Evaluation Report 1998-21

LIDAR System for Area Sensing of Vehicle Emissions: Final Evaluation Report

Minnesota Guidestar

Technical Report Documentation Page

1. Report No.	2.	3. Recipient's Accession No.
MN/RC - 1998-21		

4. Title and Subtitle	5. Report Date
LIDAR SYSTEM FOR AREA SENSING OF VEHICLE EMISSIONS: FINAL EVALUATION REPORT	January 1998
	6.

7. Author(s)	8. Performing Organization Report No.
David L. Hofeldt	

9. Performing Organization Name and Address	10. Project/Task/Work Unit No.
University of Minnesota Department of Mechanical Engineering 111 Church Street, S.E. Minneapolis, MN 55455	11. Contract (C) or Grant (G) No. (C) 72323 TOC # 151

12. Sponsoring Organization Name and Address	13. Type of Report and Period Covered
Minnesota Department of Transportation 395 John Ireland Boulevard Mail Stop 330 St. Paul, Minnesota 55155	Evaluation Report - 1994-1996
	14. Sponsoring Agency Code

15. Supplementary Notes

16. Abstract (Limit: 200 words)

This report presents an assessment of the effectiveness of an elastic LIDAR system (wavelength of 1.06 um) for wide-area remote sensing of pollutant concentrations associated with particulate plumes near urban roadways. Traditional point-sampling instruments were also used to measure mass concentrations of particulate matter and carbon monoxide (CO) concentrations near the roadways. The size distribution of the particulate matter was also measured, and variations in the size-resolved particle concentrations were compared to the LIDAR signal. We found that the LIDAR signal was most sensitive to the concentration particles whose characteristic dimensions were slightly larger than the wavelength of the laser used, and that a relation exists between the two. Hence, when used at low elevations near roadways, the 1.06 um wavelength LIDAR system located plumes of particles whose aerodynamic diameters fell in the 1-5 um size range, and tracked changes in their concentrations. Particles in this size range lie primarily in the coarse size range of respirable aerosols, and are readily made airborne by vehicle-induced air motion and thermal drafts associated with pavement and vehicle exhaust.

The bulk of this report summarizes the operating characteristics of the LIDAR system; issues regarding field deployment, including eye safety, reliability, and operator training; requirements for image display and interpretation; and correlations between the LIDAR signal, pollutant concentrations, and traffic. The influence of varying weather conditions, primarily wind speed, direction, and relative humidity, is discussed. Recommendations for further development are also given, including comments on the feasibility of fine particle LIDAR and species specific LIDARS. Firm conclusions regarding the air quality impacts associated with the operation of a portable traffic management system designed to minimize traffic congestion cannot be drawn at this time due to uncertainties associated with the effectiveness of the traffic management system and large variabilities introduced by varying weather and traffic conditions.

17. Document Analysis/Descriptors		18. Availability Statement
light detection and ranging laser beam particulate mass	PM-10 standards size-resolved particle portable traffic management system	No restrictions. Document available from: National Technical Information Services, Springfield, Virginia 22161

19. Security Class (this report)	20. Security Class (this page)	21. No. of Pages	22. Price
Unclassified	Unclassified	278	

LIDAR SYSTEM FOR AREA SENSING OF VEHICLE EMISSIONS: FINAL EVALUATION REPORT

Final Evaluation Report

Prepared by:

David L. Hofeldt, Assoc. Professor
Department of Mechanical Engineering
University of Minnesota
111 Church Street, S.E.
Minneapolis, MN 55455

January 1998

Published by:

Minnesota Department of Transportation
Office of Research Services
Mail Stop 330
395 John Ireland Boulevard
St. Paul, MN 55155

ABSTRACT

This report presents an assessment of the effectiveness of an elastic lidar system (wavelength of 1.06 μm) for wide-area remote sensing of pollutant concentrations associated with traffic activity. The lidar system was used to obtain spatially and temporally resolved images of particulate plumes near urban roadways. Traditional point-sampling instruments were also used to measure mass concentrations of particulate matter and carbon monoxide (CO) concentrations near the roadways. The size distribution of the particulate matter was also measured, and variations in the size-resolved particle concentrations were compared to the lidar signal. We found that the lidar signal was most sensitive to the concentration particles whose characteristic dimensions were slightly larger than the wavelength of the laser used, and that a linear relation exists between the two. Hence, when used at low elevations near roadways, the 1.06 μm wavelength lidar system located plumes of particles whose aerodynamic diameters fell in the 1-5 μm size range, and tracked changes in their concentrations. Particles in this size range lie primarily in the coarse size range of respirable aerosols, and are readily made airborne by vehicle-induced air motion and thermal drafts associated with pavement and vehicle exhaust.

The bulk of this report summarizes the operating characteristics of the lidar system; issues regarding field deployment, including eye safety, reliability, and operator training; requirements for image display and interpretation; and correlations between the lidar signal, pollutant concentrations, and traffic. The influence of varying weather conditions, primarily wind speed, direction, and relative humidity, is discussed. Recommendations for further development are also given, including comments on the feasibility of fine particle lidars and species specific lidars. Firm conclusions regarding the air quality impacts associated with the operation of a portable traffic management system designed to minimize traffic congestion cannot be drawn at this time due to uncertainties associated with the effectiveness of the traffic management system and large variabilities introduced by varying weather and traffic conditions.

EXECUTIVE SUMMARY

Elastic lidars operate on the same principle as conventional weather radars, only with a laser beam swept through the atmosphere rather than a radio wave. In fact, lidar is actually an acronym which stands for light detection and ranging, just as radar is an acronym which stands for radio wave detection and ranging. The lidar signal is generated as the laser beam scatters off aerosol particles in the atmosphere, similar to the way a radio wave scatters off rain droplets. The lidar scans are converted to images which display maps of aerosol concentrations within the region swept out by the beam, analogous to conventional radar images of the intensity and location of storms. As with radar images, the lidar images can be obtained sequentially in time in order to show the time history of aerosol plumes within the range of the lidar system. Such images contain information on the magnitude of pollutant concentrations, the source of plumes and how they disperse under the prevailing weather and traffic conditions, and temporal variations in plume concentrations.

The primary goal of this operational test was to determine the usefulness of lidar technology as an air quality monitoring tool. To do this, we had to establish whether a quantitative relationship existed between the lidar signal and pollutant concentrations near urban roadways, and if so, what combination of local weather and traffic conditions might enhance or mask this relation. We also had to evaluate whether software developed to display the lidar images superimposed over a regional GIS map enabled interpretation by a varied audience of public policy makers, air quality regulators, regional planners, transportation engineers, and atmospheric scientists. If a quantitative relationship existed and the data was readily displayed, the lidar images could be used to monitor pollutant concentrations over relatively wide areas and indicate exposure levels of individuals traveling in the area. Thus, the lidar scans could be used to assess the air quality impacts of various traffic management strategies. Finally, lidar data sets could be used to develop next generation dispersion models which would account for the complex turbulent mixing environment associated with urban roadways. These models could then be used to predict the air quality impacts of new traffic management strategies and business developments.

Four tests of the lidar system were performed in urban and suburban locations in Minnesota under widely varying weather conditions during July-November 1994. The sites chosen were generally surrounded by residential neighborhoods, but included local attractions

which could lead to traffic congestion during special events. Lidar data was taken before, during, and after such events. No scans were taken in central business district areas. Since the field-of-view of the lidar images is limited by line-of-sight access between the laser source and the points of interest, three types of lidar data were collected: 1) line (one-dimensional) profiles of aerosol concentrations along rays directed over the inlets of the point-sampling instruments to establish the relationship between the lidar signal and pollutant concentrations, 2) two-dimensional scans upwind and downwind of roadways designed to demonstrate the impact of various traffic conditions, and 3) two- and three-dimensional scans of relatively broad areas at elevations just above treetop level (typically above 20 m, or 60 ft) designed to show the dispersion of aerosol plumes generated by the events. The maximum range of the lidar system tested was about 10 km, although most of the data analyzed was in the 1-5 km distance range.

An additional test to establish the particle size dependence of the lidar signal was carried out in Albuquerque in June of 1995. Several point sampling instruments capable of size-resolved particle concentration measurements with time resolutions of about 30 seconds were fielded. Comparisons between the lidar data and the particle concentration measurements showed a linear relationship between the lidar signal and the number concentration of particles whose characteristic sizes were slightly larger than the wavelength of the laser used. Hence, for the particular lidar system tested (laser wavelength of 1.06 μm), the lidar signal effectively measured the number concentration of particles whose aerodynamic diameters fall in the 1-5 μm size range. This size range is respirable (particles < 10 μm are considered respirable) and included within the current EPA particulate matter air quality standards (referred to as the PM-10 standards because the regulations specify allowable mass concentrations of particulate matter less than 10 μm).

It is important to understand the significance of particle size when considering particulate concentrations near roadways. Typical atmospheric aerosols are bimodal, with one group of particles having sizes larger than about 2.5 μm (termed coarse particles) and another group with sizes less than 2.5 μm (termed fine particles). Near roadways, the mass associated with the coarse particles generally dominates the total respirable particulate mass; this occurs because turbulence created by the motion of vehicles and thermal updrafts caused by hot exhaust and convection from the road surface continually re-entrain soil and tire dust particles from the roadway, replenishing particles which settle out due to gravity. The 1-5 μm aerodynamic size range observed by the

lidar accounts for a significant fraction of the total particulate mass allowed by the current PM-10 standards, and hence the lidar images are very useful in identifying aerosol plume sources near roadways and tracking their dispersion. However, we must point out that changes to the current PM-10 standards have recently been proposed: at issue is the relative importance of health effects associated with mass concentrations of coarse particles compared to the health effects of the more numerous but lighter submicron (fine) particles, which can penetrate farther into the lungs.

Correlations between the lidar signal and ambient CO levels do not exist in general, but might occur under certain combinations of traffic and wind conditions. For example, when the sampling location is downwind of the roadway, stop-and-start traffic flow conditions exist (either due to signal changes or traffic congestion), and winds are light, the correlation between time-averaged (over several minutes) ambient CO concentrations and time-averaged coarse particle concentrations could be fairly strong. Hence, under some circumstances where a significant particle plume is generated by a roadway, the plume could also exhibit a fairly high CO concentration. It must be emphasized that an elastic lidar signal would still be only an indirect indicator of CO levels under these circumstances, not a quantitative measure. Elastic lidars could therefore have a role in identifying roadway-generated plumes in which CO levels were likely to exceed allowable levels, but quantitative spatially-resolved measurements would require the use of more sophisticated species-specific lidar systems tuned to measure CO concentrations directly.

The table at the end of this section summarizes the criteria used to evaluate the lidar technology as a traffic-related air quality monitoring device, and the conclusions of this study. In general, the correlation between the lidar signal and time-resolved roadside particle concentrations was quite strong, ranging from 0.80 - 0.98 under the short durations (3-6 hours) that we conducted. In one case, a particle event probably associated with a golf course sprinkler system located upwind of the sampling point apparently caused a large change in particle composition and number density, and the correlation including that event with periods surrounding it decreases to about 0.7. Longer duration tests or tests over periods involving large changes in relative humidity would probably need to incorporate corrections for variations in the particle compositions, and a means of calibrating the lidar system gain, perhaps using a small portable calibration target, would be needed.

The secondary goal of this project was to analyze the air quality impact associated with the deployment of a portable traffic management system (PTMS) designed to minimize traffic congestion associated with special urban events. In other words, the question to be answered was whether minimizing traffic congestion in a local area brought about a significant reduction in pollutant concentrations or merely shifted the problem to a different location. Due to uncertainties associated with the effectiveness of the traffic management system and a limited amount of lidar data with which to assess the impact of varying weather and traffic conditions, firm conclusions cannot be drawn at this time.

TABLE *i*: EVALUATION CRITERIA AND SUMMARY OF RESULTS

Criteria	Evaluation Conclusions
Locate and track pollutant plumes, qualitative indication of particulate concentrations	Excellent spatial resolution provided line-of-site access exists. Temporal resolution is on the order of 1 sec. for a single point or a line, 2 min. for 2-D slices, and 10-15 min. for 3-D sectors. Can be used to identify conditions where high CO concentrations might exist, but will not provide a quantitative measure of CO.
Auxiliary measurements required for quantitative interpretation of signal	The lidar signal in near-ground applications near roadways is nominally proportional to the number concentration of particles with aerodynamic diameters of 1-5 μm. Linear correlation coefficients are typically 0.80-098 for short term (2-8 hour) periods. Correlation coefficients will decrease if particle compositions change, for instance if a large-scale sprinkler system turned on upwind, or if the lidar system gain is not periodically calibrated. Inertial impactors or related instruments are required to obtain quantitative particle mass concentrations, and may be combined with particle counters to provide information on effective particle material density. Humidity measurements would be needed to estimate scattering correction factors if measurements were made over a wide range of humidity levels.
Issues for field deployment:	
Field-of-view and range	Measurable volume limited by line-of-sight access. Elevated site or portable platform required; wide-area resolution requires elevation over treetops & buildings. Maximum range of system tested was approx. 10 km.
Operating requirements	Two trained operators, 5 kW portable generator, ambient temps. between 32 and 110°F, no rain, wind limit depends on site location. Set up and check out requires approximately 1/2 day.
Portability	Excellent; can be flown to city, transported to site in 12 ft. moving van, carried up to desired platform.
Reliability	Moderate; some down time caused by power supply or control circuitry failures; complete spares would be advisable for critical tests. Constraints on ambient conditions given above.
Eye safety	The laser beam in this system was not eye safe to the unaided human eye within the first 1.2 km. This limits the near-field resolution in ground-level applications, which is important in urban environments where obstructions are common. FAA approval is required to ensure no interference with flight paths. The eye safety issue can be overcome by using a 1.5 μm wavelength or by increasing the diameter of the beam.
Image display and interpretation	Near real-time display of the data is needed, including time stamp and directional heading of the lidar beam. Ideally, the display would show the lidar data superimposed on the road grid. A fixed marker (a small target generating a repeatable lidar signal) would be useful in orienting the lidar images and monitoring system response. Ability to display traffic video in small inset within image would be useful, but not required.
Potential for model development and validation	Strong potential for evaluation and development of plume dispersion models for urban settings. Potential for coarse resolution of unobstructed wind fields provided aerosol plumes are present. Dial systems or fluorescence detection could be used for species specific detection, for example of NO_2, SO_2, volatile organic compounds, etc.

FORWARD TO LIDAR PROJECT EVALUATION:

Project Approach Considerations For Future Operational Tests

The two primary goals of this project were to validate the LIDAR System, and then use it to assess the environmental impacts of another ITS project. In addition to the scientific and deployment observations and recommendations reported in the following evaluation, this project revealed other issues which should be considered for future operational tests of this nature.

The LIDAR Project was unique in that much of the data used by the evaluator was collected and reduced by the private partners. This arrangement was considerably different from other operational tests where most, if not all, of the evaluation data was generated and collected by the independent evaluator. This made for challenges in managing the deployment of the equipment and the data supplied by the private partners, and often times modifications to the deployment strategies were made via group consensus only a day or so in advance of the field tests.

A large number of data sets were required to accurately characterize traffic and meteorological conditions as well as site-specific background pollutant concentrations and terrain variations. Many of the data sets had to be sampled with a high degree of temporal resolution in order to assess the effects that changes in each of these variables might have on the lidar signal. The fact that instruments were supplied and operated by different groups made data sampling, reduction, and output file formats difficult to standardize. In addition, since these groups were stationed at physically separate sites during the tests, automated synchronization of sampling intervals would have required a very sophisticated data acquisition protocol. Thus, data coordination was arranged by synchronizing watches and communicating via walkie-talkies during the tests.

The large number of time-resolved data sets resulted in tremendous volumes of data. However, despite the large volume, the number of instances in which only one variable would be undergoing significant variations, while the others remained nominally constant, was limited. This made the accuracy of all of the instruments important in order that a reliable statistical analysis could be performed. In a few cases, the scientific accuracy of the instruments and processed data sets was not up to the standard which would have been desired by the evaluator.

The marriage of this project to another operational test raised an additional challenge due to the tight and ever changing schedule of events and site locations. Changing site locations made it more difficult to establish baseline conditions, and the short time between events made it difficult to fully analyze the results of one test before starting the next. The two project goals would have been better achieved through separate operational tests, one to collect sufficient data for the verification of the LIDAR system, and presuming that to be successful, a second designed specifically to evaluate the impacts of ITS subject to the limitations in the technology identified in the first.

In spite of these challenges, the team did make strong and effective efforts to accommodate the situations, and collected enough data to achieve the project's primary goal.

The following list summarizes the key points which should be considered for future operational tests of this nature:

1. Appoint an independent data manager of considerable relevant scientific background, who can oversee the project plan, deployment procedures, calibration efforts, and data reduction. This person should have authority to ensure that personnel assigned to carry out data acquisition or data reduction tasks have the necessary experience or are properly trained for such functions. This may require special agreements with private partners. This person should also play an integral role in the project conception.
2. Provide sufficient time to develop an appropriate project scope and an effective evaluation plan. This would enable the document to be circulated for peer review.
3. Establish a more rigid event schedule, and allow sufficient time between events for the reduction, verification, and analysis of the data.

Michael A. Manore, P.E.
Lidar Project Manager

ACKNOWLEDGMENTS

We gratefully acknowledge the support of the Federal Highway Administration and the Minnesota Department of Transportation for funding this study. Appreciation is also due to Mr. Richard Schoenenberg of the Federal Highway Administration (FHwA), Ms. Lee Ann Byrd of the Environmental Protection Agency (EPA), and Mr. James R. Wright of Minnesota Guidestar for their insights into the project direction. Mr. Michael Manore, the project director, deserves commendation for his ability to overcome last minute changes in operating plans and in keeping everyone working together, as well as for his involvement in and understanding of the project.

In addition, the author would like to thank the personnel at Santa Fe Technologies; the lidar personnel at Los Alamos National Laboratory, especially Dr. William Eichinger and Mr. Larry Tellier, and Nancy Collins at IBM for their help and professionalism in carrying out this project. Finally, I must acknowledge the assistance of several graduate students at the University of Minnesota who assisted with data collection and some of the analysis for various pieces of this project: Dr. Sumantra Chakravarty, Mr. Bernard Olson, Mr. Imad Abdul-Khalek, and Mr. Phil Dieck, as well as useful discussions with my colleagues, Dr. Ken Rubow and Prof. Virgil Marple of the Particle Technology Laboratory.

CONTENTS

LIST OF FIGURES

LIST OF TABLES

OVERVIEW OF LIDAR TEST

Motivation

National ambient air quality standards were established by the Clean Air Act of 1970 in response to degradations of air quality in urban areas. Respirable particulate matter (PM; particles with characteristic sizes less than 10 μm), carbon monoxide (CO), and ground-level ozone (O_3) were among the regulated pollutants because of their known or suspected health effects. The Clean Air Act Amendments were enacted in 1990 largely as an effort to speed attainment of the air quality standards. These amendments reiterated allowable pollutant levels and established specific programs to be implemented by areas exceeding the limits. In urban areas, a significant source of the pollutants listed above can be traced to emissions from automobiles and trucks; in fact, the principal source of CO in urban areas is motor vehicle exhaust [Seinfeld 1986].

As Intelligent Transportation Systems (ITS) continue to develop, we should have the ability to manage increased traffic levels with less congestion. Smoother traffic flow associated with less congestion should reduce vehicle emissions, but the question arises as to whether the reduced emissions will be offset (or overcome) by expected increases in the number of vehicle miles traveled. In other words, while ITS technology may better service the desire for rapid personal transportation, its impact on the environment is not yet known; if the net effect of implementing ITS technologies would be a degradation in air quality in such areas, then such investments would be very costly mistakes under current regulatory policies. Since many regions considering ITS systems are also non-attainment areas with respect to one or more of the pollutants listed above, the question is an important one to answer.

In order to assess the air quality impacts of ITS projects, one needs to know the relationship between traffic conditions, weather conditions, local geography, and pollutant concentrations over fairly wide areas. Complex interactions between vehicle emissions, transport and mixing in the surrounding air, and chemical reactions control pollutant concentrations in the real world. Dispersion (*e.g.* (Dabbert, 1973; Hanna, 1982) and air quality models (*e.g.* EPA's CAL3QHCR and Urban Airshed Model; Los Alamos National Laboratory's Higher Order Turbulence Model for Atmospheric Circulation--HOTMAC, and Regional Atmospheric Modeling System--RAMS)

are necessarily simplified (Braverman, 1995; Cottingame 1995) and cannot provide quantitatively accurate predictions of pollutant concentrations over the tremendous range of climate and terrain conditions. Hence, measurements are required (*e.g.* Heinz *et al.*, 1994). A real-time, wide area remote sensing technology would address many of the requirements for evaluating the impacts of vehicle traffic on local air quality. Data on dynamic variations in the spatial distribution of pollutants caused by changing traffic and/or weather conditions could be provided by such a system. Such data would enable 1) the impact of traffic management strategies on air quality to be monitored; 2) the development and validation of next generation air quality models useful for predicting the air quality impacts of various traffic scenarios; and 3) feedback to adaptive traffic control systems based on minimizing pollutant concentrations rather than traffic congestion.

Light detection and ranging (lidar, *a.k.a.* laser radar) is a wide area remote sensing technology which has been used to map concentrations of various particulates and gaseous species in the earth's atmosphere since the 70's. Recently, it has also been used to map air pollution in various urban locations in the United States and Europe [Butler 1993; Leonelli, J., 1995; Kolev *et al.*, 1996;]. It is arguably the only remote sensing technology which can obtain measurements in real-time over relatively wide-areas (hundreds of square kilometers). As such, it represents one of the only available methods of monitoring the impact of new traffic control systems on air quality. Fielding enough conventional point sampling air quality monitoring instruments to accomplish even partial coverage of such a region would be numerically overwhelming and prohibitively expensive in any practical application.

Objectives of the Lidar Test

The principle objective was to evaluate the usefulness of elastic lidar technology for monitoring traffic-related air pollutants. The evaluation of usefulness for ground level pollution sensing applications was based on five criteria: 1) the ability to identify the source of particulate plumes, track their dispersion, and qualitatively indicate changes in particulate concentrations; 2) auxiliary measurements required to enable the lidar signal to be interpreted as a quantitative measure of pollutant concentrations; 3) ease of field deployment, *i.e.* portability, reliability, field-of-view, range, operating requirements, and safety; 4) versatility of lidar image display software for enabling acquisition and interpretation of images by an audience varying from public policy

makers, regional planners, and air quality regulators to transportation engineers and atmospheric scientists; and 5) potential for providing useful data for development and validation of atmospheric models. These criteria should be kept in mind when reading the report. A table summarizing the conclusions of this study regarding these criteria can be found in the Executive Summary and Conclusion sections.

A secondary goal of this project was to use the lidar to evaluate the air quality impact of the Minnesota Department of Transportation (MN-DoT) Portable Traffic Management System (PTMS). The PTMS consists of various portable traffic monitoring and control technologies designed for use at events which may lead to temporary but substantial increases in local traffic volume and hence traffic congestion. The realization of this goal was dependent not only upon the usefulness of the lidar data as an air quality monitor, but also on the ability to measure the impact of the PTMS system on traffic flows. Moreover, since only a small number of events were monitored, the results were susceptible to variations caused by non-repeatable traffic or weather conditions occurring on days when the PTMS was operational or idle. Since this was the first attempt at applying lidar technology to evaluate roadside air quality, such a limited test matrix was advisable to ascertain the likelihood of success before embarking on more ambitious tests.

BACKGROUND

Description of Lidar Technology

Elastic lidars operate on the same principle as conventional weather radars, only with a laser beam swept through the atmosphere rather than a radio wave. In fact, lidar is an acronym which stands for light detection and ranging, just as radar stands for radio wave detection and ranging. The lidar signal is generated as a pulsed laser beam scatters off aerosol particles in the atmosphere, analogous to radar signals generated when radio wave pulses scatter off rain droplets. The lidar scans are converted to images which display maps of aerosol concentrations within the region swept out by the beam, similar to conventional radar images of storm intensity and location. As with radar images, the lidar images can be obtained sequentially in time in order to show the time history of aerosol plumes within the range of the lidar system. Such image sequences contain information on the magnitude of pollutant concentrations, the source of plumes and how they disperse under the prevailing weather and traffic conditions, and temporal variations in plume concentrations.

The use of the term "light" within the name is sometimes confusing to those unfamiliar with laser technology: the laser beam in a lidar system is not necessarily visible, despite the generic definition of light. In fact, for applications near roadways, it is highly desirable for the beam to be invisible in order to avoid distracting drivers. (Technically, the laser beam lies in the optical frequency part of the electromagnetic spectrum, whereas radio waves -- which are also invisible -- lie in the radio frequency part of the spectrum. However, some of the original systems did use visible light, and "lidar" made a better sounding acronym than "opdar.") For simplicity, we will use the term light to refer to the laser beam.

A typical elastic lidar system is depicted in Figure 1. The laser emits a very short pulse of light (10 ns, or 10^{-8} sec. in duration for our system) in a known direction. The light travels some distance before it scatters off aerosol particles suspended in the beam path. Some of the scattered light is reflected back to the instrument, where it is collected by a telescope and focused onto a sensitive detector. The amount of light received by the detector depends in part on the concentration and size of the aerosol particles. The spatial distribution of the aerosol along the beam path is found by recording the return signal as a function of time. This works because light

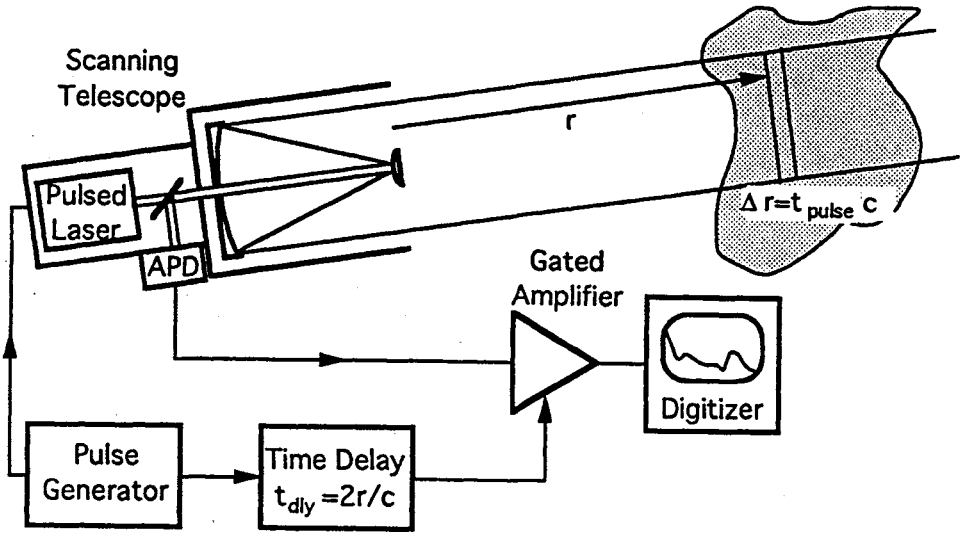

Fig. 1: Schematic of a lidar system.

travels at a velocity of roughly one foot every nanosecond. Thus, the 10 ns pulse is roughly 10 feet long, and it would take 200 ns for the light pulse to travel to a position 100 feet from the laser, scatter off particles, and return to the laser again. Thus, recording the signal 200 ns after the pulse is emitted gives a measure of the particle concentration in a volume defined by a 10 foot length along the cylindrical beam path at a distance of 100 ft from the laser. By sending out a sequence of pulses, the particle distribution along the beam path can be monitored over time. If in addition the beam is scanned through a sequence of directions and elevations, two and three-dimensional maps of aerosol concentrations can be acquired and mapped out over time.

The relationship between the lidar signal and the aerosol concentrations is discussed in more detail in App. A, but the key points can be summarized as follows:

1) The lidar signal can be related to the number density or mass concentration of particles along the beam path. The response is not equally sensitive to particles of all sizes; rather, the signal response per unit mass of particulate matter is strongest for particles whose diameters are on the same order as the wavelength of the laser employed in the lidar system. For example, in the system tested, the laser wavelength was 1.06 μm, and the peak response was to particles of about 3 μm in diameter.
2) The volume of the aerosol sampled at any instant by the lidar pulse is on the order of several cubic meters. This is a relatively large sample volume compared to conventional instrumentation, and yet it is small enough to retain more than adequate spatial resolution for resolving the spread of aerosol plumes. The large volume is advantageous because it decreases the statistical uncertainty in ambient aerosol measurements.

3) The temporal resolution depends on the total scanned volume and the desired resolution. Measurements at a single point or along a single line-of-sight can be obtained with better than one second resolution; high resolution two dimensional sector scans typically require on the order of a minute, and three-dimensional pie slices generally require on the order of 10-15 minutes.

4) Inverting the lidar signal to obtain quantitative predictions of aerosol concentrations requires knowledge of properties which affect the amount of light scattered and absorbed by the particles. To obtain mass concentrations, the effective density of the material which comprises the particle must also be known. Estimates for such particle characteristics are available in the literature, but more accurate results can be obtained by employing fast response particle sampling instruments to obtain calibration data at one or more points within the lidar field of view .

The main difficulty encountered when applying lidar technology to monitor ground-level pollution is the need for line-of-sight access between the laser source and the target air volume. This imposes several limitations: 1) the laser beam must be "eye-safe," since terrain variability may result in the possibility of bystanders within the beam path, 2) an elevated site from which desired ground-level areas can be seen is required, 3) wide-area scans will be limited to treetop or building-top levels and higher.

In this test, the laser beam was not eye safe within the first kilometer of distance from the laser. Hence, the beam was not allowed to reach the ground or other areas where humans might be (including aircraft) within 1 km of the laser. Scan directions were always overseen by a laser safety officer. Even with this precaution, the potential for eye damage, however remote, creates a public relations problem, especially if one considers the beam as a hazard to birds. It would be a relatively simple matter to expand the laser beam diameter such that it was safe to view even at the output of the laser. The farther the desired range, the higher the required laser power, and the larger the beam diameter would have to be, but this could easily be taken into account. An even more fail-safe system would be to use an eye-safe pre-pulse to detect objects entering the beam path at undesired locations, and prevent the lidar laser from firing if an object were detected. This would be more expensive because of the need for a second system, but it may be necessary if the lidar system is used for automated ground-level measurements.

An elevated site allows line-of-sight access to the ground along rays which aren't blocked by trees or buildings. Portable lifts located alongside straight roadways can provide adequate access to particular roadways, but wider area scans require the lidar to be situated on a tall building,

bridge, hill, or even a water tower. Wide area scans at heights above the treetops or building-tops can be obtained in a straightforward manner, and theoretically could be extended to ground level in unobscurred directions. The latter measurements would require a detailed topographical scan to be acquired by the lidar at a time when particle concentrations were minimum, *e.g.* during early morning hours. Such detailed knowledge of local topography would be necessary to ensure that the lidar signal near the ground corresponded to aerosol concentrations rather than scattering from objects on the ground. No measurements of this sort were attempted in this study.

Atmospheric Aerosols

A basic understanding of the properties of ambient aerosols is important in order to assess the usefulness of the lidar data. The size distribution of the aerosol particles is particularly significant, since both the lidar response and the particle characteristics are strong functions of particle size. Particles less than 10 μm in aerodynamic diameter can penetrate into the lungs and may deposit there; hence they are classified as respirable and are regulated as part of the National Ambient Air Quality Standards (see Hinds, 1982, p. 221-2). The particle standards are often referred to as the PM-10 standards, because the regulations specify allowable levels for mass concentrations of particulate matter less than 10 μm. The aerodynamic diameter, D_{AD}, is a characteristic size defined as the diameter of a homogeneous spherical particle with a density of 1 g/cm^3 which will behave in the same aerodynamic fashion as the actual physical particle, where the latter in general has a density other than 1 g/cm^3 and a morphology which is generally not perfectly homogeneous or spherical. The physical diameter of the particle is generally cited as a characteristic length, D, of a spherical particle which would have the same volume and the same mass as the actual particle, and an effective density of ρ. The aerodynamic and physical diameters are related according to $D_{AD} = D \times \sqrt{\rho}$. As the particles increase in size from 1-10 μm, an increasingly larger fraction are filtered out before they penetrate into the deepest region of the lungs, the alveolar sacs. Essentially 100% of particles less than 1 μm in aerodynamic diameter penetrate into the alveolar sacs, but this drops off rapidly to 50% of particles slightly larger than 3 μm, and 0% particles 10 μm or larger. Thus, 10 μm aerodynamic diameter is the cutoff for respirable particles. We will use the term respirable mass to indicate the mass of the fraction of particles less than 10 μm in diameter which actually penetrate into the deepest region of the lungs.

Typically, plots of the mass concentration distribution of atmospheric aerosols are shown on axes like those appearing in Figure 2, and generally two or three distinct modes are evident. The diameters are most often reported as aerodynamic diameters. Figure 2 shows the average aerodynamic particle size distribution measured over a period of approximately twelve hours during one of the Minnesota tests. In our roadside tests, the minimum of the valley between the sub- and super-micron modes consistently fell in the 1-2 μm range, with total concentrations were on the order of 30-50 $\mu g/m^3$.

In regulatory jargon, particles larger than 2.5 μm in diameter are termed coarse particles, whereas those with diameters less than 2.5 μm are termed fine particles. Particles in these different ranges have distinctly different properties and health effects. The larger particles contain primarily oxides of aluminum, silicon, calcium, and iron, and are mostly solids with characteristic densities of about 2-2.5 g/cm^3. Many of the particles whose sizes exceed 5 μm are filtered out in the nose or tracheal-bronchial tracts. Fine particles contain more sulfates, nitrates, and hydrocarbon species, which tend to be more biologically active (some are known carcinogens), and are often liquids with characteristic densities closer to 1 g/cm^3. Roughly about a quarter of the particles in any given size range from 0.1-2.5 μm which are inhaled can deposit in the deepest

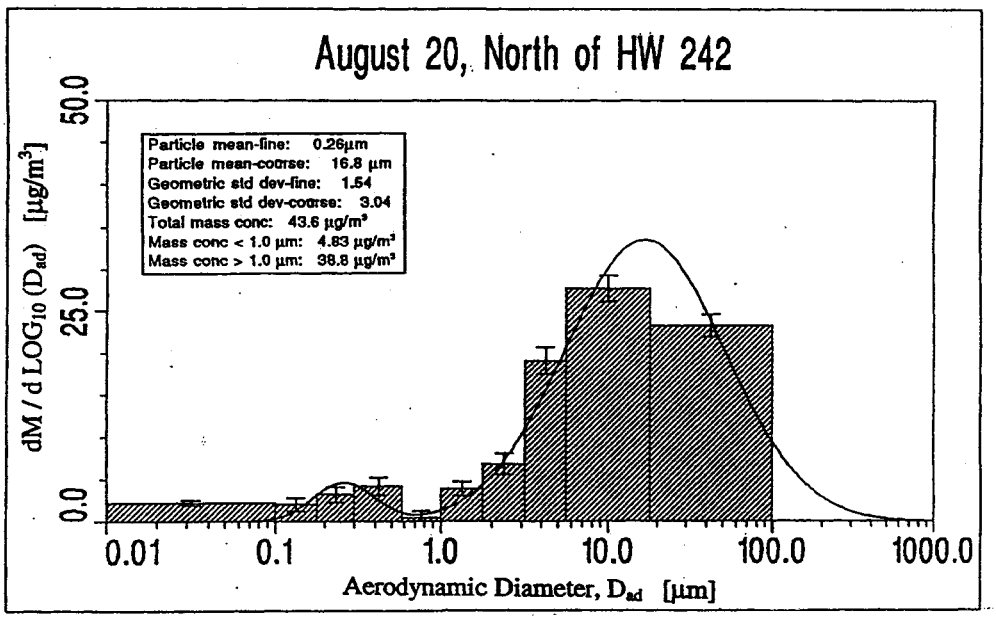

Fig. 2: Typical atmospheric aerosol size distribution averaged over 12-hours (taken on 8/20/94 just north of Trunk Highway 242 on Hanson Blvd., Coon Rapids, MN, at an elevation of 24 ft). Mass median aerodynamic diameters appear in the legend.

regions of the lungs, the alveolar sacs. Some of these particles are re-expelled, but others are absorbed or remain deposited.

At typical breathing heights near roadways, the mass associated with the coarse particles often dominates the total respirable particulate mass. This occurs because mass scales with the cube of particle diameter, and so a small number of large particles contain as much mass as a very large number of small particles. Both turbulence created by vehicle motion and thermal updrafts caused by hot exhaust and convection from the road surface continually re-entrain relatively large soil and tire dust particles from the roadway which otherwise may have settled out as a result of gravitational forces. Thus, large particle concentrations near roadways are somewhat elevated. The 1-5 μm size range accounts for a significant fraction of the total respirable particulate mass allowed by the current PM-10 standards; hence, the lidar images are useful in identifying sources of respirable aerosol plumes and tracking their dispersion.

Entrainment processes can also serve as sources of fine particles, but many more are formed as a result of photochemical reactions or coagulation and condensation of products emitted from combustion sources, *i.e.* engines. Soot particles from Diesel vehicles are one example, but a substantial fraction of fine particles are actually liquid droplets (Hinds, 1982, p. 280; Sheridan *et al.*, 1993). A critical point to realize is that although the mass associated with the fine particles may be as little as 20-30% of the total respirable particulate mass in a given volume of ambient air, the number of fine particles is orders of magnitude larger than the number coarse particles. Hence, if equal fractions of fine and coarse particles deposit somewhere within the respiratory tract, a far larger number of small particles have been deposited. If the number of incidences is more important than the volume of the deposited particles, the concern shifts to smaller particles, and even more so if the greater biological activity is also taken into account.

The current particulate standards enforced by the U.S. Environmental Protection Agency (EPA).are based on the total mass concentration of respirable particles (those less than 10 μm), and are often called the PM-10 standards. As indicated above, the total respirable mass concentration will be significantly impacted by, if not dominated by, the number of particles in the coarse mode, especially if the measurements are taken near roadways. However, results of recent epidemiological studies have indicated that mass concentrations of fine particles are much more strongly correlated with increased death rates in urban areas than are mass concentrations of

coarse particles. (Pope *et al.*, 1995, Wilson, 1995) This seems to corroborate the concern raised above, and is in fact the principal reason behind the particulate standard review currently underway at EPA.

Lidar Signal Response

A fairly complete although somewhat simplified discussion of how the lidar signal varies with particle size is contained in App. A, but the main points can be summarized as follows:

1) The lidar signal is proportional to the product of the number concentration of particles in the beam path multiplied by their optical cross section. Since the cross section varies with particle size, the particle size distribution must be known if the lidar signal is to be used as a quantitative measure of particle concentrations. Accurate size information is not easily obtained from lidar signals; hence, one or more instruments which can independently measure the particle size distribution must be located with the lidar field-of-view if the signal is to be interpreted as a quantitative measure of particle concentrations. If such size distribution measurements are not possible, the lidar signal is still an excellent qualitative indication of the relative strength of different aerosol sources within the field-of-view.
2) The lidar signal response can also be analyzed on a per unit mass of particulate matter basis. Such an analysis shows that the response is strongest for particles whose diameters are on the same order as the wavelength of the laser employed in the lidar system. For example, in the system tested, the laser wavelength was 1.06 μm, and the peak response was to particles of about 3 μm in diameter.
3) The volume of the aerosol illuminated at any instant by the lidar pulse is on the order of several cubic meters. This is a relatively large sample volume compared to conventional particle instrumentation, and yet it is small enough to retain adequate spatial resolution for resolving the spread of aerosol plumes. The large volume is advantageous because it decreases the statistical uncertainty in measuring ambient aerosol concentrations.
4) The temporal resolution of lidar image sequences depends on the scan volume. Measurements at a single point or along a single line-of-sight can be obtained with better than one second resolution; high resolution two dimensional sector scans typically require on the order of one or two minutes, and three-dimensional pie slices generally require on the order of 10-15 minutes.
5) Inverting the lidar signal to obtain quantitative measurements of aerosol concentrations also requires knowledge of the average optical cross sections of the particles, which vary with particle composition and morphology. To obtain mass concentrations, the effective density of the material which comprises the particle must also be known. Estimates are available in the literature (see App. A), but more accurate results can be obtained by employing fast response particle sampling instruments at one or more points within the field of view of the lidar for the purpose of providing calibration points.

We should point out, however, that one of the most useful features of the lidar image sequences is their ability to resolve *changes* in particle concentrations from point to point and time to time; the absolute magnitude of the particle concentration at a given point and time is important, but can often be estimated based on experience or obtained by other instruments. The signal distribution within an image enables the source or sources of relatively high concentration aerosol plumes to be located, *i.e.* ownership can be established, and the temporal resolution enables the conditions leading up to such high concentration events to be identified. These pieces of information are absolutely necessary if one is going to design strategies to avoid such occurrences or mitigate their impact. The results presented later indicate that the lidar signal can be inverted to provide quantitatively accurate measurements of absolute particle concentrations, but significant additional effort is required to obtain the particle characteristics listed above.

Comparison of Lidar Response with Particle Mass Concentrations

The principle objective of the test was to evaluate the strength of the correlation between the lidar signal and airborne particulate concentrations near roadways and relate that to traffic conditions present at the time. In addition, a number of other measurements were required to check for parameters which could interfere with the lidar-particulate matter correlation. Local meteorological conditions had to be monitored, as changing conditions in wind speed or direction could have major impacts on the physical characteristics of the particles as well as their concentrations, and hence the lidar signal. Background concentrations were also dependent on local terrain, industrial and residential buildings and operations, and prevailing wind speeds and directions. Relative humidity levels and temperature were also monitored to ascertain if changes in these parameters affected the scattering properties of the aerosol particles. For example, if the aerosol particles were hygroscopic, they would both increase in size and change optical properties under high humidity conditions, but the mass concentrations measured under controlled humidity conditions would not reflect this. Temperature was monitored in case some chemical process unrelated to relative humidity changes might be operative to change the structure, composition, or size of the airborne particles.

The results presented in the body of the report as well as the theoretical description given in App. A show that the lidar signal is essentially linearly proportional to the particle number

concentration in the 1-5 μm size range. As indicated above, regulatory standards are written in terms of particle mass concentrations, and are applicable to particles 10 μm in diameter and smaller. Thus, the purpose of this section is to illustrate how the lidar signal compares to roadside aerosol mass concentrations.

Figure 3 shows the cumulative fractions for the particle mass and lidar signal which result from the roadside aerosol concentration distribution of Fig. 2. Both aerodynamic and equivalent spherical particle sizes are indicated along the ordinate, to help orient readers who are familiar with either aerosol measurements or light scattering measurements. The relationship between the two was discussed at the outset of the Atmospheric Aerosol section. The cumulative fraction curves enable one to see which particle size range contributes the largest portion to the PM-10 and respirable aerosol mass concentrations, as well as which size range contributes the largest portion to the lidar signal. The cumulative fraction for the particle mass contributed by particles less than 10 μm in diameter (PM-10) shows that most of the mass was contributed by the coarse mode aerosol, but a much larger fraction of the respirable particulate mass was contained in submicron particles. The lidar signal is dominated by the response to particles in the 1-5 μm size range, and corresponds fairly well to the mass contributed by these same particles, although it rises much more steeply than does the cumulative mass fraction in this range. If one examines

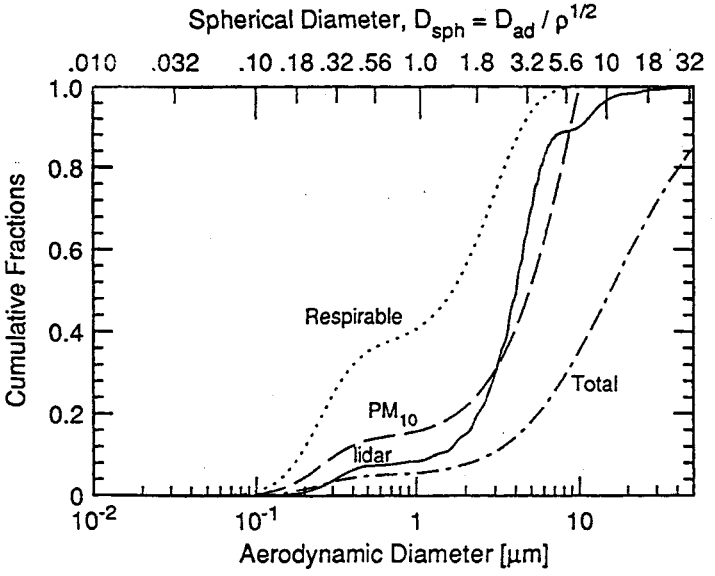

Fig. 3: Cumulative particle mass fractions compared to lidar signal fraction for the size distribution given in Fig. 2. Respirable, PM-10 and total mass fractions are shown. The equivalent spherical diameters assume a smooth increase in particle material density from 1 to 2.2 g/cm^3 between D_{ad} of 0.8 to 2.5 μm.

similar plots for other roadside particle size distributions which we measured, one finds that the respirable mass fraction associated with the fine particle mode shifts around quite substantially, but that the PM-10 and lidar signal fractions are much more stable. The stability of the latter two is apparently related to the fact that both of these fractions are dominated by contributions from relatively narrow portions of the coarse aerosol mode, and the shapes of the distributions in this size range appear to be fairly constant.

The fact that the lidar signal rises quite steeply in the 2-4 μm size range relates to its relatively high sensitivity to particles in this size range. As long as it is known that the lidar response is actually a measure of the number concentration of particles in this size range, the results are still very useful and adjustments can be made to estimate mass concentrations from the lidar signal. Perhaps of greater importance, however, is the fact that the lidar signal does not track the respirable aerosol mass very well. This stems from the fact that the lidar system used in this test employed a laser with a wavelength of 1.06 μm, which causes the response to be most sensitive to particles in the 1-5 μm size range. Thus, the current lidar system cannot detect the submicron particles in the presence of normal concentrations of particles in the 1-5 μm range. If, as indicated above, the air quality standards are redefined to place more emphasis on the smaller particles, then the spatial distribution of the respirable particles will become of greater interest. New lidar systems utilizing shorter wavelength lasers (probably in the near ultra-violet part of the spectrum) could be developed to monitor the fine particle concentrations. Such short wavelength lidar systems should behave similarly to the current system, except that the range will probably be reduced because of extinction of ultraviolet wavelengths by the atmosphere. And since there is increasing evidence that the number concentration of these small particles may be more important than their mass concentration, the fact that the lidar signal is proportional to particle number concentration may be highly advantageous.

Relations with Roadside CO Concentrations

Another goal was to determine whether the elastic lidar signal could be used as an indicator of local CO levels associated with traffic conditions. For this to work, there would have to be a reasonably strong correlation between traffic-generated particulate concentrations and CO concentrations, at least during intervals with high CO levels, since the lidar signal responds to

variations in particulate concentration and not directly with CO concentration. Hence, we first had to understand the relationship between the lidar signal and particulate concentrations, and then we could look for correlations between particulates and CO. There will obviously be instances where a link between concentrations of particulates and CO near roadways would break down, because although CO concentrations will be dominated by vehicle emissions, particle concentrations come from a large number of sources, including vehicle emissions (e.g. soot), condensation processes (primarily hydrocarbons), road and tire dust, and background particles carried to the location by the wind. Hence, one might expect the link to be somewhat tenuous and subject to local traffic and weather conditions.

Still, both CO and particulate violations are known to be "hot spot" problems, and one might anticipate that under certain conditions when local CO concentrations were high (*e.g.* low wind, temperature inversion, and lots of stop/start traffic flow), one might also observe higher particle concentrations. This is really all one needs in an air quality monitoring tool, because one is not generally concerned with how *clean* the air is, but rather whether it is approaching an unacceptably *dirty* level. We suspected that the correlation would be stronger if one could look only at submicron particle concentrations, as particles in this range would be created from condensation of hydrocarbon emissions, which occur under the same engine conditions that give rise to increased CO emissions. Moreover, the mixing processes which are responsible for dispersing particles on the order of 1 μm in size and smaller are similar to those which control the dispersion of CO in the atmosphere. The concern for the lidar signal was whether the signal was sensitive enough to the expected increased particle concentrations in the smaller size range.

INSTRUMENTATION AND PROCEDURES

Point Sampling Instruments

In order to obtain the desired correlations and determine the impact of traffic conditions, the time-resolved lidar signal had to be compared with time- and size-resolved particulate concentrations made by accepted monitoring methods, and the latter in turn compared with local traffic conditions. As previously described, we wanted to gather data on particle size distribution, wind conditions, humidity, fleet composition, and background particulate levels. At the time of this test, quantitatively accurate techniques for measuring particulate matter, CO concentrations, humidity, temperature, and traffic flow levels in a field test all involved point sampling instruments. Some measurements of wind fields have been made using lidar techniques (Sutton, 1994; Eichinger, 1995; Overbeck, 1996), but such measurements were beyond the scope of this project. Table 1 lists the instruments used in the tests along with some of their characteristics.

The point sampled data had to be available with relatively high temporal resolution in order to relate changes in the time-resolved data to changes in the lidar signal. As indicated in Table 1, the various point sampling instruments had a variety of sampling intervals. The situation was made more difficult because most of the instruments did not support external triggering, which meant that the sampling times for the different instruments could not be locked to a master clock. Hence, in order to compute correlations between the lidar signal and other time-resolved data sets, running averages were computed over a least-common-denominator sampling interval, with linear interpolation used to estimate the average values at corresponding times on all instruments. This added a significant amount of data processing and some uncertainty to the resulting correlations. Nevertheless, if, for example, a correlation between the lidar signal and 1 μm particle concentrations remained nominally constant over time even though changes in wind speed and direction occurred, then one would conclude that the correlation probably existed over space as well. Such a relation between space and time would be expected for small particles, since they remain airborne for fairly long intervals and are carried fairly long distances by the wind and vehicle wake fields. Such invariant correlations would greatly increase the value of the lidar signal, as single point calibrations could be applied to the entire field of view.

Table 1: Instrumentation Used in Field Tests

QUANTITY MEASURED	INSTRUMENT (# DEPLOYED)	DEPLOYMENT GROUP	DEPLOYMENT TESTS	TYPICAL SAMPLE INTERVAL (VOLUME)	COMMENTS
Lidar Signal					
	Aerosol Lidar System (1)	LANL	All	1-2 sec per point or line 1-2 min per 2-D slice 15-20 min per 3-D sector (approx. 2 m^3 = 2000 liters at each point)	50 Hz Nd:YAG laser, 1.06 μm wavelength, 100 mJ pulses with 10 ns duration, 8" telescope, avalanche photodiode detector. 10 km range, peak response to 1-5 μm particles.
Particle Concentrations					
Size-resolved, time-averaged particle mass concentrations	MOUDI: Micro-Orifice Uniform Deposition Impactor (2)	U of MN	All	8-12 hours (17,000 liters in 10 hrs)	0.1-10 μm size range, 4 bins per decade, each with uniform logarithmic width
Size-resolved, fast-response particle mass concentrations	QCM: Quartz Crystal MOUDI (1)	U of MN	Bunker Hills Golf Course, Blaine, MN	2 minutes (56.6 liters)	MOUDI with quartz crystals imbedded in impactor stages. Unreliable due to crystal frequency drift with temperature, particle bounce, and water vapor outgassing.
Size resolved, fast response, aerodynamic number concentrations	APS 3310: Aerodynamic Particle Sizer, TSI Inc. (1)	U of MN	Rosedale, Roseville, MN; and Albuquerque, NM	30 second sample period, data recorded approx. every 40 sec. (0.500 liters)	Size classified in terms of aerodynamic diameter; range 0.75-10 μm, larger diameter counts may be subject to double trigger error
Size resolved, fast response, optical number concentrations	Climet CI 226 (1)	U of MN	Rosedale, Roseville, MN; and Albuquerque, NM	30 second sample period, data recorded approx. every 70 sec. (3.54 liters)	Size classified by optical cross section with visible (white) light, 0.39-4.0 μm, but lowest and highest ranges somewhat suspect
Size resolved, fast response, optical number concentrations	LAS-X Laser Aerosol Spectro-meter, Particle Measurement Systems, Inc (1)	U of MN	Albuquerque, NM	30 sec sampling interval for any range, 2 minute cycling interval through 4 ranges (0.300 liters each)	Size classified by optical cross section at 632.8 nm, cycles through 4 ranges: 0.12-0.21 μm, 0.15-0.30 μm, 0.24-0.84 μm, 0.60-3.00 μm

Table 1: Instrumentation Used in Field Tests (cont'd)

QUANTITY MEASURED	INSTRUMENT (# DEPLOYED)	DEPLOYMENT		TYPICAL SAMPLE INTERVAL	COMMENTS
		GROUP	TESTS		
Carbon Monoxide Concentrations					
Time-resolved CO concentrations	CO Monitors, Langan Model L-15 (8)	Santa Fe Technologies;	All; (U of MN ran Albuquerque calibrations)	1 minute	Subject to amplifier drift, hence not reliable for ambient monitoring without repeated on-site calibrations; no real-time display caused several cases of improper set up to go unnoticed.
Time-resolved CO concentrations	Dasibi Environment Corp Model 3003 CO monitor (1) (supplied by NM Environ. Health Dept, c/o Steve Walker, Alonzo Archuleta)	U of MN	Albuquerque, NM	Approximately 5-10 seconds	Non-dispersive infrared analyzer, generally accurate, but intermittent bad ppm data recognizable by rapidly fluctuating high and low readings.
Traffic Conditions					
Time-resolved traffic count	Air-pulse type, usually with directional capability (number varied)	Santa Fe Technologies;	All Tests; MN: NM:	15 min resolution; 2 or 10 min res.	The traffic counts registered by the counters didn't always agree with counts recorded by video camera; no calibration was performed
Time-resolved traffic count, flow condition, and fleet composition	Video cameras (1 or 2)	U of MN	All	1 second	Distance scale of field of view was noted to enable speed check; camera clock was synchronized with data acquisition computers
Meteorological Conditions					
Time-resolved wind speed, horizontal wind direction, temperature, relative humidity	Davis Weather Monitor II and Weather Wizard III Met. Stations (1 ea)	U of MN	All	1 min. readout interval, humidity and temp. response times closer to 5 min.	Also records maximum wind gust during one minute interval
Positions					
Locations relative to road grid	GPS locator	Santa Fe Technologies;	All MN tests	Hand held instrument carried from point to point	Differential GPS locators would have given more precise locations

SIZE-RESOLVED PARTICLE CONCENTRATION INSTRUMENTS - The importance of the aerosol size distribution data is evident in the number of instruments listed in Table 1. The original intent was to use conventional MOUDI (Micro-Orifice Uniform Deposition Impactor) devices to characterize the time-averaged but size-resolved mass concentrations of the roadside aerosol. These devices essentially draw in a continuous flow of ambient air and direct it through a series of jets aimed directly at a set of impactor plates. The gas stream simply makes a sharp bend and flows around the impactor plates, but particles are relatively massive, and depending on their inertia, some of them will impact on the plate. If a very thin grease layer is applied to the plate, the particles will stick to the plate. There is a relatively sharp cutoff between particles which will impact out and those which will continue to follow the gas flow; the cutoff size can be controlled by controlling the characteristics of the gas jet. The size distribution can be measured by arranging a set of impactor plates in series with successively smaller cutoff sizes. The MOUDIs we used incorporated 8 impactor plates spanning 2 orders of magnitude in aerodynamic diameters (0.1-10 μm), with the bins spaced uniformly with respect to the logarithm of the diameters. In other words, the bins were 0.100-0.178, 0.178-0.316, 0.316-0.562, 0.562-1.00, 1.00-1.78, 1.78-3.16, 3.16-5.62, and 5.62-10.0 μm, respectively.

The MOUDI data was to be augmented by a time-resolved version of the same instrument: small quartz crystal oscillators were imbedded in the impactor plates and connected to a power supply. The resonant frequency of the crystals is a function of the mass of the crystal, including any particle layer on its surface. Thus, by recording the oscillation frequency of the crystals with a high resolution frequency counter, the particle mass accumulated over time could be measured. The derivative of the signal is related to the instantaneous particle mass concentration of the particles which impact on the crystal. While this can be calibrated fairly well in a laboratory setting, in a field experiment there are several difficulties associated with changing ambient temperatures and changing relative humidities. The former also causes the oscillation frequency of the crystals to drift, and the latter causes the particles collected under high relative humidity conditions in the morning to lose water vapor mass over a long time period as the relative humidity of the sampled air stream drops. While in theory these problems could be overcome with careful design and development, the tight time schedule of the events did not allow sufficient

development time between the first field test which identified the difficulties and subsequent test dates. Hence, the development effort was suspended.

Since the QCM data was not quantitatively reliable, commercially available particle counting devices were deployed during the Rosedale (Roseville, MN) and Albuquerque, NM events. These instruments were not employed at the outset because they measure particle number concentrations classified into various size bins rather than particle mass concentrations as specified in the ambient particulate matter regulations. Additional information on the effective particle material density is then required in order to arrive at a particle mass concentration. Moreover, several types of instruments which operate on different principles are commercially available, and these give somewhat different size distribution classifications. Moreover, often the instruments do not cover the full 0.1-10 μm range of the MOUDIs, and so several instruments would have to be deployed and their data combined. The cost associated with renting or buying the instruments listed for the entire testing period would have been quite high.

Nevertheless, the evaluation required some indication of the time history of the particle size distribution in order to analyze changes in the lidar signal. The Climet CI 226 white light optical particle counter and a TSI model 3310 Aerodynamic Particle Sizer (APS) were lent to us by the Particle Technology Laboratory at the University of Minnesota. They were deployed side-by-side with a single sampling inlet (10 ft elevation) at the Rosedale test. The same two instruments plus a Particle Measurement Systems LAS-X laser aerosol spectrometer (a size-resolved particle counter) were fielded in the Albuquerque tests. The size ranges covered by these instruments vary as indicated in Table 1, but together they essentially cover the desired 0.1-10 μm size range.

The APS instrument works on the principle that aerosol particles possess larger inertia than gas molecules, and hence they will lag behind gas velocities when a particle-laden flow undergoes acceleration. The APS takes an aerosol flow and accelerates it to a known velocity by passing it through a nozzle. It then measures the velocities of particles which pass through a small measurement volume and sorts them into various velocity bins. The velocity of the particle relative to the gas stream is an indication both of the drag force which results as the gas slips past the particle and the particle inertia. Hence, the particle size, morphology, and mass (and hence the effective particle material density, ρ_{eff}) all affect the measurement. Therefore, results are reported in terms of number concentrations and equivalent aerodynamic diameter (the diameter of

a spherical particle with a density of 1 g/cm^3 which would exhibit the same velocity when accelerated through the nozzle). Since the sampling interval and volumetric flow rate are known, the number of particles per unit volume which have aerodynamic diameters corresponding to a given bin width can be calculated. The characteristic physical diameter of a spherical particle with a homogeneous density of ρ_{eff} is related to the aerodynamic diameter according to $D = D_{AD}/\sqrt{\rho_{eff}}$, so one needs the effective density. (for details, see Hinds, 1982).

The Climet and LAS-X instruments are both optical particle counters that measure the amount of light scattered from individual particles. Particles are binned into size ranges according to the amount of light they scatter, and the bin counts in a given time period are converted to a number concentrations using the instrument flow rate. The LAS-X instrument uses a monochromatic light source at 632.8 nm (red helium-neon laser beam) and collects the scattered light over a fairly large range of forward angles, while the Climet uses white light (broadband continuous wavelength distribution in the visible region of the spectrum) and collects light scattered into a range of angles to one side of the particle. In either case, the amount of light received at the detector depends on the particle cross section relative to the light source and its effective refractive index in the illumination wavelength band. The former obviously depends on the characteristic physical size of the particle, but both can be influenced by the morphology and orientation of inhomogeneous, non-spherical particles. The important distinction is that the measurement is binned according to a characteristic optical size, which although related to a physical size for homogeneous spheres, can be a fairly sensitive function of morphology for inhomogeneous, non-spherical particles. Thus, large number counts should be obtained in all bins such that undersizing and oversizing errors associated with variations in morphology and orientation do not lead to biased particle counts. These counts should in general be similar to those measured by the APS provided proper calibrations are done, but they are in fact measuring slightly different things. None of these instruments actually gives particle mass concentration in a given size range without assuming a value for the effective particle density, ρ_{eff},.

The flow rates through these instruments were sufficient to record particle counts every 30 seconds, although the counts in the upper size bins (particles greater than 3 μm or so) exhibited significant statistical fluctuations because of poor counting statistics (less than 20 particles in a

sampling interval). The counts were obtained from a continuously flowing gas sample rather than by trapping bag samples and measuring the concentrations in the bags. The continuous count is analogous to the way the traffic count data is obtained, and simplifies the comparison of these data sets. In essence, continuous counts are running averages of the instantaneous rates averaged over the sampling interval; thus, they can be readily compared to the lidar data by taking a running average of the lidar data over the same sampling interval.

Each of the particle counting instruments (optical and aerodynamic) has some advantages and disadvantages when used to measure atmospheric aerosols; we list several of the important ones here, but many more can be found in the literature (Cheng *et al.*, 1990; Hering and McMurry, 1991; Stein *et al.*, 1994; Lilienfeld, 1996).

CO CONCENTRATION MEASUREMENTS - Trace gases in the atmosphere are generally detected by optical or electro-chemical effects. The Langan L15 CO samplers monitor the electro-chemical current of the following reaction:

$$2\,CO + 2\,H_2O \Rightarrow 2\,CO_2 + 4\,H^+ + 4\,e^- \qquad (1)$$

to measure the CO concentration. This reaction is followed by oxidation to water

$$O_2 + 4\,H^+ + 4\,e^- \Rightarrow 2\,H_2O \qquad (2)$$

to complete the circuit. Since CO is present at the PPM (parts per million) level in typical urban environments, water vapor and oxygen are always available in excess within the sampled air and do not need to be externally supplied. Other trace gases can undergo similar electro-chemical reactions, but their interference can be minimized by proper choice of filters and electrodes.

The Langan monitors were selected by Santa Fe Technologies as one of the few portable instruments with built-in data loggers and time response capabilities of a minute. They had also been used in previous tests by the California Air Resources Board for atmospheric monitoring. The L15 was designed to be operated as a stand alone unit powered by a small battery pack. Therefore, they had relatively low sample flow rates, and hence were measuring fairly small currents from the electro-chemical reaction. Because of this, two key limitations arose: 1) the

least significant bit uncertainty arising from the amplifiers and digitizing circuits corresponded to ±0.5 ppm of CO; and 2) variations in ambient temperature and humidity during the day caused the amplifier gains and offsets to drift, such that absolute concentration measurements required calibration points to be taken throughout the day.

The instrument sensitivity was insufficient for the majority of the conditions we encountered, as roadside CO levels were most often below 3 ppm. We attempted to reduce the uncertainty by asking that pairs of detectors be mounted side-by-side. If the monitors were properly set up and functioning with fully-charged battery packs, the CO levels recorded by each monitor in the pair generally showed good agreement. However, since ambient CO concentrations are known to exhibit hot spots, the need to operate the instruments in pairs reduced the probability of monitoring a hot location downwind of a roadway and within the field of view of the lidar, as well as our ability to monitor background conditions. The former was necessary to determine the strength of the correlation between the lidar signal and roadway-generated CO and particulate concentrations, while the latter was used to check the background conditions. The background correlation was tested in order to indicate the significance of the downwind correlation; one would expect to see different correlations between aerosol lidar signals and CO levels upwind and downwind of roadways because the relations between the particle and CO concentrations would supposedly be substantially different in these two regions.

The latter calibration procedure, although suggested, was not performed by Santa Fe either during the Minnesota field tests or in subsequent laboratory tests. Response calibration data was taken by the evaluation team during the Albuquerque test, and showed significant variation through the course of each day. Such response drifts render the CO data from the Langan monitors useful only as qualitative indicators of CO concentrations over relatively short time periods. This was a significant disappointment with regard to the goals of the operational test, and the choice of CO monitors would have to be re-examined and tested prior to future tests.

INSTRUMENT CALIBRATION - The ideal way to perform instrument calibrations for field tests is to perform periodic on-the-spot calibrations interspersed with actual data collection efforts. The logic behind field calibrations is not only to measure the response under actual field sampling conditions, but also to monitor the calibration in case changes occur for some reason during the field test, for example due to amplifier drifts associated with changes in ambient

temperature. If such response changes occur, the calibration data points indicate how much and when the responses shift, and enable correction factors to be applied to the data. Often however, either because of the amount of instrumentation and/or time required to obtain accurate calibrations, such calibrations are not always possible. In such cases, before and after response calibrations are the next best thing, preferably done over a range of conditions similar to the actual sampling conditions.

The amount of instrumentation and time required to obtain periodic size-resolved particle concentration calibrations would have meant that significant blocks of time would have been consumed during the field tests. The responses of the particle sizing instruments (APS, Climet, and LAS-X) were thus calibrated against each other in laboratory tests taken before and after the field tests. The calibrations were done by generating aerosols containing monodisperse (*i.e.* single size) polystyrene latex (PSL) particles of known diameter and having all instruments sample from the same flow. We never observed any changes in the before and after responses, so we assumed that no response degradations had occurred during any of the tests. And since there were several instruments monitoring the same size range, any drift in the responses of the instruments associated with changes in the ambient conditions would likely show up as differences in the measured concentrations recorded by the various instruments.

By comparison, it is relatively simple to monitor the responses of gas concentration monitoring equipment by periodically sampling from a gas stream which contains a known concentration of the desired gas. Calibrations with gas concentrations near zero and near the maximum levels to be encountered in the test are useful for determining instrument offset and gain as a function of time during the test. These are referred to as zero and span calibrations, respectively. Periodic zero and span calibrations of the Langan CO monitors were taken by the evaluation team during the Albuquerque test, and an additional EPA-approved monitor supplied by the New Mexico Environmental Health Dept. was fielded for comparison. The results indicated substantial drift in the zero concentration offset of the Langan monitors as the ambient temperature changed from around 60 °F in the early morning to over 100 °F in the afternoon. Since such calibration data was not taken during the Minnesota tests, then the uncorrected Minnesota data should be viewed only as an indication of changes in CO concentrations over relatively short time periods, but not as quantitatively accurate CO concentrations. We did not

feel that it was appropriate to apply response correction factors which could have been derived from the Albuquerque data to the Minnesota tests because a significant amount of time elapsed between these tests, and because the setups of all of the CO monitors were checked and adjusted just prior to the Albuquerque tests.

METEOROLOGICAL DATA - Davis model 7440 weather monitoring instruments were deployed on the instrument platforms. These included sensors which recorded horizontal wind speed and direction, temperature, and relative humidity (RH). It was decided that a single RH measurement should suffice because of the proximity of the sampling sites. The vertical component of the wind speed was not measured because budgetary constraints did not allow us to purchase three component anemometers. LANL brought along a 3-D Sonic Anemometer for the Rosedale event, but it did not work under the cold ambient temperature (20^{o}F) conditions. The 3-D Sonic Anemometer was also deployed during the Albuquerque test, but the data was never made available to the evaluation team. Regional weather data for the event days was also obtained from local meteorological offices.

Linkage with PTMS Test Sites

The lidar project was originally envisioned in connection with a second ITS operational test of MN-DoT's Portable Traffic Management System (PTMS). The PTMS is designed to be taken to local special events which are expected to draw significant vehicle traffic into areas where the roadways are not designed to handle such a load. The PTMS operators can monitor traffic conditions in real-time and make adjustments in traffic control strategies to prevent or alleviate congestion. The idea of coupling the two projects arose primarily from the desire of FHWA and MN-DoT to ascertain whether traffic control strategies designed to relieve vehicle congestion had a positive impact on air quality in a region, or simply moved a region of relatively high pollutant concentrations (hot spot) from one location to another. In order to evaluate the impact of expected changes in traffic flow, one had to be able to monitor relatively wide areas rather than just a few points. Hence, the lidar project. The idea was to utilize the wide-area capabilities of the lidar to evaluate the impact that changes in traffic conditions had on local air quality.

Several difficulties arose from this linkage. First and foremost, before we could use the lidar system to evaluate the impact of the PTMS, we had to establish the quantitative accuracy of the

lidar signal. This was indeed the primary goal of the lidar project. The best way to accomplish this goal would have been to set up the lidar system at a single site and monitor the lidar signal along with the variables described above under a wide variety of conditions. This would have enabled us to work out the optimum location for line-of-site access to locations of interest identified by both the lidar and traffic data. In fact, the original test plan called for most of the tests to be carried out during events at the National Sports Center (NSC) in Blaine, MN.

Unfortunately, several of the events at the NSC were either canceled by the NSC management or predicted by the PTMS team to have insufficient traffic volume to allow adequate testing of the PTMS effectiveness. Thus, only one event of the three which were originally scheduled was actually conducted at the NSC. This meant that other test events had to be added to enable both the PTMS and the lidar systems to be evaluated. Events and sites were selected by personnel from Castle Rock Consultants (the PTMS evaluators) based on historical traffic data which had indicated congestion. They chose to conduct tests at four different sites (see maps in App. B), and the timing between several of the events was quite tight (see Table 2). From the PTMS standpoint, multiple sites would enable the portability and versatility of the PTMS to be evaluated. Unfortunately, the variation in sites meant that some of the parameters which could influence the correlation between the lidar signal and the particle concentrations would change, thereby increasing the complexity of the statistical analysis. In addition, the needs for eye-safe line-of-sight access between the lidar and point sampling instruments and time to reduce previous data sets prior to new tests were not priority concerns. The net result was that the variation in test sites and the changing schedule greatly increased the difficulty of the lidar evaluation.

TABLE 2: LIST OF PTMS + LIDAR EVENTS

Event and Site	Lidar Test Dates	PTMS Test Date(s)	Event Date(s)	Comments
Drum and Bugle Corps Contest, National Sports Center, Blaine, MN	July 25-26, 1994	July 26, 1994	July 26, 1994	Traffic congestion was minimal; lidar beam elevated above sampling sites due to access restrictions.
Burnet Senior Classic PGA Golf Tournament, Bunker Hills Golf Course, Coon Rapids, MN	Aug. 17-22, 1994	Aug. 19-21, 1994	Aug. 18-21, 1994	Lidar beam was slightly elevated above sampling inlets due to concern for eye safety; lidar system was down most of the day on 8/17; good 2-D and 3-D data sets. Aerosol plume from unpaved overflow parking lot dominated much of the time, but traffic flow impacts were observed.
Minnesota State Fair, St. Paul, MN	Aug. 24-27, 1994	Aug. 25-28, 1994	Aug. 25-Sept. 4, 1994	Generally windy conditions; Lidar was down 8/25 after wind toppled system overnight, sampling instrument platform actually blown down by gust on 8/27.
Post-Thanksgiving weekend shopping rush, Rosedale Shopping Center, Roseville, MN	Nov. 23, 25, 1994	Nov. 25-26, 1994	Nov. 25-26, 1994	Lidar not operational most of first day due to cold temperatures. Line-of-sight access restrictions meant beam was very high. No aerosol lidar signal was observed.

Lidar and Sampling Instrument Placement and Operation

The locations of the lidar system and point sampling instruments were determined by the goals of the test: to evaluate the correlation between the lidar signal and local pollutant concentrations, and to analyze the impact of various traffic conditions and traffic control strategies on air quality. To address the latter goal, the lidar system was located as high as possible during the Minnesota tests to provide an elevated vantage point and minimize the number of viewing directions which were blocked by trees, buildings, or power lines. To address the former goal, we needed to have time-resolved particle concentration data at points as near as possible to the lidar beam path in order to minimize the impact of spatial variations in the particle and wind fields. During any single test, we could monitor pollutant concentrations and the associated meteorological data at most two points; more points would have required more instruments, more operators, and further increased the already large volume of data. The two point scenario was a compromise to stay within budgetary constraints while providing some idea

of the spatial variability of the lidar correlation. Locations of the lidar and sampling sites are indicated on the maps in App. B.

Since the comparison data was gathered by point sampling instruments at only one or two points in space, it was critical that the lidar beam pass as close as possible to the sampling instruments; the further the separation between the lidar beam and the sampling location(s), the more likely it would be that spatial variations in the sampled data would degrade the correlations between the lidar signal and the other data sets. Thus, the lidar beam had to pass almost directly over the instrument inlets. This implies not only line of sight access, but also that the beam path be known with an accuracy of a few feet. The beam could not envelop the inlets, lest the inlet tubes themselves reflect a signal back to the detector and partially obscure measurements farther along the beam path. Nor was it desirable to have the beam pass several feet above the inlets, as different heights could allow larger particles to settle, thereby creating a difference between the size distribution viewed by the lidar and that sampled by the aerosol instruments. Hence, since characteristic dimensions associated with the wind and particle fields were expected to be of the order of 10 ft, the center of the beam had to pass somewhere within about 4 to 8 feet from the inlets. The spacings given allow for beam diameters of several feet at the inlets without generating false return signals or having part of the measurement volume extend beyond the 10 ft limit. The single-reading GPS locators could not be counted on for such accuracy, although differential GPS techniques would have worked. Instead, the beam path had to be determined by "pinging" the beam of an object with a known height and location.

MINNESOTA TESTS - Gaining line of sight access to the sampling inlets turned out to be the biggest limitation to the Minnesota tests, primarily because sites and wide-area viewing requirements were dictated by the simultaneous PTMS test, but also because eye safety issues restricted where the beam could strike the ground. The lidar system in this experiment employed a Nd:YAG laser which operated at a wavelength of 1.06 μm. This near infrared wavelength is not visible, but the beam intensity was high enough that eye damage could occur if one were to stare directly into the beam from a distance of less than about 1.2 km. For added safety, the eye-safe viewing distance was taken to be 2 km or greater. However, this specification applies to the unaided eye. Since we could not guarantee that individuals traveling to the National Sports

Center (or other sites) would not be curious enough to look back at the lidar system with binoculars, we did not allow the lidar beam to strike the ground within 5 km of the laser.

Lest the eye safety issue be misinterpreted, we must point out here that the hazard was associated with the lidar system which was tested, not lidar systems in general. It should be possible to address the eye safety issue by using a larger beam telescope to further expand the beam and thereby reduce its intensity to a very safe level. Because the larger beam would have an even smaller divergence angle, the increased beam size should not affect the spatial resolution of the lidar beam. In fact, the larger telescope would in fact increase the amount of scattered light which was collected, thereby increasing the system range. We therefore recommend that such a modification be available for use in future lidar systems applied to ground-level measurements.

Hence, during the Minnesota tests, the beam height was kept at least 20 feet above the ground for distances of at least 5 km. In many directions, the height was even higher due to obstructions caused by trees, buildings, or telephone/power lines. Since the locations of the point sampling instruments were most often less than 5 km from the lidar unit (see maps in App. B), the instruments were elevated to heights of 24 ft in order to minimize the distance between the lidar beam and the sampling inlets. Although this is well above the height desired for ambient pollutant monitoring, the need to minimize the possibility of spatial variations masking actual correlations outweighed the desire to obtain measurements at standard monitoring heights.

The 24 ft sampling height simply reflected the maximum height of the portable lift platforms which were available from local rental agencies. These lifts were chosen because they had reasonably small footprints so that they could be readily positioned alongside roadways. We chose the maximum height in anticipation that in some cases we would not be able to reach the beam, and we did not want a variable sampling height to add yet another consideration to the analysis of the measured pollutant concentrations. Somewhat higher elevations yet would have been desirable to get closer to the beam at all sampling sites, but the stability of the moderate footprint platforms in wind gusts was a limiting factor. In fact, one of the platforms actually blew down during a gust which occurred during the Minnesota State Fair test. Fortunately, the direction which the platform fell missed the operators, the data acquisition equipment, and the roadway, and even more amazingly, all of the equipment survived the fall.

As indicated earlier, the sensitivity of the Langan CO monitors was about 0.5 ppm. Unfortunately, at 24 ft elevations, the CO concentrations as recorded by the monitors were often near this limit. To reduce statistical scatter, the CO monitors were mounted in pairs on the instrument platforms. Even this failed to improve the data quality to an acceptable level. The instrument pairs were lowered to 8 ft elevations for the Rosedale and Albuquerque events, with somewhat higher concentrations recorded, but with accuracy concerns as indicated in the previous section.

ALBUQUERQUE TEST - Primarily because the need for near coincidence of the lidar beam and sampling inlets was not always satisfied in the Minnesota tests, an additional test was conducted in Albuquerque, NM. The sole purpose of this test was to characterize the lidar signal response at a single point which was located at the same elevation and within 10 feet of the sampling inlets. In this test, several time-resolved particle concentration instruments (APS, Climet, and LAS-X) drew samples from a single inlet pipe which was open to the atmosphere at a height of 10 ft. The size distributions and concentrations measured by the instruments were calibrated using polystyrene latex particles in a laboratory setup. These calibrations were done the day before the field tests and again the day after (before the instruments were.shipped) to check for any changes during the tests. No significant changes were found.

The Langan CO monitors were carefully set up prior to the test and checked with zero and span calibration gases (0 ppm and 20 ppm CO, respectively). In addition, the span gases were used to periodically calibrate the monitor responses during the field test.. The zero and span calibration points showed that significant drifts in the zero concentration offset of the Langan monitors were present, most likely related to changes in temperature during the day. The calibration points provided a means to correct for the drifts. An EPA-certified CO monitor supplied by the local air quality office was also used as a check; it too, was periodically calibrated with the zero and span gases.

Traffic counters with two minute resolution were placed on the main thoroughfare (Gibson Blvd.) in front of the sensors, with additional counters with 10 minute resolution placed on the less active nearby side street (Girard Ave.). The rest of the traffic video and weather monitoring instrumentation was positioned and operated as in the Minnesota tests.

Data Display

IBM was the subcontractor responsible for displaying the all of the data sets superimposed on a grid of the local road map. An IBM RISC-6000 workstation running IBM's Data Exploration (DX) Software package was used to render the lidar images, area maps, point sensor pollutant data, and traffic data. An SGI Indigo 2ZX housed at the University of Minnesota was used for corroborative image exploration and some data analysis. The IBM software is designed to run under IBM's AIX operating system; it was possible to get it to run on the SGI machine running the Berkeley UNIX operating system, but some of the driver programs had to be special versions supplied by IBM.

Most of the analysis reported in the results section was done on the original point-sampled data sets together with the time history of the lidar signal at a single point near the sensors rather than using values from the displayed images. This was done to avoid introducing additional uncertainty associated with the image display interpolation algorithms. (The interpolation algorithms are needed because the lidar image data actually consists of time histories of the signals from many individual points in space; the interpolation algorithms are essentially curve-fitting routines which allow a smooth, continuous image to be drawn in based upon the point values from the lidar data sets.)

Test Participants and Responsibilities

We would like to close this section by listing the personnel involved and their responsibilities for deploying the instruments and supplying the data for the evaluation. The project was directed by the MN-DoT / Minnesota Guidestar office headed by James Wright, with Michael A. Manore responsible for the project management. Santa Fe Technologies, Inc. (SFT) was the prime contractor responsible for carrying out the operational test. Howard Kraye directed the project team. SFT personnel were responsible for operating the Langan L15 CO monitors, time integrated PM-10 monitors, traffic counters, and the GPS locator. Lisa Albright, Thomas Albright, Dishayne Garcia, John McClenahan, Joe Stone and Don Weddle assisted Howard Kraye in the data collection effort. Additional time-averaged total particulate and CO concentrations were to have been collected using saturation monitors supplied by the U.S. EPA, but the data was not reliable when compared to other instruments. The cause was most likely the lack of training

of SFT personnel for operating the instruments, and the effort was dropped from all but the first test at the National Sports Center. The lidar system was operated by Los Alamos National Laboratory personnel under a subcontract with SFT. Dr. Bill Eichinger was the chief lidar scientist, with assistance from Larry Tellier and Dan Cooper. IBM was a subcontractor responsible for data display. Ken M. Pascutoi was the client representative, but Dr. Nancy Collins bore the lions' share of the work for importing the data sets into IBM's Data Explorer visualization software package and for developing additional algorithms for displaying the data sets on top of the GIS maps. Dr. Chris Doehlert also provided some assistance during the early stages of the project, and Randy Evans of SFT provided some assistance during the latter stages.

The University of Minnesota (U of MN) was responsible for obtaining the particulate matter, meteorological, and traffic video data. The MOUDI and QCM instruments were operated by Phil Dieck and Bernard Olson, with assistance from Brian Gabrios and Mike Witzmann. Their efforts were directed by Prof. Marple and Dr. Ken Rubow of the Particle Technology Laboratory, with additional supervision from Prof. Hofeldt. The time-resolved particle instruments were operated by Bernard Olson, Imad Abdul-Khalek, and Prof. Hofeldt, with assistance from Phil Dieck, Wilson Poone, and Jeremy Ames. The Davis weather monitoring instruments were operated by Sumantra Chakravarty. Some area-wide weather data was obtained from the Minnesota Weather Access System (MnWAS) by MN-DoT. Traffic conditions at the sampling sites were recorded on videotape by members of the U of MN team. Some additional traffic data was obtained by the PTMS evaluation and was provided by Robert H. Bamford of Castle Rock Consultants, with assistance from Marthand Nookala of Minnesota Guidestar.

As outlined above, various test participants were responsible for collecting and formatting the raw data sets, but the data analysis was performed by the U of MN evaluation team. Prof. David L. Hofeldt was the principal evaluator, with assistance from Sumantra Chakravarty. A minor exception regarding the data analysis was that Bill Eichinger of Los Alamos performed some initial pre-processing of the lidar data to minimize the effect of atmospheric extinction.

RESULTS AND DISCUSSION

Major results of the individual tests are summarized here according to the chronological order of the tests. More details on the Minnesota tests can be found in the various milestone reports filed with Minnesota Guidestar / MN-DoT shortly following the test periods (Chakravarty and Hofeldt, 1994a, 1994b, and 1995a). Since the Albuquerque test took place at the very end of the contract period, this is the only document which includes data from that test. Most of the evaluation of the quantitative relationship between the lidar signal and the ambient particulate concentrations is based upon the results of the Albuquerque test. Several representative images obtained during the Bunker Hills test are included and discussed to illustrate the usefulness of the temporal and spatial information available from the lidar data.

National Sport Center, Blaine, MN

The first test was conducted at the National Sports Center (NSC) on Monday, July 25, and Tuesday, July 26, 1994. The first day was a non-event day, meaning that no special events were occurring at the Sports Center that day, and PTMS was not in operation. This day was included in order to establish the normal traffic levels and patterns associated with the area. It took roughly two-thirds of the day Monday to set up all of the instrumentation and obtain the GPS point measurements. Two sampling stations were chosen based on recommendations from the PTMS team as to where traffic congestion was likely to occur (see Fig. B2 in App. B). One sampling station was located alongside the four-lane artery (Trunk Highway 65, speed limit 45 mph) leading past the Center. The lidar system was located about 3 km south of this sampling station on an unused overpass over Hwy. 65. Highway 65 is very straight in this region, so that the lidar beam could be directed almost straight down the roadway. The other sampling station was located between 1 and 2 km to the west, along a secondary access route to the Center (Radisson Rd.).

Mass distribution data from the MOUDIs can be found in App. C, grouped together with data from other tests for ease of comparison. Table 3 summarizes some of the main observations of the NSC test and the recommendations made by the evaluation team for subsequent tests.

Table 3: Observations and Recommendations from NSC Test

OBSERVATION	RECOMMENDATION
The lidar beam passed well above the inlets to the sampling instruments at both sampling stations because of obstructions caused by power lines over the road and the sports center structure itself.	Line-of-sight access to the sampling inlets had to be verified by "pinging" the lidar beam off the sampling instrument towers to verify beam location.
Two-dimensional lidar images showed what appeared to be hot spots located along Hwy. 65 coincident with the locations of stoplights.	Enough single point correlation data had to be taken over the sampling inlets interspersed with two- and three-dimensional image sets to enable statistical correlations between the lidar and point data to be established.
Traffic levels were significantly lower than expected. No significant traffic congestion occurred around the Sports Center either prior to or after the event.	No recommendation made.
The MOUDI instruments showed that the mass concentration of particles with aerodynamic diameters less than 10 μm was less than 40 $\mu g/m^3$. We had expected higher levels alongside roadways due to entrainment of road dust into the wakes of moving vehicles.	The instruments should be located downwind of roadways if possible to increase the observed mass concentrations and improve accuracy.
Several of the EPA saturation monitors failed to operate, and those that did had been supplied with fiberglass particulate filters. The particulate mass concentration data was considered unreliable because several filters indicated negative mass change values, most likely because of loss of filter substrate material incurred during filter handling.	Proper operation of the saturation monitors needs to be verified prior to use, and Santa Fe personnel must familiarize themselves with details of use. Location and operation should be checked with qualified EPA or local air quality agencies. Teflon filters should be used to collect the particulate matter to increase accuracy.
Five of the eight Langan CO monitors either did not function properly or produced inaccurate data. Some of the malfunctions were later linked to improper setup by Santa Fe personnel. Those instruments that did read what appeared to be reasonable concentration levels showed values near the resolution limit of the instruments.	The instruments should be checked for proper operation prior to the field tests. They should be located in pairs and downwind of roadways if possible to increase the observed concentrations and provide improved accuracy.
	The data should be imported into the rendering software as soon as possible to enable the spatial relationships to be checked.

Some of the issues raised in this initial set of recommendations were never completely resolved by the various participants responsible, and continued to cause difficulties for the evaluation during subsequent tests.

Bunker Hills Golf Course, Coon Rapids, MN

The second operational test was conducted Aug. 17-22 adjacent to the Bunker Hills Golf Course in Coon Rapids, MN. The Burnet Senior Classic Golf Tournament (a scheduled event on the PGA Senior Tour) is held annually at the course, and draws significant crowds of spectators to the course. The tournament was held Thursday-Sunday, Aug. 18-21. Data was to be gathered on Wed., Aug. 17, before the event started, and on Thursday, the first event day, without the PTMS in operation. These data sets were meant to establish the baseline pollutant and traffic levels in the area without and with an event, respectively, and without PTMS control. Unfortunately, the laser power supply on the lidar system broke down during shipment from Los Alamos, and the lidar system did not come on line until the 18th. The test date on Monday, Aug. 22 was added to compensate for the missing baseline data.

The lidar system and the two sampling stations were located roughly in line at three positions along the east side of Hanson Blvd. (see Fig. B3, App. B). The lidar system was farthest north, roughly 3 km north of Trunk Hwy 242, a major east-west arterial through the region (speed limit 55 mph). One sampling station was roughly 2 km south of the lidar and 1 km north of the intersection with TH 242, where Hanson Blvd is a two-lane road with a 35 mph speed limit. Access to the overflow parking lot at the golf course lay between the lidar system and the north sampling station. The other sampling station was located just a few hundred feet south of the intersection with TH 242, where Hanson Blvd is a 4 lane thoroughfare with a 45 mph speed limit. The wind during this time of the year in Minnesota is generally out of the west or northwest, hence the choice of sampling locations on the east side (expected downwind side) of Hanson Blvd. The lidar system was elevated to a height of about 40 ft using a portable man-capable scissors lift. The particle instrumentation included two MOUDIs and one quartz crystal MOUDI designed to obtain time-resolved particle measurements. EPA saturation monitors were not deployed since Santa Fe personnel were not trained to obtain accurate data. The MOUDIs were elevated on lifts to 24 ft heights as previously described. Because of trees along the roadway and undulations in the local terrain, the lidar beam was once again somewhat higher than the sampling inlet heights (estimated at 20 ft above the north station an 30-40 ft above the south).

Large capacity high voltage power lines ran along the west side of Hanson Blvd and crossed the road just south of the southernmost sampling station, where Hanson Blvd. takes a jog

to the south-southwest. The large towers limited the field-of-view "upwind" of Hanson Blvd., effectively preventing the acquisition of a clear picture of the background conditions in the area without influence from the roadway. The main golf course parking lot lay roughly parallel to Hanson Blvd but slightly under 1 km to the east. The overflow lot was located in a grass field which extended off the main lot all the way over to Hanson Blvd. When present, vehicle activity in the unpaved overflow lot kicked up a significant aerosol plume which was convected downwind from that point. In addition, a condominium development project was under construction at the northeast corner of Hanson Blvd. and TH 242, and a fairly large area of soil was exposed due to prior landscaping work. Some equipment was operating in the area on Thursday and Friday, but we were somewhat surprised that the area did not appear to be a major dust source during our tests.

The previous description was given in a effort to provide some background for interpreting the lidar images which follow. As was indicated in earlier sections, the principle advantage of the lidar system is its ability to record image sequences of spatially-resolved aerosol plumes as they develop and disperse over distance and time. Knowledge of the spatial and temporal characteristics of the aerosol concentrations is the first step in formulating effective controls. With image records, not only can one judge the relative strengths of different aerosol sources and assess their extent, but one can also identify conditions leading up to high concentration events. Moreover, locations which show representative "average" concentration histories such as might be experienced by individuals in the region can be identified. The former are useful for deciding where controls are needed and what controls might work best, whereas the latter is needed for monitoring regional air quality and assessing exposure levels.

Because of the multiple potential aerosol sources described above, the Bunker Hills site provided an excellent opportunity to demonstrate the benefit of having such wide area images. And since the beam elevation had to be higher than the inlets anyway, a greater emphasis was placed on the acquisition of two- and three-dimensional image sets. The remainder of this section gives a detailed analysis of some of the images obtained, while Table 4 is intended to provide a brief summary of the results. MOUDI data is again given in App. C.

Figures 4 and 5 (located at the end of this section) illustrate how "hot spot" areas and/or times can be identified and associated with particular aerosol sources and wind patterns. The

figures show relative aerosol concentrations in a particular two-dimensional vertical slice at two different instants in time. These lidar images were taken during the early evening on Saturday, August 20, 1994, looking south down Hanson Blvd. near the Bunker Hills Golf Course in Coon Rapids, Minnesota, as people gradually filtered away from the golf tournament. The images were superimposed over the local road grid and displayed with the proper distance scale, orientation, and perspective using the Data Explorer software package. The various colors represent different lidar return signals, and the legends indicate major roads in the local road grid, the distance scale, and the wind velocity and direction at the two different instances. The structure shown is interpolated from the high resolution, two-dimensional lidar data points by the software.

Table 4: Summary of Observations and Findings from Bunker Hills Test

OBSERVATION	CONCLUSION
When observed, hot spots are often observed near intersections.	Concentrations of vehicles and vehicle accelerations produce significant levels of aerosol particles.
Even with similar traffic levels and wind conditions, the distribution and magnitude of aerosol plumes above intersections can vary dramatically with respect to the phase of the image relative to the period of the signal lights.	The vehicle exhausts and thermal plumes generated by vehicle acceleration transients combined with relatively low vehicle wake turbulence associated with low speeds can lead to the observation of relatively concentrated plumes above intersections. By contrast, lower vehicle loads and higher wake turbulence associated with free flowing traffic conditions lead to relatively dispersed plumes and lower aerosol concentrations.
Lidar technology is capable of observing changes in aerosol concentrations associated with different traffic flow conditions.	Changes in aerosol concentrations due to some combination of increased vehicle emissions, increased roadway dust entrainment, and decreased dispersion cause an easily observed change in signal, but additional measurement techniques would be needed to assess which factor is most important.
A larger number of lidar images taken over the roadway would have helped us to better identify the relative importance of wind, traffic volume, and traffic flow conditions.	Since real-time display of the images was not part of the lidar system, the scan sequence couldn't really be optimized on-line to examine particular details observed within the lidar field-of-view. Real-time display would increase the analytical usefulness of the technology.
Absolute locations of the lidar images were most easily established by linking stationary objects to the stationary return signals.	The GPS data is useful for getting approximate locations, but differential GPS or pinging measurements must be included to establish accurate positions.

We should note that high resolution lidar scans of the angular extent shown here require on the order of a minute to acquire. Hence, the images are not really one-minute exposure snapshots, but rather represent an entire series of adjacent rays, each acquired with a relatively short exposure time (about one second). The figures thus are analogous to the persistent image one would see as a radar image was swept out on a screen, albeit with a fairly slow scan rate associated with very high spatial resolution. The aerosol concentration contours can be blurred out somewhat due to motion of the plume during the image sweep period, but the effect is not generally significant under typical combinations of wind speed and spatial resolution.

The bottom-most ray of the slices shown was located roughly 30-50 feet above the roadway; the exact elevation varies slightly due to gentle undulations in the terrain (they aren't

really steep enough or tall enough to be called hills). This elevation was chosen so that the bottom-most ray clears trees which line Hanson Blvd. south of 242. The images show vertically oriented cross-sections through the aerosol plume generated by vehicle traffic down Hanson Blvd.: the vehicle motions and exhausts create turbulent air currents which entrain and lift particles from the roadway, where they are in turn picked up and dispersed by the wind. In these images, a light breeze was blowing nominally out of the north-north-east, almost parallel to the road but just slightly across it. The wind carried the aerosol plume generated by vehicles through the vertically oriented slice. Since vehicle traffic along Hanson Blvd. is the aerosol source, the size distribution and composition of the particulate matter is probably fairly constant throughout the field-of-view of the images, and hence the images can be interpreted as color-coded contour maps of the relative aerosol concentrations at the two instances.

The hot spots visible in the images occur 1) near the intersection of Hanson Blvd. and TH 242, 2) at the bend in Hanson Blvd. which brings it underneath the lidar slice, and 3) where the unlabelled cross-street (Northdale Blvd, *a.k.a.* Cty. Rd. 11) cuts under the lidar slice. The difference in the aerosol distributions in the images is quite remarkable; yet if one examines the traffic counts for the 15 minute intervals containing the lidar "exposures", one finds that the count for the period surrounding the 17:34:40 image is in fact slightly higher than that for the 18:24:48 image, as one might anticipate from the tournament schedule. The slight difference in the wind heading and magnitude between the two image times would cause some of the roadway-generated aerosol to be carried underneath the lidar slice in the 17:34:40 image, but probably would not account for the differences observed. Upon examination of the videotapes of the traffic flow recorded at the two different instances, it was found that the traffic light at the intersection of 242 and Hanson Blvd. changed from red to green just prior to the latter exposure allowing for a slight time delay for aerosol transport from the roadway to the elevation of the lidar image. We concluded that the difference in traffic flow conditions must have been the primary cause of the difference in the observed aerosol concentrations. It is likely that the higher vehicle loads produced during acceleration transients create fairly strong vehicle exhaust jets with significant thermal buoyancy. And since the vehicle speeds are fairly low under such conditions, the penetration of the exhaust jets should increase while the turbulence levels associated with the vehicle wakes decreases. It is not clear whether increased vehicle emissions of sub-micron

particles during acceleration transients, actually contribute to the increased lidar signal. Recalling that the lidar is most sensitive to particles in the 1-5 mm range, the increase in small particles would have to be sufficient to overcome the signal due to roadway dust, the entrainment of which may also be increased under these conditions. What is clear is that the low vehicles speeds appear to be accompanied by reduced dispersion, and the thermal buoyancy of the plumes appears capable of carrying the particulate matter to fairly high elevations under low wind conditions.

The dependence on traffic flow described above could have been investigated by acquiring a continuous sequence of similar images and looking for repeatable patterns which occurred with roughly the same interval as the stoplight period. Unfortunately, since the lidar system did not have the capability to display the images in real-time as they were being acquired, the strength and location of the hot spots was not known until April of 1995, when the images were properly oriented with the road grid in the Data Explorer software. Thus, there was no feedback during the test or prior to subsequent tests which would have shown the benefit from such a repeated sequence of such images, so most of the data sets are part of 3-D scans or point data sets for correlation with sampling instruments.

Two key findings arise from these observations:

1) The image sequence demonstrates the ability of the lidar system to resolve impacts of changing traffic conditions on local air quality, and hence with a large enough set of images, one should be able to analyze the impact of various traffic control strategies.
2) Real-time display of the lidar images, preferably superimposed over the roadway grid, should be developed for subsequent use with the lidar system. Display during acquisition would enable the lidar users to quickly analyze the images with respect to observed traffic and weather conditions and select the type and location of scan which would provide the most useful information.

The slices shown in Figures 4 and 5 were themselves part of a sequence of similar 2-D slices which, taken together, map out the three-dimensional distribution of the aerosol concentration in the region. Figures 6 and 7 (again inserted at end of this section) show how such slices can be put together by the rendering software to depict the 3-D distribution. Figure 6 highlights several vertical slices which were combined to make the 3-D scan. The highlighted slices are not adjacent slices; several additional 2-D slices exist in between the highlighted ones, but are not emphasized to maintain image clarity. Recalling that each high resolution 2-D slice takes on the order of 1-2 minutes to acquire, one realizes that the highlighted slices will be

separated in time by several minutes, and that a 3-D scan with reasonable horizontal resolution might require on the order of 15 minutes to acquire. The software can interpolate a continuous three-dimensional contour between the 2-D slices, and in fact, Fig. 7 highlights the horizontal plane of such an interpolated volume. However, one must be careful when interpreting such 3-D images, because different sections were obtained at different points in time: highlighting the horizontal plane of an interpolated 3-D image as is done in Fig. 7 leaves the impression that the data was acquired by scanning in a horizontal plane. While the lidar system could have been programmed to scan the 3-D volume by taking a series of relatively short duration, nominally horizontal scans, in fact, the data was taken as a sequence of vertical slices. Thus, the assumption of a relatively short horizontal scan implied by Fig. 7 may lead erroneous interpretation since the data in different parts of the horizontal plane were actually taken at different points in time. This example is included only to illustrate that the image processing and display algorithms employed are important to the interpretation of the image, and hence their effects must be properly understood when they are used.

The main difficulty in analyzing the images described above was a relatively long delay in obtaining them superimposed over the GIS road map in the DX format. The delay developed because some preliminary file conversion steps were necessary to prepare the lidar image files for importation into DX. Originally, this file conversion was handled by Randy Evans at Santa Fe Technologies, but the responsibility was eventually transferred to Nancy Collins at IBM when difficulties arose. When the DX images did become available, a small angular error appeared to exist between the coordinate frame used to aim the lidar system during the test and the coordinate frame associated with the GIS road map and GPS data points. The error was discovered because the DX images suggested that the lidar scans which supposedly passed directly over the north sampling site were actually about 200 meters from the sensor platform at the closest point. Since the lidar unit was only about 1 km from the sensor platform, this seemed like an unrealistic error in that the lidar operators could probably "eyeballed" the alignment to within say 50 meters (*i.e.* a $\pm$2-3° accuracy). We did not think that such an error would have escaped observation by the lidar operators, and they had in fact "pinged" the sampling tower to establish the beam direction, so we thought that an error might have occurred in importing the lidar images into the GIS coordinate frame used in displaying the road grid. Upon re-examination of the data, a coordinate frame error

was discovered, and the lidar images were re-imported into the DX format. The correctly displayed images still indicated an azimuthal separation from the sampling stands of about 10 meters.

This separation still seemed larger than what we had expected owing to the fact that the lidar operators had aimed the lidar unit by "pinging" the beam off the sampling stand, as requested by the evaluators in pre-test meetings. The accuracy of the "pinging" was never checked, as for instance could have been done by raising and lowering the sampling instrument stand, simply because we didn't recognize a need to do so in advance -- there were no images which showed what seemed to be a distance error, and the pinging and multiple GPS measurements were thought to be sufficient. In fact, the GIS road maps used in the DX images have some positional inaccuracies, and in addition, the single-sensor GPS locators have built-in errors of as much as 100 meters to prevent misuse by terrorists or unfriendly militaries. Hence, even with multiple GPS data points, the accuracy with which the lidar image was displayed on the GIS road map was less than what could be determined by knowing the estimated beam size and "pinging" a real object.

An example of the positional accuracy of "pinging" is displayed in Fig. 8. After seeing Figs. 4 and 5 and reading the associated discussion, viewers typically interpret the regularly spaced bright spots as plumes from stop signs or signal lights at adjacent intersections. However, even without knowing whether such intersections existed, one should be struck by the regularity of the spacing, signal strength, spatial dispersion, symmetry, and timing of the presumed aerosol plumes. If one recalls that the lidar signal along any given ray is acquired in a time of only about a second, then it seems extremely unlikely that such uniform aerosol plumes would have existed at essentially the same instant at all the presumed intersections.

In fact, the signals result because the bottom of the field-of-view of the lidar beam clips the top of high voltage towers which run along the west side of Hanson Blvd. until just south of TH 242, where the wires continue in straight line while Hanson Blvd. jogs slightly west and cuts underneath the wires. The signal continues to be generated even though a small part of the beam is blocked by each subsequent pole because the beam path and the line of poles probably do not perfectly coincide, and the width and divergence of the beam continue to create return signals from each tower. Only a very weak part of the beam needs to hit a solid object to create a large

return signal--the main part of the beam can still pass by relatively unaffected. Thus, lidar signals from similar concentrations of particles before and after the obstruction can be the same, because the weak part of the beam which is blocked only contributes a significant amount of scattered light when an obstruction is present. The symmetry and smoothness of the signals displayed in the image are a result of the interpolation algorithms employed by the DX software in displaying the distributed point data set. This image enables one to ascertain not only the azimuthal direction of the lidar beam, but also its elevation above the ground.

In concluding this section, we should also note that the schedule change to include the State Fair test immediately following the Bunker Hills test was not desirable from a field test standpoint. Because we had to select sites and prepare the instrumentation for the State Fair test, there wasn't time for anything but an extremely cursory look at the data from the Bunker Hills test. Except for the troublesome CO monitors, the lack of data analysis did not end up leading to any repeated instrument errors during both the Bunker Hills and State Fair tests, although such errors could have occurred.

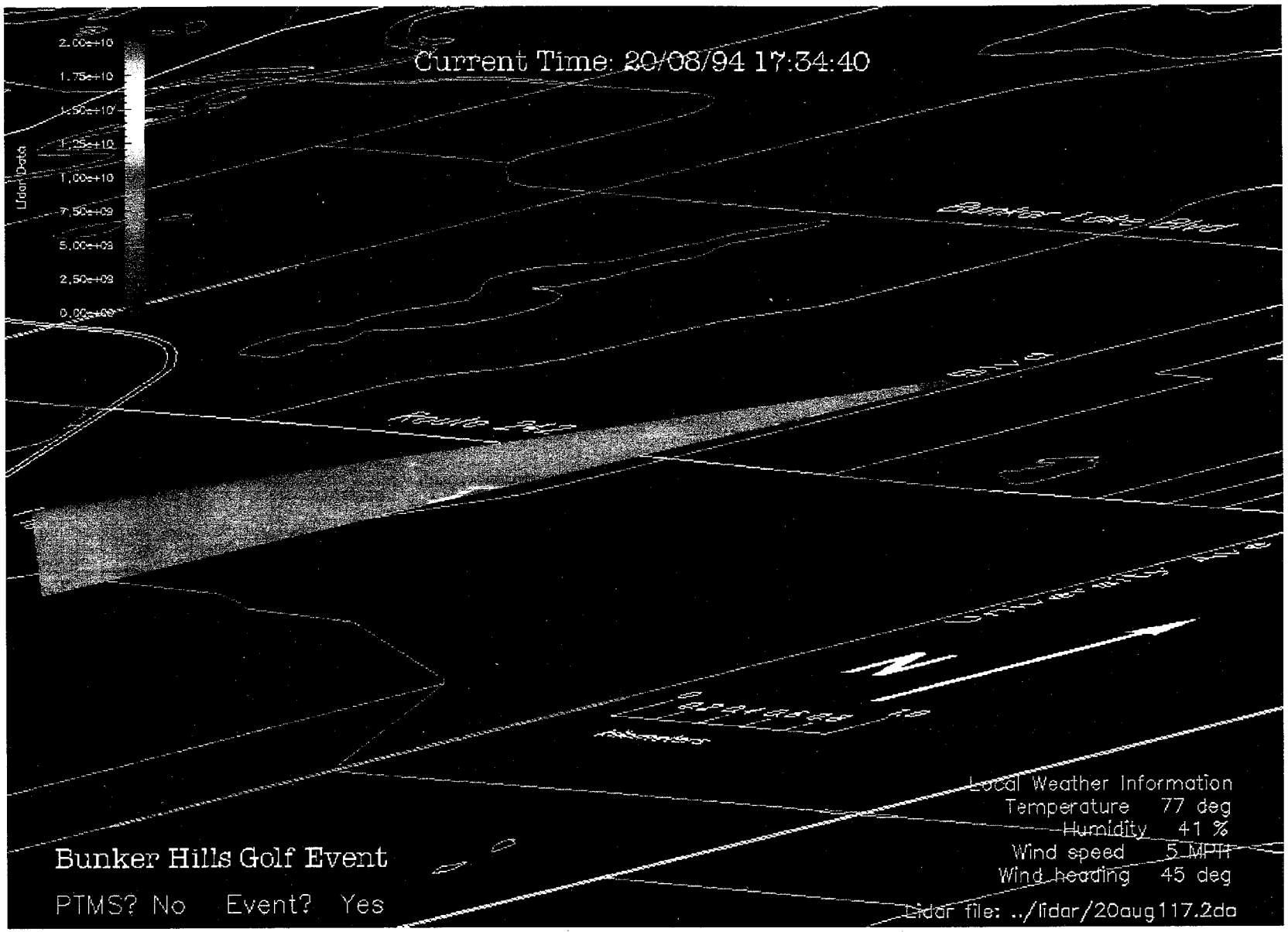

Fig. 4: Vertically oriented two-dimensional slice showing aerosol distribution along Hanson Blvd. early Saturday evening (5:34 p.m., Aug. 20, 1994). The distance scale (center bottom, hard to read) is one kilometer and the wind direction and magnitude is shown in the legend at the bottom right.

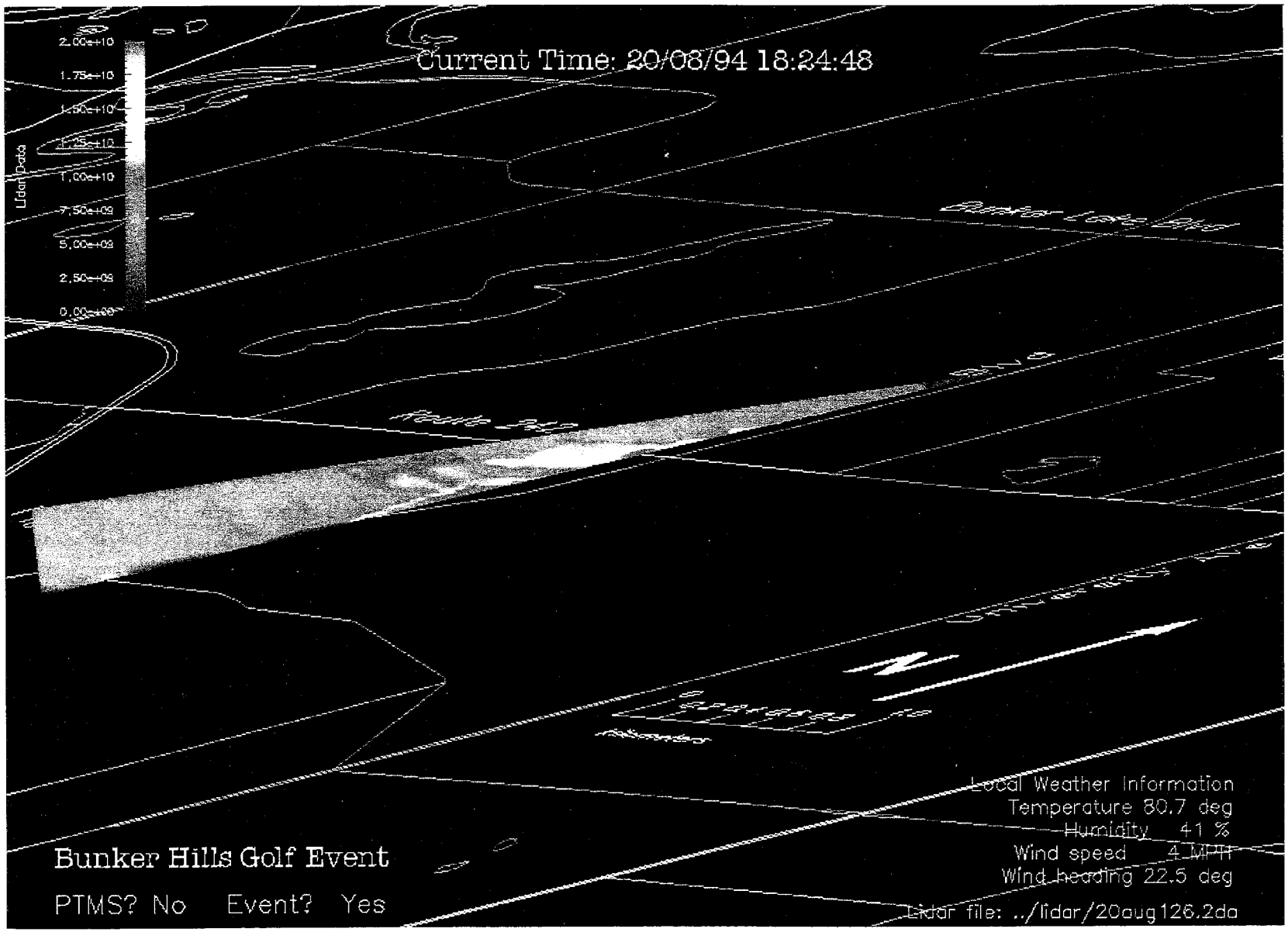

Fig. 5: Same vertically oriented two-dimensional slice looking down Hanson Blvd. as shown in Fig. 4, only about an hour later (6:24 p.m., Aug. 20, 1994). The distance scale (center bottom, hard to read) is one kilometer and the wind direction and magnitude is shown in the legend at the bottom right.

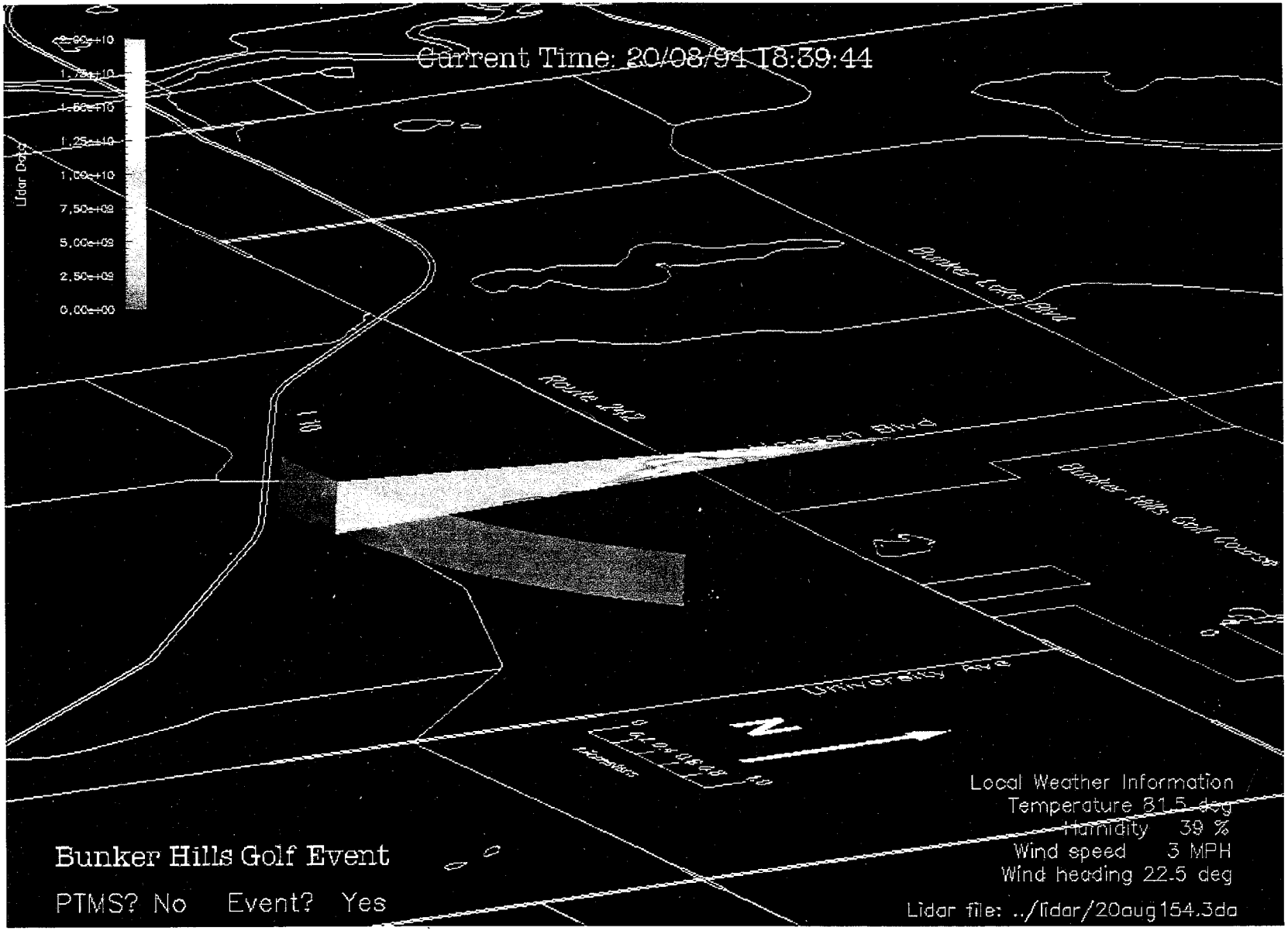

Fig. 6: Illustration of how a sequence of vertically oriented 2-D slices are put together to form a 3-D scan. A single slice is highlighted to show the cross-section of the aerosol distribution at this plane. The image display software can interpolate a continuous 3-D distribution through multiple slices.

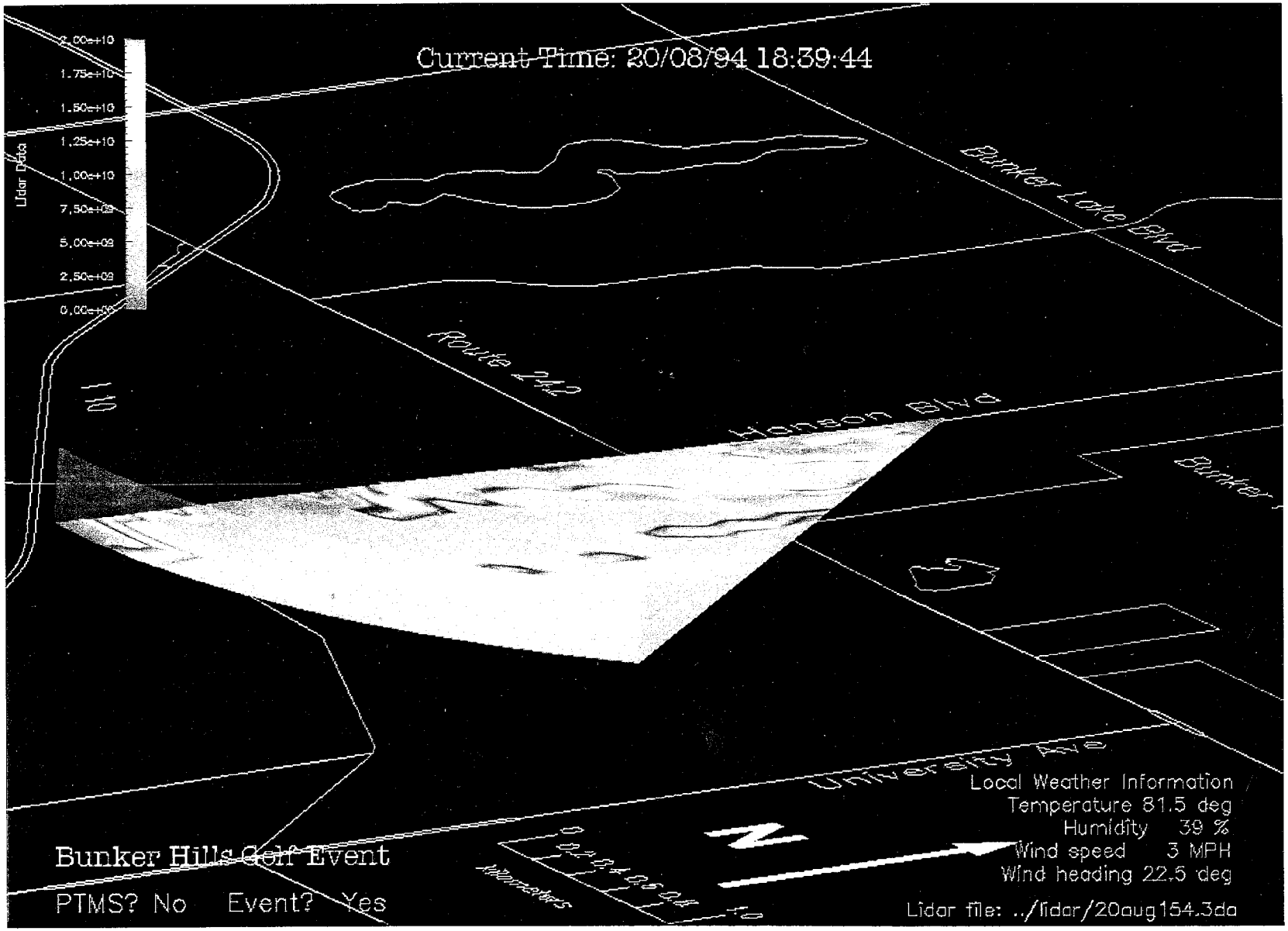

Fig. 7: Same 3-D scan sequence as shown in Fig. 6, but this time the lowermost plane (roughly horizontal) is highlighted for viewing. Since the 3-D distribution is interpolated from a sequence of 2-D which are acquired over time, the concentrations indicated in the lower plane occur over a fairly long interval.

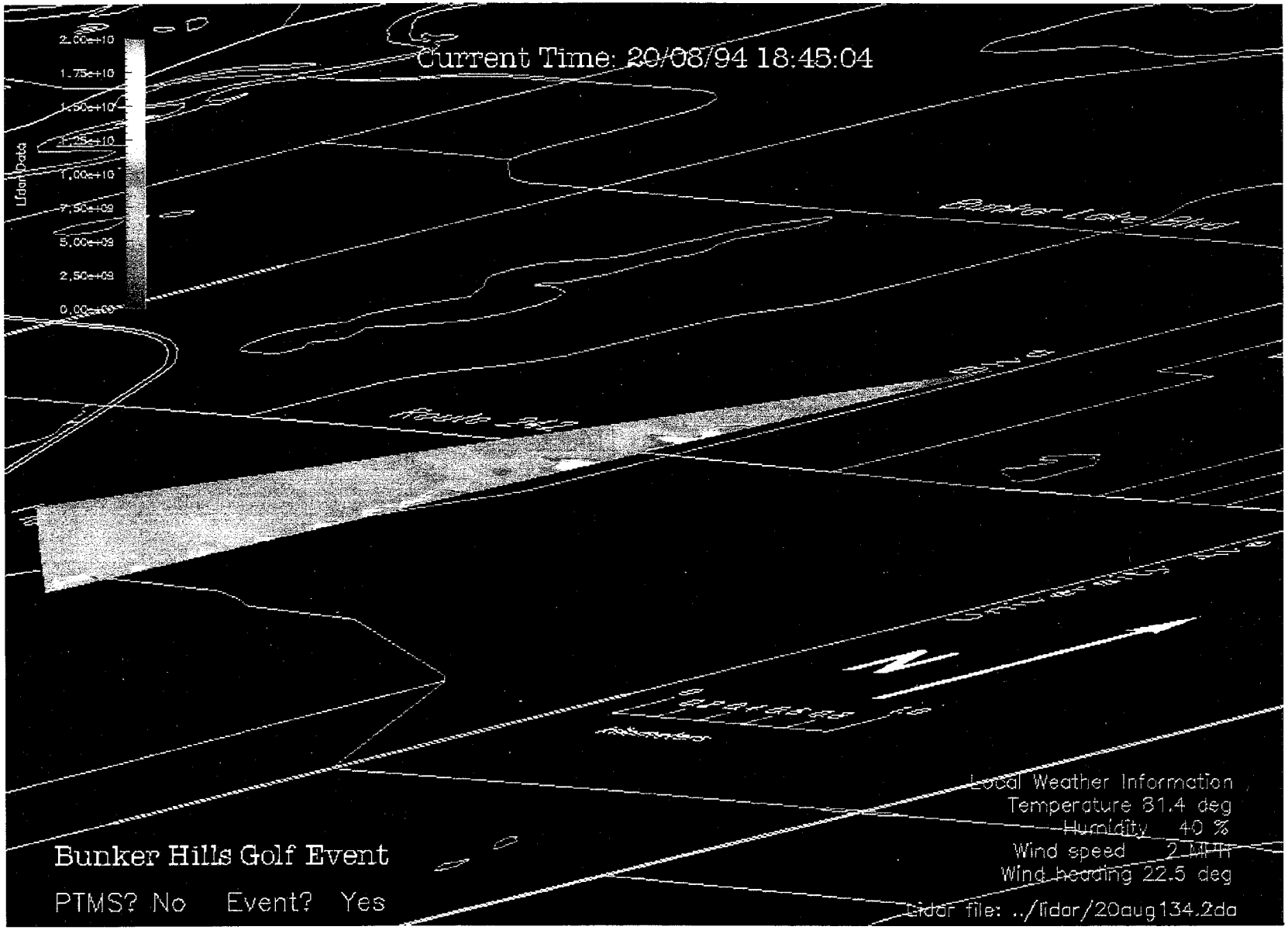

Fig. 8: Two-D vertical scan nearly parallel to Hanson Blvd. and along its west side. The regularly spaced signals along the lowermost rays of the slice actually result from the beam clipping the top of high voltage towers which run beside the road, as discussed in the text.

Minnesota State Fair, St. Paul, MN

The State Fair tests were conducted immediately following the Bunker Hills test from Wednesday, Aug. 24, through Sunday, Aug. 28, 1994. The Minnesota State Fair is purportedly the largest state fair in the country located on grounds within metropolitan city limits which are surrounded principally by residential neighborhoods. It draws large crowds to the area, and significant traffic congestion can result, especially during the morning rush hour as people try to get into the close-in parking lots and again when the grandstand shows let out in the late evening. A map of the area is shown in Fig. B4, App. B.

The lidar unit was set up on the roof of a 24 story apartment building located roughly 5 km away from the center of the fairgrounds. This location provided a view of the entire fairgrounds, as well as the major east-west freeway approaches from Interstate 94 and Hwy. 36 and the major north-south thoroughfare which passes by the entrance to the grounds, Snelling Avenue. The sampling stations were located on the east and west sides of the Snelling Avenue overpass over Energy Park Drive, just south of the main fairgrounds entrance.

Lidar scans were taken at above-building heights, and alternated between large area 3-D scans over the fairgrounds area, scans over the freeway area, and scans over the Snelling and University air quality monitoring station. Single line scans over the particulate sampling sites were interspersed between the multi-dimensional scans. The plan was to place a greater emphasis on the acquisition of a relatively large number of multi-dimensional scans during the first several test days, as requested of the project manager, Michael Manore, followed by a higher emphasis on line scans on the latter test days. The idea was to show off the range capability of the system and the extent of different aerosol plumes which may arise in an urban environment. Since most of the residences and small businesses in the area are two to three story buildings, the lidar location on top of the single high-rise apartment building in the area provided a unique opportunity to do this. The shift to line scan emphasis was to occur in order to increase the number of comparison data points.

Several problems developed as a result of very gusty winds during the test days. First, the lidar unit was toppled by a gust of wind which occurred overnight on Aug. 24. All of the equipment survived the fall except the support yoke for the telescope. Locating a replacement part and having it shipped in meant a day of down time. The system was once again operational

on Friday, Aug. 26. A similar accident struck one of the sampling stations late Saturday afternoon, Aug. 27, when a very strong wind gust actually toppled the sampling platform while data was being collected. Fortunately, the lift fell in a direction which missed all of the people and the data acquisition equipment. The particle sampling instruments and CO monitors actually survived the fall from the 24 ft height with only superficial damage, but the particle sampling equipment had to be recalibrated the next day. The two MOUDI samplers were part of a matched set owned by the Particle Technology Laboratory, and the calibration of the one which fell had to be rechecked against that of its mate. The recalibration had to be done on Sunday, because the set was scheduled to be used in another experiment the next week.

The combination of these two events greatly reduced the number of comparison points available between the lidar data and the point sampled data. In addition, there was a significant delay in importing the images into the DX format because of a backlog from previous experiments. When several images became available in October in the DX format, an obvious discrepancy existed between the viewing angles recorded by the lidar operators and the coordinate frame derived from the GPS measurements. This was evident because the lidar scans were not properly oriented over the fairgrounds on the displayed image; the magnitude of the discrepancy indicated that the error probably arose from another mistake in translating the angular reference data from the lidar system into the GIS coordinate frame of the DX image rather than an error in aiming the lidar.

Obviously, the lack of a rapid image display capability was very damaging in this instance, because the angular reference error would have been caught as soon as the images were displayed. With a rapid (preferably near real-time) display capability, the source of the angular discrepancy could have been identified and corrected during the test. However, because of the error, not only were the images incorrectly positioned, but it also wasn't possible to determine with certainty where the lidar beam passed relative to the sampling stations during the single line scans. Correlations between the lidar signal and the sampling sites would have been useless unless the point of closest approach was well known. With more investigation, the angular error could probably have been found, but because the DX formatted images had already been delayed by several months, the evaluators asked the image display team (at this time, Nancy Collins of IBM, with some help from Bill Eichinger of Los Alamos) to concentrate on data from the Bunker Hills

Golf Course event. As a result, much of the lidar data acquired during the State Fair Event was never imported into the spatial grid in the Data Explorer format.

Thus, a combination of problems involving down time of the lidar, down time of the sampling stations, and delays in importing the images into the DX format (the first images arrived in October, much too late to enable the angular error to be discovered and corrected during the test) plagued the State Fair data. As a result, none of the lidar data was useful for quantitative comparison with the data from the point sampling stations. The important conclusions which could be gathered from the test included the importance of securing all instrumentation, the relative durability and reparability of the lidar, and the need for real-time display of the lidar data relative to the road grid.

Rosedale Shopping Center, Roseville, MN

The Rosedale test was scheduled for the Wednesday before Thanksgiving and the two days immediately following, Nov. 23, and 25-26, 1994. The purpose was to try to monitor the impact of the post-Thanksgiving holiday shopping rush on the local air quality. The lidar system was located roughly 6 km to the south of the shopping center on the roof of an 8 story building (see Fig. B5, App. B). Time-resolved particle concentration measurements were obtained using a Climet CI 226 optical particle counter and a TSI model 3310 Aerodynamic Particle Sizer (APS). These used a common sampling inlet (10 ft elevation), adjacent to one of the MOUDI sites.

The ambient temperatures were below freezing on the test days. This caused a problem with the lidar control electronics and the laser itself. The problem with the control electronics was related to the cold ambient temperatures. This was fairly simple to diagnose, and the problem was solved by moving the instrumentation close to the roof access door and leaving the door open. While this was not very efficient in terms of building heat usage, the warm air draft was sufficient to keep the instrumentation working properly. The problem with the laser was much more subtle, and required slightly more than a half day for Dr. Eichinger to diagnose. A small amount of cooling water had been spilled inside the laser housing during normal flashlamp maintenance. The spill created a locally high humidity condition inside laser, and the water vapor then condensed onto the surface an optical element in the laser cavity known as the Q-switch, which was cold because of the cold ambient temperature. This would reduce the laser power

beyond an acceptable level. When the cavity was opened to investigate the cause of the low output power, the condensation evaporated. Thus, the problem was difficult to spot, and upon closure of the cavity again, the laser would operate for a few minutes again before gradually losing beam power. The cause was eventually discovered, and the solution involved drying the cavity and renting a propane heater to direct a stream of warm air past the laser. As a result of this difficulty, the lidar system was not operational until midmorning of Friday, Nov. 25.

No aerosol lidar signal was observed over the Rosedale site, although both the APS and Climet instruments showed measurable aerosol concentrations at a 10 ft height. Apparently the lidar beam elevation was too high to observe any 1-5 μm particles, even though these particles were present at lower elevations. Optical access was limited because the shopping center actually sits somewhat lower than the terrain located just slightly to the south across Hwy. 36, and the beam had to be directed above trees located there. The result was that the lidar beam did not even reflect off any of the parking lot light poles, each of which was about 50 ft high. This meant that the lidar beam elevation was more than 50 ft above the ground over the parking lot. The thermal buoyancy of the vehicle plumes apparently was not sufficient to carry the larger 1-5 μm particles to such heights, and the concentrations of the smaller particles was apparently not high enough to generate a measurable return signal. Thus, with no lidar data available and a snowstorm moving into the region on Saturday evening, the planned Sunday test was canceled.

Gibson Boulevard Thoroughfare, Albuquerque, NM

Much of the lidar image data acquired during the Bunker Hills and State Fair tests did not become available for evaluation until April, 1995. It then became apparent that this data would not be sufficient to accomplish the primary project goal of establishing a quantitative relationship between the lidar signal and particle concentrations. An additional test was scheduled to take place in Albuquerque, NM, to address this need. The test was held in Albuquerque to minimize the travel costs for participants from Santa Fe Technologies and Los Alamos National Laboratory, and the timing was controlled by the availability of the lidar system and the ending date for the project contract. The test was designed by the evaluation team to compare the lidar signal at a single point to the size-resolved particle concentrations at the same point. Thus, the test was different than all of the Minnesota tests because the lidar beam was not scanned. A

secondary goal was to check the instrument accuracy of the Langan CO monitors under field conditions using on-site calibrations and comparing the results with an EPA-approved air quality monitor. The key to success was selecting a site which ensured line-of-sight access between the lidar and a sampling site located alongside a major roadway at a nominal height of 10 feet.

The intersection of Gibson Boulevard and Girard Avenue was chosen as the test site. A map op the surrounding area is included in Appendix B, Fig. B6. Gibson Blvd. is a major east-west thoroughfare (three through lanes in each direction plus left and right turn lanes) which runs past the metropolitan airport and connects with a freeway several miles from the test site. Girard is an improved local connector (4 total lanes south of Gibson carrying some traffic to and from the airport, merging down to two lanes on the north side of Gibson). It is not a major access route to the airport. A golf course occupies a significant area to the north and east of the intersection; this was considered ideal with regard to background aerosol concentrations. Line-of-site access to the intersection was possible along a line nearly paralleling Gibson Blvd. at roughly a constant height of 13 ft. The lidar field-of-view was restricted to the north side of the road along Gibson by trees which lined the golf course. A small parking lot located about a quarter mile east of the intersection served as a convenient site for the lidar system truck, and some small trees located just west of the intersection provided a convenient beam stop. The north particulate and CO sampling site was located on the sidewalk adjacent to Gibson Blvd., at a point about 70 feet east of the intersection. Several sites on the south side of Gibson were used to obtain additional aerosol measurements and provide information on background or roadway aerosol contributions, depending on the wind direction (see Fig. B6). Finally, the headquarters of Santa Fe Technologies is only a half block from the chosen intersection, and hence could be used as a convenient base for overnight instrument storage.

As with other tests, the particle concentrations, CO concentrations, wind speed and direction, relative humidity, ambient temperature, and a video record of the traffic flow were recorded at the sampling site, while traffic counts were taken in several locations to determine flows in and out of the area (see Fig. B6). Several particle sampling instruments were used to monitor particle concentrations in the various size ranges. The MOUDI instruments were again used to provide daily averaged measurements of particle mass concentrations resolved into 8 logarithmically spaced bins in the range from 0.1-10 μm (4 bins per decade: 0.10-0.18, 0.18-0.32,

0.32-0.56, 0.56-1.00, 1.00-1.78, 1.78-3.16, 3.16-5.62, 5.62-10.0). Time-resolved measurements of particle number concentrations in different size ranges were obtained using a TSI, Inc., Model 3310 Aerodynamic Particle Sizer (0.6-10 μm), a Climet 296 optical particle counter (0.4-4 μm), and a Particle Measurement Systems LASX optical particle counter (0.1-3 μm). Each of these instruments obtains size-resolved average particle concentrations within nominal 30 second sampling periods. Some additional information on the instruments was given in the Background section of this document, and the instrument characteristics were summarized there in Table 1. Unlike the MOUDI data which relies on cascaded impactors to obtain the size resolution, these instruments produce analog signal outputs which are correlated with various particle sizes with a high degree of size-resolution. Due to the nonuniformity and asphericity of typical ambient aerosol particles, such resolution is not really justified; hence, the raw data from these instruments has was re-binned into logarithmic bins of equal width for comparison with the MOUDI data. Eight bins per decade were used: 0.10-0.13, 0.13-0.18, 0.18-0.24, 0.24-0.32, 0.32-0.42, 0.42-0.56, 0.56-0.75, 0.75-1.00, 1.00-1.33, 1.33-1.78, 1.78-2.37, 2.37-3.16, 3.16-4.22, 4.22-5.62, 5.62-7.50, 7.50-10.0). The integrated data from the MOUDIs is again shown in App. C.

The sampling intervals of the time-resolved particle instruments were not exactly the same, and not all of the instruments were capable of being locked to an external clock. Therefore, if the various instruments were allowed to free run, the sampled particle concentrations would not always be taken over identical time periods. This could have been solved by acquiring a relatively large volume of air quickly into a sample chamber (*e.g.* bag sampling), and then having the instruments sample from the steady state conditions in the sample chamber. The time required to obtain the sample would probably have been on the order of one or two seconds, such that we theoretically could have compared the particle concentrations with the lidar data corresponding to the sample filling interval. However, shorter duration sampling intervals would have increased the importance of exactly overlapping the lidar signal volume with the volume of sampled air, and the timing of the lidar data would have had to have been synchronized with the sampling system down to fractions of a second. The former is effectively not possible, since there must be some separation between the "edges" of the lidar beam and any solid object to avoid generating a return signal which would mask the aerosol signal, and the latter would have some fairly sophisticated triggering circuitry which would have required time to develop and debug. Hence, each

instrument was allowed to record concentrations with the fastest possible time resolution consistent with adequate particle sampling statistics for that instrument, which turned out to be about 30 seconds for the ambient concentrations encountered in most of the size ranges listed above.

Since the instruments sampled from the air, and the instantaneous particle concentrations could vary during the sampling period, which means that the measured particle concentrations represent running averages over the sampling period. The particle concentration data was therefore compared with a running average of the lidar data taken over the same period. The time synchronization requirement between the lidar and sampling instrument clocks is thus reduced to something on the order of a second, which is easy to accomplish by periodically synchronizing the clocks of the different data acquisition computers. Thus, a 30 second resolution represented the highest temporal resolution of the particle measurements; the data was actually accumulated into running averages over longer periods (*e.g.* 2 minutes) for comparison with the weather and traffic data, which were acquired at one and two minute intervals, respectively.

As described in the background section, the raw size distributions of number concentrations measured by the optical counters and the APS cannot be directly compared because the effective particle material densities of most coarse mode ambient aerosol particles are significantly different than 1 g/cm^3. Calibration experiments were run in a laboratory setting on the days immediately preceding and following the field tests, which enabled the accuracy of the number concentrations measured by the various instruments to be verified. A rough estimate of the effective material density of the particles measured by the APS was then deduced from the field test data by shifting the aerodynamic diameter distributions measured by the APS to match the smaller "physical" size concentration distributions measured by the LAS-X and Climet instruments. The particle material density was found to be 2.2 g/cm^3, and was assumed to be constant over the range of aerodynamic diameters measured by the APS (1.0 -7.5 μm, which corresponds to a "physical" size range of 0.67 - 5.06 μm) for all of the field test data. The details of the data reduction methods are given below, but the important thing to realize is that the particle sizes indicated in the figures below are given in terms of the "physical" sizes rather than aerodynamic diameters. This choice was made because the effective density of the smaller

particles measured by the LAS-X was not known, so there was no way to accurately convert them into aerodynamic diameters.

SUMMARY OF KEY RESULTS - The large volume of data associated with the time-resolved (and size resolved) instruments is problematic to display or discuss all at once. We have summarized the key results of the Albuquerque test in the table below. A detailed discussion of the data follows.

Table 5: Summary of Key Results from Albuquerque Test

In order for valid comparisons to be drawn between the lidar data and point-sampled data, the lidar beam must pass as close as possible to the inlets of the sampling instruments without reflecting off any of the sampling hardware. Minimum distance separating the lidar beam and the point sampling instruments is the most important factor affecting the correlations. For example, if the angle of the lidar beam is changed such that the lidar beam path is closer to the roadway or the ground than the sampling inlet, the lidar signal will be generated by the particle concentrations there, whereas the sampled particle counts would be from a different position. Even though the correlation between the lidar signal and the particle concentrations at the beam position could be high, spatial variations in the time histories of the particle concentrations at the two different locations would degrade the correlation between lidar signal and the sampled particle concentrations. The bigger the separation distance, the worse the correlation. The beam path can be established by recording reflections from a movable target, where the position of the target is known relative to the sampling inlet.
It would be advisable to periodically record the position of a small target within the field of view of lidar scans. This would provide a reference point from which beam alignment relative to the road grid could be verified.
When the lidar signal was taken at a position close to the inlet, the linear correlation between the number concentration of particles whose actual diameter was 2-3 μm varied between 0.72 and 0.98, provided that the beam angle stayed fixed, and the particle concentrations varied by at least a factor of 3 over the time period of the correlation (see next entry). Stronger correlations occurred over time periods of two hours or less, whereas the low value listed here came over a 6 hour period. (Correlation coefficients were obtained using conventional linear regression analysis of two minute running averages of all of the data sets.)
Ambient particle concentrations in the 1-5 μm size range were again very low, so the particle concentration data in these size ranges is fairly noisy, even after two-minute running averages were used to smooth the data. The lidar signal is actually smoother because the signal is generated from a much larger volume of particles than is sampled by the instruments. If representative correlations between the lidar data and the particle number concentrations are to be obtained, then the variation in the mean particle concentrations over time must be at least several times the level of the residual noise on the data. If the mean particle concentrations remain nominally constant during the interval of the correlation, then misleadingly low correlation coefficients will be obtained because the noise on the sampled particle counts will not correlate with the smoother lidar data. When intervals of nominally constant particle concentration are combined with time periods during which the particle concentrations vary substantially, the correlations are again in the 0.72-0.92 range.
Correlation coefficients between the mass concentration of particles whose aerodynamic diameters fell in the 1.33-7.50 μm range and the lidar signal were also in the 0.70-0.96 range. Again, the low correlations generally came when particle concentrations did not vary much, so that noise on the particle counts was important.

Table 5: Summary of Key Results from Albuquerque Test (cont'd)

Changes in particle material density or particle composition affect the aerodynamic particle diameter, the particle mass concentration, and the particle scattering cross section. This will change the relationship between the lidar signal and the aerodynamic particle concentrations. The particle event on Friday morning, June 23, apparently involved a substantial number of water particles convected from the golf course. Since the material density of water is lower than that of most roadway dust particles, the physical size of water particles is larger than the physical size of dust particles with the same aerodynamic diameters. This creates larger scattering cross sections, and is a partial explanation for the increase in the lidar signal relative to aerodynamic particle concentrations. However, since water and road dust particles have different effective refractive indices, the resultant difference in scattering is not due solely to differences in physical size. Hence, if lidar images record scattering from particle plumes, and aerodynamic particle counts are obtained from those plumes, then the combined information can be used to help identify the type of particles present.
Sorting the data by wind speed or wind direction did not increase the correlation coefficients substantially. With the exception of the particle event, this would indicate that variations in particle composition and material density with source direction were not in general large enough to substantially change the relationship between the lidar signal and particle concentrations over the relatively short period of this test. Thus, the relatively large sampling volume of the lidar is advantageous in reducing variability because a large number of particles is sampled at each instant. Very high volume sampling instruments would be require to achieve similar particle statistics.
Because ambient aerosols are generally somewhat hygroscopic, large changes in relative humidity will impact the correlation between the lidar signal and aerodynamic particle concentrations. This would be expected because the absorbed water changes both the effective density and the optical properties of the particles. The data from the Albuquerque event are not sufficient to analyze the magnitude of this effect due to the limited range of relative humidities encountered and the impact of interfering parameters.
Lidar systems operated at different wavelengths would respond to particles in different size ranges. Since different size ranges may have different effective material densities and compositions, particle counts in the different size ranges would still be needed to help calibrate the different lidar signals.
Wind field data with relatively coarse spatial resolution can be found by analyzing plume dispersion in a sequence of lidar images (*e.g.* Sutton and Bennett, 1994; Eichinger, 1995). The spatial resolution usually depends on spatial scales of the plumes, whereas the temporal resolution depends on scan speed and the number of velocity components desired. The following times apply to our system: single components along a line: a few seconds; two-components within a plane: several minutes: three components within a small sector 15-20 minutes.
The sensitivity of the Langan L-15 CO monitors is not sufficient for most ambient monitoring applications. This could probably be improved with the use of a higher resolution digitizing circuit. The L-15 monitors can be used to record relatively high ambient CO concentrations (above 10 ppm), but correction factors for drifts in the amplifier gains and offsets must be obtained using on-site calibrations if the data are to be useful.

DETAILED DISCUSSION OF PARTICLE CONCENTRATION AND LIDAR CORRELATIONS - The discussion which follows goes in detail through the analysis which led to the above conclusions. In order to make the data assimilation task manageable, we have plotted the time histories of the various data sets over contiguous three hour intervals. We first discuss the data obtained on the second test day, Friday, June 23, 1995, because it contains several interesting features which demonstrate both how the data analysis took place as well as the correlation between the lidar and the particle concentrations.

The particle concentrations during the early morning period from 6:00-9:00 a.m. as measured by the APS and LASX instruments are shown in Figure 9 (figures are again placed at the end of this section, and the size and scales are chosen to simplify comparisons). The number concentrations represent the 30 second average concentration measured by each instrument plotted versus time. The size labels represent estimates of the physical diameters of the particles as measured by the different instruments: the optical diameters recorded by the LASX instrument are not corrected, whereas the aerodynamic diameters of particles greater than 0.75 μm measured by the APS were scaled by a factor of $1/\sqrt{2.2} = 0.674$ to correct them back to physical diameters assuming particle material density of 2.2 g/cm^3 for all APS size ranges. The scaling was done to check the correspondence between the lidar signal and particle concentrations as predicted by scattering theory; however, note that regulations are written in terms of aerodynamic diameters, and hence the diameters should be rescaled by a factor of 1.48 to obtain the corresponding aerodynamic diameters. Note also that the number concentrations decrease exponentially with size. Hence, the number concentrations for the largest particle size shown (5 μm) are low enough that only a relatively small number (on the order of 10) are contained within the volume sampled by the APS during the 30 sec sampling interval. This results in significant statistical fluctuation in the numbers of particles contained in adjacent sampled volumes, which then appears as the fluctuations in the number concentrations indicated on the plot.

From Fig. 9, we note that there was some sort of event which occurred from about 7:15-8:15 a.m. Friday which caused an hour-long jump in particle concentrations larger than 0.5 μm, but not much change in the smaller size ranges. Figures 10a and 11 show the lidar signal nearest the sampling inlet, and the wind speed and traffic count along Gibson Blvd., respectively, for the same 6-9 a.m. time period displayed in Fig. 9. Logarithmic scales with the same number of decades have been used on all of the ordinates of these plots such that changes in variables by equal multiplicative factors show up as the same vertical distance changes on the plots, regardless of the absolute magnitude of the numbers. Fig. 12 shows the weather data on a linear scale in order to allow the wind direction to be shown. Comparing the signal profiles from the logarithmic plots, only the lidar signal displays a profile which is similar to the rectangular feature observed in the coarse particle concentrations. This coincidence of profiles implies that there is a strong linear correlation between the two data sets, since changes in particle concentration by some factor are

matched by similar changes in lidar signal. In fact, the correlation coefficient between the data displayed in Figs. 9 and 10 is $r = 0.76$. The strength of the linear correlation between the data sets can be readily visualized by making a transparency of the lidar plot (Fig. 10a) and overlaying it on top of the particle concentration data, sliding it up and down to compare the lidar signal to concentrations in different size ranges. The linear correlation between the lidar signal and the particle concentrations in the 1-5 μm size range is exactly what one would predict from basic particle scattering theory (refer to App. A for details). Considering the approximations in the theory, the level of agreement is quite surprising.

Thus, the procedure for analyzing the data was to make plots of the time-histories of the various measured parameters and to look for interesting features in the data, then check other data sets for any related responses. Breaks in the data sets for the particle sampling instruments occur when the files were backed up to disk. The same is true for the lidar data.

The time period from 7:15-8:15 a.m. Friday for which various data sets are displayed in Figs. 9-12 is a good period during which to examine the relation between the lidar signal and the particle concentrations because the wind speed (nominally 3-5 mph), direction (nominally out of the north), and traffic count along Gibson Blvd. remained relatively constant over that time period. In addition to changes in emissions by local particle sources, these three observable parameters are presumably the major factors which could cause significant changes in the particle size distribution, effective composition, or concentration which reached the sensors. In this case, the roadway was downwind of the sensors, so the traffic level shouldn't have greatly influenced the measured particle concentrations anyway. Therefore, the logical conclusion to the hour-long increase in particle concentrations was that either a new particle source came on during this period or an existing source increased its output concentration by about a factor of three. Since the golf course was located just upwind of the sampling site, the most likely activities would be course-wide mowing of greens, raking of the sand traps, or watering/spraying the grounds. The uniformity of the distributions described in App. E[1] would suggest the latter.

Although the correlation between the lidar data and the particle concentrations in the 1-5 μm size range appear very good in Figs. 9 and 10a, close examination reveals that there is a steady drift in the relationship between the two signals over the period between about 7:45 and

[1] Images of the lidar signal along the beam path (available after draft printing) suggest sprinkler use -see App. E.

8:30 a.m., after which point the relationship becomes steady again This reduces the correlation between the data sets from the value of 0.98 which occurs for the 6:00-7:15 interval to the value of 0.76 cited above for the period from 6:00-9:00. Fig. 10b shows the lidar signal again along with the difference between the lidar signal and a linear fit derived from the entire morning's data.

One possibility for the drift is that the lidar signal plotted in the figures corresponded to a position slightly offset from the position of the particle sampling inlet. However, it seems unlikely that the particle concentrations between two points would drift apart in such a steady fashion and remain that way through the remainder of the day. A more plausible scenario involving beam position might be that the mounting hardware on the lidar telescope relaxed somewhat and the beam path actually drifted a little. That this might occur early in the morning shortly after the system was aimed is possible. In order to detect such a drift, one would have to scan the beam in a narrow sweep in the vicinity of a marker whose position was known, such that the marker location would be accurately recorded in the scan. We did accurately determine the beam position between about 9:15 and 10:20, as described below, but this would not rule out the possibility of beam drift in the period in question.

A second possibility is that there was a drift in the gain or offset of the amplifier which processes the signal from the lidar detector, such as often occurs with changes in temperature. This does not seem likely, partly because the lidar amplifier is temperature corrected and the temperature change during the period in question is only 72-80 °F (even uncorrected amplifiers would be expected to have a flat response over this range), but primarily because no other such drifts were observed at other times during the experiment, as would be expected in such a case.

The third possibility is that there is a drift in the flow rates through the aerosol counters. Again, this possibility cannot be ruled out, but other such drifts would then also have been expected to occur during the remainder of the day.

A fourth possibility is the impact of an interfering variable, such as relative humidity or particle composition. A change in either could cause a gradual shift in the optical properties or effective density of the particles (see App. A). Referring to Fig. 12, we note that the relative humidity data does show a negative rectangular time response during the 7:15-8:15 period, but nothing peculiar which begins at 7:45. The sudden drop in humidity appears correlated to the particle event, because the ambient temperature continues a very gradual climb during this period,

and the relative humidity tracks inversely with the change in temperature except during this particle event window. The slight time lag between the particle event and the change in the relative humidity is due to the relatively slow time response of the humidity sensor. Now, if the particles were extremely hygroscopic, they might absorb water vapor from the air, which would cause them to grow. This would show up as a slight increase in the concentrations of larger particles and an increased lidar signal. However, it would be impossible for the low concentration of aerosol particles present to absorb the mass of water vapor associated with a nearly 10% drop in the relative humidity as indicated in Fig. 12. The particles would grow so heavy that they would simply settle to the ground. Thus, we do not think the indicated change in relative humidity during this period is real, but rather results from an interference between particle concentrations of whatever type were present during this period and the relative humidity sensor. Since the humidity sensor works on the principle of measuring the change in capacitance of the air caused by changes in the relative humidity level, it is possible that charged particles could have influenced the measurement. We note that this is the only instance in which a strong correlation was observed between particle concentrations and relative humidity, and hence we feel that the interference was peculiar to the source which generated the particles between 7:15 and 8:15, rather than a problem of general concern. However, in future experiments, it might be advisable to use a different type of humidity sensor, or at least to monitor the average aerosol charge.

The final possibility is that the particle scattering properties drifted during this period. As will be shown later, a linear fit between the lidar signal and the aerodynamic concentrations shows an increase during the particle event relative to the correlation observed at other times. This would be consistent with particles carrying a significant amount of adsorbed water, which would reduce the effective particle material density. This also would cause particles of a given aerodynamic diameter to have a slightly larger physical size. For example, the average material density of dry particles in the 1-5 μm aerodynamic size range is about 2.2 g/cm^3, whereas water has a density of 1.0 g/cm^3. If the particles which came from the golf course had similar dry composition and morphology but were 16.7% by volume water, then their effective density would have decreased to 2.0 g/cm^3, and the physical particle size corresponding to equal aerodynamic diameters would have increased by nearly 5%. If the particles had been 100% water, the material density would have been 1.0 g/cm^3, and the physical diameter corresponding to the same

aerodynamic diameter would have increased 50%. The larger physical particle size would have outweighed the reduced scattering associated with the optical properties of water, resulting in an increased lidar signal from a given class of aerodynamic diameter particles. This would explain the slightly larger increase in the lidar signal relative to the increase in aerodynamic concentrations during the particle event. The slow decay in lidar signal during the event could reflect either a decrease in the percent water in the particles, or a decrease in the fraction of water particles.

Based on this discussion, the cause of the signal drift between 7:45-8:15 would remain uncertain; however, the distributions described in App. E, coupled with observations of sprinkler use would indicate that a compositional change is most likely. This is further supported by the fact that the correlation which exists as of 8:15 continues to hold quite well through the remainder of the day, regardless of changes in wind speed, direction, ambient temperature, and humidity.

Continuing on to Figs. 13-14, the lidar signal once again tracks the particle concentrations from 8:30 to 9:15 a.m., at which time the signal trends substantially downward before recovering to track particle concentrations from about 10:20 to noon. In fact, from 9:15 to 10:00, the lidar signal level decreases by almost an order of magnitude, but similar changes were not observed in other variables which might cause such a change. This drop is easily explained: during this period, we were attempting to establish the exact location of the lidar beam in relation to the sampling inlets by "pinging" the lidar beam off an opaque object. To do this, we constructed a cardboard target (approximately 1 ft by 1 ft) mounted on the end of a pole, and swept in back and forth through the air surrounding the sampling station. Because we were so close to the laser transmitter, the gain on the lidar detector was turned down to avoid saturating the electronics. This explains the decrease in the lidar signal during the 9:20-11:00 period. Small blips on the signal represent the target and/or support pole passing through at least part of the beam. The gain was eventually turned back up just before 11:00, after we had confirmed the beam location several times with the target (see the large signals in Fig. 14 between 10:15 and 10:45).

The point at which the lidar signal shows a maximum return value should correspond to the point at which the center of the beam strikes the target. We were thus able to determine that lidar beam angles of 6.18° azimuth, 0.26° elevation placed the beam axis roughly parallel to Gibson Blvd, 3.5 ± 1 feet (1.1 ± 0.3 m) above and 7 ± 1 feet (2.1 ± 0.3 m) north of the sampling inlet (approximately 4.1 m above the ground and 5.2 m north of the northernmost curb of Gibson

Blvd.). Also, by examining a real-time plot of the lidar signal along the ray, the distance between the sampling inlet and the lidar unit was estimated to be 385 ± 5 meters. (The uncertainty reflects the ability to read the graph, not the lidar resolution.) The relatively low height was purposely chosen to demonstrate the ability to get near-ground level measurements, and as long as no one climbed a ladder or tree directly in the beam path and looked directly back at the lidar unit, there was no eye safety hazard. And since the beam path nearly parallel the fence line of the golf course, we were assured that no other individuals or vehicles could cross through the beam path.

The process of determining the beam location took quite a bit of time (approximately 9:20-11:00), primarily because we didn't want to sweep the beam to find the target in order to avoid introducing positional uncertainty into the early morning data. In addition, the spatial profile of the beam made it more difficult for us to zero in on the target. Because we were so close the lidar transmitter, the beam was not a simple pencil-like beam, but rather a primary central beam with a half-power diameter of about one foot surrounded by a lower power ring about two and one-half feet in diameter. The annular ring surrounding the main beam is fairly typical of laser - telescope systems such as that used in the lidar unit at this distance. (The intensity distribution is known as the near-field beam profile in scientific jargon.) When we were satisfied that we knew the beam position accurately, a slight change was made to the beam angles at 11:23 to bring the beam to 6.14° azimuth, 0.10° elevation, *i.e.* the beam axis was nominally at the same height as the sampling inlet (10 ft above the ground) and 6 ± 1 feet (1.8 ± 0.3 m) north of it to avoid beam reflections from the inlets. The small change in the elevation may have caused a slight change in the lidar signal vs particle concentration relationship, but because of the relatively large diameter of the lidar beam, it would not be expected to be large.

Continuing to Friday afternoon, there is a large spike which occurs at about 12:15 p.m. on the particle concentrations in all size ranges (see Fig. 17), and two smaller spikes at about 12:00 and 12:25. These events were actually caused by a member of the evaluation team, although not purposefully. At this time, we were in the process of setting up a second sampling station directly across Gibson Blvd. (on the south side) in order to evaluate the impact of the roadway (the wind was generally out of the north). Doing this required transferring a generator, table, pump, awning and various miscellaneous hardware across the street in the bed of a pickup. However, the driver (Sumantra Chakravarty) was a little timid in pulling the truck over the curb and onto the parkway

on the south side of Gibson, and he ended up spinning the wheels with one tire on the sandy soil of the park-row and the other still in the gutter. After several tries (the "events" at 12:00 and 12:15), he wasn't successful in getting the truck to jump the curb, so another driver finished the job several minutes later (at about 12:25 p.m.).

Although it is difficult to see on Fig. 17 because the various concentration histories at 12:15 p.m. overlap, the particle concentrations recorded by the LASX instrument in the 0.5-2 μm size ranges jump by roughly an order of magnitude, while those in the 0.8-5 μm range recorded by the APS jump by almost two orders of magnitude. There are probably significant counting errors on both instruments associated with the very high particle concentrations which occurred during this short event (the APS will overcount due to false triggering by multiple small particles, and the LASX will undercount due to a particle coincidence data validation algorithm). Hence, the actual particle concentrations probably increase somewhere between one and two orders of magnitude in the 0.5-5 μm size range.

Note, however, that the concurrent increases in the lidar signal at 380 m (Fig. 18) only amount to factors of 3 or 4. The wind during the period was very light, but swirled a little between northerly at 0-4 mph to westerly at 0-4 mph (Fig. 20); assuming there was no time offset between the lidar data and the wind data, the wind would have been nominally from the west at about 3-4 mph at both times the wheels spun. The direction of wheel rotation would have thrown the particles across the roadway and a little to the west, where the particles would have been transported in the wakes of the east- and west-bound vehicles, while the wind would have convected particles at higher elevations back to the east, apparently past the inlet of the aerosol instruments and through the lidar beam. In light of the previous discussion, possible explanations for the difference between the observed changes in the lidar signal and particle concentrations were that the lidar signal at the 380 meter distance didn't correspond to the location of the sampling inlet, or that there was some kind of a drift in the lidar gain. The latter seemed unlikely since the signal levels preceding and following the event were similar to those which had been observed at other times.

We were puzzled by these results, so we eventually asked Bill Eichinger of Los Alamos to re-examine the original data set to look at the lidar signal variation with time along the entire beam path. He produced several two-dimensional plots showing a color contour maps showing

the lidar signal as a function of time and distance along the beam (see Fig. 21a). This image is essentially what would be displayed on the lidar computer monitor in real-time during lidar data acquisition. The spatial distribution of the signal at any time can be seen by analyzing the signal changes as one moves vertically upward from the abscissa, whereas the temporal history at any position along the beam can be seen by scanning horizontally along the plot. Convection of plumes along the beam can be observed in such plots. In fact, the component of the wind speed in the direction of the beam can be found by looking at the angle that the plumes make on the plot: a steep slope downward and to the right would indicate a fairly strong component of the wind moving along the beam toward the laser source (the plumes get closer to the laser in a short period of time), while a shallow slope upward and to the right would indicate a relatively small wind component in the direction of the beam away from the laser. Typically, a series of 50-100 laser pulses (which are recorded within 1-2 seconds at the 50 Hz laser firing rate) are averaged together to reduce the inherent noise in collecting the low light level return signal. The time resolution of the image is thus about 1-2 seconds, which is generally sufficient for most ambient aerosol events.

The signal variation shown in Fig. 21a is consistent with a fairly concentrated plume cutting across the lidar beam with an east-directed wind velocity component. A portion of the data displayed in Fig. 18 corresponds to data displayed in the horizontal profile at 380 m in Fig. 21a. However, Fig. 21a is a low resolution image which displays a running average of several adjacent points. Since each point is spaced 7.5 m apart, the signal magnitude of a concentrated narrow plume whose characteristic width was less than about 10 m across would be smoothed out if displayed this way. Fig. 21b displays the full resolution of the lidar data without any spatial averaging, and we do indeed see a much stronger signal (max. of 2×10^7 as opposed to the maximum of 2×10^6 displayed in Fig. 21a). The highest signal is located at about 400 m and is a factor of about 40-50 times higher than signals at nearby locations and times.

This increase in signal magnitude agrees quite well with the concentration changes observed by the particle counters, indicating that the previously observed correlation probably continued to hold quite well even at very high local particle concentrations. The fact that the maximum signal location appears at a slightly longer distance than we would have anticipated based on the cardboard target pinging results probably occurs because of a combination of

factors: 1) the lidar beam path is further north of Gibson than the sampling inlet; 2) the plume has a strong spatial variation with position; and 3) the ±10 ft uncertainty in determining the distance of the cardboard target. The sketch in Fig. 21b shows how the strongest concentrations could have been observed at two different locations at slightly different times. The variation in the lidar signal over the relatively small distances examined in this case demonstrates quite dramatically the need for good spatial resolution when interpreting concentration fields which contain highly localized concentrations.

During 12:45-1:05 p.m., several spikes show up on the 0.15 and 0.2 μm fine particle concentration histories as well as on the 0.5 - 3 μm histories. These are also picked up by the lidar signal. The changes in the fine particle concentrations appear unusual because not many changes such as this had been recorded outside of the tire-spinning episodes described above. Referring to Fig. 20, the wind was generally quite calm during this period but with variable direction; the spikes in the small particle concentration appear during times when either westerly or easterly winds existed. Such winds would carry particles along the roadway at relatively low speeds. We think the fine particle spikes correspond to plumes from diesel vehicles undergoing acceleration transients, since diesel vehicles are known to emit large numbers of soot particles in the 0.2 μm size range and below. Because of the relatively light winds, the plumes would not disperse very quickly, and the increase in the small particle concentrations would be observed by the LASX. The coarse particle concentrations also exhibit smaller spikes during these instances, but the fluctuations appear rather less dramatic because the concentrations typically fluctuate up and down more substantially due in part to higher variability in the counting statistics for the larger particles.

At about 1:45 p.m., the lidar signal exhibits a significant increase by almost a factor of 10. This coincided with a strong wind gust out of the east (see Fig. 20). The particle concentrations showed an increase of only about a factor of 3-4 during this time. Unfortunately, although the particle concentrations did exhibit larger fluctuations from about 2:00-2:30, the lidar system was not operating during this period: the power supply had become exposed to sunlight, and had overheated; it was moved to a shaded location and allowed to cool down before the system was restarted. In addition, the wind direction indicator appears to have frozen from about 2:15-3:00. Due to the lack of data, we can only speculate on the reasons for the lidar signal behavior relative

to the particle concentrations during the brief interval preceding 2:00. It is possible that the sudden shift in wind direction caused the particle scattering characteristics to change, but it is more likely that the difference is related to 1) false return signals generated because of tree movement (there are some data points where the detector saturates, similar to what will be discussed regarding Thursday's data shortly), or 2) spatial variations in the particle concentrations and the separation between the sampling inlet and the lidar beam.

After 2:00, the LASX data stops because it was transferred to the south side of Gibson to try to pick up more clearly the impact of vehicle traffic based on the prevailing wind. It was restarted at about 3:00 p.m. The APS continued to sample on the north side of Gibson during this period. Fig. 22 shows the upwind concentrations measured by the APS, while Fig. 23 displays the downwind concentrations measured by the LASX. The downwind LASX data shows quite a number of spikes in the submicron particle concentrations. Several of these spikes occur across the entire submicron range of the instrument, while others have a smaller extent. In some of these instances, there are corresponding spikes exhibited by the APS instrument, but they are definitely not as pronounced as those recorded by the LASX.

The wind direction sensor appears to get stuck at about 4:40 p.m., as indicated by the flat data, but the wind speed data appears to remain valid. Notes taken at the site indicate that the big gust which occurred at 4:55 actually came from a southerly direction, while fairly calm westerly winds existed at 5:00 and 5:25, southerly wind at 5:30, and finally shifting around to northerly or north-easterly by about 5:40. The spikes on the LASX channels do not appear closely correlated to the wind gusts, with the exception of the small increases in 0.15, 0.2, 0.87, and 2.05 μm concentrations which occurred during the strong southerly gust at 4:30. In fact, notes and traffic video data indicate that the spikes correspond to times when trucks or buses went by on the roadway and the wind direction was such that the particulate emissions were carried to the particle counters.

One of the most interesting events occurred at about 4:45. Two large lawn mower vehicles had driven down the maintenance road (paved) which surrounded the airport field on the south side of Gibson Blvd. The drivers noticed our test stations and came over to inquire what was happening before they began mowing. When they found out it was an aerosol study, they immediately agreed to proceed to a much different part of the airport grounds so that their

mowing operations wouldn't interfere with our measurements. The lawnmowers had been parked about 150 feet south of the LASX sampling station when they restarted the vehicles, and the wind was moderate out of the south (2-5 mph). Not quite two minutes after the vehicles started and drove off to the south down the paved road, large spikes appeared on the concentrations of 0.15 and 0.2 μm particles, but not much occurred on the larger particle channels. The wind speed and direction at this time would have carried any particles generated by the vehicles to the LASX site in about a minute's time. Together with the delay time associated with the transit time of the particles through the sampling tube, these concentration spikes were almost certainly related to the startup of the mowers, as no other events were observed at this time which could have led to a transient jump in the small particle concentration. Assuming this is correct, this event points to the potential significance of cold and hot vehicle starts on local submicron particle concentrations.

We now discuss the data from the first test day on Thursday, June 22. Figures 27-40 display the data in the same manner as used for Friday. The first thing one notices is that the lidar signal level appears to shift between the breaks in the data during the morning, although little change is seen in the particle concentrations in the 1-5 um range at these times. These shifts occurred because the lidar telescope was being re-aimed in an attempt to avoid interference from a tree located about 360 m from the laser. During these adjustments, the lidar signal was not recorded; hence, the breaks in the data. Both the azimuthal and the elevation angles of the beam were changed slightly, and the beam location relative to the aerosol inlet moved by about 5-10 ft in both horizontal and vertical directions. The interference from the tree signal appears at the same distance from the laser at all times in the distance-time plots shown in Figs. 31 and 32. Since lidar signals farther down the beam were not greatly affected, the interference must again arise from a relatively weak part of the beam. Software interpolation artificially spreads the interference over a longer part of the beam path than is actually the case.

After several adjustments, we still encountered some interference from the tree, so we obtained permission to tie the tree branches back to limit their movement. Because the position of the lidar beam relative to the sampling inlet changed several times on Thursday, we did not perform the detailed pinging procedure to establish the exact location of the lidar beam relative to the aerosol inlets until Friday morning. The instrument locations were marked so that they could be exactly re-positioned, and the elevation angles are repeatable from day to day because they are

referenced using a level. Only the azimuthal angle was not repeatable without reference to an object located some distance from the lidar. However, the azimuthal angle was limited by a street light pole and a golf course sign, both of which were located near the sampling inlet, and were spaced about 10 m apart. Hence, we will assume that the Thursday beam position can be found from the Friday beam position, although there is probably some uncertainty in the azimuthal direction. Thus, we deduce that the angles of 5.70 az. 0.70 elv. correspond to a beam position 1.2 m south of the sampling inlet and 4.0 m above it, whereas the angles of 5.50 az. 0.20 elv correspond to 2.6 m south and 0.7 m above the inlet.

The discreet beam direction changes described above would be analogous to beam direction changes that would occur if the beam had been continuously scanned, only the angular increments during a continuous scan would be smaller. Hence, at first thought, one is worried that the apparent change in the correlation between the lidar signal and the particle concentrations would indicate that the lidar signal would not be a quantitative indication of particle concentrations across the scanned volume. However, upon careful consideration, one realizes that two factors could have contributed to the apparent change in the correlation: 1) the percent of the beam which was blocked by the tree probably changed, and this would change the signal levels observed from locations downstream of the tree, and 2) the particle concentrations in the 1-5 μm size range should be fairly strong functions of vertical height and distance from the roadway, and hence one would expect to see changes in the particle concentrations at different azimuthal (horizontal) or elevation (vertical) beam angles. This implies that the lidar signal would change relative to the particles concentrations observed at the fixed aerosol sampling inlet. Furthermore, the data from Friday (discussed above) did not show any similar changes in the signal correlation (excepting of course the time during which the target was used to locate the beam position). On Friday, the beam position was held essentially constant, and although the variable wind and traffic conditions led to changes in particle concentrations and size distributions, the correlation between the lidar signal and the particle concentrations remained essentially the same. Hence, the shift in the lidar signal relative to the sampled particle concentrations on Thursday are almost certainly due to the reasons cited above rather than any change in the relationship between the lidar signal level and the illuminated particle concentrations.

The next thing one notices is that there are several instances from about 12:45-1:30 on Thursday during which the lidar signal appears to rapidly jump to a substantially higher level only to return to the previous level a very short time later. These jumps do not seem to correlate with particle concentrations or wind bursts. In fact, the original data files contain some negative signal values which are obviously not physically possible. (Note: the negative points had to be filtered out of the logarithmic plots shown in Figs. 35 and 36.) Negative signal values can arise when a sudden increase in backscattered light, such as would occur if the beam struck a solid object, reaches the detector, creating a very large signal spike which overloads the amplifiers. Even after the light flash goes away, the electrical signal from the amplifier rings (oscillates) for a period of several milliseconds, resulting in large positive and negative signal fluctuations. The signal oscillations are faithfully recorded by the digitizing system. The millisecond duration associated with the ringing is quite long compared to the time required for light to travel over relatively long distances (the round-trip time for the lidar beam to travel out to a distance of 300 m and return to the detector is only 2 μs). Hence, the ringing affects the data recorded along the entire ray path downstream of an obstruction.

The impact of saturation and ringing can be seen by comparing the distance-time plots shown in Figs. 33a and 33b, where both images were acquired with identical beam angles. Fig. 33a shows a typical distance-time plot, where we can see how the component of the wind in the direction of the beam convects and disperses the aerosol plumes with time. In the case of Fig. 33a, the nominal wind speed in the direction of the beam as indicated by the plume dispersion angle is approximately 3 ft/s (2 mph). By comparison, the wind direction measured by the sensor at the sampling site changed from west to south with an average velocity of about 4 mph over the period from 1:10-1:20. This agrees quite well with the lidar data when the difference in the vector directions is taken into account.

As an aside, note that the analysis above illustrates how distance-time histories such as those plotted in Figs. 31-33 can be used to obtain a rough map of the wind velocity component in the direction of the beam, where the spatial resolution of the velocity information depends on the number of identifiable plumes. This last fact implies that the velocity data is in general not highly detailed. The analysis can be extended to two- or three-dimensional velocity fields using two- or three-dimensional lidar scans. The idea is to use the track of dispersing plumes to determine the

wind direction, from whence the velocity field data is found from cross-correlations of subsequent images acquired at slightly different times. The total scan time required to obtain detailed three-dimensional data sets would limit the resolution of three-dimensional velocity fields, but two-dimensional vectors can be readily obtained.

Returning to the Thursday data sets, the particle concentrations, lidar data averaged from 386-396 m, traffic and weather conditions during the early afternoon period appear in Figs. 34-37. (Note: the wind direction indicator on the Davis weather monitor apparently got stuck from about 1:20-2:10 and again later after 3:45, but the rest of the direction data agrees with notes taken during the test.) Several rather large oscillations occur in the lidar signal around 12:45-1:00 (12.75-13.00) and again around 1:15-1:51 (13.25-13.85). These lidar signal oscillations did not in general correspond to times when aerosol concentrations increased or when large wind gusts were recorded, as indicated by the data displayed in Figs. 34 and 36. The lidar data from 1:08 to 1:31 corresponds to the 386-396 m data shown in Fig. 33b, and the lidar data from 1:31-1:53 comes from a lidar file which has a similar abnormal distance-time profile. Numerous negative lidar signal values appear in the 386-396 m data during these abnormal files, and we do not have any plausible explanation for their occurrence. By comparison, only a single negative value was recorded just prior to 1:00 (13.00), and the distance-time plot corresponding to this period appears normal (see Fig. 33a). Based on the stationary signal vs time displayed on Fig. 33a and the fact that the signal does not disperse as an aerosol cloud would under the wind conditions existing at the time, we think that the signals generated around 1:00 actually correspond to several instances in which part of the beam struck part of the moving sampling platform which was being raised or lowered as part of the test. Such raising and lowering took place to calibrate the CO monitors and to change the tape in the traffic video camera. These instances once again show the importance of having spatially resolved information to help in interpreting single point data.

Lastly, note that the correlation between wind gusts, spikes in the 1-5 μm aerosol concentration, and spikes in the lidar signal actually correspond quite well from 3:50 p.m. (15.83) to 5:45 (17.75). This can be seen by laying a transparent plot of the lidar signal on top of the other plots, or alternatively by looking at the data on Fig. 41. Again using the beam location results from Friday as a baseline, the path of the lidar beam at this time would have been 2.0 m south and 4.0 m above the sampling line inlet (5.58 az. 0.70 elv.). The substantial difference

between the heights of the lidar beam and the sampling inlet is probably the primary reason for the difference in the magnitudes of the changes in the aerosol concentrations and the lidar signal during the wind burst. A word of caution is also in order here: although the correlation between the lidar signal and the particle concentrations looks good for this time period, a mathematical correlation will not appear very good because the relatively small signal change and the parcity of high signal levels destroys the overall correlation. Much better correlations were obtained on Friday when the beam was oriented closer to the inlet for longer periods during which the particle concentration changed appreciably.

In summary, time-resolved measurements of particle size distributions acquired during the Albuquerque tests demonstrated several impacts associated with changes in particle sizes and compositions. Somewhat to our surprise, the size distributions were fairly constant, with exceptions caused by sprinkler use and spinning vehicle tires. We attributed the similarity of the size distributions to the stirring action of the vehicle wakes and the dominance of entrained road dust. The total beam path was relatively short (400 m), in a single direction (parallel to the road), and maintained a relatively constant elevation above (13.5 ft) and distance from the road. Since no other local particulate sources such as fast food restaurants, construction equipment, industrial smokestacks, etc. were located upwind of the test area, one can reasonably assume the particle size distribution and composition was essentially constant along the entire beam path. Thus, with the exception of the particle events, one would probably be justified in using a single measure of particle size distribution and assuming it to apply at all points along the short length of beam.

In general roadside tests, the lidar image would display a qualitative picture of the distribution of particle number concentrations, but determination of quantitative aerosol concentrations would require additional measurements of size and composition distributions. For example, one would expect large particle concentrations to drop off slowly with increasing elevation or distance from the roadway due to natural settling effects. Knowledge of the change in size distribution would be important if accurate number concentrations were to be recovered, for instance in a vertical slice. A set of size distribution measurements could be taken as a function height, and the time average values at each elevation could be used to arrive at a generally applicable vertical size distribution function which could then be applied over the image.

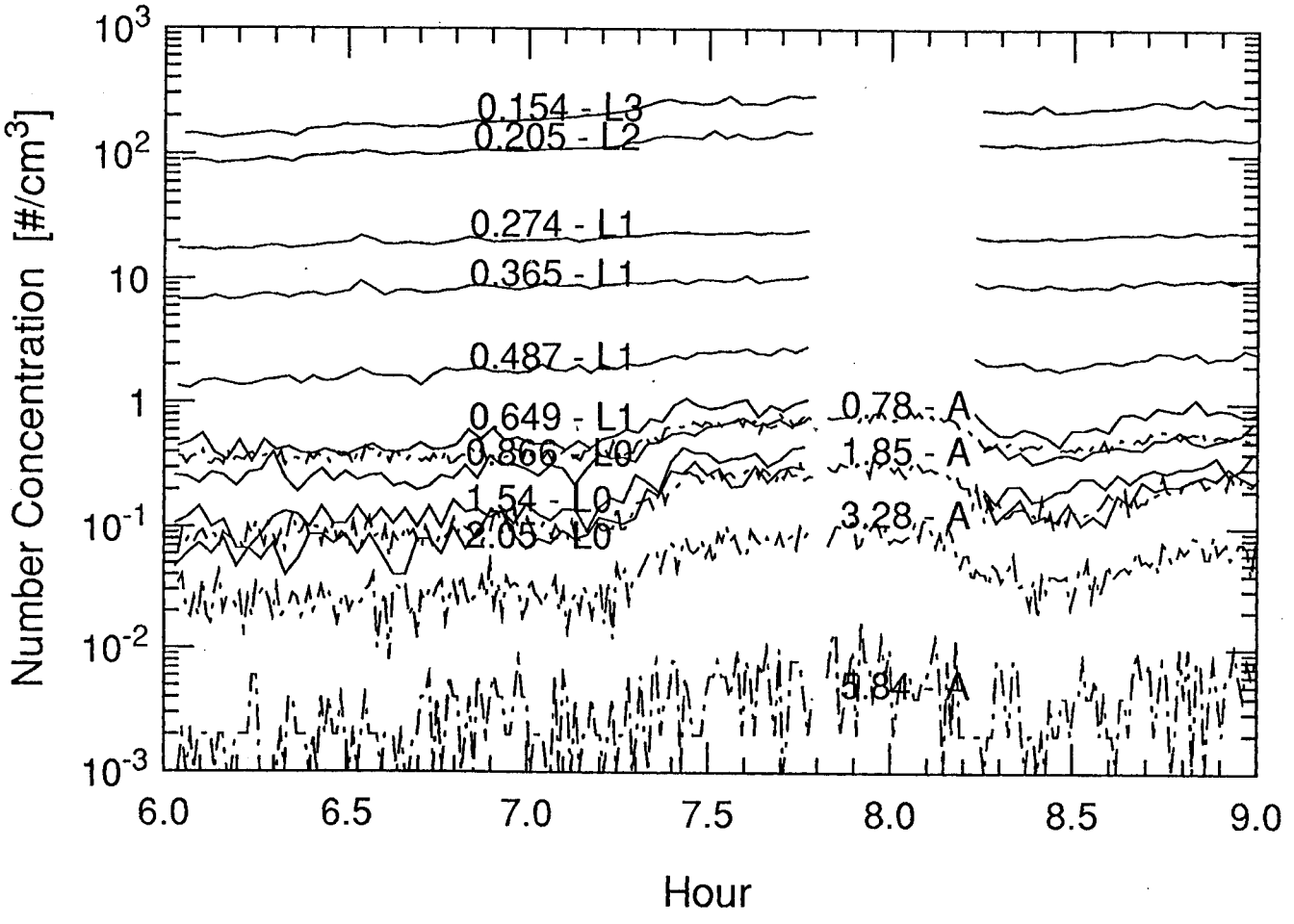

Fig. 9: Particle concentration histories during early morning hours, Friday, 6/23, north of Gibson Blvd. The legends on the traces give the logarithmic midpoint of the various size bins using approximate physical particle diameters in μm. "L#" indicates that the data was taken by the LASX instrument on range "#", while "A" indicates the data was taken using the APS.

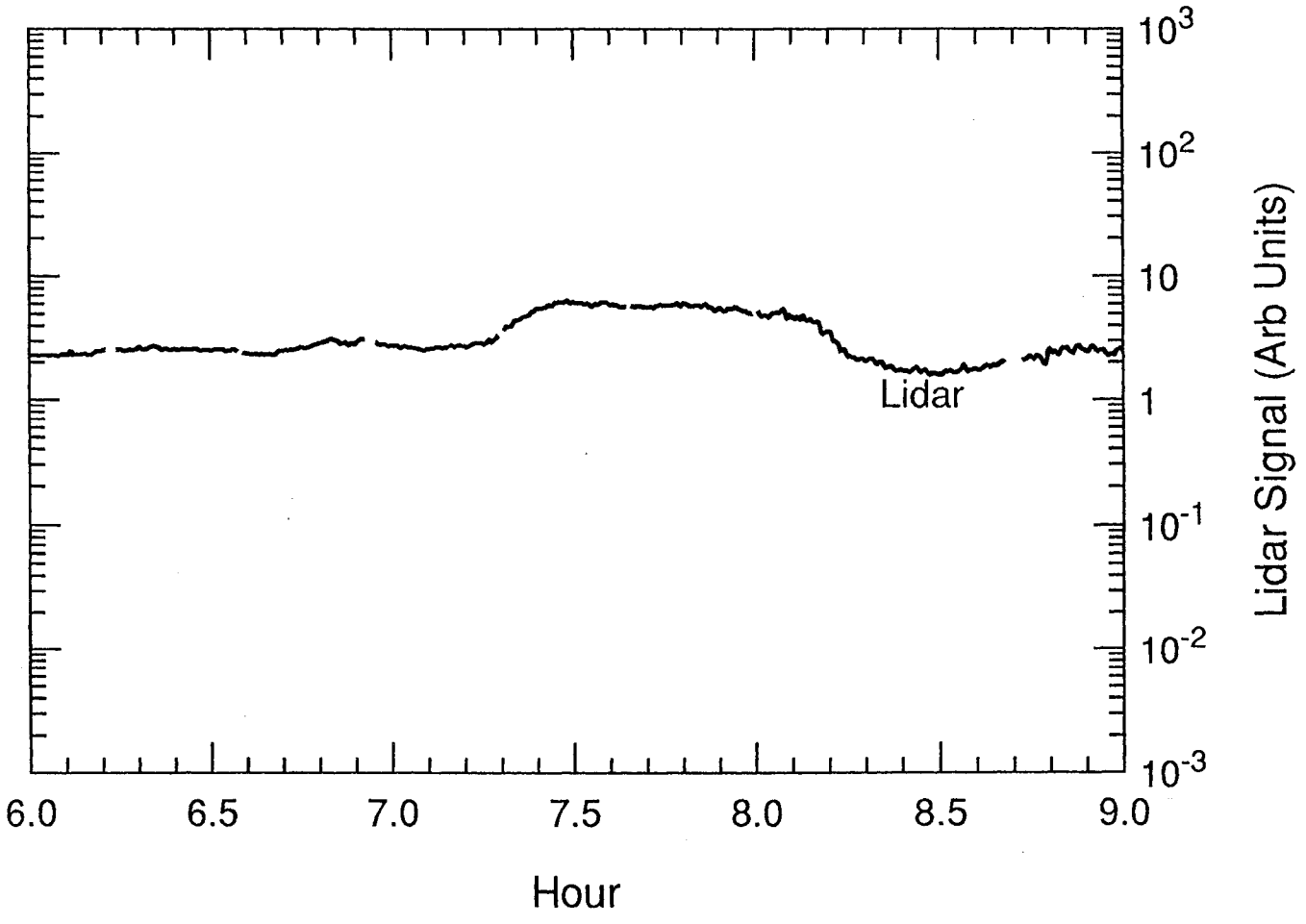

Fig. 10(a): Running 30 second average of lidar signal during early morning hours, Friday, 6/23. The location of the signal volume is north of Gibson Blvd., slightly north of and above the sampling inlet (see text).

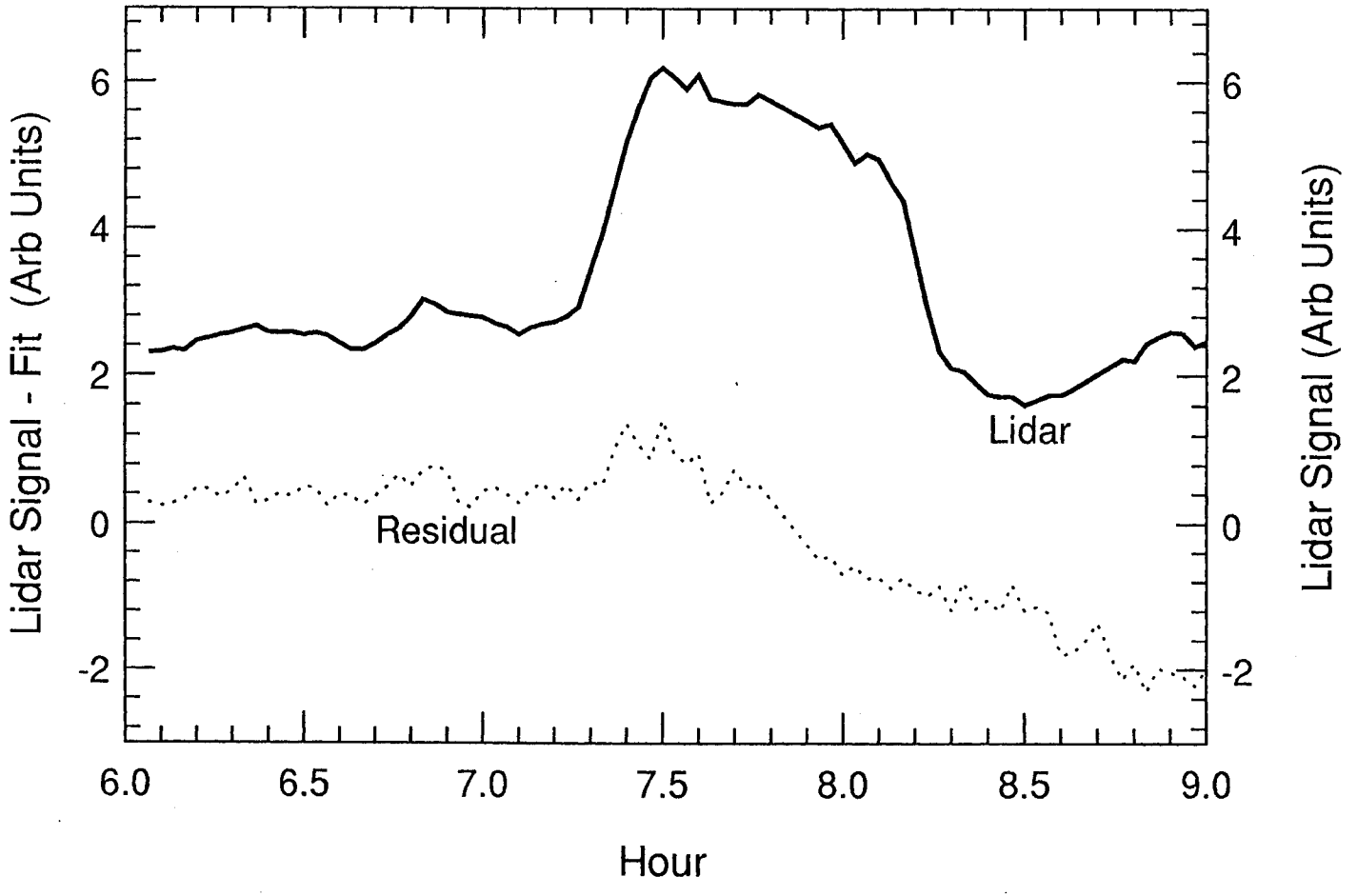

Fig. 10(b): Lidar signal repeated from (a) along with residual difference between the lidar signal and linear fit to number concentration of 1.85 μm from 7:00-8:30 (see Table 6).

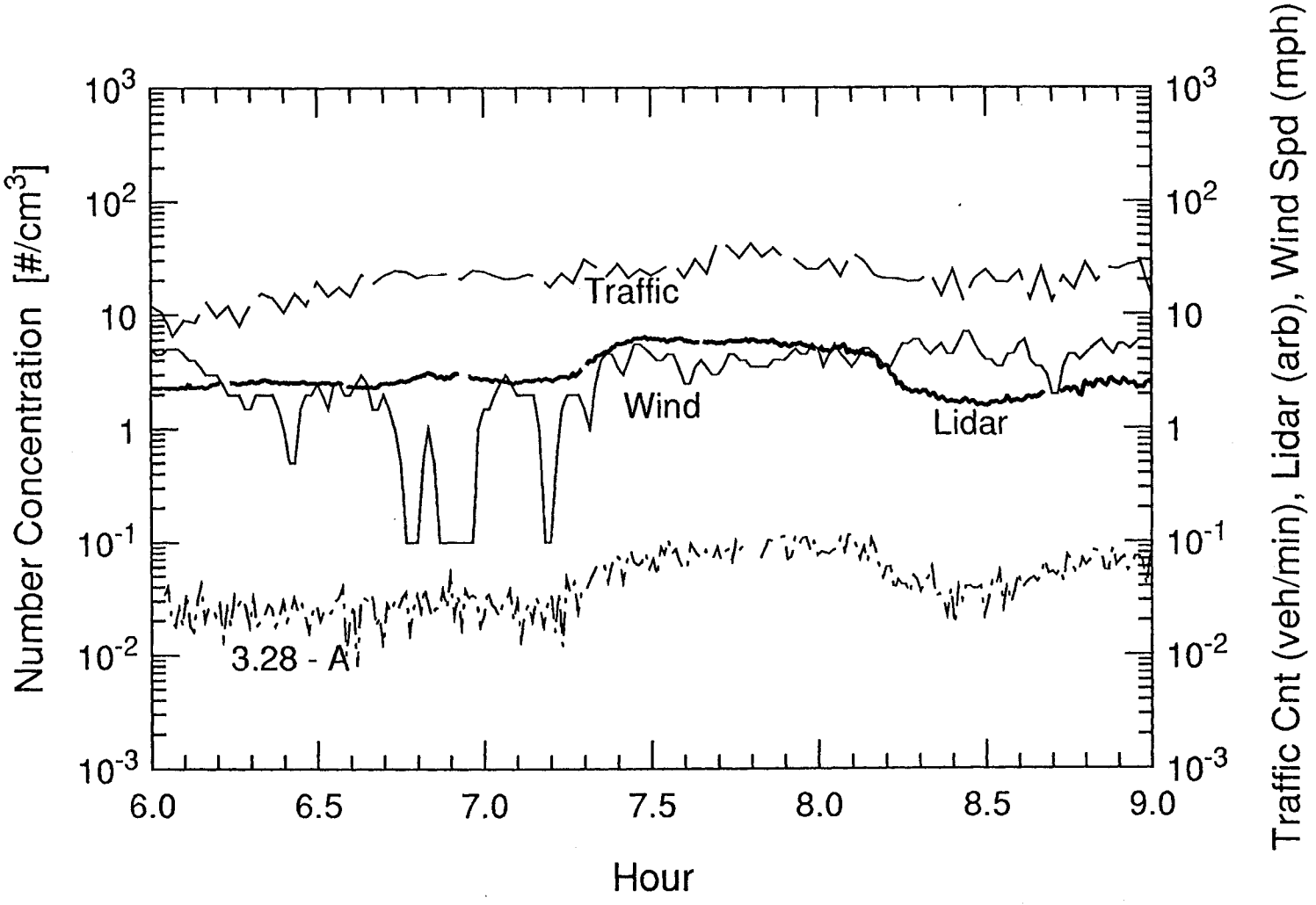

Fig. 11: Comparison of total traffic count (both directions) on Gibson Blvd, wind speed, lidar signal, and 3.28 μm particle concentration histories during early morning hours, Friday, 6/23, north of Gibson Blvd. Logarithmic scale used for visualization of correlation (wind speeds < 0.5 mph instrument resolution shown as 0.1 mph).

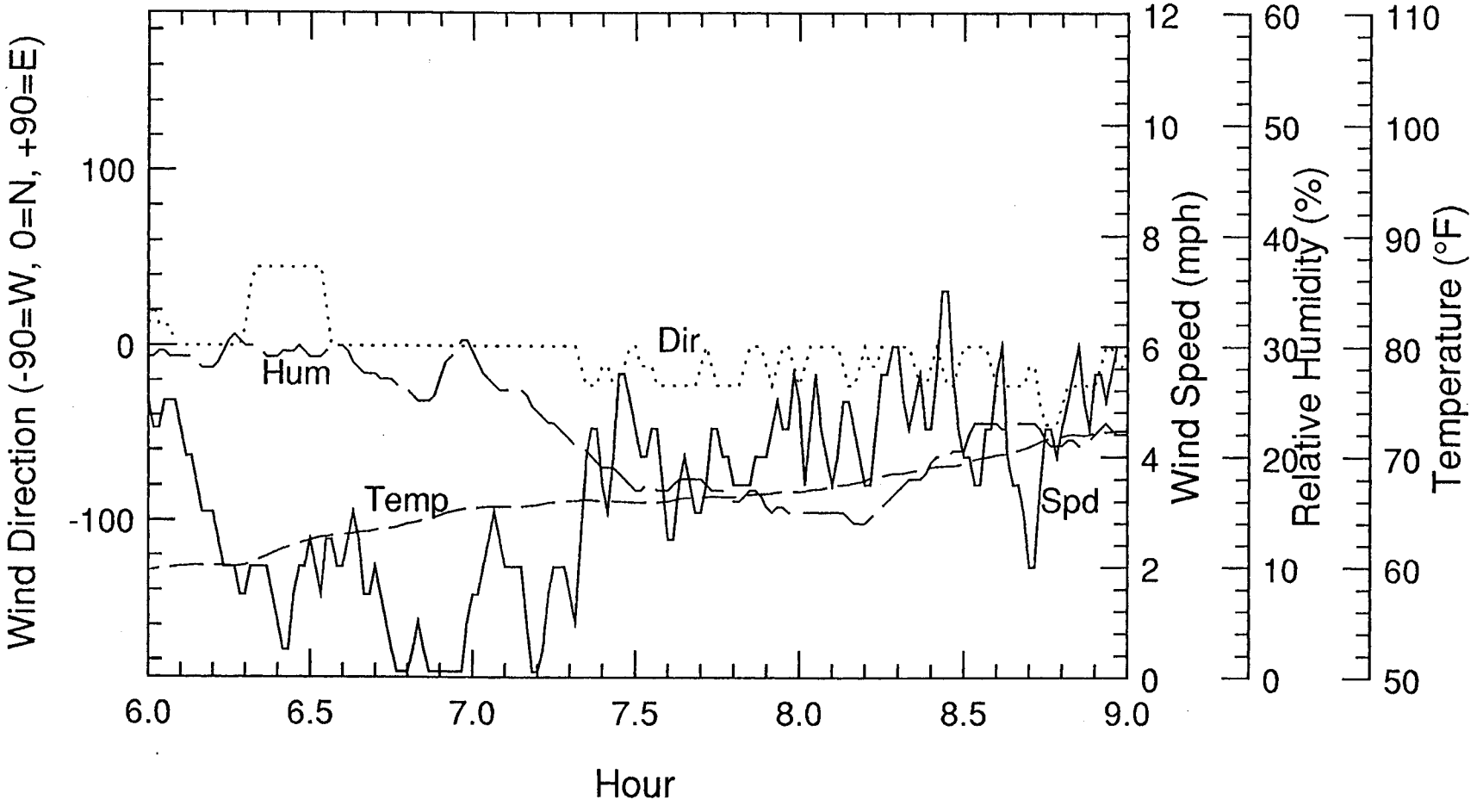

Fig. 12: Temperature, relative humidity, wind direction (0 => out of north, -90 = out of west, +90 = out of east, ±180 - out of south), and wind speed data for early morning hours, Friday, 6/23, north of Gibson Blvd. at a height of 20 ft.

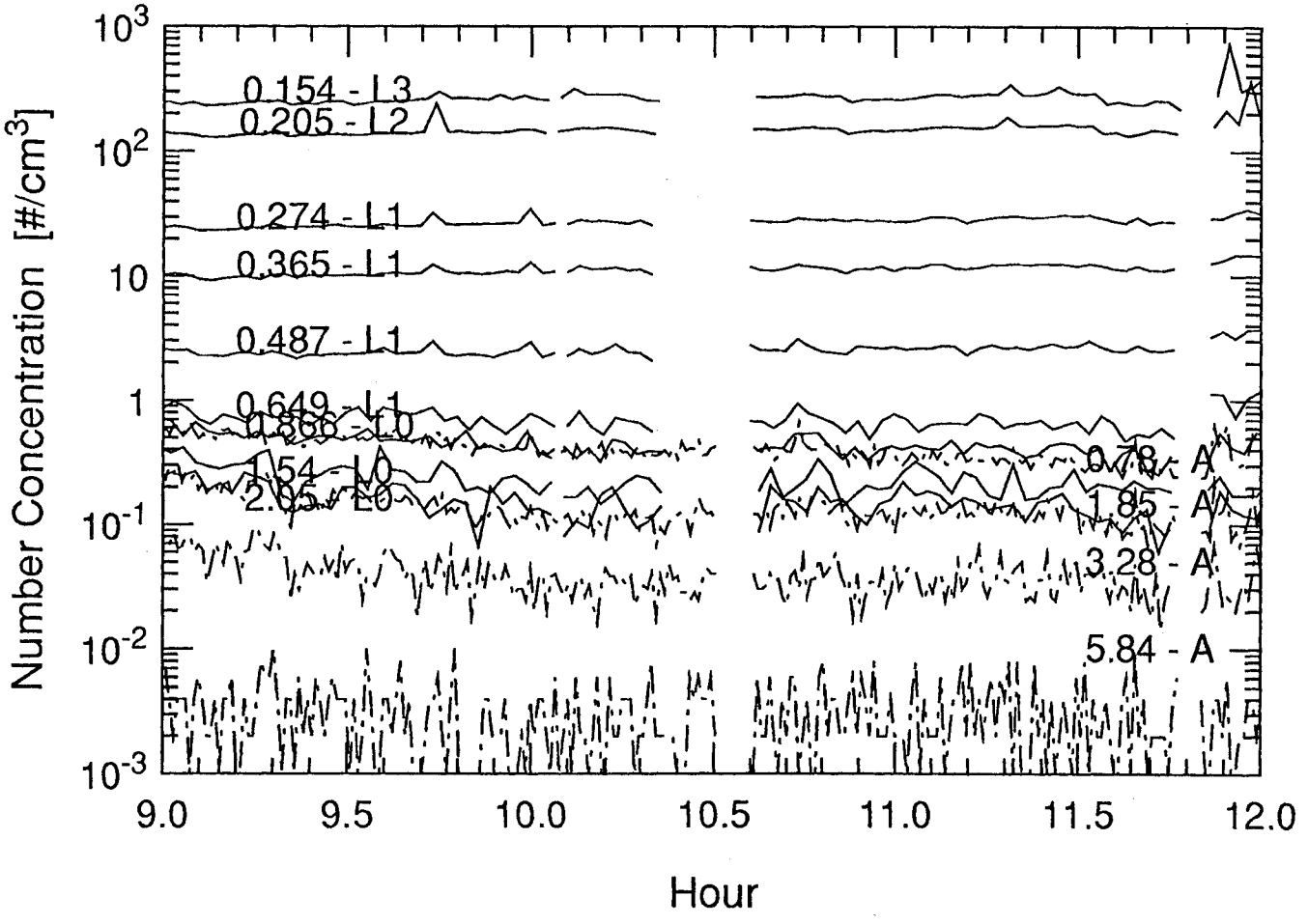

Fig. 13: Particle concentration histories during mid-morning hours, Friday, 6/23, north of Gibson Blvd. The legends on the traces give the logarithmic midpoint of the various size bins using physical particle diameters in μm. "L#" indicates that the data was taken by the LASX instrument on range "#", while "A" indicates the data was taken using the APS.

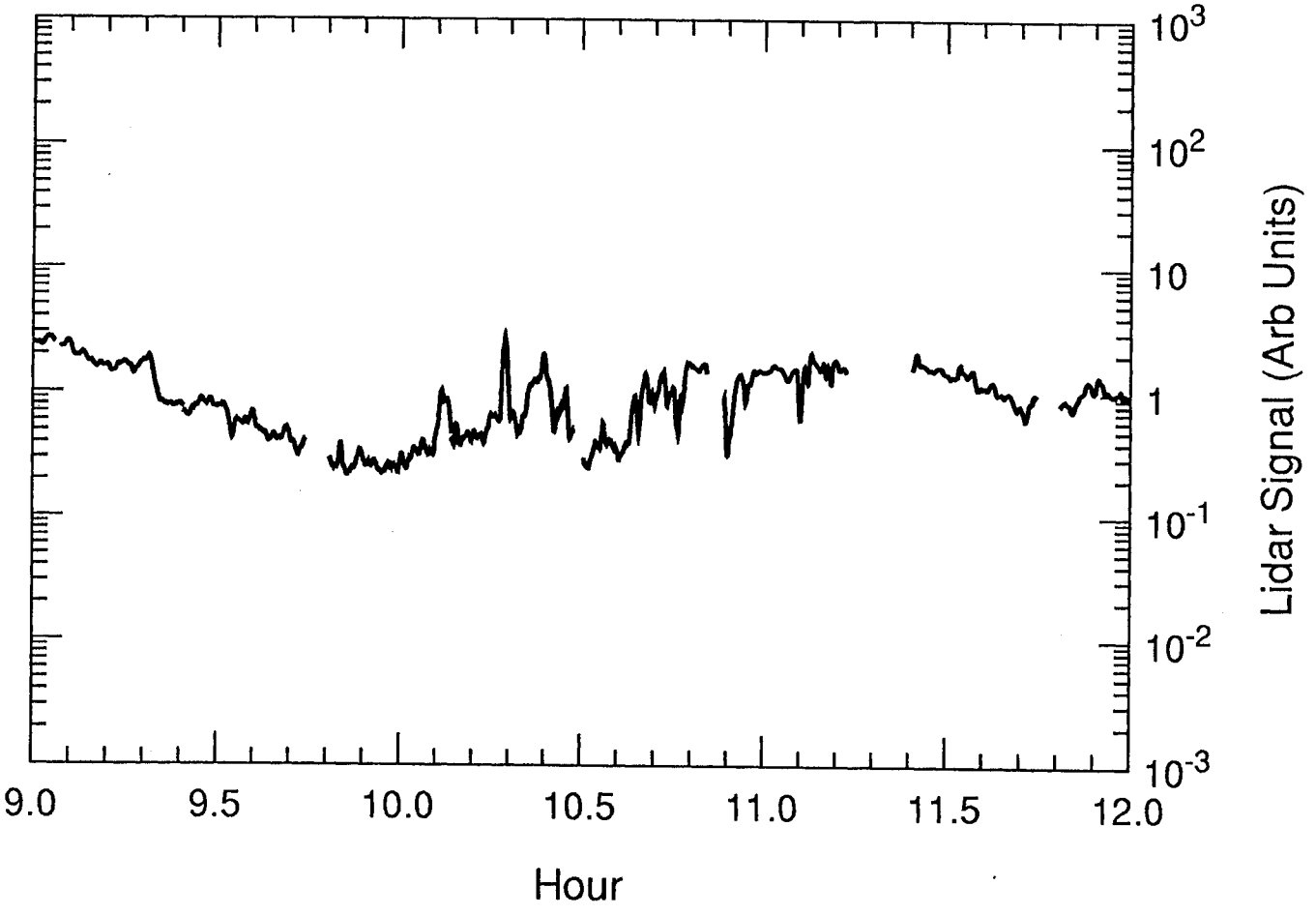

Fig. 14: Running 30 second average of lidar signal during mid-morning hours, Friday, 6/23. Signal volume is north of Gibson Blvd., slightly north, west, and above particle sampling inlet (see text).

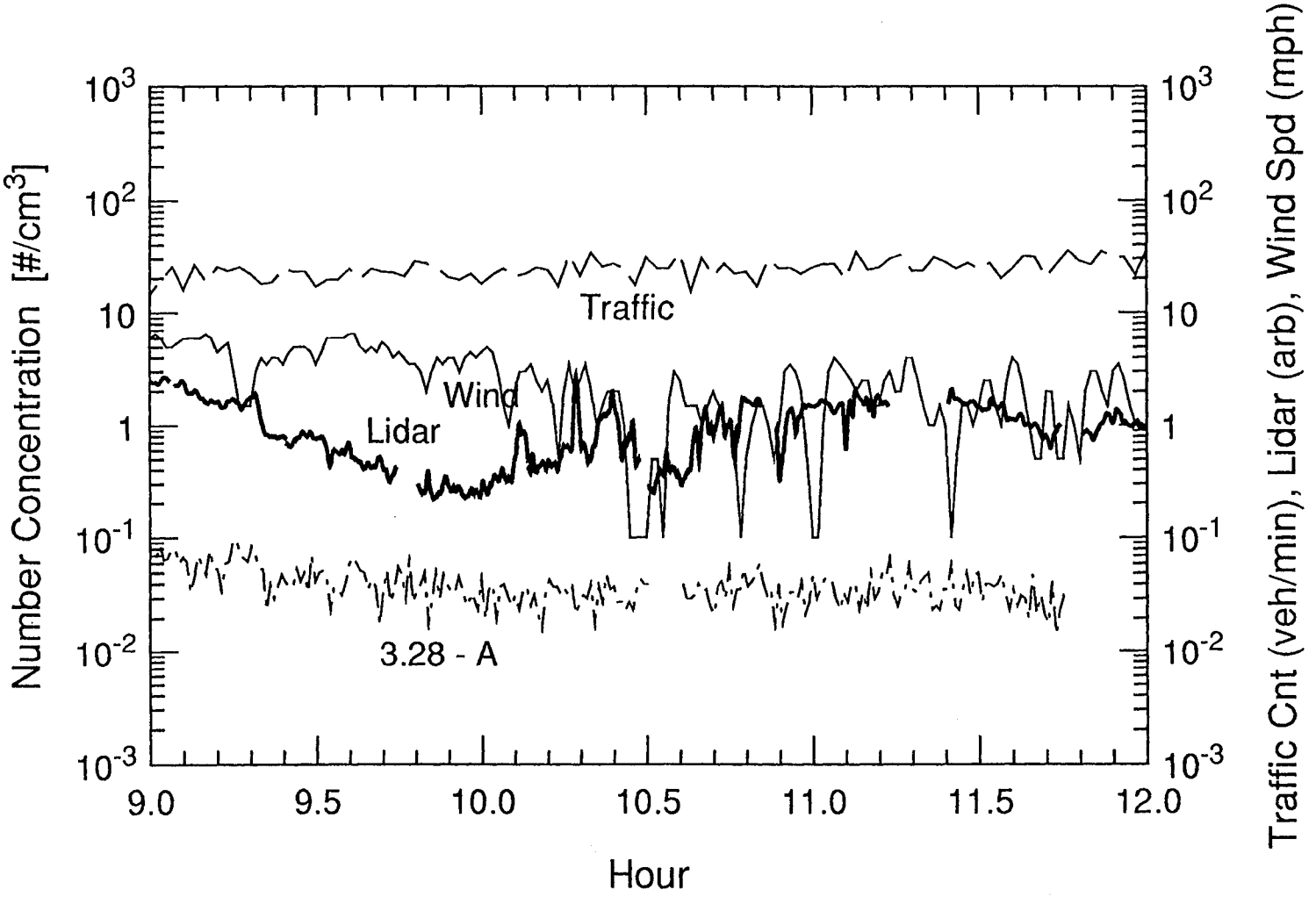

Fig. 15: Comparison of total traffic count (both directions) on Gibson Blvd, wind speed, lidar signal, and 3.28 μm particle concentration histories during mid-morning hours, Friday, 6/23, north of Gibson Blvd. Logarithmic scale used for visualization of correlation (wind speeds < 0.5 mph instrument resolution shown as 0.1 mph).

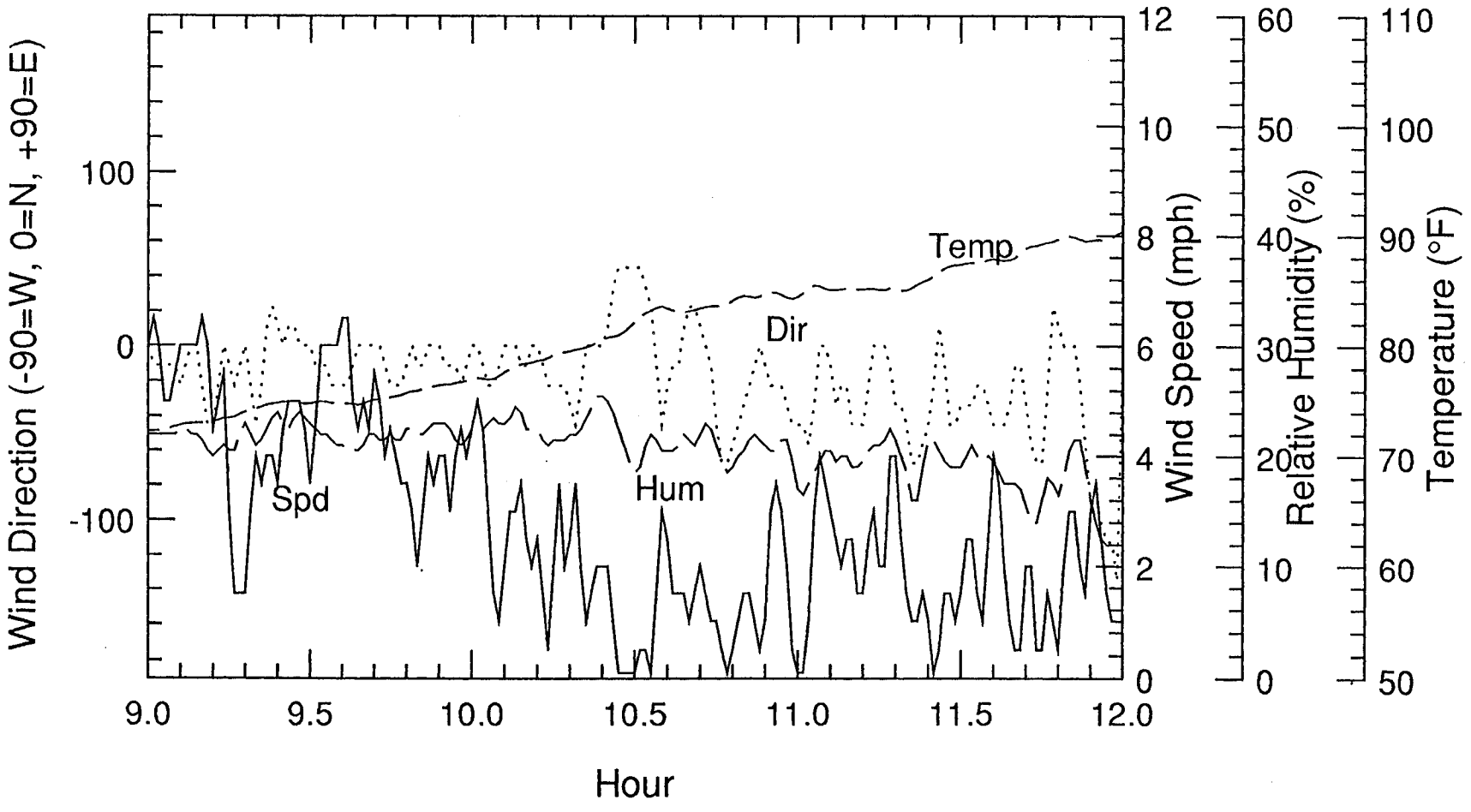

Fig. 16: Temperature, relative humidity, wind direction (0 => out of north, -90 = out of west, +90 = out of east, ±180 - out of south), and wind speed data for mid-morning hours, Friday, 6/23, north of Gibson Blvd. at a height of 20 ft.

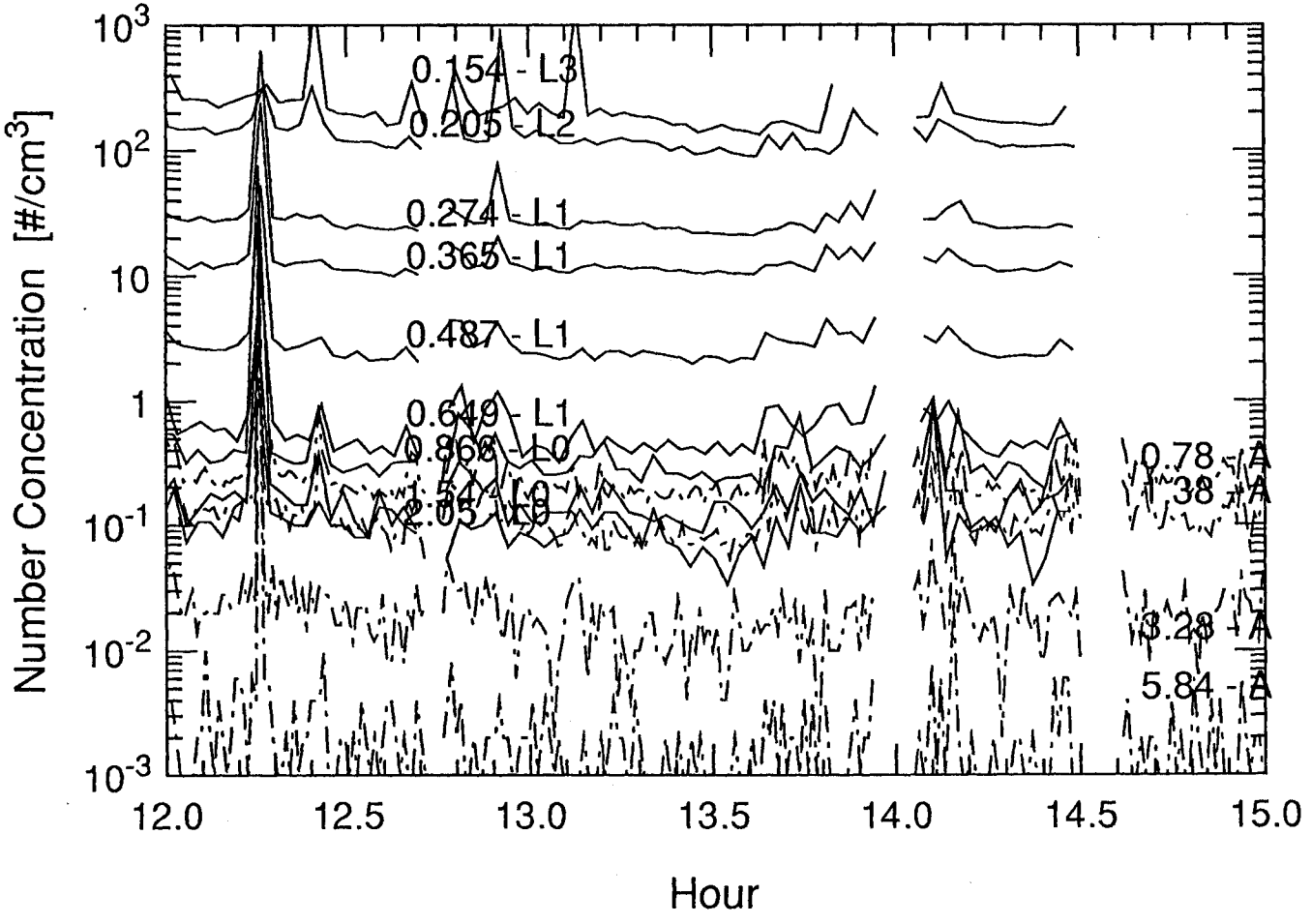

Fig. 17: Particle concentration histories during early afternoon hours, Friday, 6/23, north of Gibson Blvd. The legends on the traces give the logarithmic midpoint of the various size bins using physical particle diameters in μm. "L#" indicates that the data was taken by the LASX instrument on range "#", while "A" indicates the data was taken using the APS.

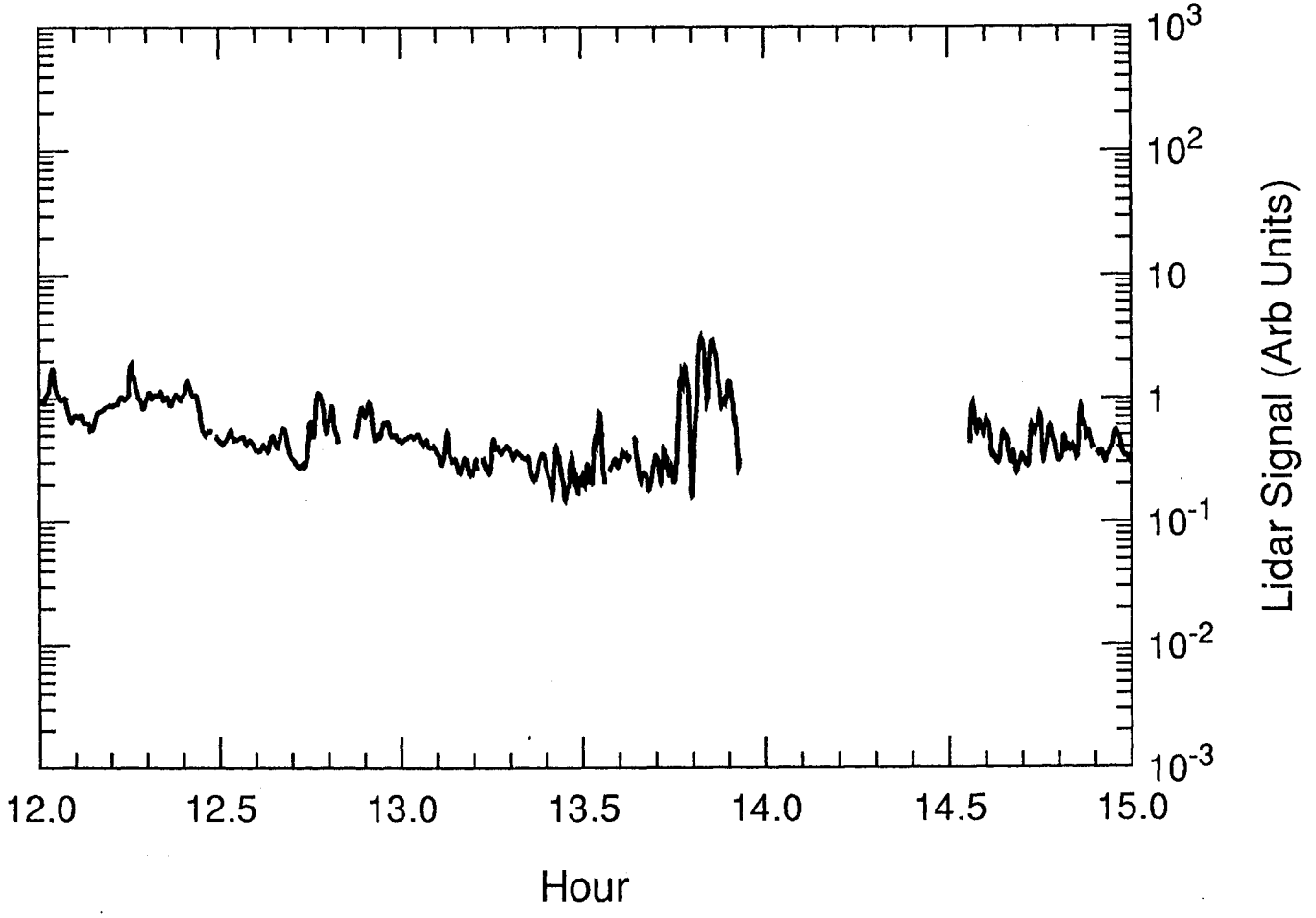

Fig. 18: Running 30 second average of lidar signal during early afternoon hours, Friday, 6/23. Signal volume is north of Gibson Blvd., slightly north, west, and above particle sampling inlet (see text).

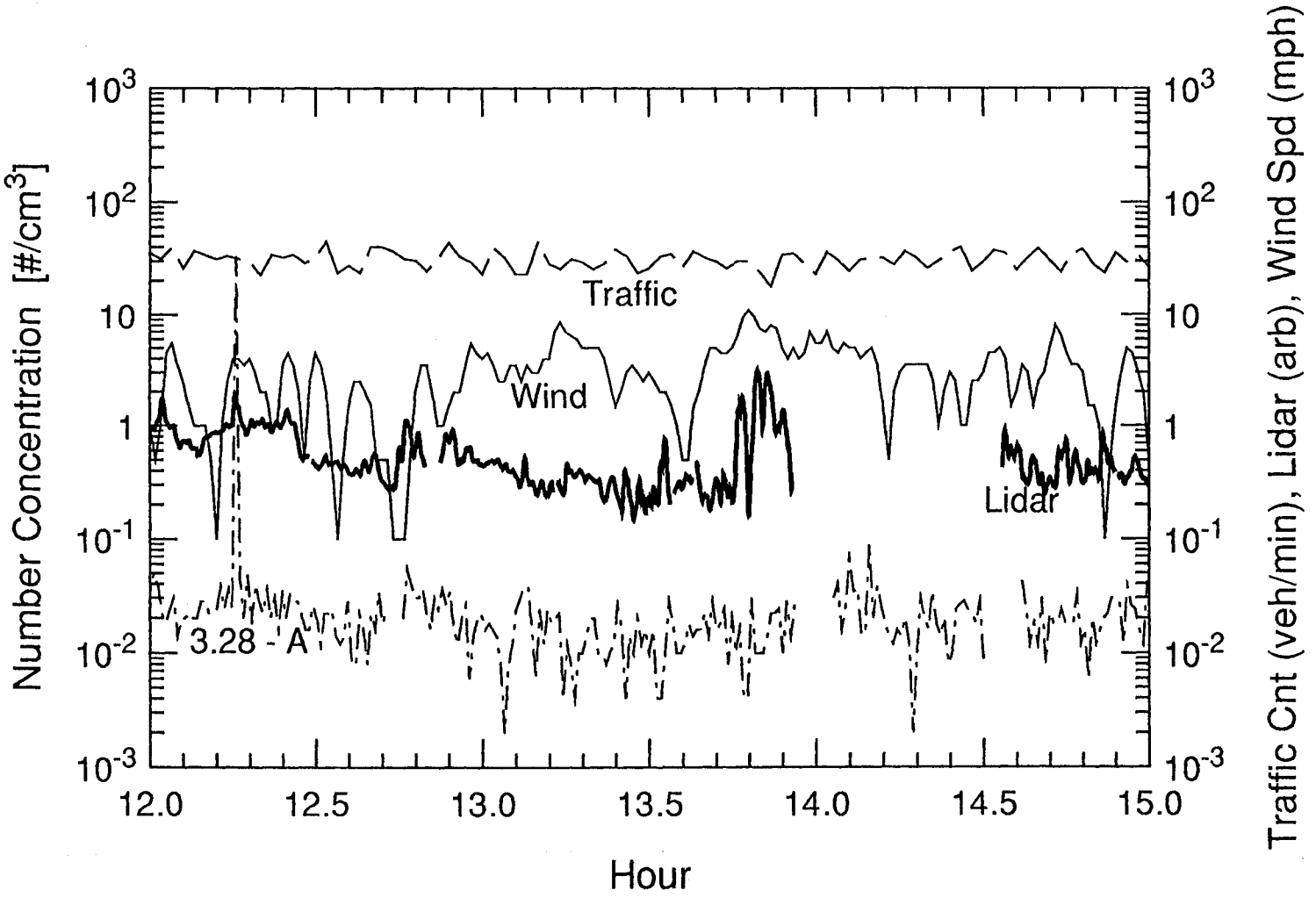

Fig. 19: Comparison of total traffic count (both directions) on Gibson Blvd, wind speed, lidar signal, and 3.28 μm particle concentration histories during early afternoon hours, Friday, 6/23, north of Gibson Blvd. Logarithmic scale used for visualization of correlation (wind speeds < 0.5 mph instrument resolution shown as 0.1 mph).

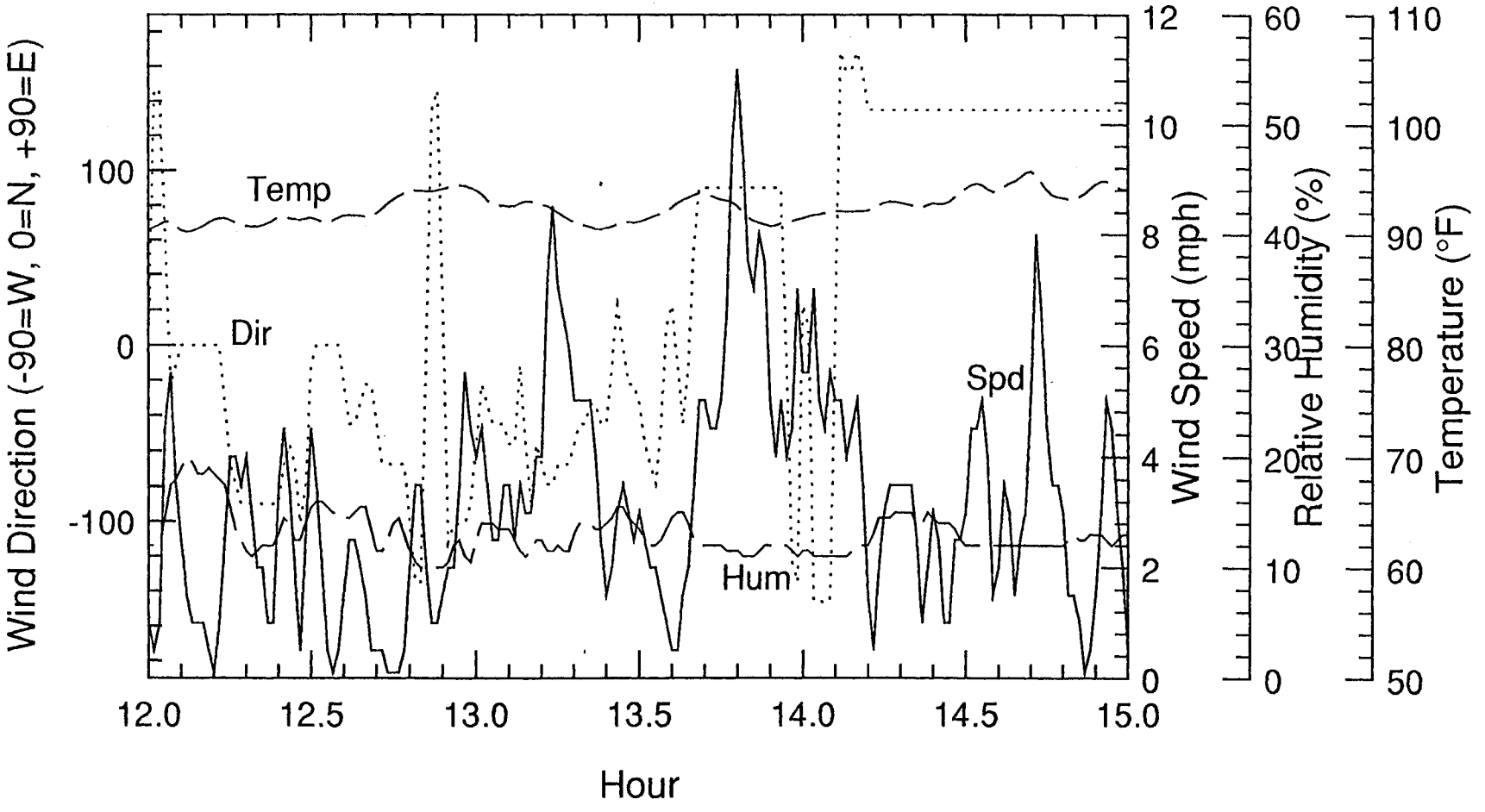

Fig. 20: Temperature, relative humidity, wind direction (0 => out of north, -90 = out of west, +90 = out of east, ±180 - out of south), and wind speed data for early afternoon hours, Friday, 6/23, north of Gibson Blvd. at a height of 20 ft.

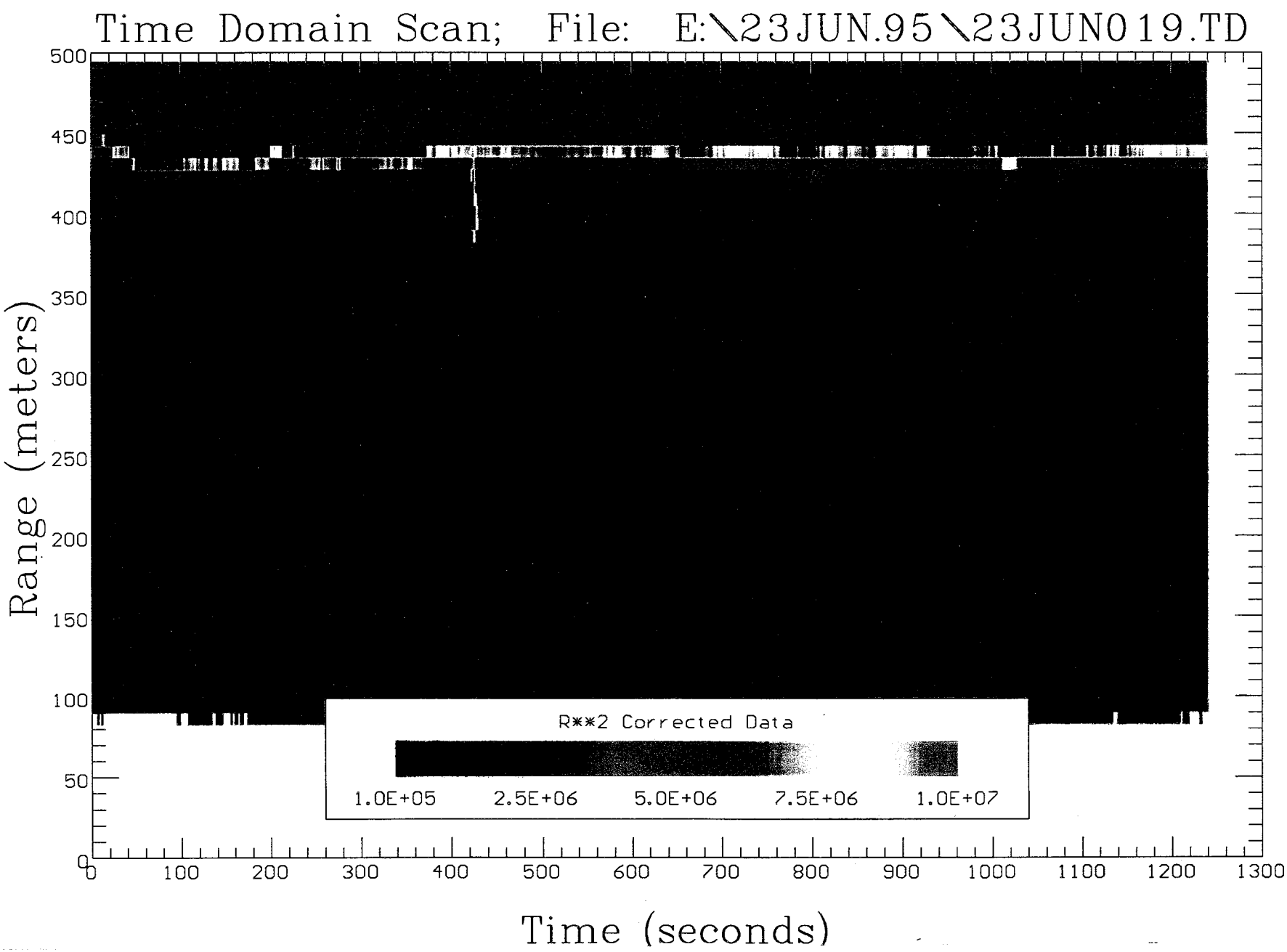

Fig. 21(a): Color-contour plot of lidar signal strength versus position during early afternoon hours, Friday, 6/23, as would be displayed in real-time during lidar data acquisition. Sharp spatio-temporal distribution of plume from wheel-spinning incident.

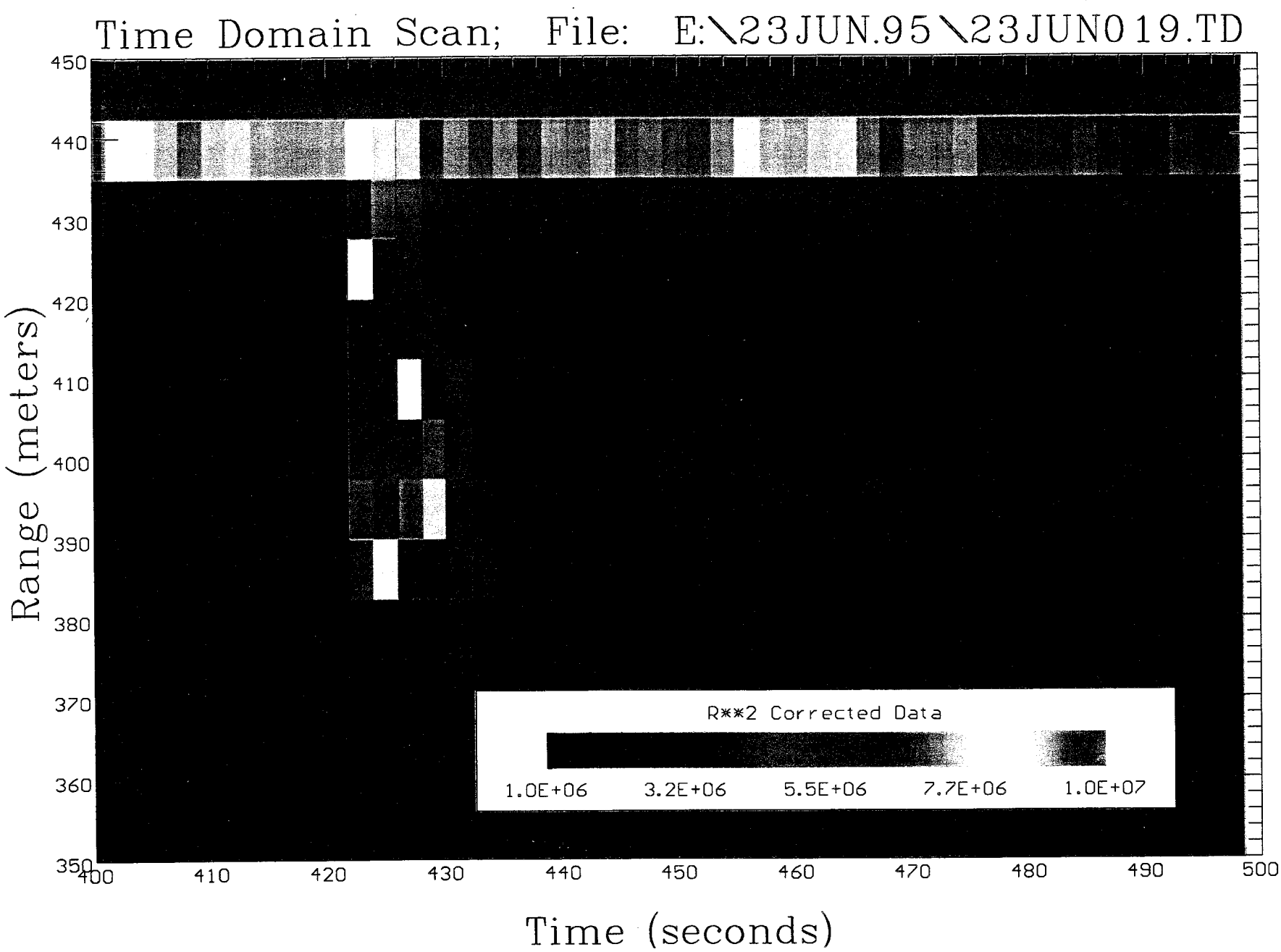

Fig. 21(b): Blow up of region containing concentrated aerosol plume from wheel-spinning incident. The 7.5 m resolution shown is the maximum available from the orignal data set. (Note: the low end of the color contour map has been changed.)

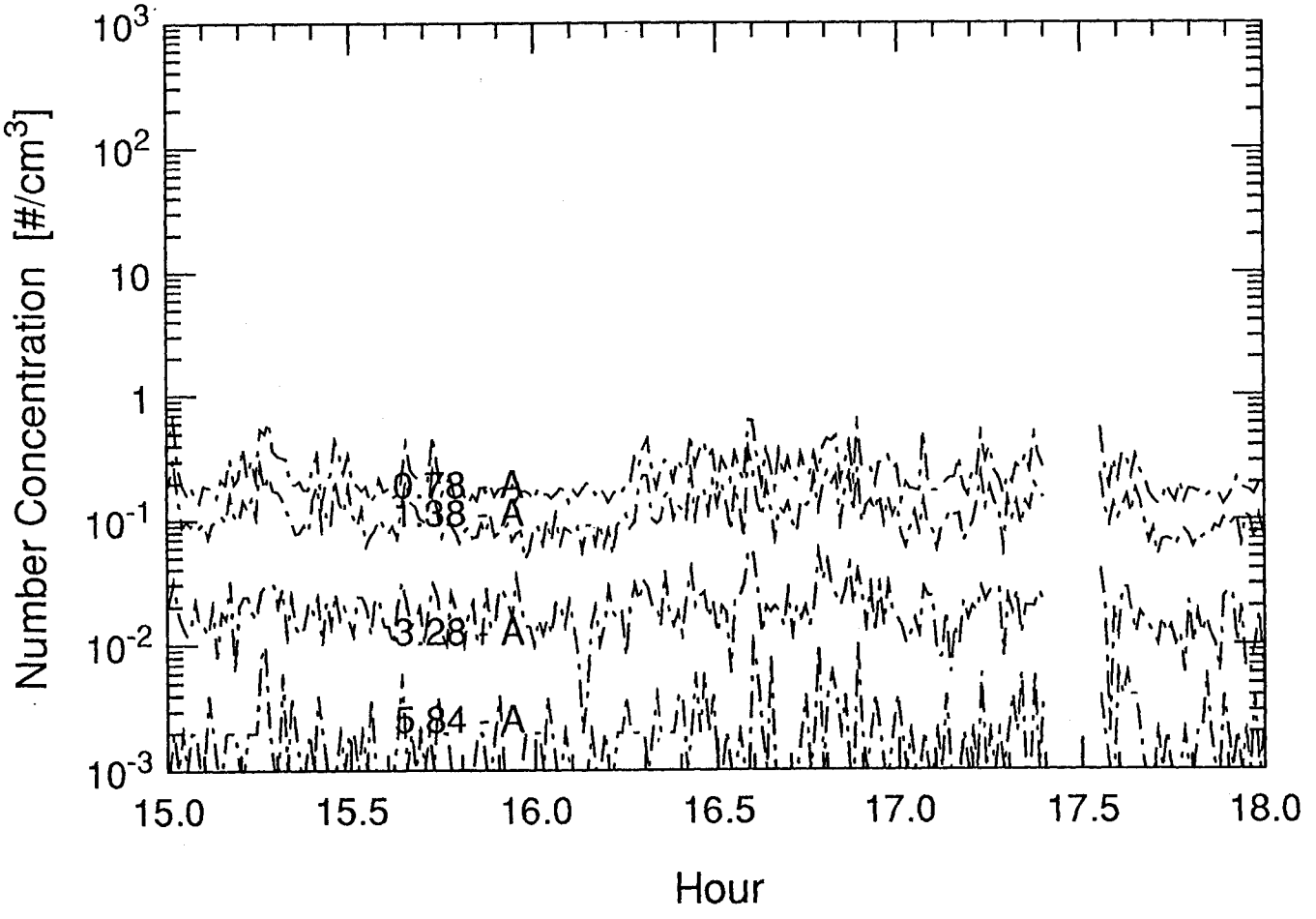

Fig. 22: Particle concentration histories measured by APS during late afternoon hours, Friday, 6/23, north of Gibson Blvd. The legends on the traces give the logarithmic midpoint diameters (in μm) of the various size bins. Aerodynamic diameters were converted to equivalent homogeneous spherical diameters assuming the density of particle material was 2.2 g/cm^3.

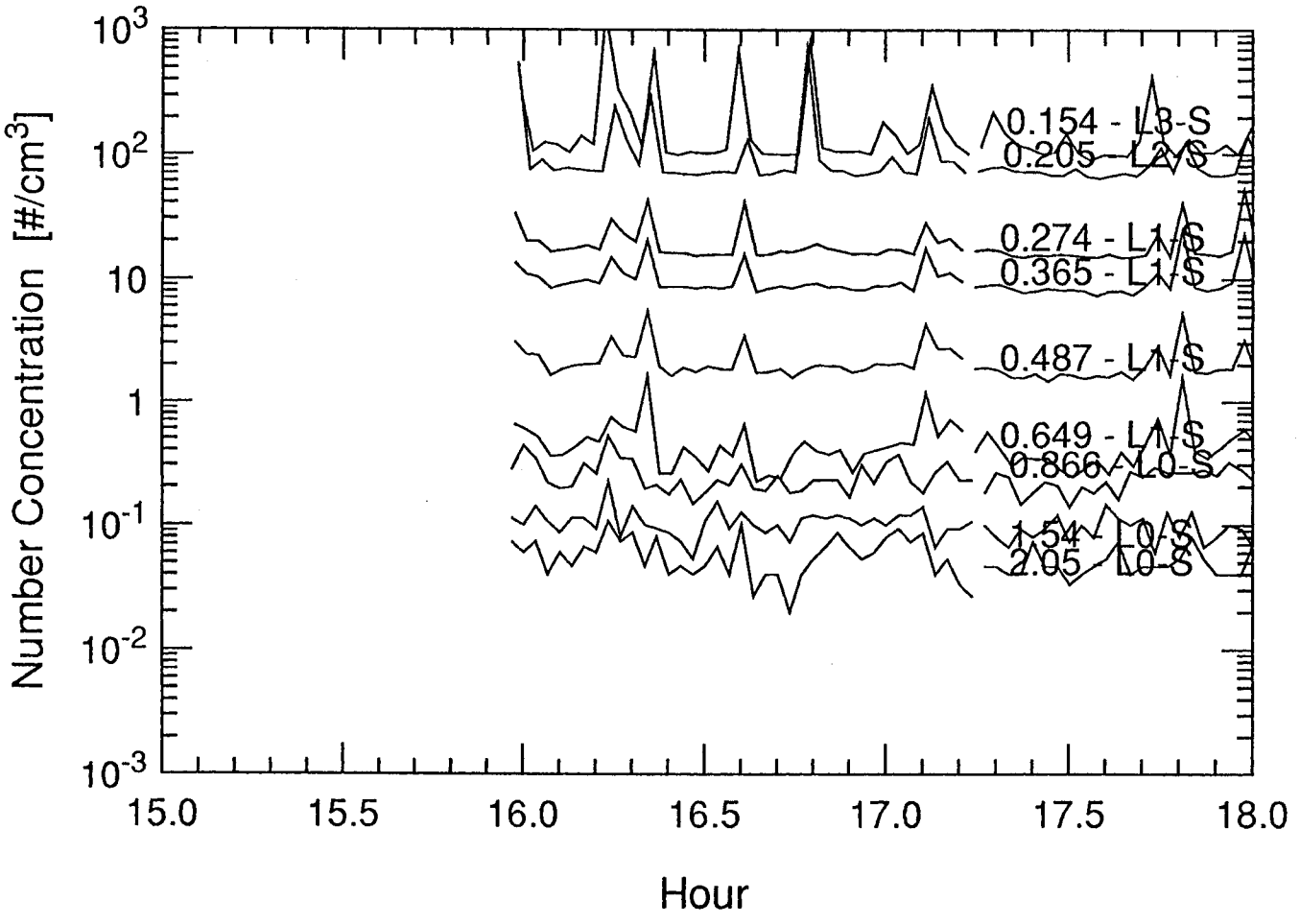

Fig. 23: Particle concentration histories measured by LASX during late afternoon hours, Friday, 6/23, south of Gibson Blvd. The legends on the traces give the logarithmic midpoint diameters (in μm) of the various size bins.

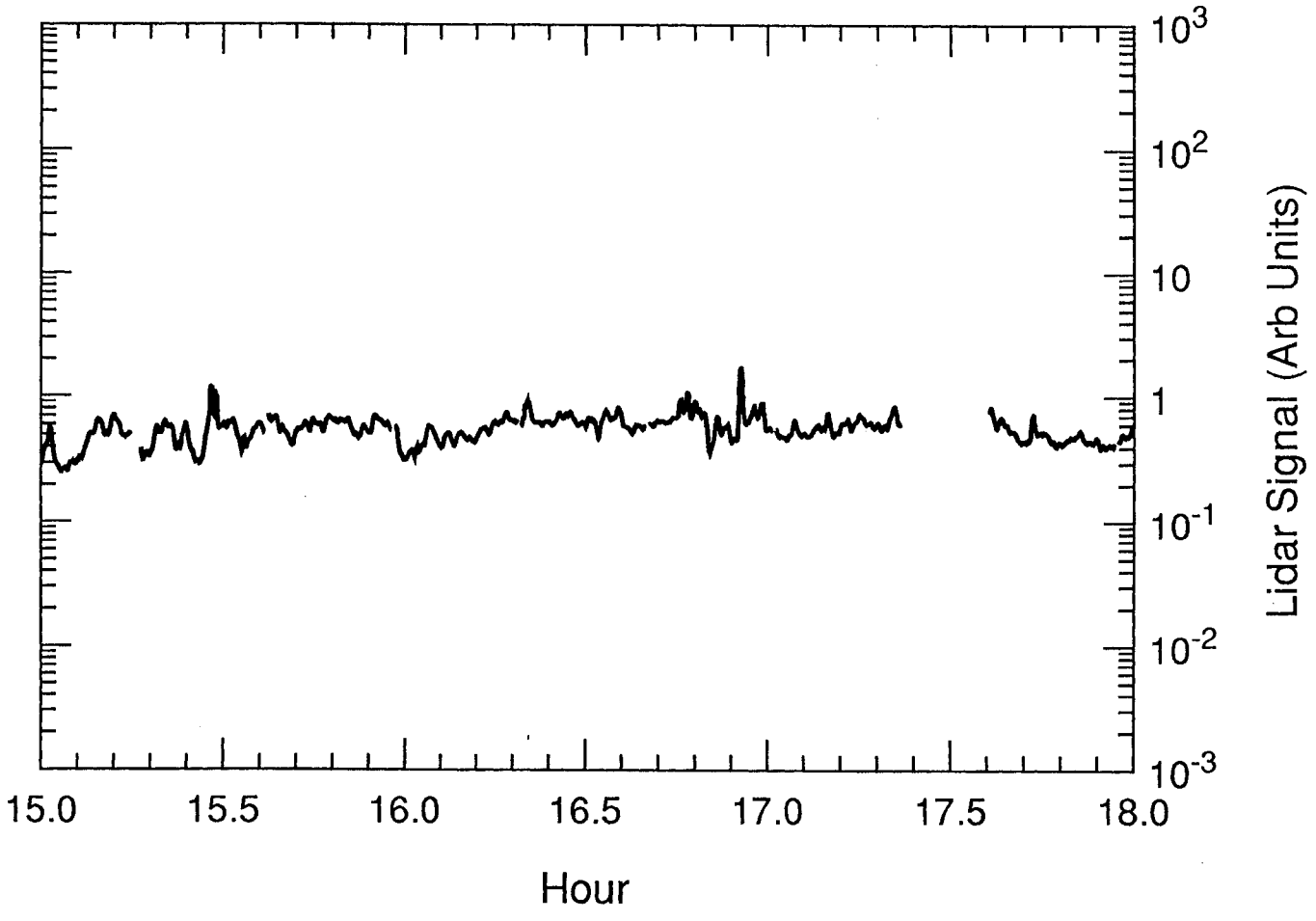

Fig. 24: Running 30 second average of lidar signal during late afternoon hours, Friday, 6/23. Signal volume is north of Gibson Blvd., slightly north, west, and above particle sampling inlet (see text).

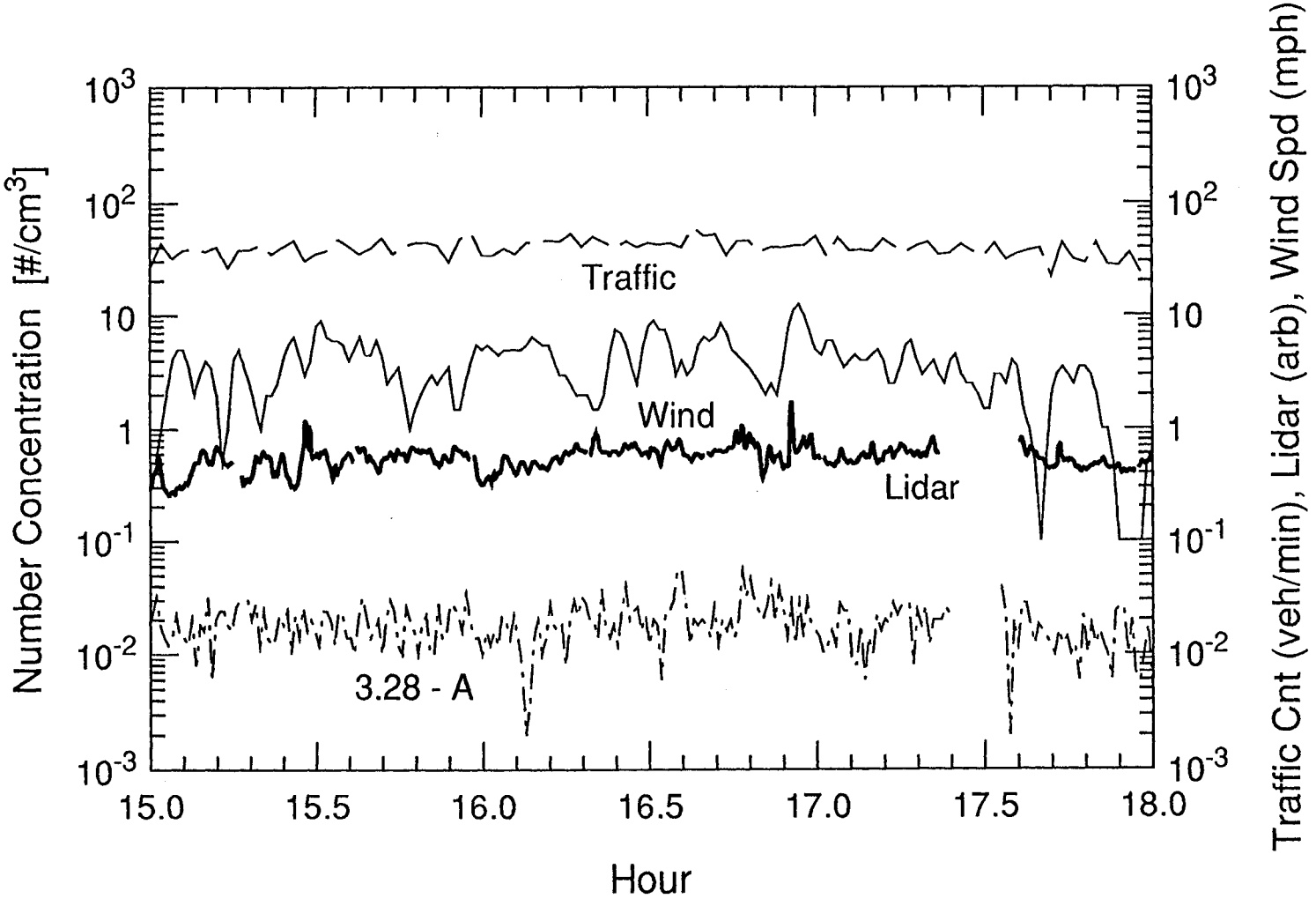

Fig. 25: Comparison of total traffic count (both directions) on Gibson Blvd, wind speed, lidar signal, and 3.28 μm particle concentration histories during late afternoon hours, Friday, 6/23, north of Gibson Blvd. Logarithmic scale used for visualization of correlation (wind speeds < 0.5 mph instrument resolution shown as 0.1 mph).

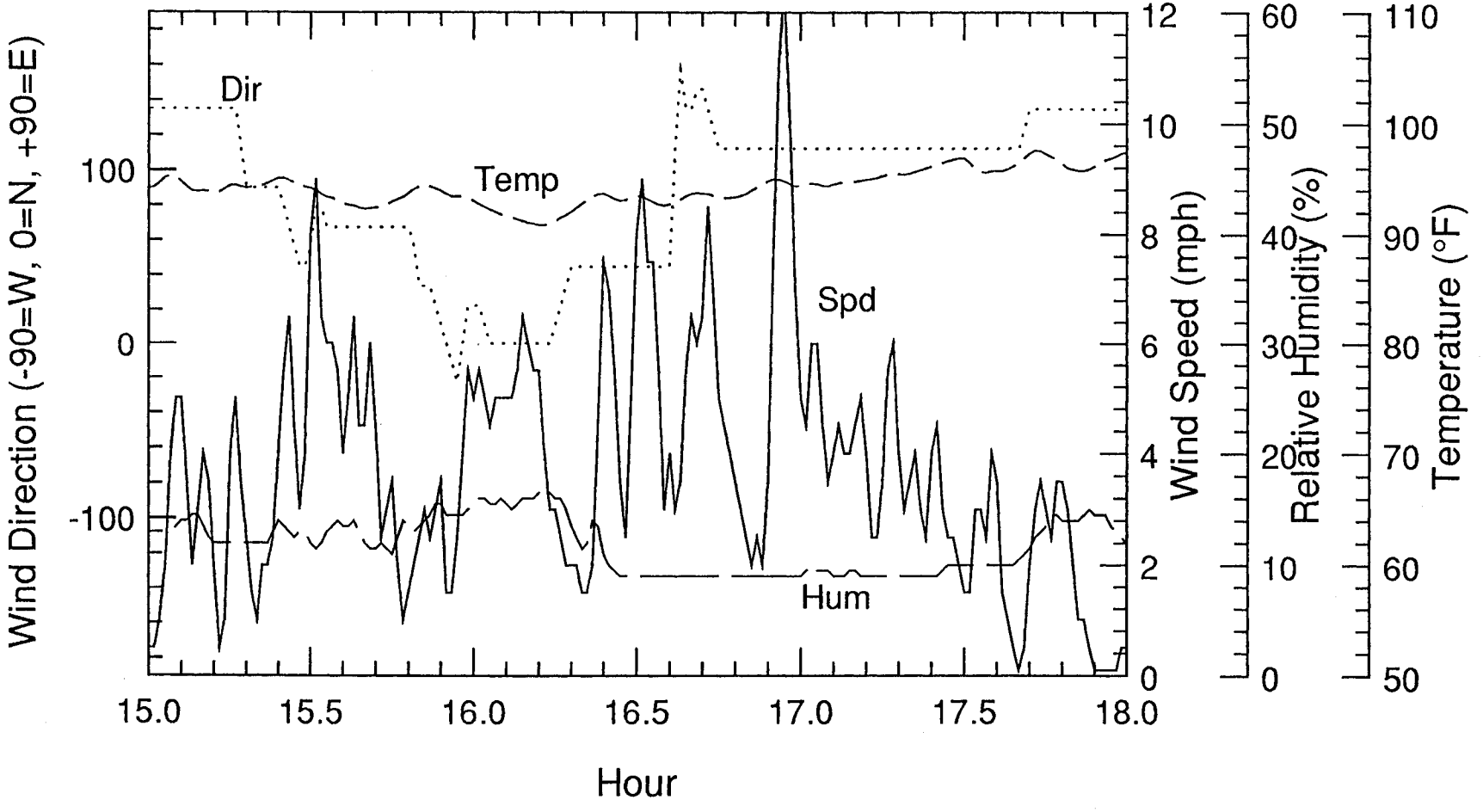

Fig. 26: Temperature, relative humidity, wind direction (0 => out of north, -90 = out of west, +90 = out of east, ±180 - out of south), and wind speed data for late afternoon hours, Friday, 6/23, north of Gibson Blvd. at a height of 20 ft.

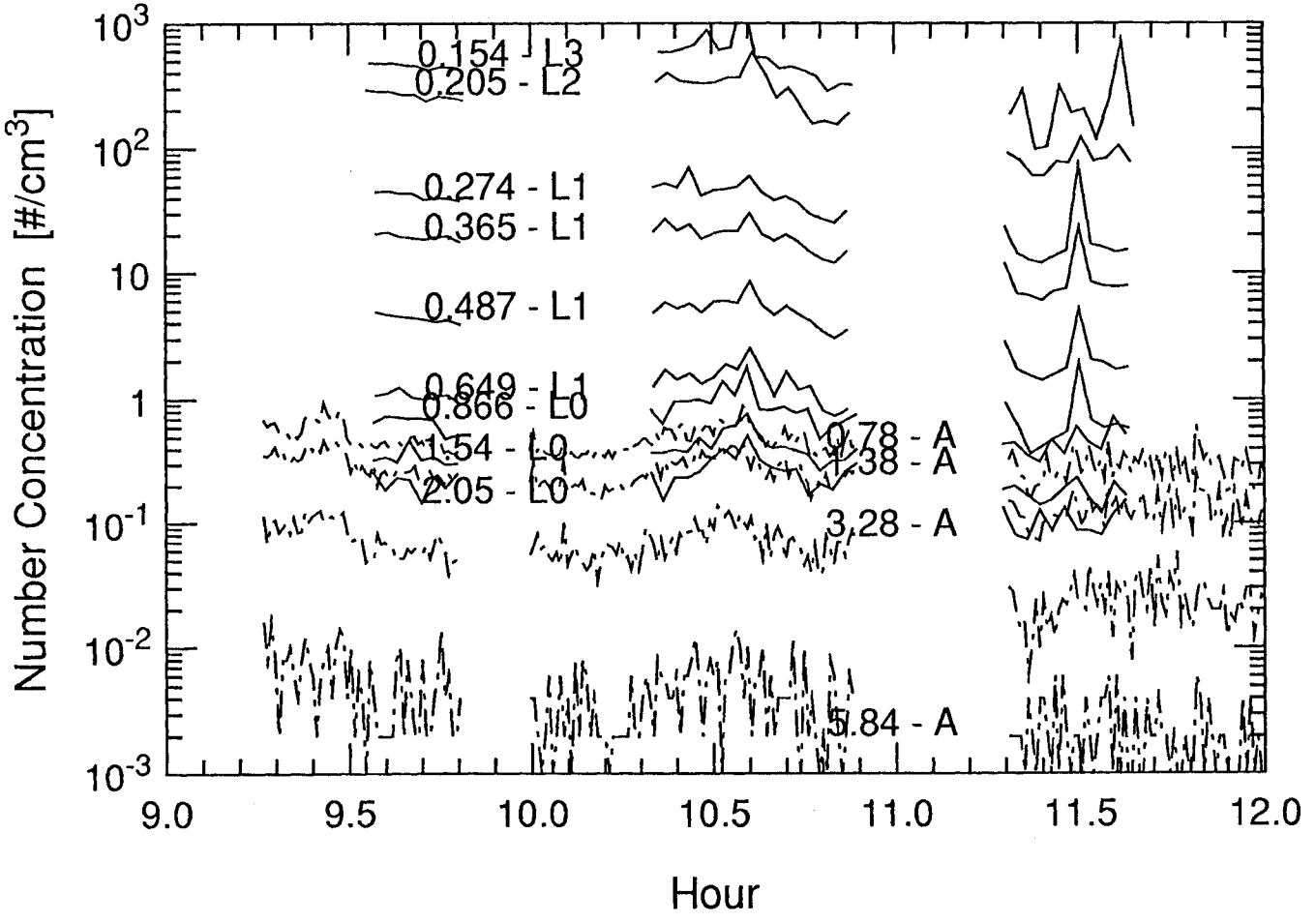

Fig. 27: Particle concentration histories during mid-morning hours, Thursday, 6/22, north of Gibson Blvd. The legends on the traces give the logarithmic midpoint of the various size bins using physical particle diameters in μm. "L#" indicates that the data was taken by the LASX instrument on range "#", while "A" indicates the data was taken using the APS.

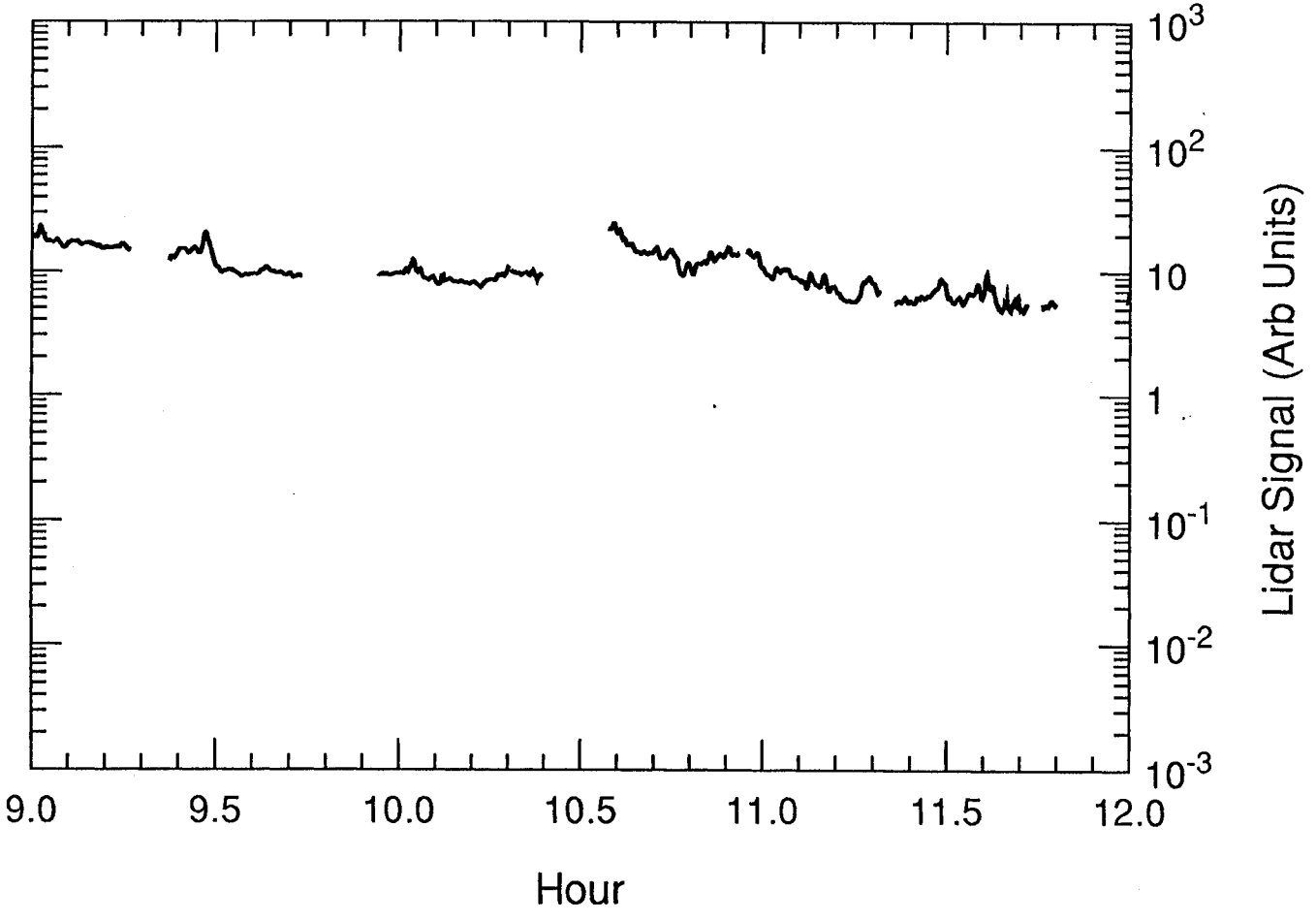

Fig. 28: Running 30 second average of lidar signal during mid-morning hours, Thursday, 6/22. Signal volume is north of Gibson Blvd., slightly north, west, and above particle sampling inlet (see text).

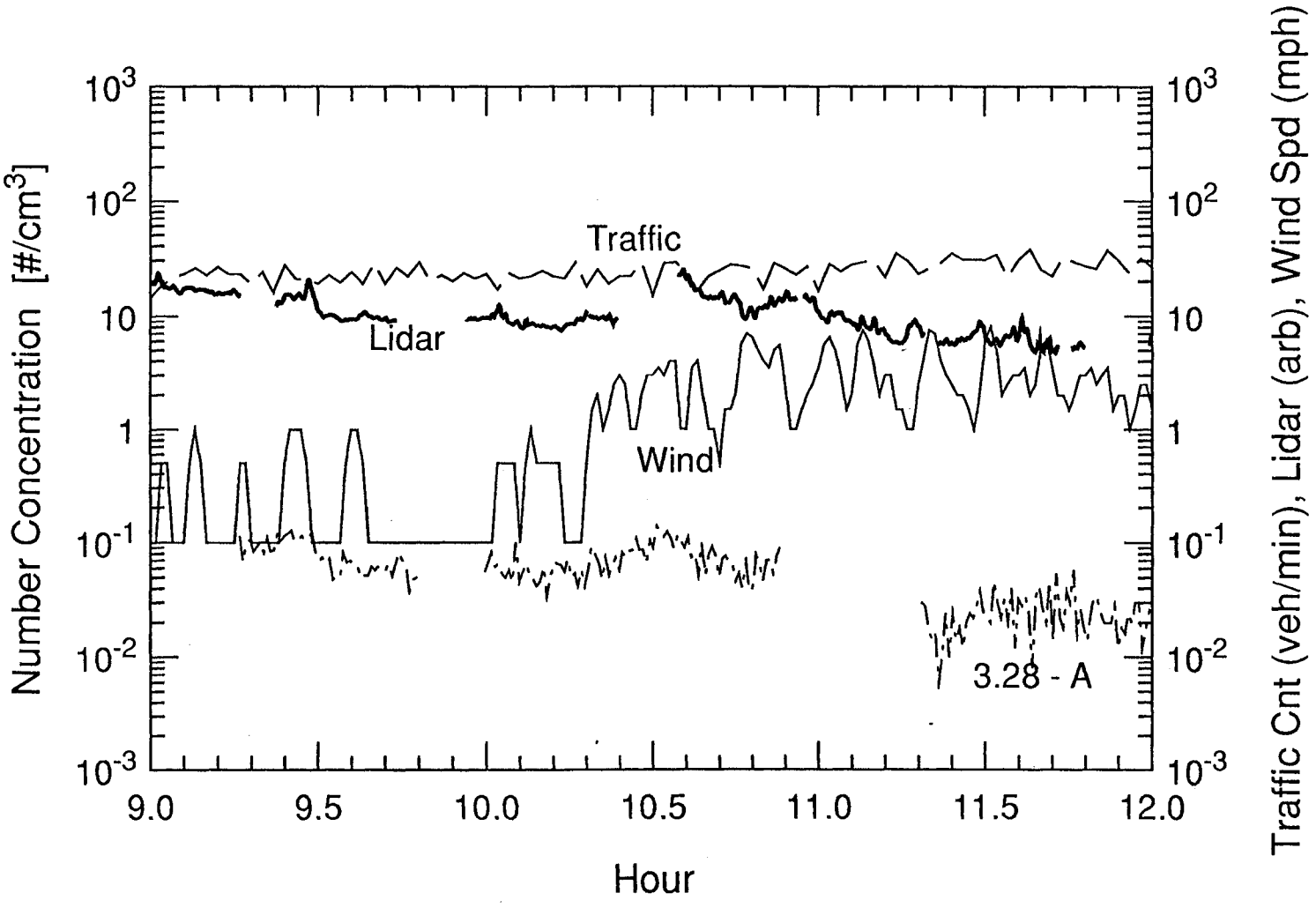

Fig. 29: Comparison of total traffic count (both directions) on Gibson Blvd, wind speed, lidar signal, and 3.28 μm particle concentration histories during mid-morning hours, Thursday, 6/22, north of Gibson Blvd. Logarithmic scale used for visualization of correlation (wind speeds < 0.5 mph instrument resolution shown as 0.1 mph).

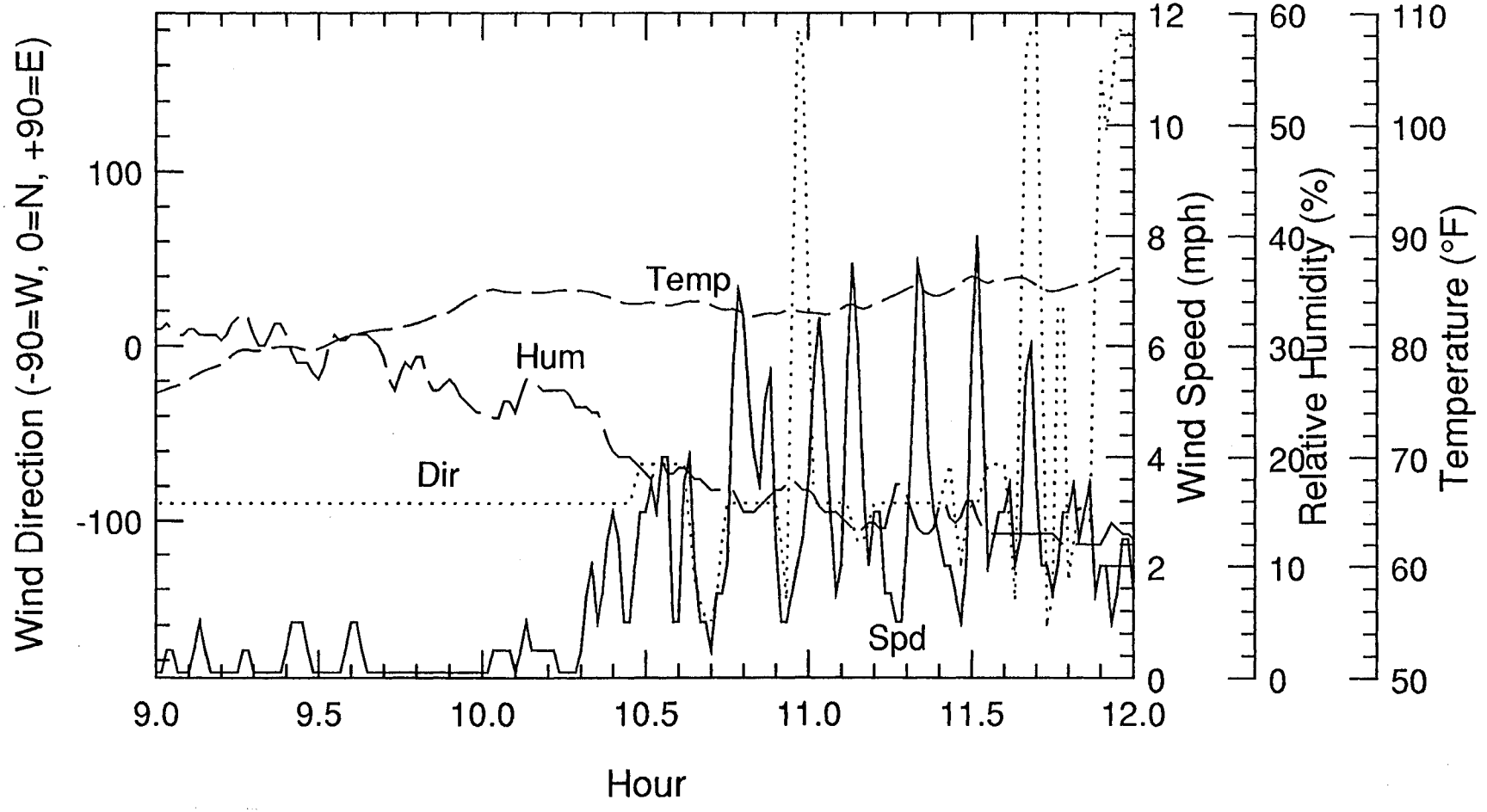

Fig. 30: Temperature, relative humidity, wind direction (0 => out of north, -90 = out of west, +90 = out of east, ±180 - out of south), and wind speed data for mid-morning hours, Thursday, 6/22, north of Gibson Blvd. at a height of 20 ft.

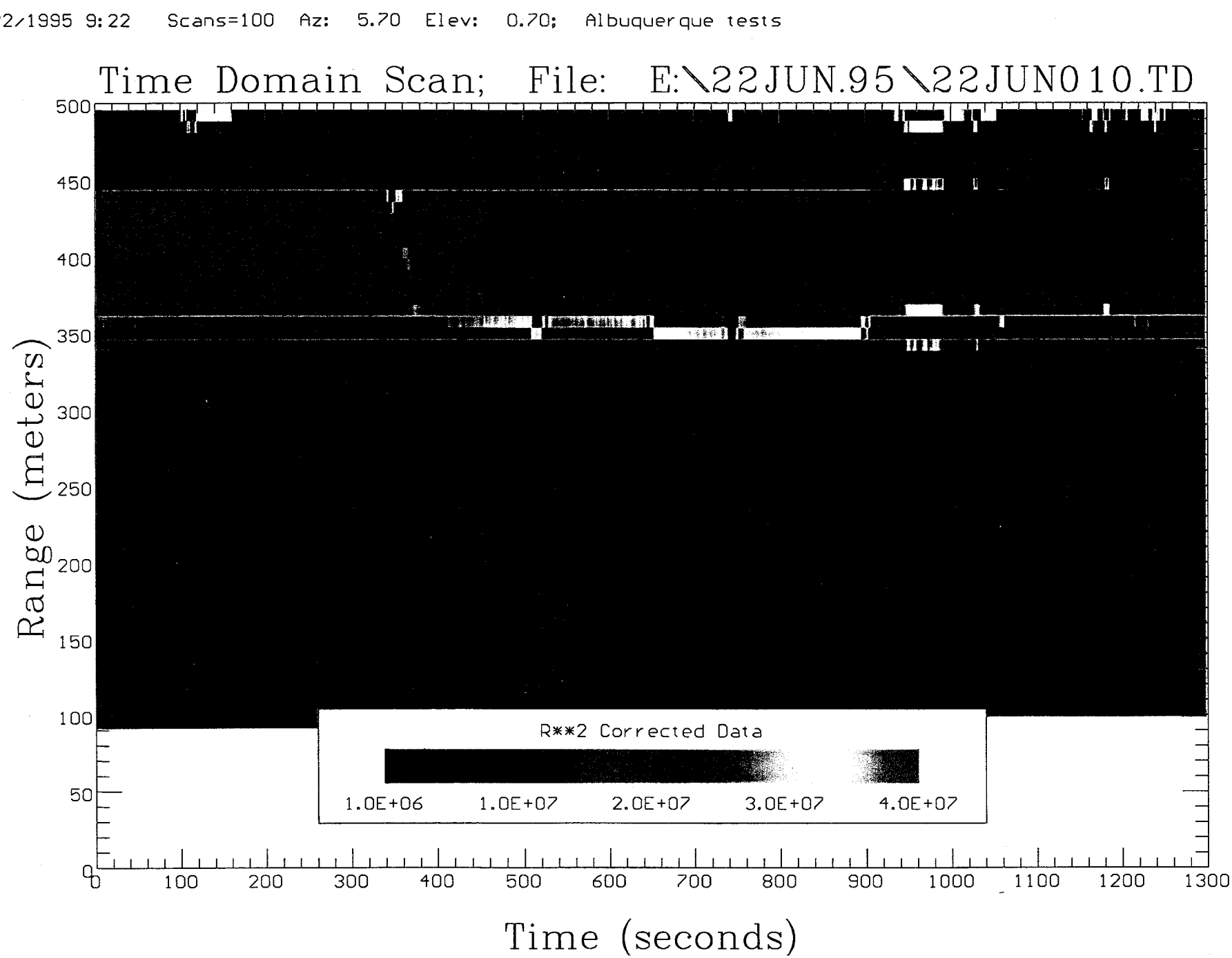

Fig. 31: Color-contour plot showing lidar signal strength as a function of position and time beginning at 9:22 a.m., Thursday, 6/22. The azimuth and elevation angles given in the legend are in degrees. The interference generated by the tree located about 360 m from the laser is evident, as is a weak signal which appears briefly at about 9:25 at a distance of 380-390 m. This object/event is directly over the sampling site, and it is responsible for the weak signal increase observed in Figs. 28 and 29.

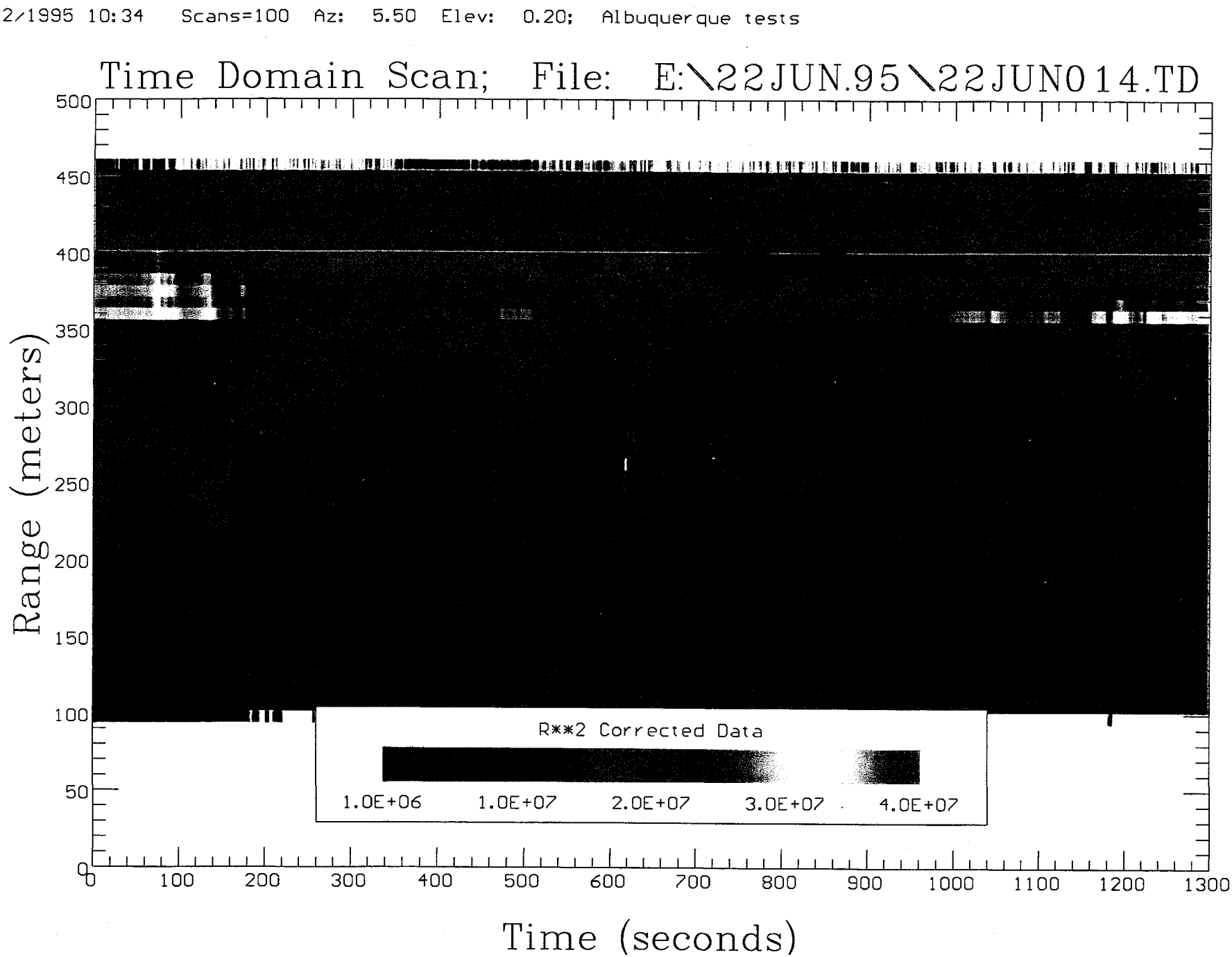

Fig. 32: Color-contour plot showing lidar signal strength as a function of position and time beginning at 10:34 a.m., Thursday, 6/22. New azimuth and elevation angles (given in degrees) reduced interference from the tree located at 360 m but did not eliminate it. Beam now stopped by trees on west side of Girard at a distance of about 400 m. Nothing too interesting appears at 380-390 m during this interval.

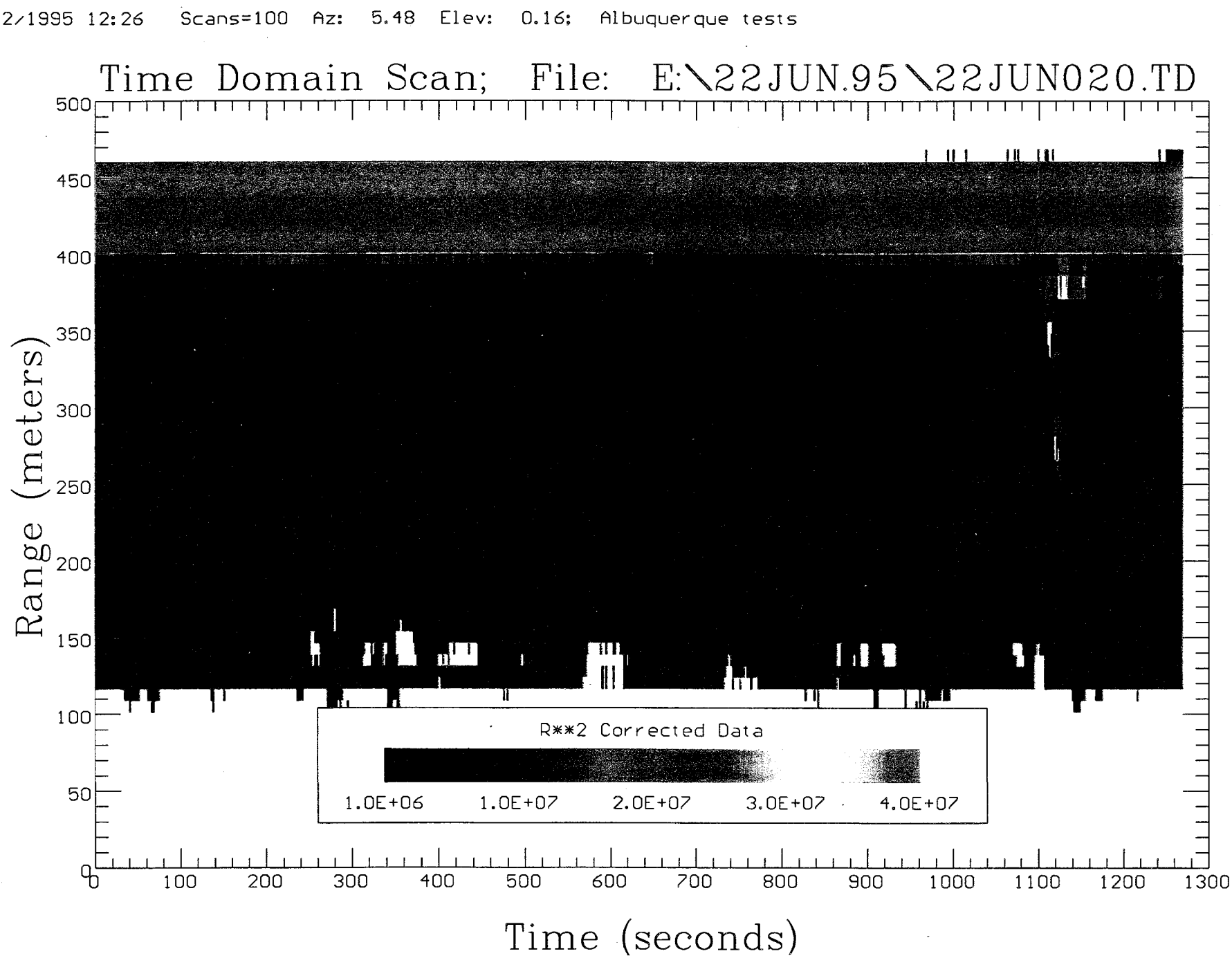

Fig. 33(a): Color-contour plot showing <u>normal</u> lidar signals as functions of position and time from 12:26 p.m. to 12:46 p.m., Thursday, 6/22. Note that something happens at a distance of 380-390 m at several instances around 12:45. A similar image also occurs for the next 20 minute interval from 12:47-1:07.

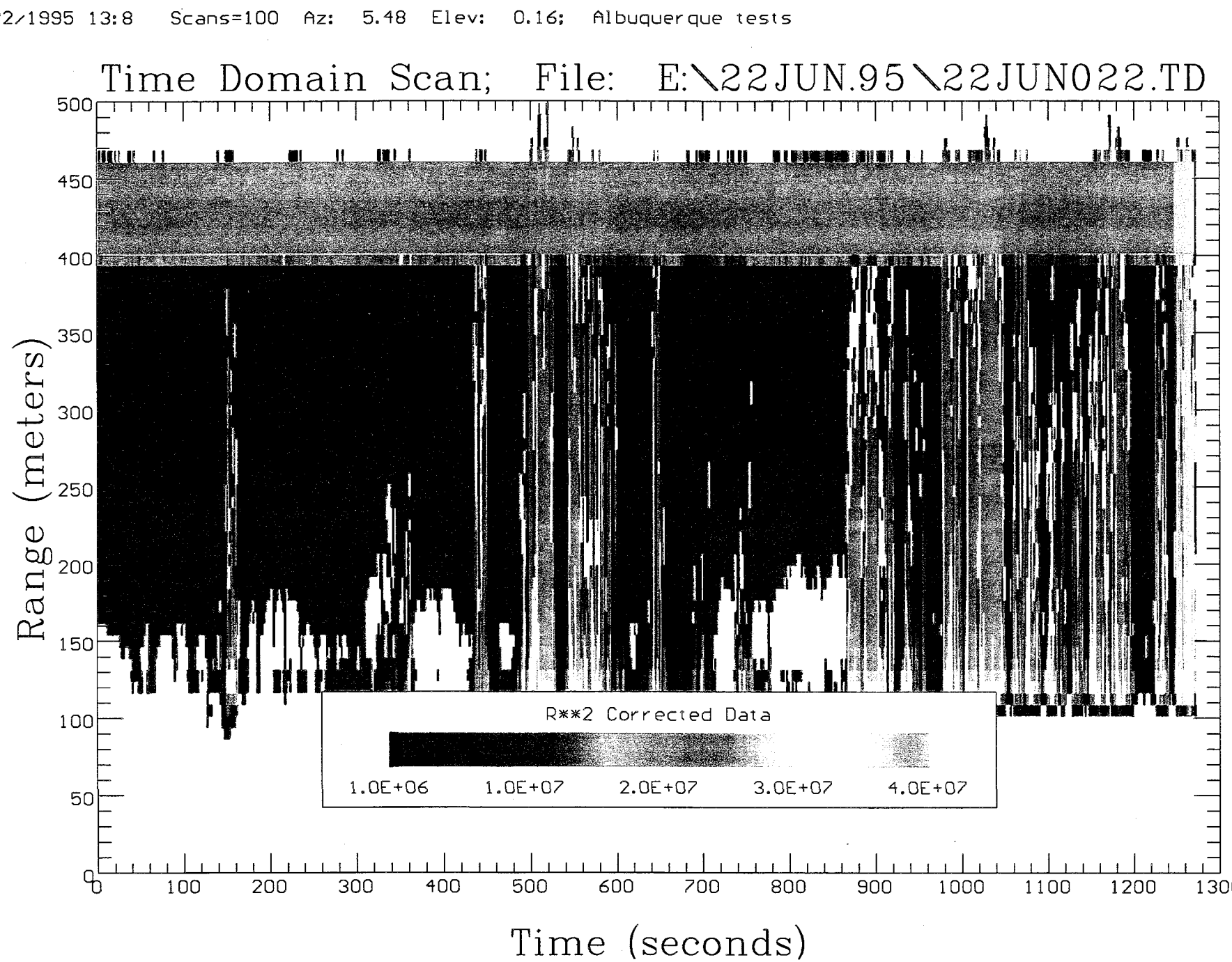

Fig. 33(b): Color-contour plot showing abnormal lidar signals as functions of position and time from 1:08:59 (shown as 13:8) to 1:30, Thursday, 6/22. The beam angles are identical to those used during the acquisition of Fig. 33a, and the wind and traffic conditions are similar. Nothing particularly interesting appears at 380-390 m relative to the rest of the beam path during this interval. The cause for the abnormal signal history is unknown.

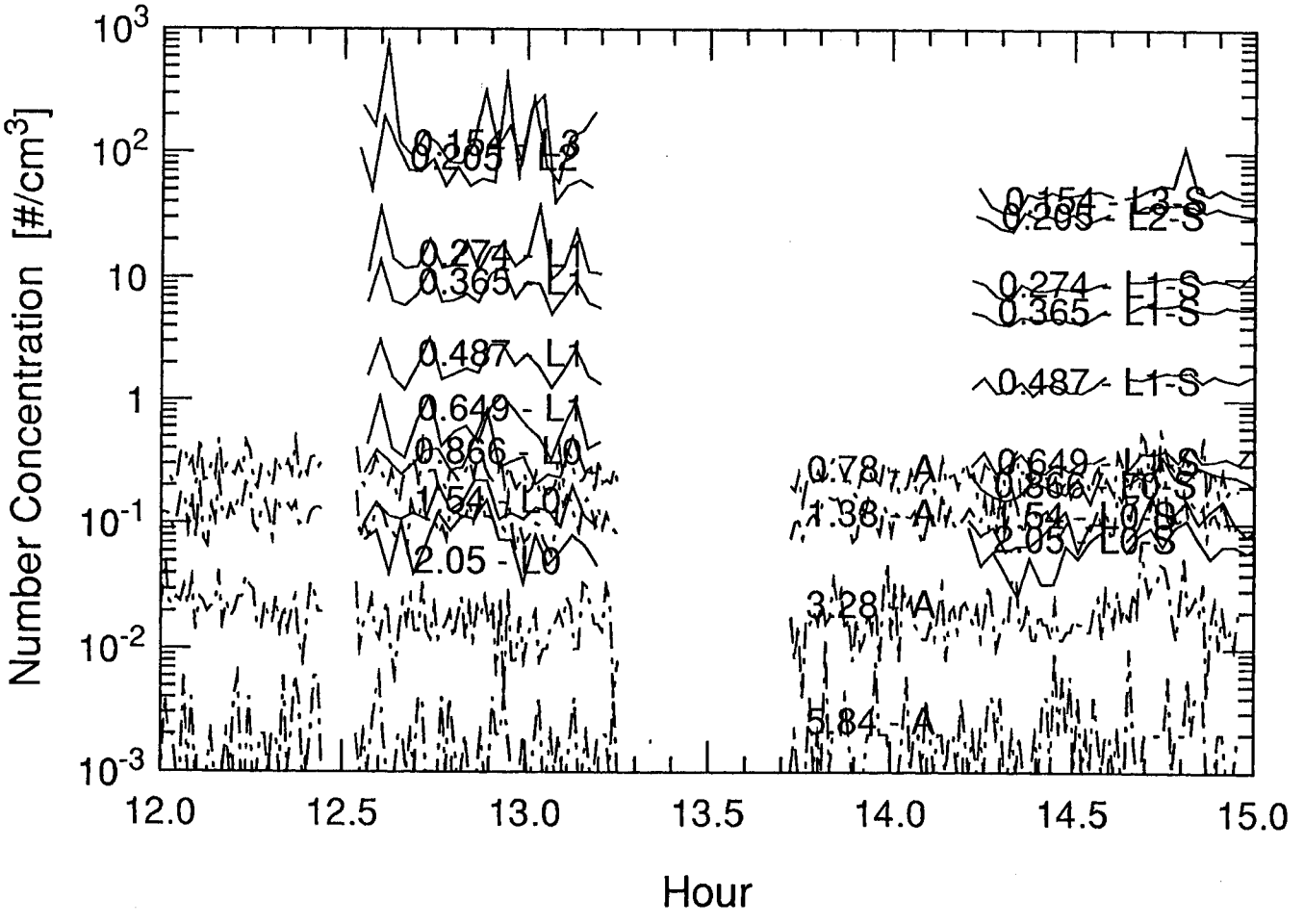

Fig. 34: Particle concentration histories during early afternoon hours, Thursday, 6/22, north of Gibson Blvd. The legends on the traces give the logarithmic midpoint of the various size bins using physical particle diameters in μm. "L#" indicates that the data was taken by the LASX instrument on range "#", while "A" indicates the data was taken using the APS.

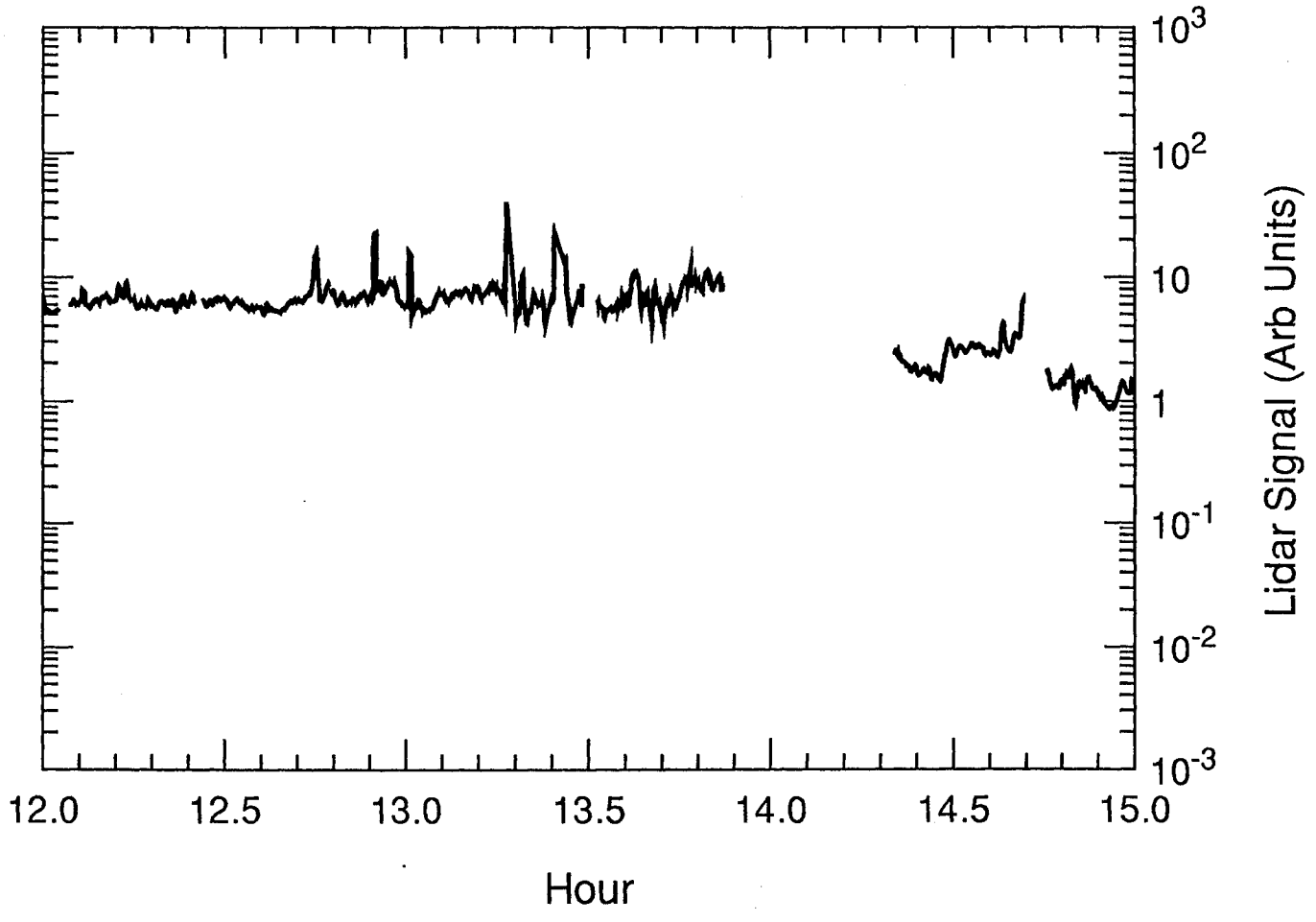

Fig. 35: Running 30 second average of lidar signal during early afternoon hours, Thursday, 6/22. Signal volume is north of Gibson Blvd., slightly north, west, and above particle sampling inlet (see text).

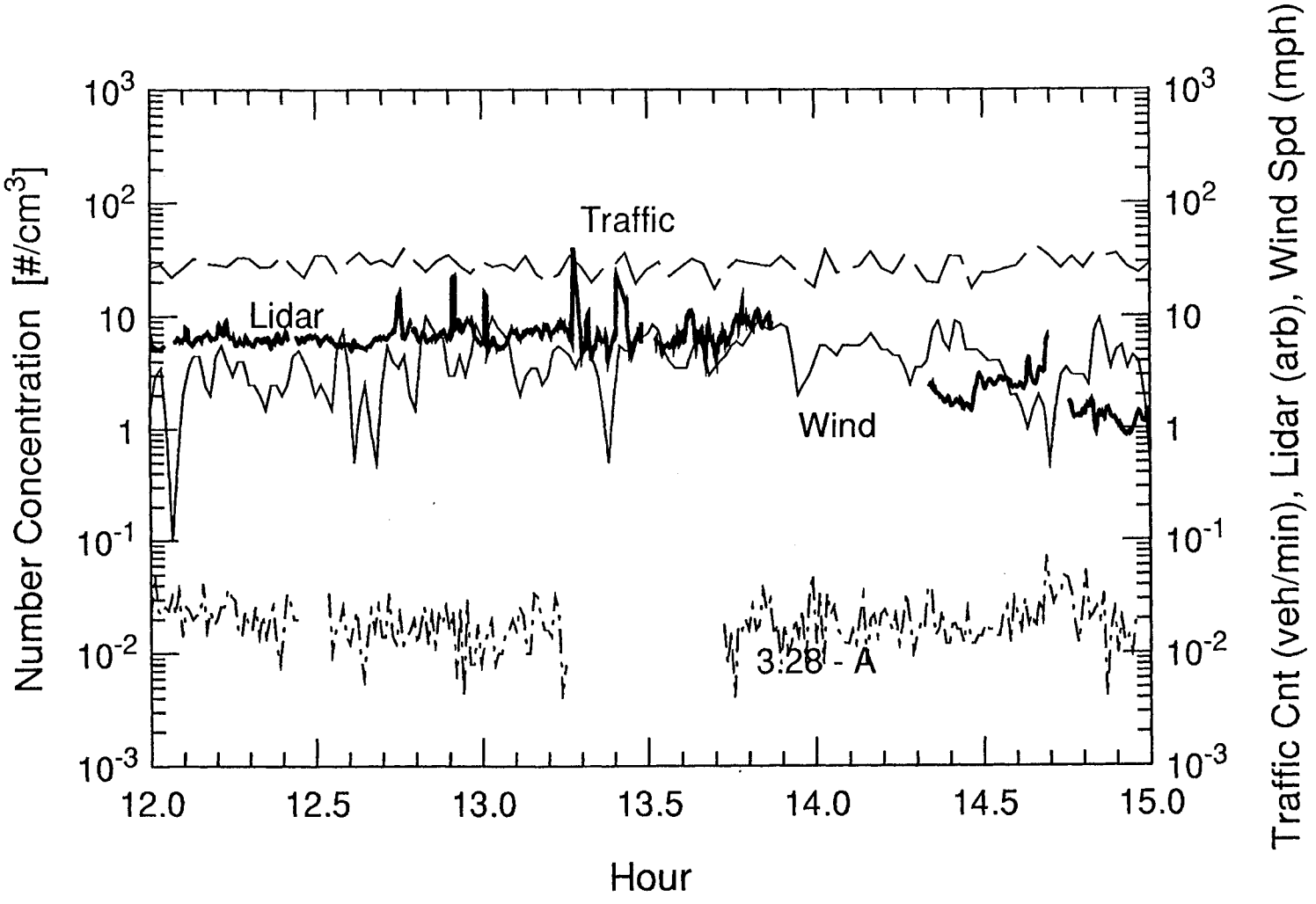

Fig. 36: Comparison of total traffic count (both directions) on Gibson Blvd, wind speed, lidar signal, and 3.28 μm particle concentration histories during early afternoon hours, Thursday, 6/22, north of Gibson Blvd. Logarithmic scale used for visualization of correlation (wind speeds < 0.5 mph instrument resolution shown as 0.1 mph).

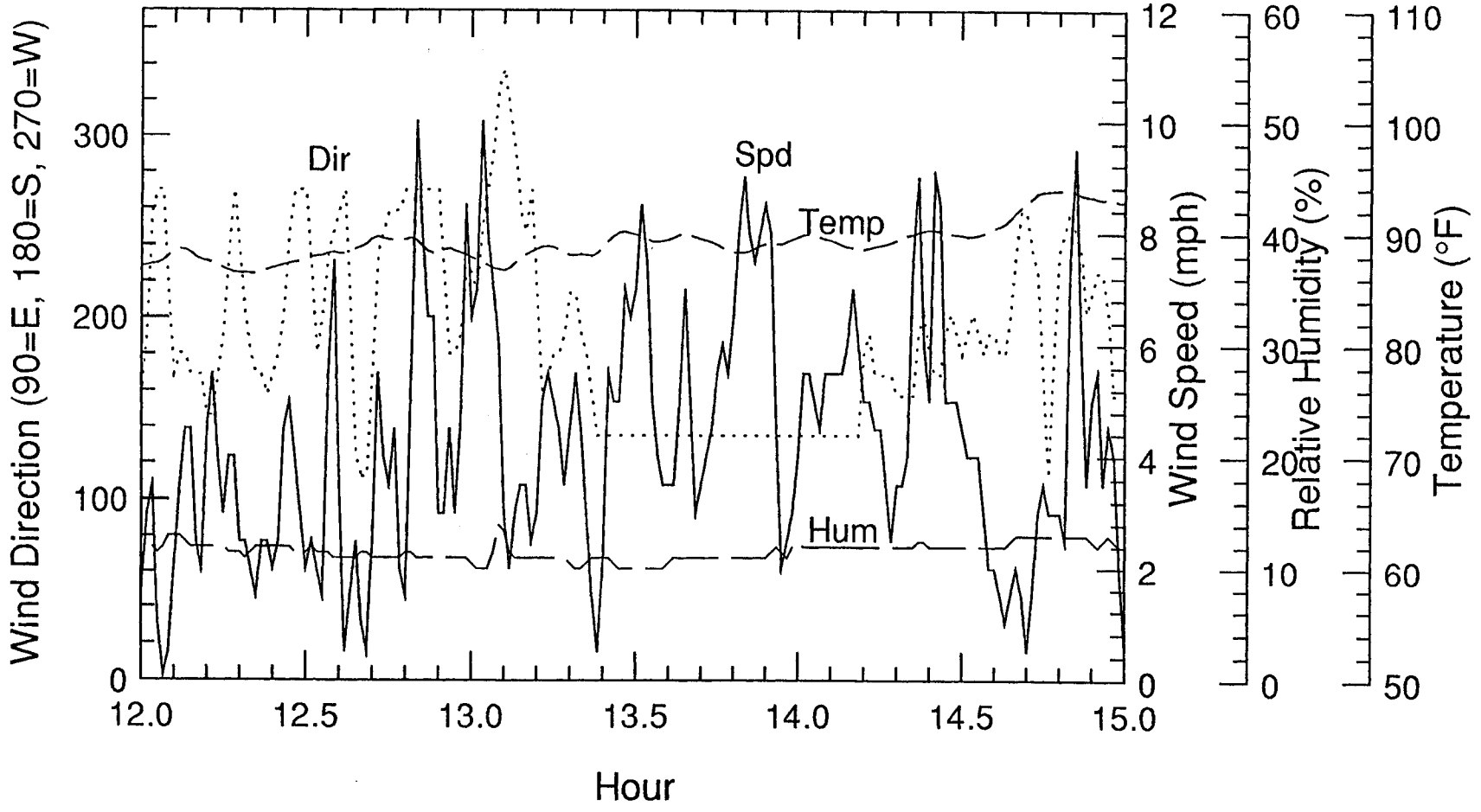

Fig. 37: Temperature, relative humidity, wind direction (0 => out of north, -90 = out of west, +90 = out of east, ±180 - out of south), and wind speed data for early afternoon hours, Thursday, 6/22, north of Gibson Blvd. at a height of 20 ft.

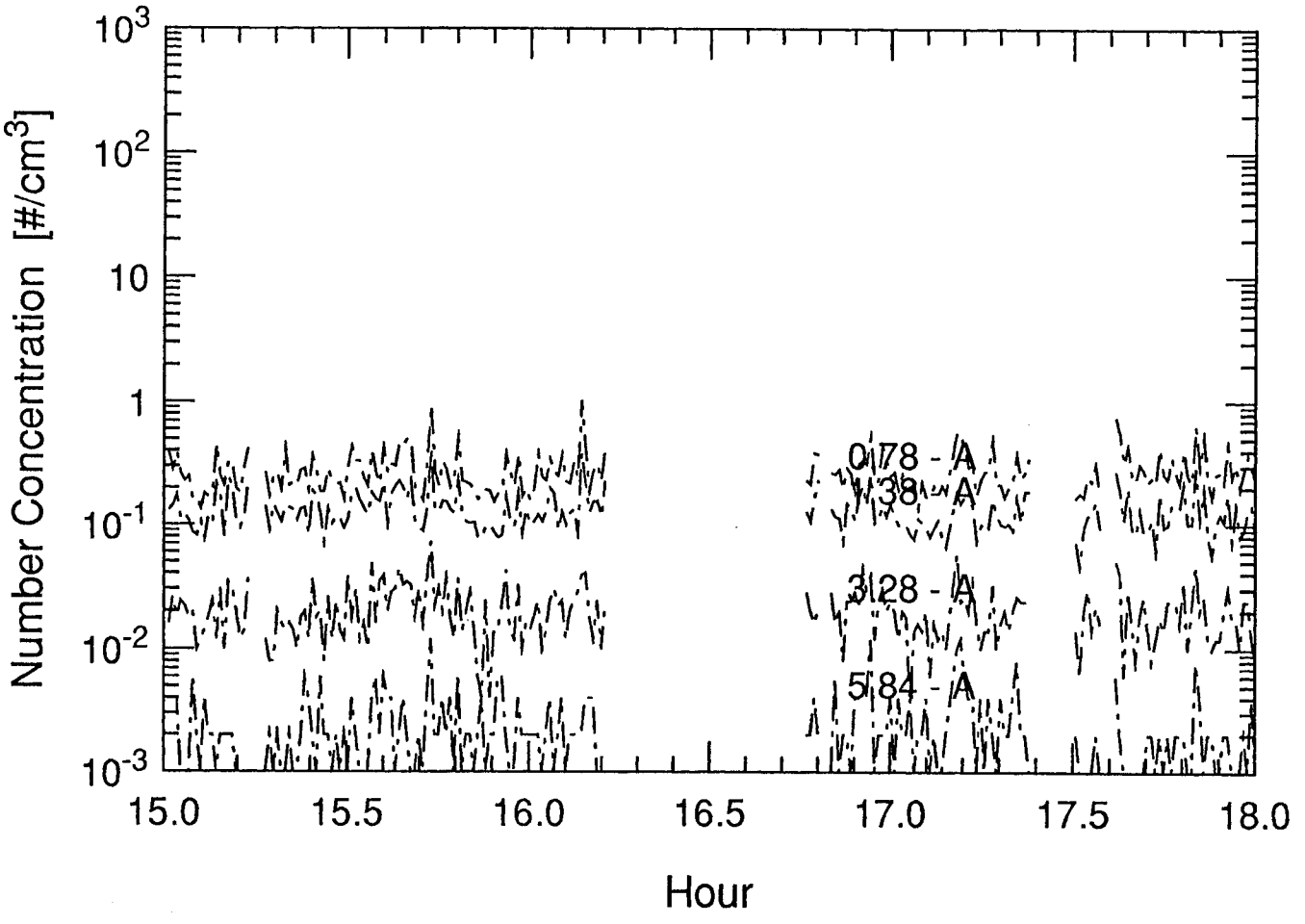

Fig. 38: Particle concentration histories measured by APS during late afternoon hours, Thursday, 6/22, north of Gibson Blvd. The legends on the traces give the logarithmic midpoint diameters (in μm) of the various size bins. Aerodynamic diameters were converted to equivalent homogeneous spherical diameters assuming the density of particle material was 2.2 g/cm^3.

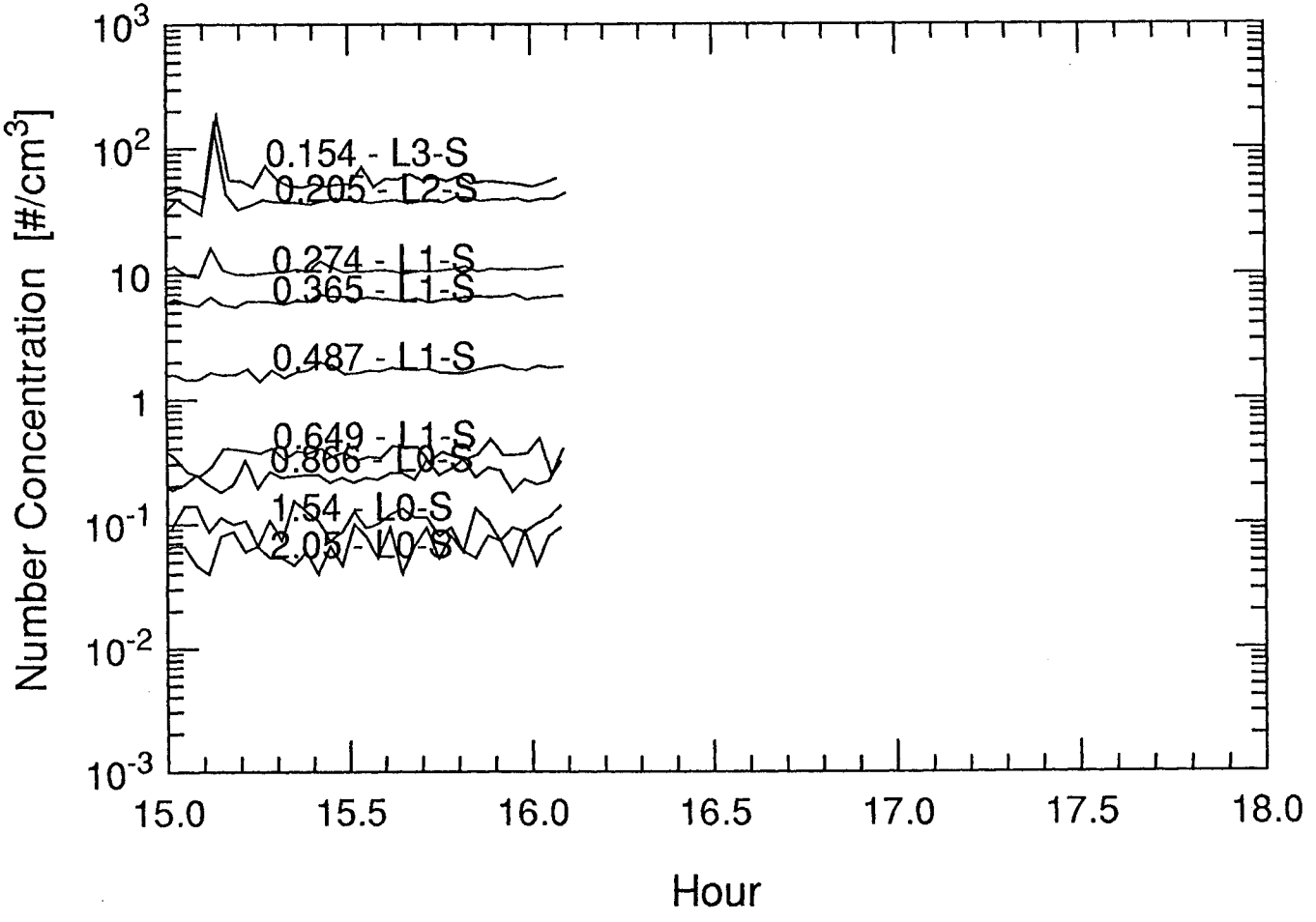

Fig. 39: Particle concentration histories measured by LASX during late afternoon hours, Thursday, 6/22, south of Gibson Blvd. The legends on the traces give the logarithmic midpoint diameters (in μm) of the various size bins.

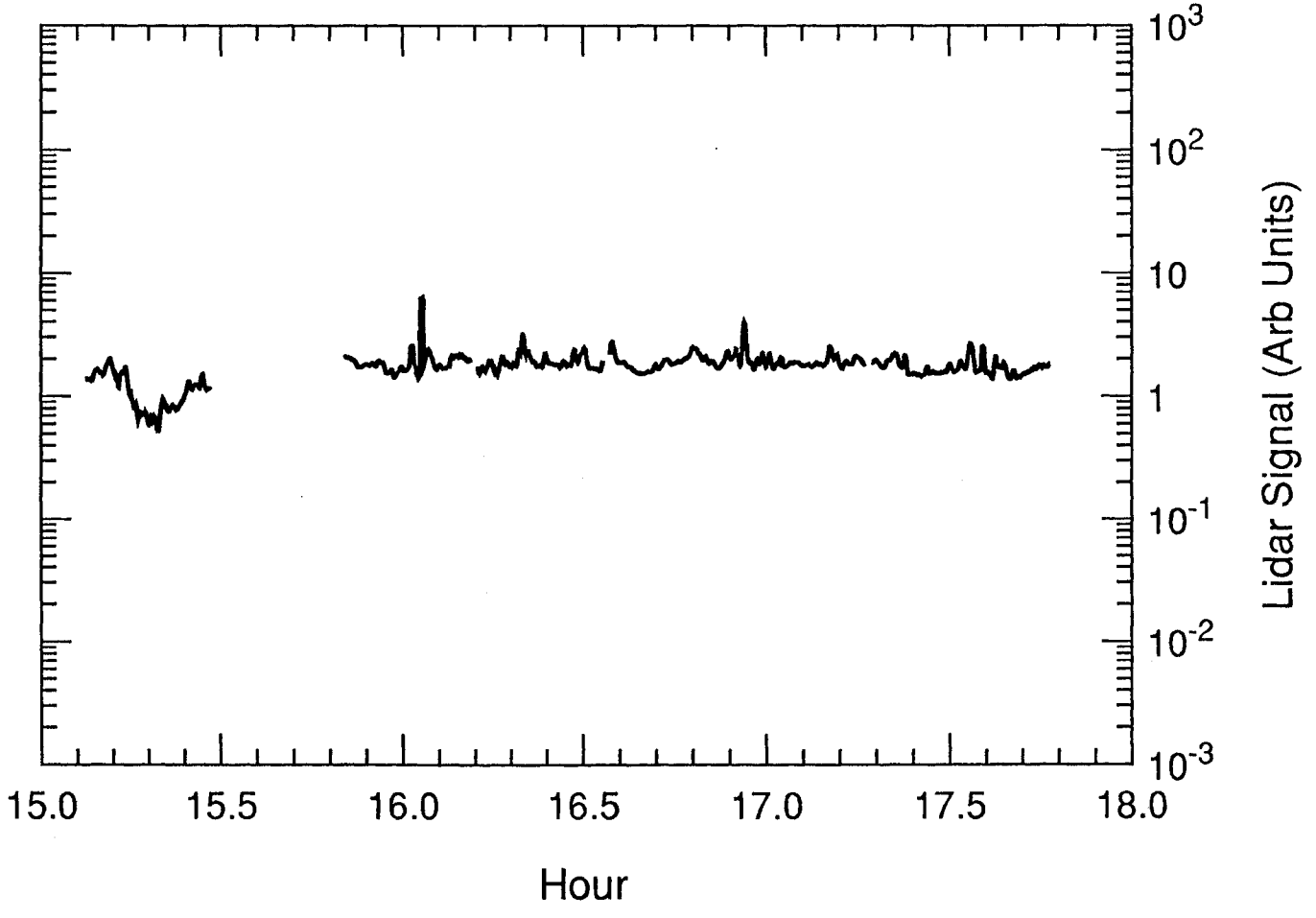

Fig. 40: Running 30 second average of lidar signal during late afternoon hours, Thursday, 6/22. Signal volume is north of Gibson Blvd., slightly north, west, and above particle sampling inlet (see text).

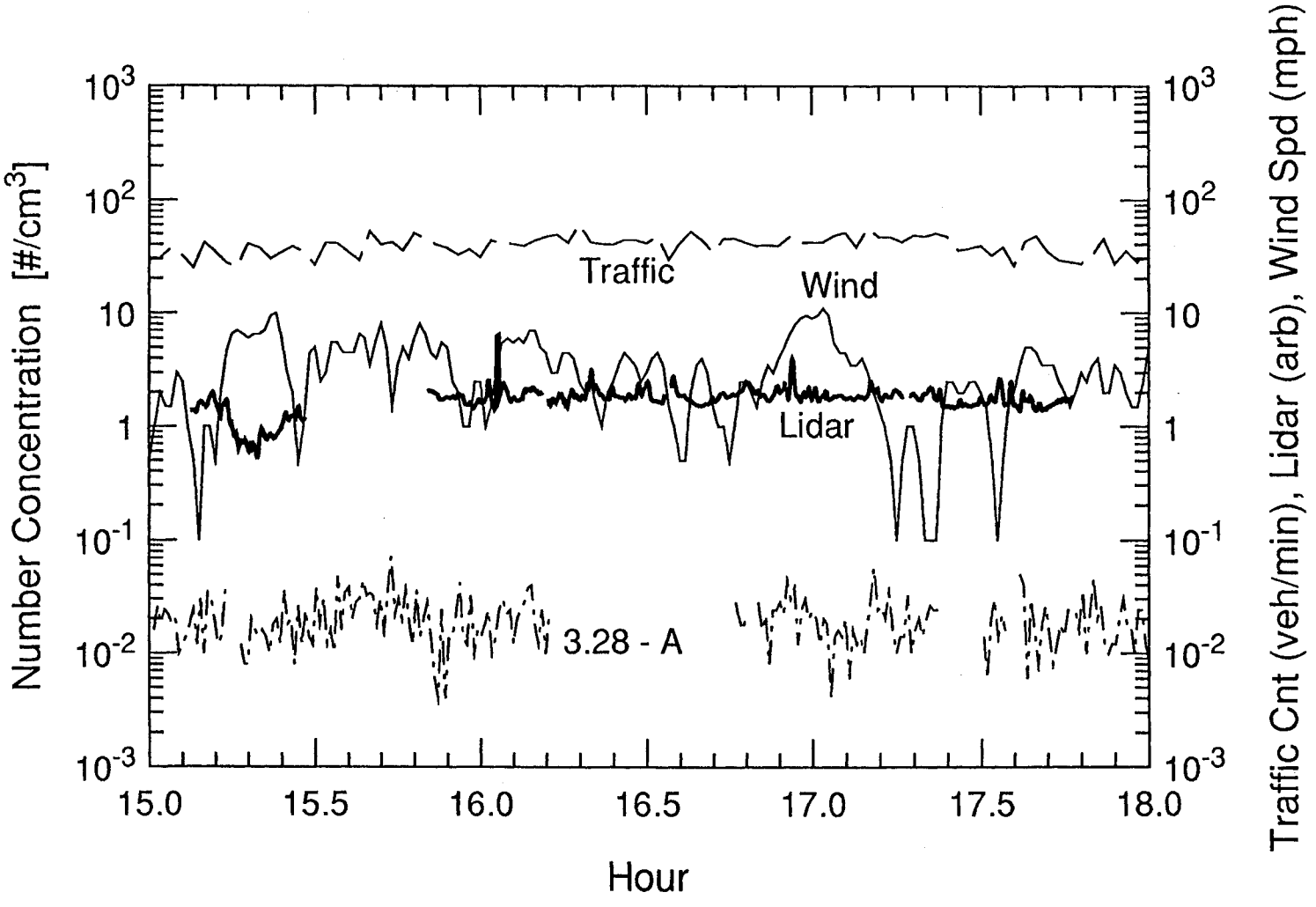

Fig. 41: Comparison of total traffic count (both directions) on Gibson Blvd, wind speed, lidar signal, and 3.28 μm particle concentration histories during late afternoon hours, Thursday, 6/22, north of Gibson Blvd. Logarithmic scale used for visualization of correlation (wind speeds < 0.5 mph instrument resolution shown as 0.1 mph).

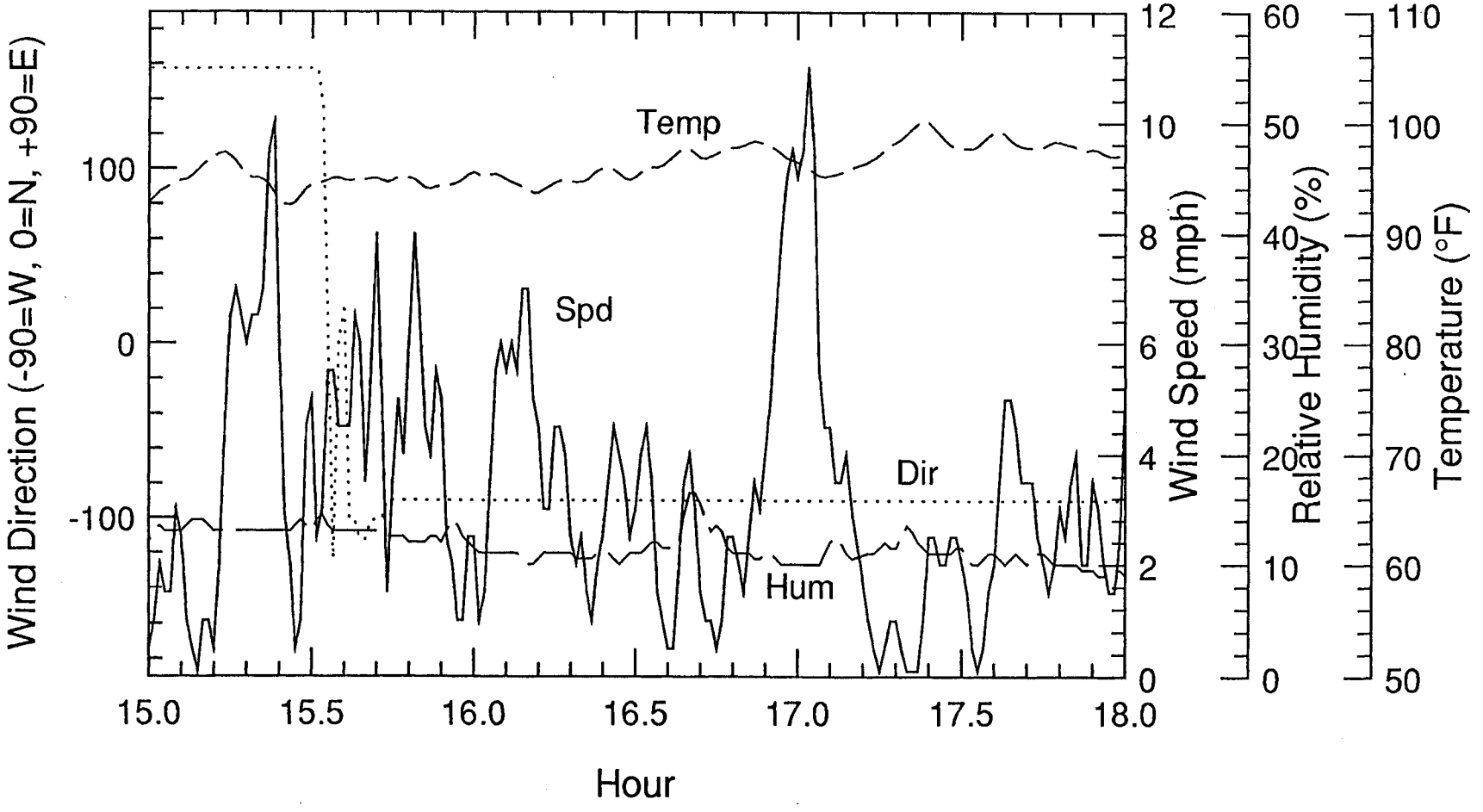

Fig. 42: Temperature, relative humidity, wind direction (0 => out of north, -90 = out of west, +90 = out of east, ±180 - out of south), and wind speed data for late afternoon hours, Thursday, 6/22, north of Gibson Blvd. at a height of 20 ft.

CORRELATION BETWEEN LIDAR SIGNAL AND PARTICLE CONCENTRATIONS - The strongest correlations were obtained for particles whose aerodynamic diameters fell in the size ranges of 2.37-3.16, 3.16-4.22, and 4.22-5.62 μm, although correlations with particles in the adjoining bins of 1.00-1.33, 1.33-1.78, 1.78-2.37, and 4.22-5.62 μm were only a few percent lower. Assuming the particle material density is 2.2 g/cm^3 for these bins, the three bins with the strongest correlations correspond to particles whose characteristic actual diameters are 1.60-2.13, 2.13-2.85, and 2.85-3.79. Particles in these size ranges would be expected to generate in excess of 50% of the lidar signal (see Appendix A for details), so the data are in agreement with the Lorenz-Mie scattering model. Representative correlations between the lidar signal and particle number concentrations for the 2.37-3.16 and 4.22-5.62 μm aerodynamic size bins are summarized in Table 6. The logarithmic mean aerodynamic diameters of these bins are 2.74 and 4.87 μm, which correspond to characteristic actual diameters of 1.85 and 3.28 μm, respectively.

Table 7 shows similar results for the correlation between the lidar signal and the estimated mass concentration of particles contained in the ranges spanning 1.33 -7.50 μm in aerodynamic diameters (0.89 -5.06 μm characteristic physical diameters). The mass concentration is estimated assuming the particle material density is 2.2 g/cm^3 and estimating the total volume of particles in the bin using the cube of the logarithmic mean diameter of the bin. Since the logarithmic mean is slightly less than the volume mean diameter and the mass concentration per size interval is generally increasing over this size range, the mass concentration arrived at this way will most likely be a slight underestimation of the true mass concentration of particles in this range.

In both cases, since the sampling intervals and digitization rates were different, the correlations were obtained by computing running averages of the various data sets, and then using linear interpolation within the averaged data to obtain points at common times. Two-minute (120 sec.) running averages were used for the lidar, APS, and wind data, incorporating approximately 60, 4, and 2 data points in the average, respectively, based on the different sampling rates of the instruments. Four-minute (240 sec.) running averages were used for the LASX and traffic data, were each average incorporated 2 data points. The averaging interval used was a compromise between time resolution, reduction of noise, and number of points left for the correlation.

As can be seen from the data in the table, the fit of the lidar signal to the particle concentrations is not single-valued, but rather can change with time. The "long time" average

response (where "long time" here means about 12 hours) appears to be fairly stable as long as the lidar beam remains in the same location relative to the sampling inlet. The effect of interference by the tree located 360 m from the lidar unit is illustrated in the correlations obtained between 9:24 and 11:42 on 6/22. The difference between the response levels (the slopes of the fits) on 6/22 and 6/23 may be caused by any of three factors, including lower amplifier gain, lower laser power, or relatively higher blockage of the beam by trees located between the laser and the sampling point. Each of these would cause the lidar signal recorded on 6/23 to decrease relative to that recorded on 6/22, and hence lead to lower slopes for the fits to the particle concentration data. It is also possible that the horizontal position of the lidar beam was further from the roadway on 6/23, which could have led to lower illuminated particle concentrations and hence lower signals. This latter explanation seems less likely due to the consistency of the fits for each day regardless of wind direction.

The best way to maintain a consistent response from day to day would be to calibrate the system response each day. In theory, this could be done by calibrating the return signal from a positional target. However, this is not as simple as it sounds, because the position of the target relative to the beam intensity profile would have to be monitored, along with its orientation relative to the beam direction. Variations in the beam intensity profile with distance from the laser would mean that more or less energy would be reflected by the target depending on its size relative to the beam diameter as well as its location in the beam. The most accurate calibration would require the generation of a plume of particles of known composition and size distribution, but this is neither simple nor desirable. Hence, in practice, it is simpler to use the size-resolved particle concentrations as a calibration measurement, and obtain information regarding the composition of the ambient particles by collecting particle samples. The only requirement then is that the beam location be returned to the same point relative to the sampling inlets.

Table 6: Correlations of Lidar Signal vs Particle Number Concentration--Albuquerque

Date	Time	Beam Angles[1] (Azimuth, Elevation)	Particle Diam. Range[2] (μm)	Linear Fit[3]: Lidar = m*#Conc + b		Correlation Coefficient, r	No. of Points	Comments
				Slope, m (x 10^6)	Intercept, b (x 10^6)			
6/22	9:24-10:22	13 pts at (5.7°, 0.7°); 11 pts at (5.4°, 0.3°)	1.85 3.28	38.1 95.9	3.01 3.72	0.91 0.88	24 24	Short break in lidar data from 9:50-10:00 as beam was re-aimed; even though beam angles shift, there's no clear shift in signal. Particle concentrations fluctuate, but drop by about a factor of 2 during this interval. Based on the strength of the correlation and the lack of a double-valued signal response, it would appear that something unusual is occurring for the 0.30° beam elevation, because it should have produced relatively higher signal values than the 0.70° elevation. An error in the recorded beam angle is possible but unlikely, since this is automatically recorded by the data acquisition system. It is also unlikely that the particle concentration at 0.30° was unusually low for an entire half-hour period. An explanation is given in the next two rows.
6/22	10:36-11:42	(5.5°, 0.2°)	1.85 3.28	72.2 182	0.443 2.19	0.96 0.94	21 21	Short break from 10:22-10:36 between lidar files to change beam angle in attempt to avoid tree. APS data not available for 10:54-11:18, which reduces number of points in the correlation. Particle concentrations vary by factor of four. Best fit slopes increased substantially from above, as would be expected--the particle concentrations should be higher at lower elevations, thus increasing the strength of the lidar signal and raising the slope of the fit.
6/22	9:24-11:42	13 pts at (5.7°, 0.7°); 11 pts at (5.4°, 0.3°); 21 pts at (5.5°, 0.2°)	1.85 3.28	46.7 112	2.52 3.80	0.83 0.79	45 45	Slopes become nearly average of above two fits. It is very odd that the correlation including the large angular jump from (5.7, 0.7) to (5.4, 0.3) is quite strong, but including data from a smaller angular shift to (5.5, 0.2) causes the correlation to decrease significantly. Apparently, a larger fraction of the beam was blocked by the tree at the 0.3° elevation, reducing those signals relative to the signals recorded at the other beam elevations.

[1]The horizontal beam angle is not repeatable from day to day. It is not referenced to magnetic north. The elevation angle should be quite repeatable from day to day, because it is referenced with a level. No data on the absolute accuracy was available.

[2]Diameter range from 1.60 - 2.13 μm has geometric mean at 1.85 μm, whereas diameter range from 2.85 - 3.79 μm has geometric mean at 3.28 μm. The geometric mean is midway through the range in log space.

[3]Number concentration is in units of #/cm^3; lidar signal is in arbitrary units as digitized.

111

Table 6: Correlations of Lidar Signal vs Particle Number Concentration--Albuquerque (cont'd)

Date	Time	Beam Angles[1] (Azimuth, Elevation)	Particle Diam. Range[2] (μm)	Linear Fit[3]: Lidar = m*#Conc+b		Correlation Coefficient, r	No. of Points	Comments
				Slope, m ($\times 10^6$)	Intercept, b ($\times 10^6$)			
6/22	9:24 - 1:06	45 pts at (5.7°,0.7°), (5.4°,0.3°),(5.5°, 0.2°), + 27 pts at (5.48°,0.16°)	1.85 3.28	41.5 99.9	3.55 4.68	0.83 0.81	72 72	Adding additional data at the nearby angle of (5.48, 0.16) doesn't affect the above correlation much; the important fact still appears to be the jump in the response between 10:36-1:06 compared to 9:24-10:22.
6/22	10:36 - 1:06	21 pts at (5.5°, 0.2°) 27 pts at (5.48°,0.16°)	1.85 3.28	63.1 158	2.02 3.58	0.90 0.88	48 48	These angles are similar enough such that the particle concentrations would be expected to be very similar. Hence, the correlation remains strong. The fact that the slope of the fit is higher at the lower elevation is expected--higher particle concentrations should exist at lower elevations, so the lidar signal increases relative to the particle concentrations recorded by the sampling instruments, because the height of the sampling inlet is unchanged. Hence the slope of the fit increases.
6/22	9:24 - 10:22, 2:24 - 5:46	24 pts at (5.7°, 0.7°), (5.4°, 0.3°), +57 pts at (5.66°,0.56°) (5.58°,0.70°)	1.85 3.28	61.5 154	-2.34 -0.992	0.94 0.95	81 81	Although the data is taken at different times of the day, the correlation is strong. The key is that the beam angles are very similar, and the particle concentrations vary enough between the two time periods to lead to a good correlation.
6/22	9:24 - 5:46 (All 6/22 data)	see above	1.85 3.28	59.1 146	-0.407 1.03	0.80 0.79	129 129	The correlation over the entire day is still very strong, even though the beam angle was changed a number times in an attempt to avoid interference from trees. This indicates that the variation in particle concentrations is not that large over the range of distances covered by these lidar beam angles, and that the fluctuations at the different heights are still fairly strongly coupled under this particular set of wind, traffic, and background conditions.

[1]The horizontal beam angle is not repeatable from day to day. It is not referenced to magnetic north. The elevation angle should be quite repeatable from day to day, because it is referenced with a level. No data on the absolute accuracy was available.

[2]Diameter range from 1.60 - 2.13 μm has geometric mean at 1.85 μm, whereas diameter range from 2.85 - 3.79 μm has geometric mean at 3.28 μm. The geometric mean is midway through the range in log space.

[3]Number concentration is in units of #/cm^3; lidar signal is in arbitrary units as digitized.

Table 6: Correlations of Lidar Signal vs Particle Number Concentration--Albuquerque (cont'd)

Date	Time	Beam Angles[1] (Azimuth, Elevation)	Particle Diam. Range[2] (μm)	Linear Fit[3]: Lidar = m*#Conc + b		Correlation Coefficient, r	No. of Pts.	Comments
				Slope, m ($x10^6$)	Intercept, b ($x 10^6$)			
6/23	6:04-7:44	(6.18,0.26)	1.85 3.28	18.6 63.9	0.924 0.962	0.98 0.96	51 51	1st running average available at 6:04; particle event starts at ≈ 7:15, 7:45 is about midway through event. Residuals show two distinct responses--lidar signal during particle event is higher. In general, slopes are much lower than on 6/22; this could be due to less beam blockage or higher system response.
6/23	7:46-11:22 (excl. target period)	(6.18,0.26)	1.85 3.28	18.5 56.6	-0.976 -0.557	0.92 0.90	54 54	Correlation starts midway through particle event, continues through rest of points at this beam angle (target finding points excluded). Again, residuals show two distinct responses, with higher signals during particle event.
6/23	7:00-8:30	(6.18,0.26)	1.85 3.28	16.5 51.9	0.674 1.013	0.86 0.83	42 42	Again, higher response during particle events evident. If hold offset to zero, slope increases slightly. Particles present during the particle event may have slightly lower average material densities, which leading to reduced aerodynamic diameters but not necessarily smaller scattering cross sections.
6/23	8:18-11:22 (excl. target period)	(6.18,0.26)	1.85 3.28	8.42 26.4	0.437 0.580	0.80 0.81	42 42	When exclude particle event, slope of fit is much lower, and residuals don't show two-valued nature; the correlation coefficient drops because the range of data is lower and noise in concentration data is important.
6/23	6:04-11:22 (excl. target period)	(6.18,0.26)	1.85 3.28	17.5 60.4	0 0	0.69 0.67	105 105	Held offset = 0 in fit, which seems to give better agreement on slopes of data sets generated during particle event and other times; without holding offset fixed, correlation coefficients are 0.72 and 0.71, respectively.
6/23	11:24-6:00	(6.14, 0.10)	1.85 3.28	7.197 23.3	0.051 0.121	0.64 0.66	157 157	Particle concentrations within this period only vary by factor of two, so correlation is degraded.
6/23	6:04-6:00 (all 6/23 data)	(6.18,0.26) am, (6.14,0.10) pm	1.85 3.28	18.8 61.8	-0.545 -0.378	0.83 0.82	262 262	Signals during the morning particle event give slightly higher responses as is verified above, but correlations during other times are very strong.
6/23	8:18-6:00	(6.18,0.26) am, (6.14,0.10) pm	1.85 3.28	11.38 36.9	-0.219 -0.102	0.87 0.87	199 199	Removing particle event during a.m. removes dual valued response; remaining data gives narrow response despite slight change in the lidar beam angle (vertical beam height changed only by about 3.5 feet = 1.1 m).

[1]The horizontal beam angle is not repeatable from day to day. It is not referenced to magnetic north. The elevation angle should be quite repeatable from day to day, because it is referenced with a level. No data on the absolute accuracy was available.

[2]Diameter range from 1.60 - 2.13 μm has geometric mean at 1.85 μm, whereas diameter range from 2.85 - 3.79 μm has geometric mean at 3.28 μm. The geometric mean is midway through the range in log space.

[3]Number concentration is in units of #/cm^3; lidar signal is in arbitrary units as digitized.

113

Table 7: Correlations of Lidar Signal vs Particle Mass Concentrations --Albuquerque

Date	Time	Beam Angles[1] (Azimuth, Elevation)	Aerodynamic Diameter Range[2](μm)	Linear Fit[3]: Lidar = m* Mass Conc + b		Correlation Coefficient, r	No. of Points	Comments
				Slope, m ($x 10^6$)	Intercept, b ($x 10^6$)			
6/22	9:24-10:22	13 pts at (5.7°, 0.7°); 11 pts at (5.4°, 0.3°)	1.33-7.50	0.625	3.63	0.93	24	The comments in Table 6 regarding the 0.30° beam angle still apply; we expect a dual valued response when signals from two significantly different beam angles are correlated against point mass concentrations, but did not observe this.
6/22	10:36-11:42	(5.5°, 0.2°)	1.33-7.50	1.29	1.13	0.96	21	With the beam at a lower elevation, we do expect a higher signal response, and the higher slope of the fit supports this. The small number of points is the result of a generator failure which shut down the APS from 10:54-11:18.
6/22,	9:24-11:42	13 pts at (5.7°, 0.7°); 11 pts at (5.4°, 0.3°); 21 pts at (5.5°, 0.2°)	1.33-7.50	0.757	3.43	0.81	45	When points at the 0.20° elevation are included with those of the 0.30° and 0.70° elevations, the correlation degrades significantly. Referring to the discussion in Table 6, we suspect that significant beam blockage is occurring at the 0.30° elevation.
6/22	10:36-1:06	21 pts at (5.5°, 0.2°) 27 pts at (5.48°,0.16°)	1.33-7.50	1.13	2.65	0.91	48	The change in beam angle corresponds to less than a 1 foot change in elevation at the sampling site located 400 m from the lidar transmitter. Hence, a single response is observed with a strong correlation.
6/22	All 6/22 data	see above	1.33-7.50	0.991	0.401	0.79	129	see Table 6.

[1]The horizontal beam angle is not repeatable from day to day. It is not referenced to magnetic north. The elevation angle should be quite repeatable from day to day, because it is referenced with a level. No data on the absolute accuracy was available.

[2]Aerodynamic diameter range from 1.33 - 7.50 μm corresponds to characteristic diameter range from 0.89 - 5.06 μm assuming constant particle material density of 2.2 g/cm^3. The mass concentration in each of the six logarithmically spaced bins is estimated using the logarithmic mean diameter of the bin and the measured number concentration.

[3]Mass concentration is in units of $\mu g/m^3$; lidar signal is in arbitrary units as digitized.

Table 7: Correlations of Lidar Signal vs Particle Mass Concentrations --Albuquerque (cont'd)

Date	Time	Beam Angles[1] (Azimuth, Elevation)	Aerodynamic Diameter Range[2](μm)	Linear Fit: Lidar = m* Mass Conc + b		Correlation Coefficient, r	No. of Points	Comments
				Slope, m ($x 10^6$)	Intercept, b ($x 10^6$)			
6/23	6:04-7:44	(6.18,0.26)	1.33-7.50	0.363	0996	0.93	51	see Table 6.
6/23	7:46-11:22 (excl. target period)	(6.18,0.26)	1.33-7.50	0.364	-0.854	0.92	54	see Table 6.
6/23	7:00-8:30	(6.18,0.26)	1.33-7.50	0.321	0.802	0.87	42	see Table 6.
6/23	6:04-11:22 (excl. target period)	(6.18,0.26)	1.33-7.50	0.286	0.644	0.73	105	Includes sprinkler event, no correction made to account for changes in scattering cross sections or material densities associated with water droplets or water-coated particles.
6/23	11:24-6:00	(6.14, 0.10)	1.33-7.50	0.145	0.064	0.67	157	During this period, particle concentrations are low and do not change much, so the correlation is significantly degraded by variations in the particle counting statistics.
6/23	6:04-6:00 (all 6/23 data, Friday)	(6.18,0.26) am (6.14,0.10) pm	1.33-7.50	0.375	-0.492	0.83	262	see Table 6.
6/23	8:18-6:00	(6.18,0.26) am, (6.14,0.10) pm	1.33-7.50	0.229	-0.193	0.87	199	see Table 6.

[1]The horizontal beam angle is not repeatable from day to day. It is not referenced to magnetic north. The elevation angle should be quite repeatable from day to day, because it is referenced with a level. No data on the absolute accuracy was available.

[2]Aerodynamic diameter range from 1.33 - 7.50 μm corresponds to characteristic diameter range from 0.89 - 5.06 μm assuming constant particle material density of 2.2 g/cm^3. The mass concentration in each of the six logarithmically spaced bins is estimated using the logarithmic mean diameter of the bin and the measured number concentration.

[3]Mass concentration is in units of $\mu g/m^3$; lidar signal is in arbitrary units as digitized.

115

In any event, calibration measurements would be needed in any long-time application of the lidar system if quantitative aerosol concentrations were desired.

Short time averages can also show significant deviations associated with particular particle events, as is illustrated above and also in Fig. 10b. This would be expected, and in fact can be used as an indicator that some new particle source has come on line which may warrant further investigation. The large jump in the slope between the lidar signal and the aerodynamic diameters during the particle event is consistent with a jump to a large number of pure water droplets, as might be expected at this time due to watering activity at the golf course located upwind of the measurement volume. This is an illustration of the effect of particle composition and density changes. In general, one would also expect a change in the scattering characteristics of the particles if the relative humidity varied over a significant range, as this would once again change both the optical properties and the effective material density of the particles. Such changes in the scattering relationship could provide clues as to the likely source of a given particle plume.

CALIBRATION OF PARTICLE CONCENTRATION INSTRUMENTS AND DETERMINATION OF MATERIAL DENSITY - The instrument calibrations were done by sending a clean air flow seeded with polystyrene latex (PSL) particles of several known sizes (0.1, 0.4, 0.8, and 2.9 μm), and simultaneously measuring the size distributions recorded by all of the particle counters. PSL particles are essentially perfect homogeneous spheres with a material density of 1.05 g/cm^3, which means that the number concentrations measured by all of the particle sizing instruments should be comparable in all bin ranges. Since the size ranges of the instruments overlapped, this provided a check on the instrument calibrations. The number concentrations reported by the APS and Climet instruments agreed, but the number concentrations reported by the LAS-X were low by almost exactly a factor of two. The flow rates were double checked with a gilibrator, but no error was found. Hence, the number concentrations reported by the LAS-X during the field tests were also increased by a factor of two.

With this correction, the number concentrations reported during the field tests by the Climet and the corrected LAS-X data agreed within expected uncertainty bounds, but the raw APS number concentrations, reported in terms of aerodynamic diameters, were shifted to the right. Again, this was what we expected, since atmospheric aerosol particles with sizes on the order of a micron and larger typically have material densities ranging from 2 - 2.5 g/cm^3,

depending on the local soil composition. Assuming an effective particle material density of 2.2 g/cm^3 and plotting the APS results in terms of the characteristic physical size $D = D_{AD}\sqrt{1/2.2}$ once again brought the number density distribution functions for all instruments into agreement (see Fig. 43). The Climet data was very sporadic due to a thermal problem with its data acquisition computer in the hot ambient temperatures. Hence, we only used the results from the Climet as a periodic check of the results from the LAS-X. For reasons of clarity which will be obvious when one looks at the figures below, only the LAS-X data is plotted.

By comparing the number concentration data from the LASX and the APS in the domain of the diameters in which they overlap, one could get a rough idea of the effective particle material density for each size bin at all times; however, the uncertainties associated with the number counts and morphologies do not really justify this level of detail. Thus, we simply assumed a constant particle material density of 2.2 g/cm^3 for all particles whose aerodynamic diameters were in the range of 1.0 -7.5 μm. We stress that this effective density would not hold for submicron particles, where previous data indicates that effective material densities approach numbers slightly greater than one as the particle sizes decrease into the submicron range.

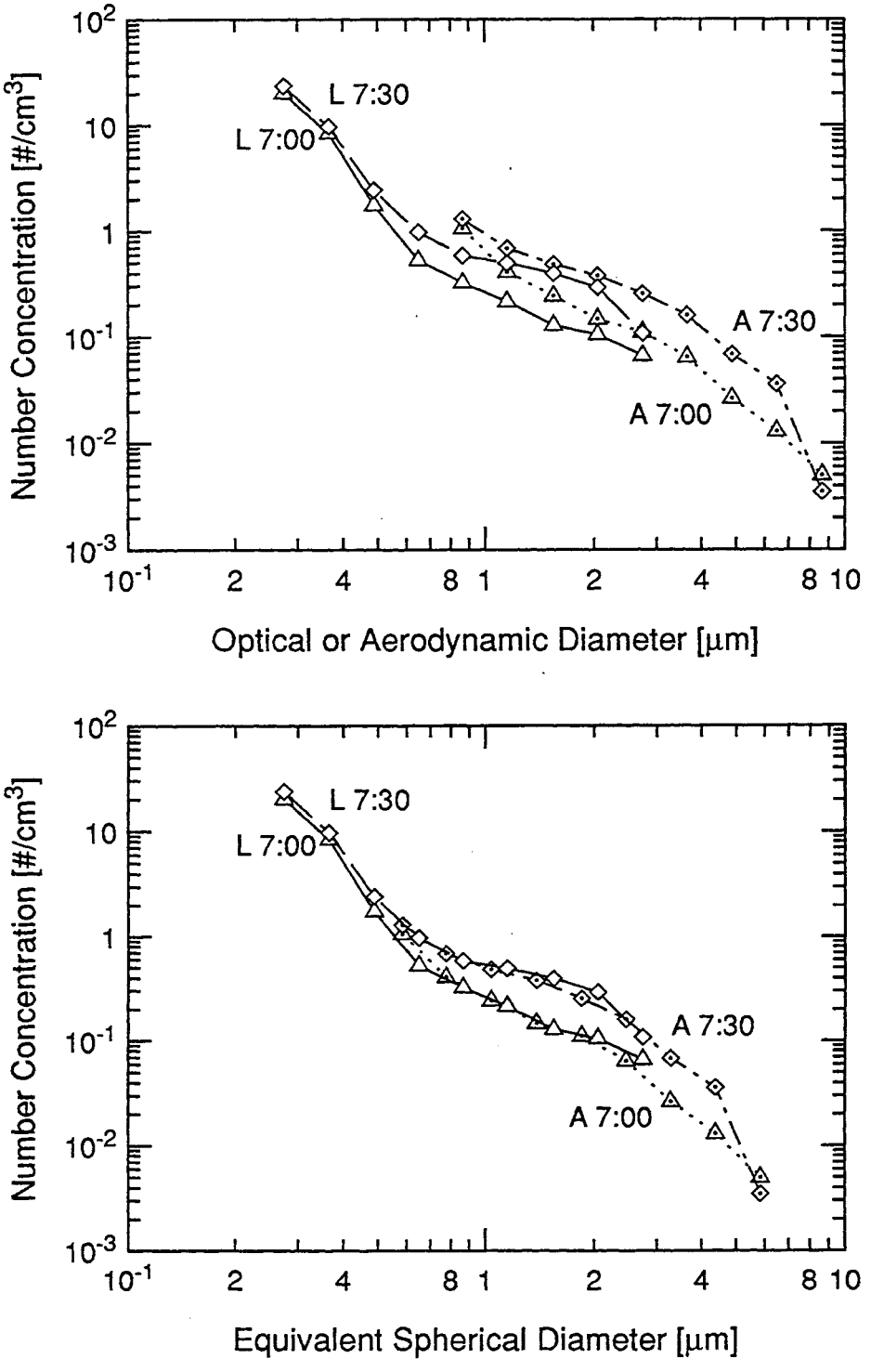

Fig. 43: Determination of effective material density from particle counter data: (a) Number concentrations from LAS-X and APS versus "optical" and "aerodynamic" diameters, respectively, as determined from measured data and PSL calibrations. (b) Same data, but with aerodynamic diameters shifted to smaller equivalent spherical diameter corresponding to a material density of 2.2 g/cm^3. Data are shown for several different time periods with differing total number concentrations.

CORRELATION BETWEEN LIDAR SIGNAL AND CO CONCENTRATIONS - As was stated above, a secondary goal was to check the accuracy of the Langan model L-15 CO monitors under field conditions using on-site calibrations as well as through comparisons to simultaneous measurements taken with an EPA-approved CO concentration monitor (Dasibi Environment Corp Model 3003) supplied by the local air quality agency, the New Mexico Dept. of Environmental Health. Six Langan monitors were located in pairs at the test site. The results were meant to document variability of the monitors such that the usefulness of previous data from the Langan monitors could be assessed. We did not set out to test the hypothesis that conditions during which high CO concentrations were observed might be correlated with conditions of high particle concentrations and hence high lidar signal levels, which would have meant that we should have chosen a location known to generate high CO concentrations during some part of the day. As we have indicated above, one would not in general expect a correlation to exist between roadside CO concentrations and roadside particle concentrations in the 1-5 μm size range, so one would also not expect a very good correlation between roadside CO concentrations and the lidar signal. And since high CO levels are known to be somewhat localized in extent and often occur overnight during temperature inversions, we chose a sight designed to gather data on the lidar - particle correlation rather a lidar CO concentration.

Santa Fe Technologies personnel carefully set up the CO monitors in consultation with the manufacturer in an attempt to ensure the highest accuracy for the Langan instruments. This was a more rigorous setup than had been followed in the previous tests. Hence, the Albuquerque data serves as a good test of the accuracy of the CO monitors, but does not necessarily prove the accuracy of data from the Minnesota tests, since different setup procedures were used. A total of six Langan CO monitors were mounted in pairs at three slightly different locations to test the instrument accuracies as well as provide some idea of CO variability. Monitors 1633 and 1648 were mounted to the particle sampling inlet at a height of 10 feet. Monitors 1632 and 1635 were located on the table supporting the particle sampling instruments at a height of about 3 feet. Monitors 1630 and 1663 were located on a streetlight pole adjacent to the roadway near the northeast corner of Gibson and Girard, at a height of about 10 feet. The Dasibi 3003 drew its sample from the sampling inlet line, so it should provide calibration data for monitors 1633 and

1648. Several times during each test day, span (20.3 ppm CO) and zero (0 ppm CO) gases were fed to the sampling inlets of each instrument to provide calibration reference points.

(Note: a complete set of graphs from the Langan instruments, as supplied by Santa Fe Technologies, is given in Appendix D. The graphs are included in order to provide a record of the Langan CO data. The ASCII data files supplied by Santa Fe Technologies, which were supposed to correspond to the graphs, were incomplete or missing-- see Table D-1 in App. D. However, enough data was supplied to demonstrate the behavior of the sensors, all of which exhibit similar characteristics when the instruments are properly set up and the data is properly reduced. This is sufficient to address the goal of this test: establishing how the CO data taken in Minnesota without calibration could be interpreted.)

Figures 44-47 below compare some of the CO concentration measurements made by several of the Langan monitors as well as the Dasibi device. The span calibration times are easily picked out by the jump up to much higher CO concentrations associated with the 20 ppm span gas concentration. The zero gas calibrations are somewhat more difficult to pick out because of the generally low ambient CO levels, but they are present as can be verified by a close examination of the data files together with notebook logs. Figures 44 and 45 clearly indicate the baseline drift that occurs on the Langan monitors as the sensor temperature warms up. Since sensor 1630 was not located at the sampling inlet (no files for sensors 1633 or 1648 were available), we cannot directly compare the readings. In other words, sensor 1630, located adjacent to the roadway and close to the corner of Gibson and Girard, shows more variability in CO concentrations, as one might expect. If one were to subtract the baseline offset using the data from the Dasibi 3003, it appears that the gain of the Langan monitors is relatively stable.

The Langan monitors do exhibit fairly uniform response from sensor to sensor when they are properly set up. This is illustrated by Figs. 46 and 47, which display the outputs from monitors 1630 and 1663, which were mounted side-by-side on the streetlight adjacent to the roadway. These two instruments show remarkable agreement considering the resolution of the digitizers in the Langan instruments is only 0.5 ppm. This indicates that the sensitivity of the sensor itself is actually better than 0.5 ppm, but that a more sensitive amplifier / digitizer combination should be used to record the output. Since most of the roadside data is at very low

CO concentrations (under 3 ppm), the uncertainty associated with the discreet digitization would dominate the precision of the result after the baseline biases were corrected.

In fairness, we must also point out that some difficulties were also encountered with the Dasibi instrument under the high ambient temperature conditions encountered in Albuquerque. This Dasibi instrument was used as supplied by the State of New Mexico Environmental Health Dept., presumably as they would use it in other ambient tests. It came equipped with only a strip-chart recorder for data recording. We noticed that very high frequency oscillations would show up at seemingly random times. These oscillations were much faster than could have been produced according to the sample flow rate and detection volume size of the instrument, so they had to arise from electrical noise in either the instrument or the chart recorder. We were unable to locate the source of the noise during the field tests, but the noise is readily recognizable as random bursts of nearly vertical lines on the chart recording. These occurred at relatively infrequent periods and were simply ignored when the strip chart data was later digitized.

Regardless of the absolute accuracy of the output signals, the relative fluctuations in CO concentrations can be compared to check to see if the various instruments are at least responding to similar events. In general, the Dasibi instrument shows more fluctuations that do the Langan monitors. The main reason is that the output signal level can be adjusted to the low range of the CO concentrations, and hence very small fluctuations can be recorded, whereas the Langan instruments are limited by the least significant bit resolution of 0.5 ppm. More fluctuations are observed when the roadway is located downwind of the sensors as would be expected. Other than the noise however, the instrument was almost perfectly calibrated. We observed essentially no drift in the baseline, and the voltage output was within (+2%, -0%) of what one would expect for a 20.3 ppm span gas. This uncertainty is well within the uncertainty limits of the equipment and calibration gas that we used.

Figures 48-53 display the Dasibi CO data along with average traffic counts, lidar signal, wind speed, and particle concentrations. The traffic, lidar, and particle concentrations have appeared in previous graphs. The wind direction is indicated as follows: periods with the wind blowing nominally across Gibson Blvd. toward the monitors (from the south ± 45°) are shown with a medium level gray shading, periods with the wind nominally parallel to Gibson Blvd. (east or west ± 45°) are indicated with light gray shading, and periods with the wind blowing nominally

from the golf course to the monitors (north ± 45°) are indicated in white. Low wind velocities and slow traffic motion conditions presumably reduce the amount of dilution of the exhaust plumes emitted by the vehicles, so we would expect slightly higher CO concentrations to be observed under these conditions. Some such trends were indicated in the data, but the parcity of instances with the wind blowing from the south (roadway downwind of instruments) makes the statistical significance of these events impossible to confirm.

In general, two-minute average CO concentrations did not necessarily track the traffic counter data very well. However, both the small particle and CO concentrations showed an increased number of short duration spikes when the wind was nominally parallel to the roadway, although not necessarily at the same times. These spikes could be the result of individual "high polluter" vehicles. For example, some of the small particle spikes apparently correspond to instances when unusually dirty Diesel vehicles (buses or trucks) underwent a transient acceleration slightly upwind of the sensors, as recorded by the video data of the scene. However, very little correlation is evident between the CO and lidar data sets, which might be expected at these low CO and particle levels. Although gasoline-powered vehicles emitting high levels of CO during acceleration transients are the likely source of the CO spikes, there is no way to confirm this from the video data. Moreover, although it is likely that high hydrocarbon emissions would accompany the high CO transients and could condense into very small hydrocarbon droplets, it is not likely that these would have sufficient time to grow into the size ranges monitored by the particle devices between the time that they were emitted with the vehicle exhaust and the time that they were sampled. It is more likely that the source of the small particle spikes was the transients in the exhaust flows which must accompany the acceleration transients -- these could either re-entrain small particles from the walls of the vehicle exhaust system, or they could entrain additional particles from the roadway surface.

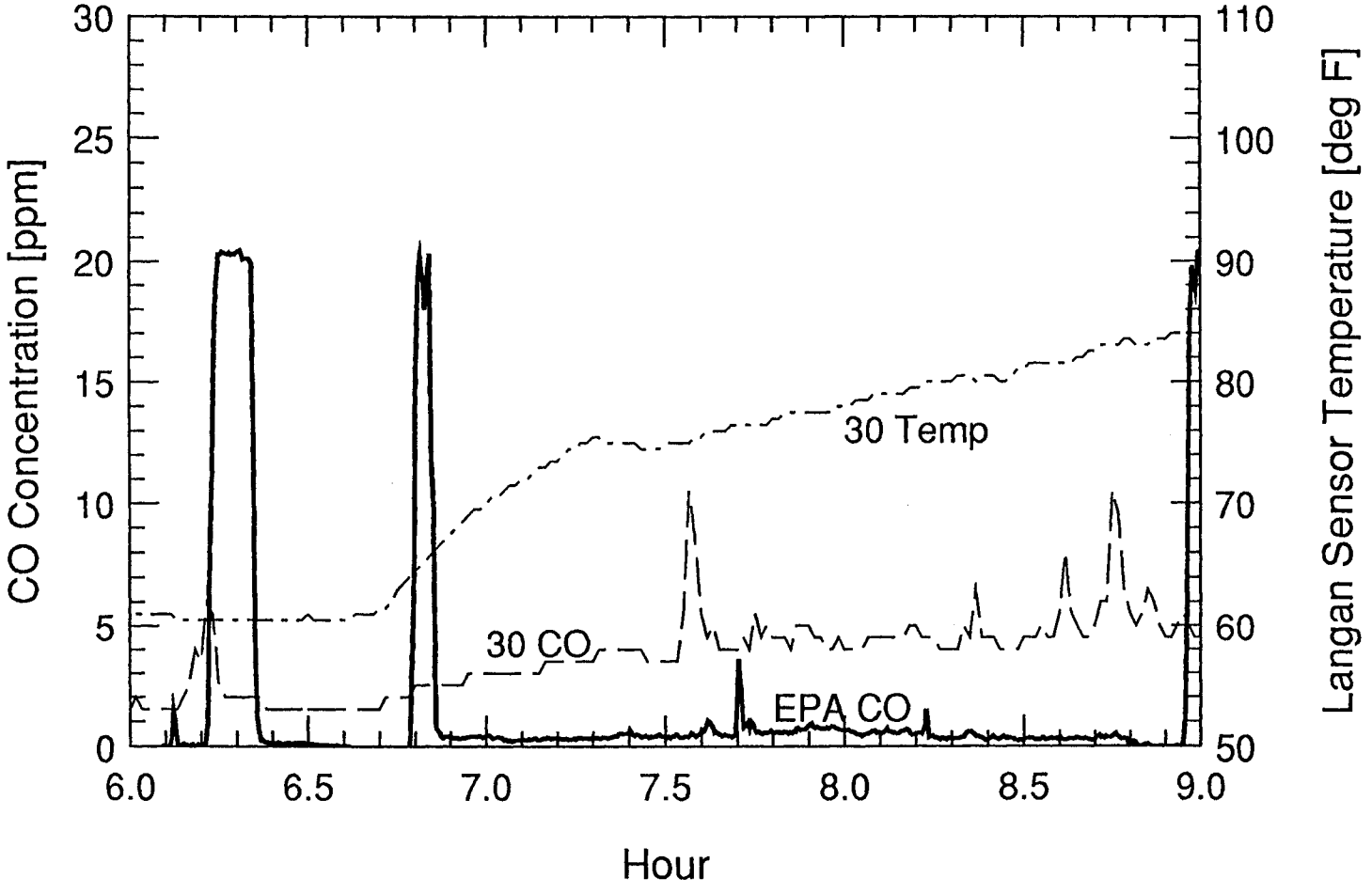

Fig. 44: Early morning CO concentrations (6/23) as measured by Langan L-15 CO monitor 1630 and Dasibi 3003 on loan from NM Environmental Health Dept. (EPA-approved). Both monitors sample from elevations of approximately 10 ft. The 20.3 ppm span calibrations are evident on the EPA monitor trace, as is the drift in the Langan output with sensor temperature.

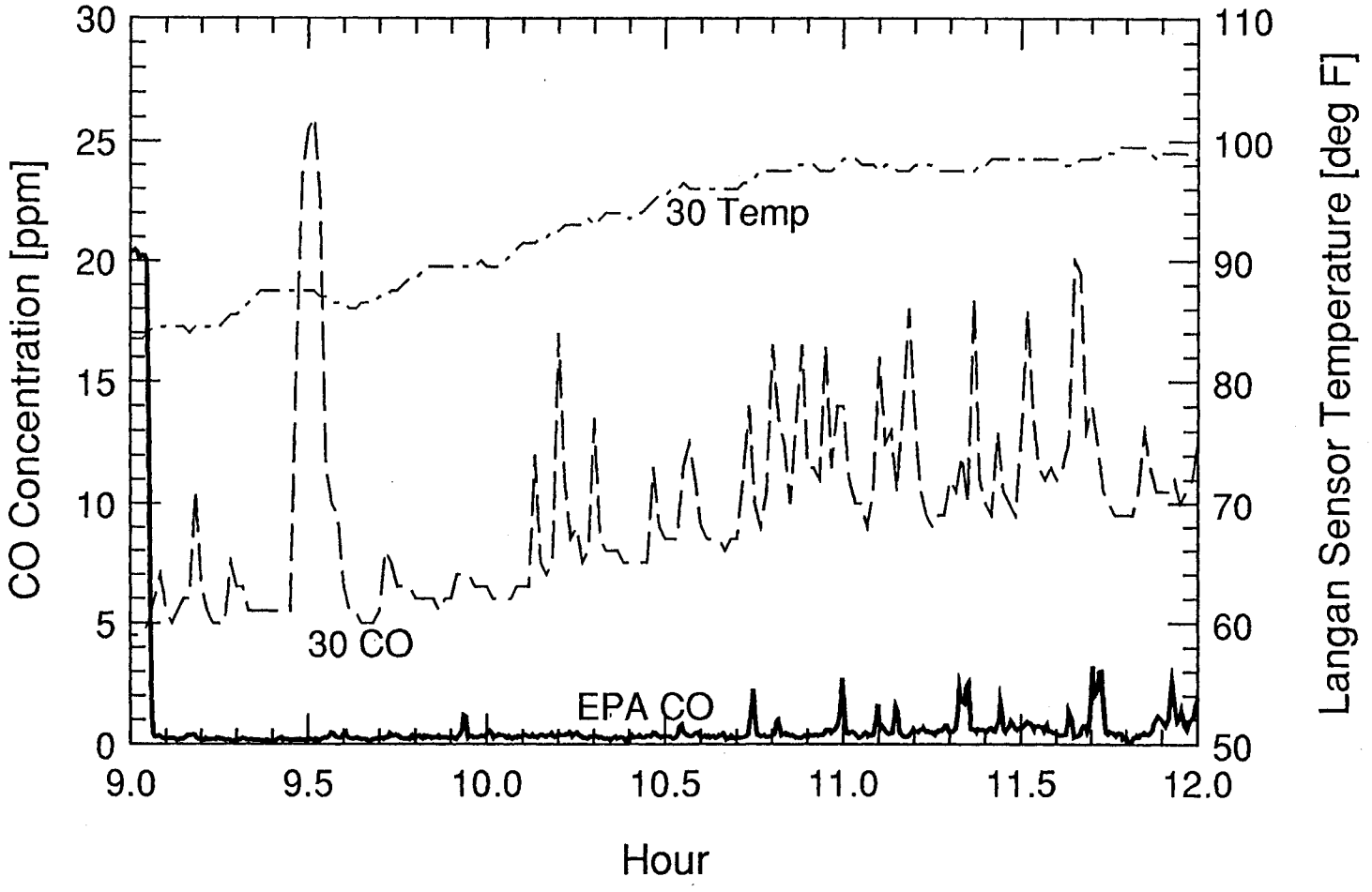

Fig. 45: Mid-morning CO concentrations on Fri.,6/23, as recorded by Langan L-15 CO monitor 1630 and Dasibi 3003 on loan from NM Environmental Health Dept. (EPA-approved). Both monitors sample from elevations of approximately 10 ft. The end of 20.3 ppm span calibrations at 9:00 is evident on the EPA monitor and a zero and span calibration is also shown for the Langan. The Langan offset continues to drift with temperature, but the gain appears correct.

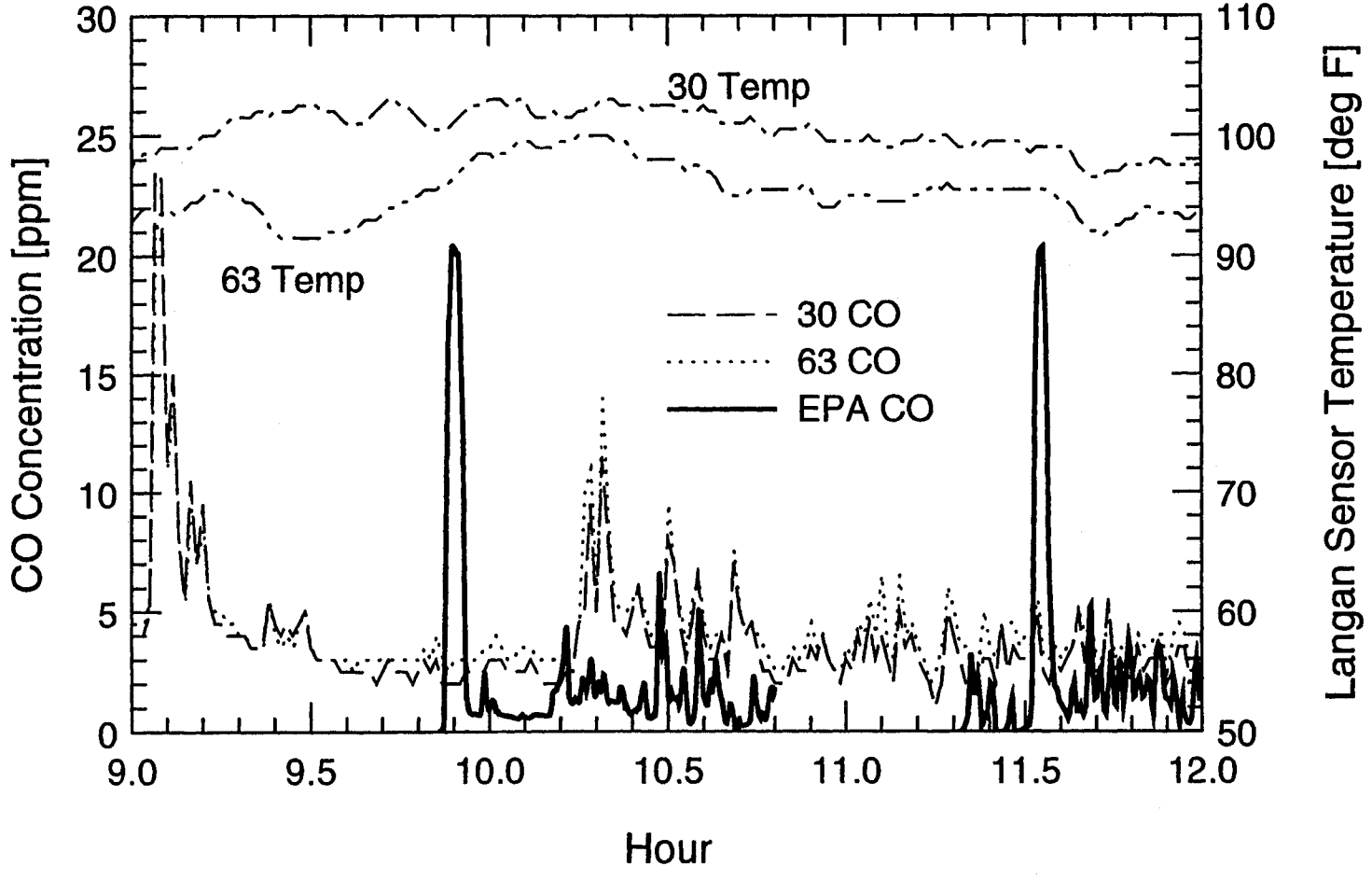

Fig. 46: Mid-morning CO concentrations on Thurs., 6/22, as recorded by Langan L-15 CO monitors 1630 and 1663. Monitors were mounted side-by-side on a streetlight adjacent to Gibson Blvd., near northeast corner of Gibson and Girard. The inlet heights were both approximately 10 ft above the ground. The relative agreement is real -- the outputs have not been shifted or scaled.

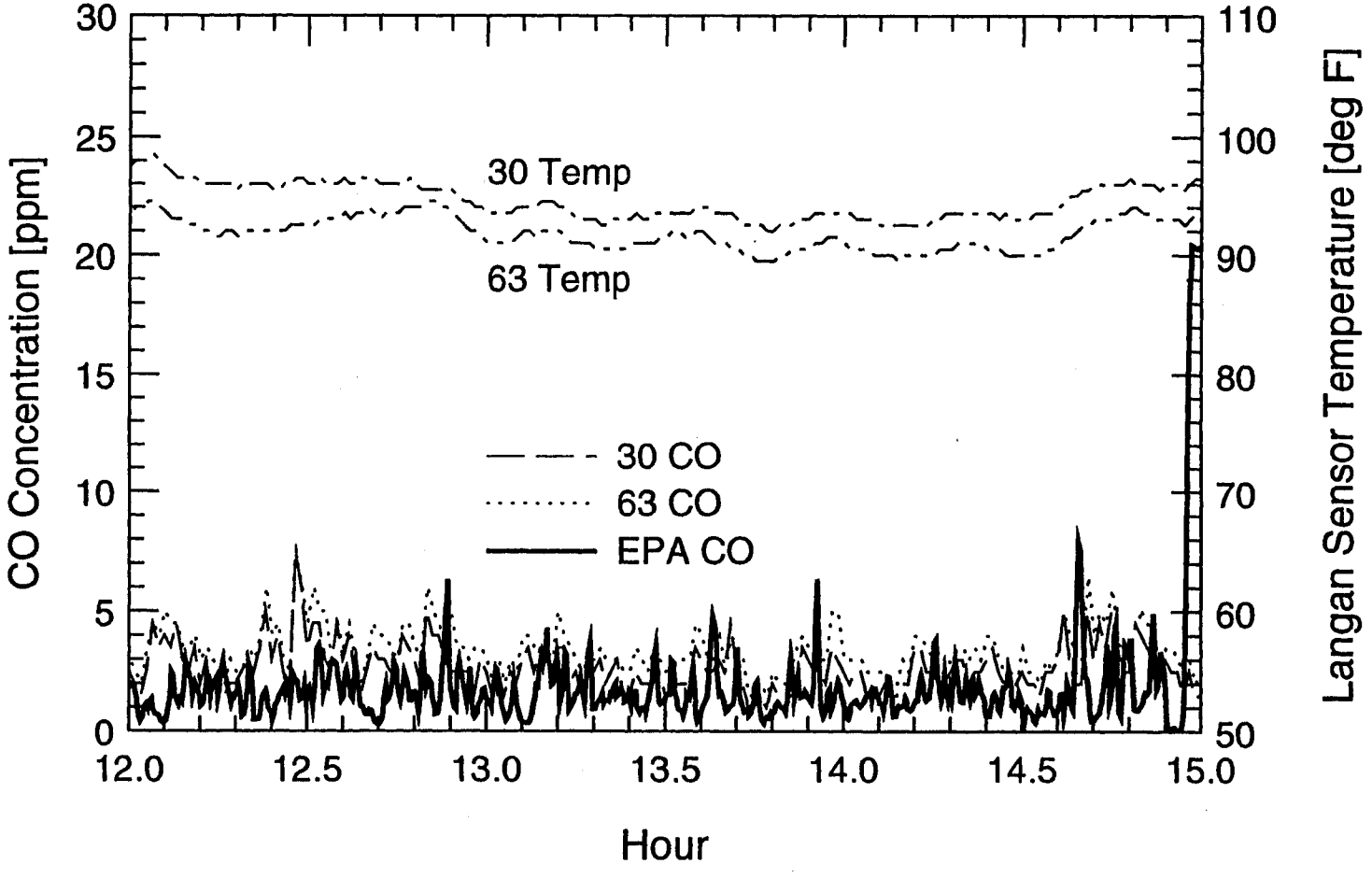

Fig. 47: Early afternoon CO concentrations on Thurs., 6/22, as recorded by Langan L-15 CO monitors 1630 and 1663. Monitors were mounted side-by-side on a streetlight adjacent to Gibson Blvd., near northeast corner of Gibson and Girard. The inlet heights were both approximately 10 ft above the ground. The relative agreement is real -- the outputs have not been shifted or scaled.

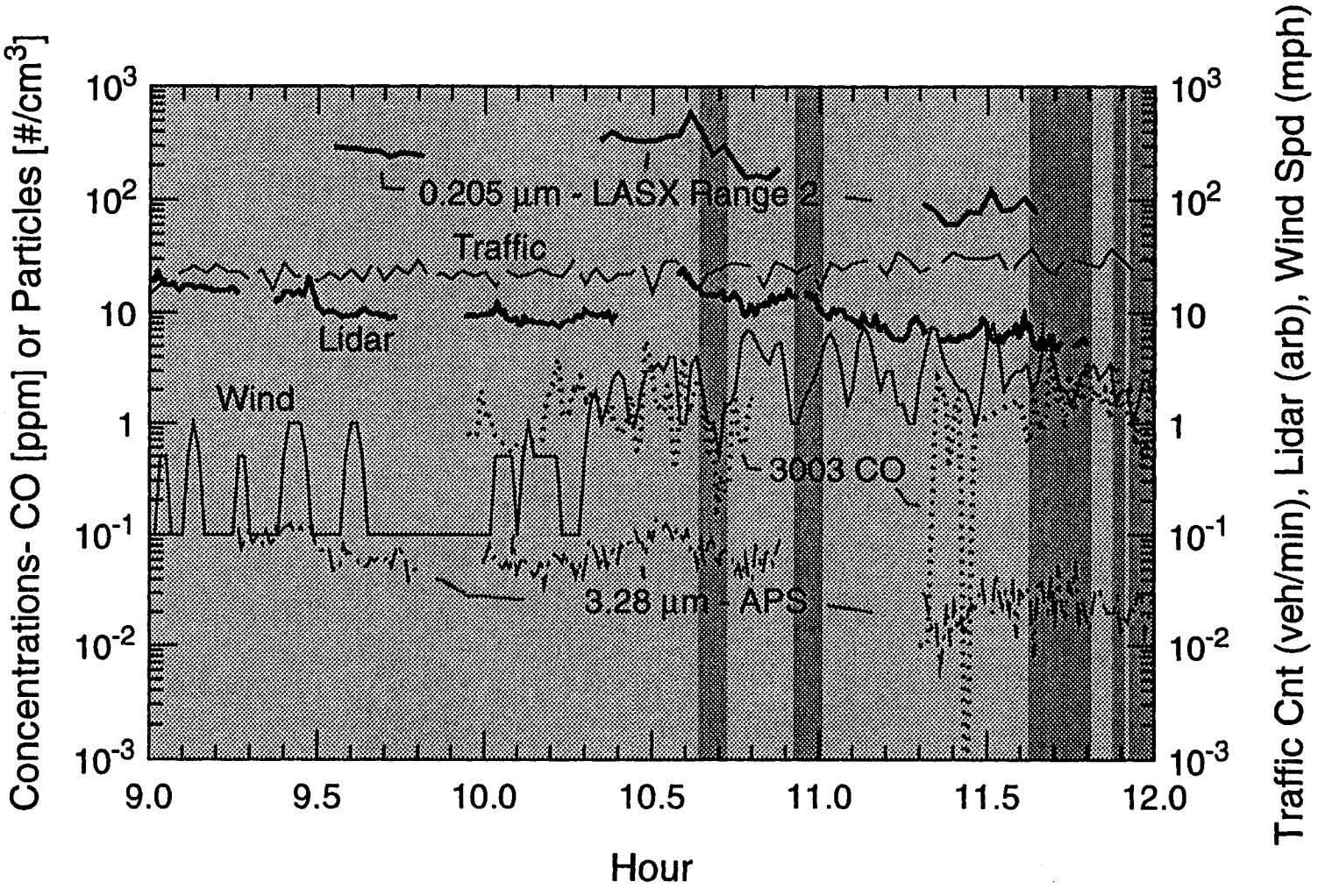

Fig. 48: Albuquerque CO concentrations (Dasibi 3003) compared to traffic counts, particle concentrations, wind speed, and lidar signal during mid-morning hours, Thursday, 6/22. Wind directions are indicated in quadrants as follows: N ± 45° -- white; E ± 45° or W ± 45° -- light gray; S ± 45° -- medium gray.

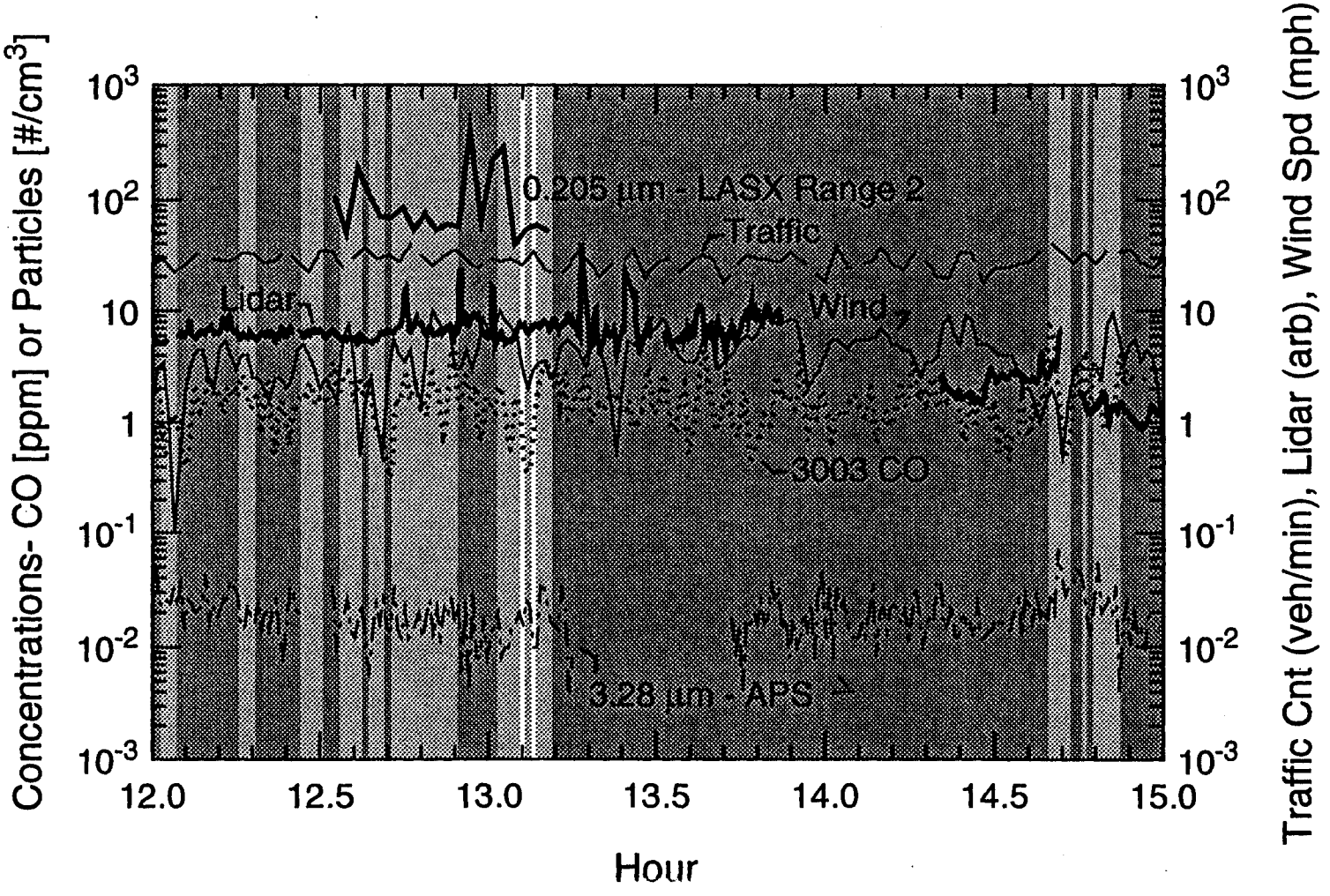

Fig. 49: Albuquerque CO concentrations (Dasibi 3003) compared to traffic counts, particle concentrations, wind speed, and lidar signal during early afternoon hours, Thursday, 6/22. Wind directions are indicated in quadrants as follows: N ± 45° -- white; E ± 45° or W ± 45° -- light gray; S ± 45° -- medium gray.

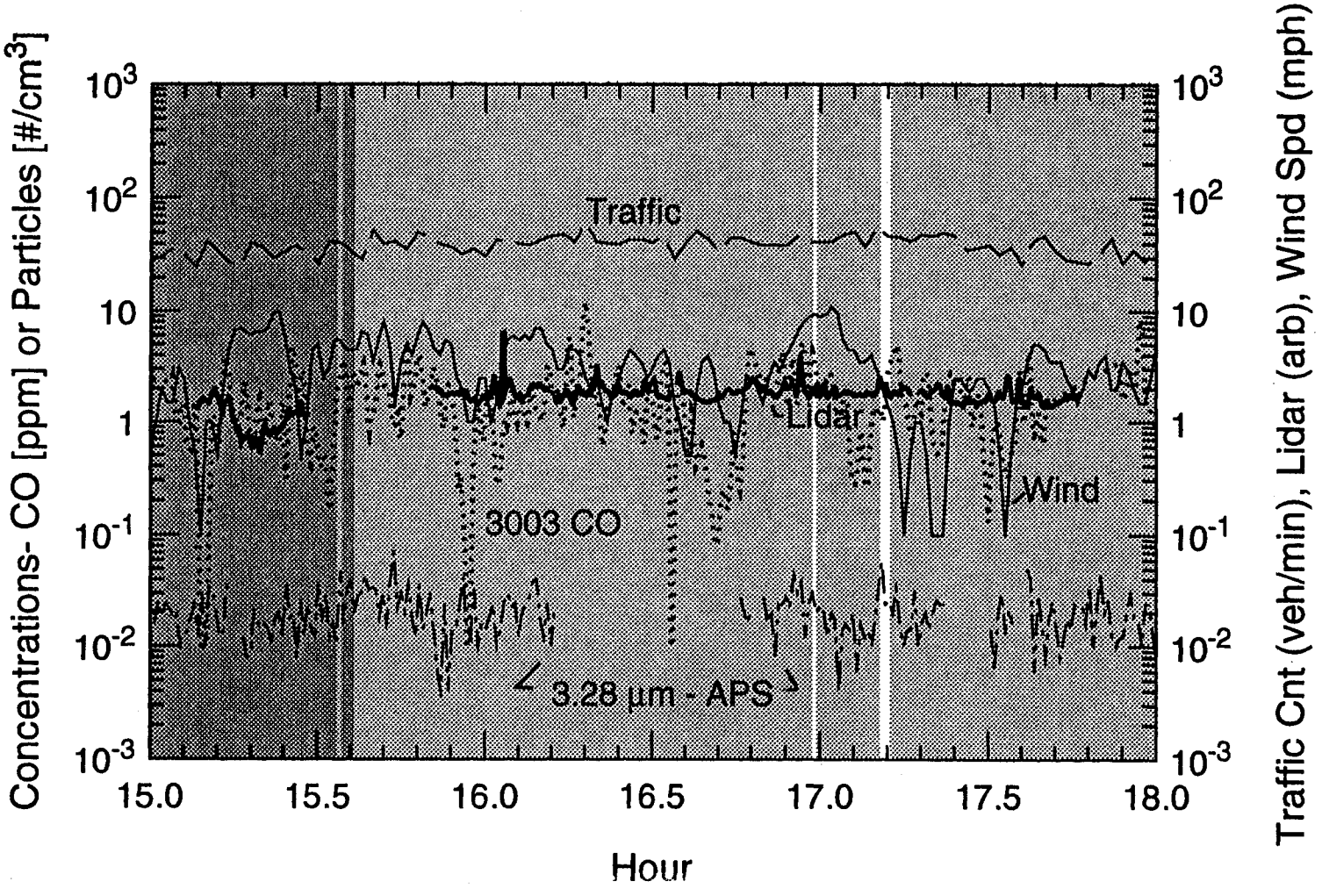

Fig. 50: Albuquerque CO concentrations (Dasibi 3003) compared to traffic counts, particle concentrations, wind speed, and lidar signal during late afternoon hours, Thursday, 6/22. Wind directions are indicated in quadrants as follows: N ± 45° -- white; E ± 45° or W ± 45° -- light gray; S ± 45° -- medium gray.

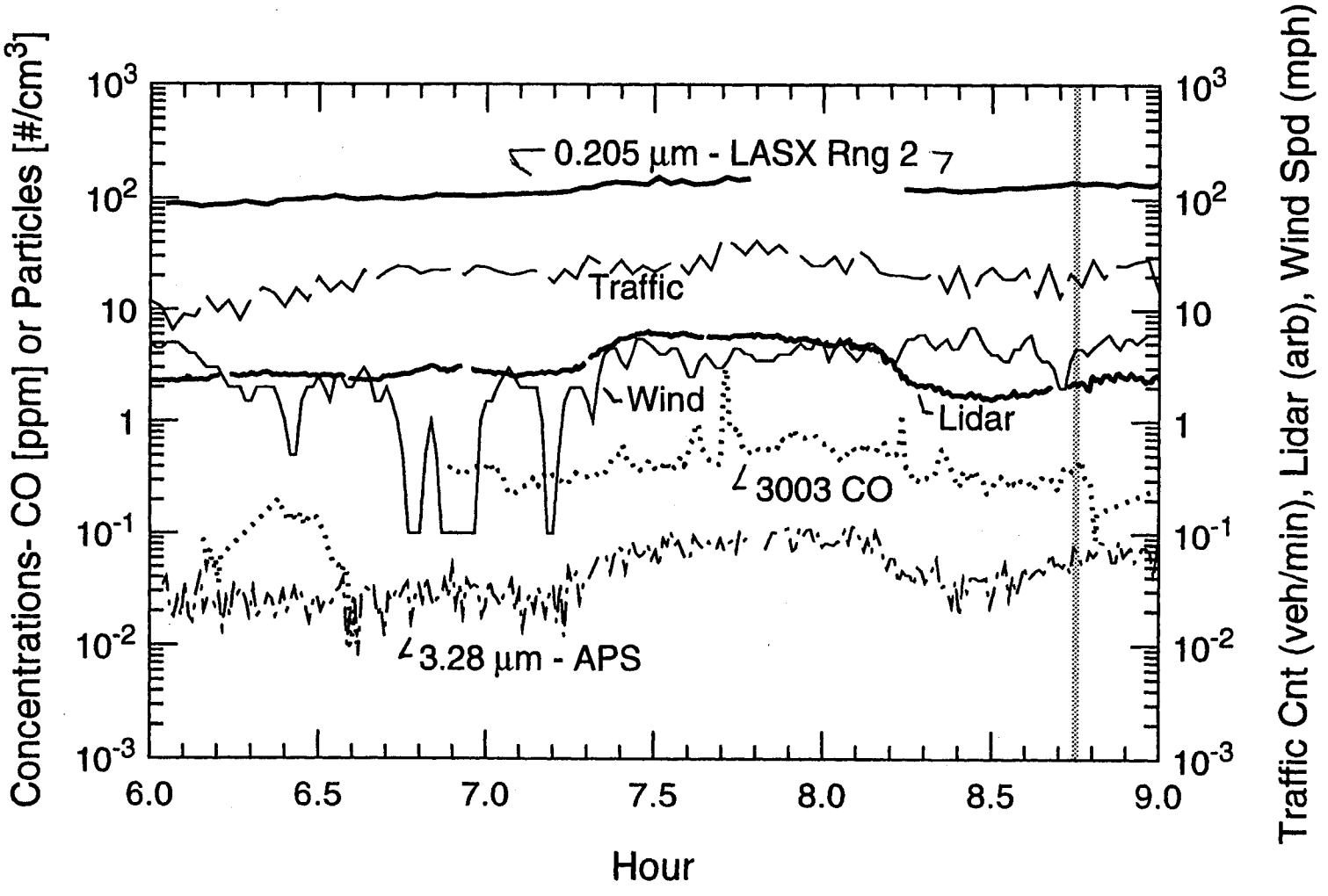

Fig. 51: Albuquerque CO concentrations (Dasibi 3003) compared to traffic counts, particle concentrations, wind speed, and lidar signal during early morning hours, Friday, 6/23. Wind directions are indicated in quadrants as follows: N ± 45° -- white; E ± 45° or W ± 45° -- light gray; S ± 45° -- medium gray.

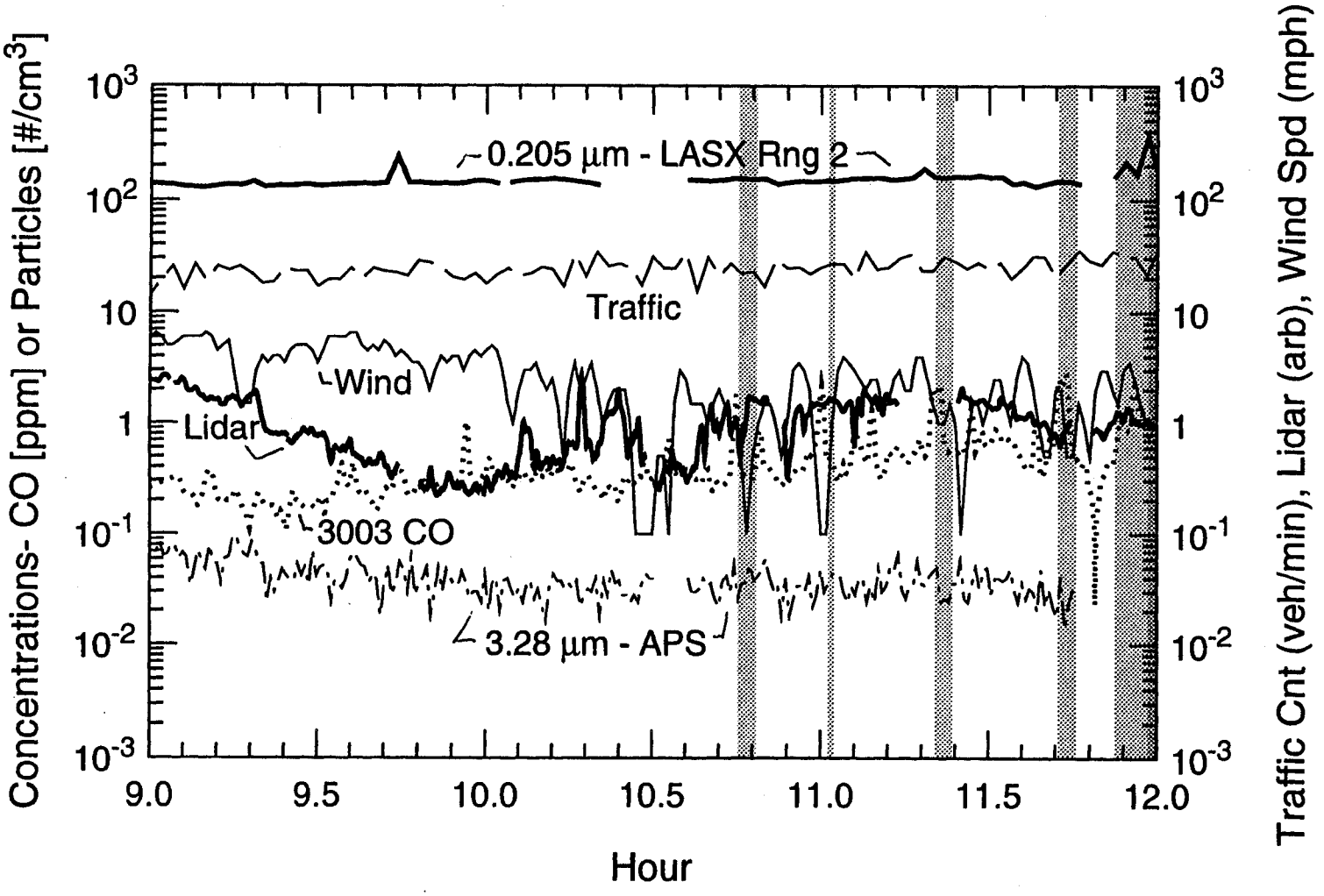

Fig. 52: Albuquerque CO concentrations (Dasibi 3003) compared to traffic counts, particle concentrations, wind speed, and lidar signal during mid-morning hours, Friday, 6/23. Wind directions are indicated in quadrants as follows: N ± 45° -- white; E ± 45° or W ± 45° -- light gray; S ± 45° -- medium gray.

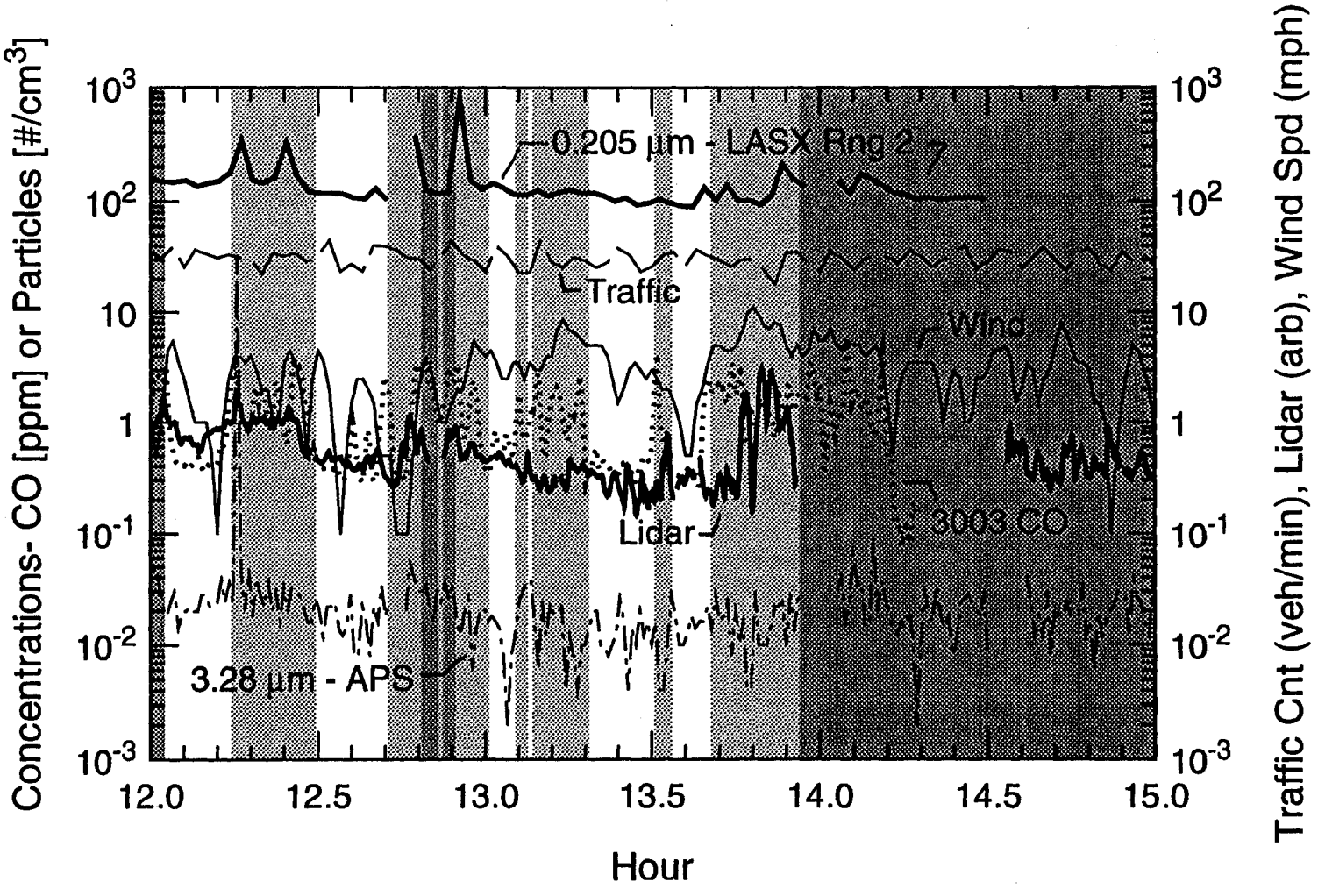

Fig. 53: Albuquerque CO concentrations (Dasibi 3003) compared to traffic counts, particle concentrations, wind speed, and lidar signal during early afternoon hours, Friday, 6/23. Wind directions are indicated in quadrants as follows: N ± 45° -- white; E ± 45° or W ± 45° -- light gray; S ± 45° -- medium gray.

Lidar Durability and Portability

The lidar system was sufficiently portable and rugged to enable field measurements to be made. However, several failures did occur. The yoke that holds the telescope of the lidar system broke when the entire unit was toppled by a wind gust during the Minnesota State Fair event. This shows that lidar system may not be left unattended under all possible weather conditions unless special precaution are taken. This may not be a serious limitation with respect to pollutant monitoring because pollutants generally disperse rapidly on windy days and buildup is not generally significant. The lidar operation was also hindered during the Rosedale event because of the cold ambient temperature. This could be overcome with improved lidar system design. Access to ground level measurements was somewhat restricted by field-of-view obstructions and eye safety considerations. In particular, during the Rosedale event, the lidar access was severely limited because of obstruction from an elevated highway located between the Rosedale Mall and the lidar located on the University of Minnesota St. Paul campus. The air was also very clean during this event because of occasional snow fall. We could not find any lidar data suitable for correlation calculation from the Rosedale event. Finally, in Albuquerque, when the laser power supply was subjected to sunlight and an ambient temperature of 100 F, it overheated several times. It had to be operated in the shade when the temperature was that high.

Rendering System Effectiveness

As the data above have demonstrated, lidar technology has the ability to yield information on aerosol distributions and their relationship to traffic events; however, its acceptance into the traffic control, regulatory, and urban planning communities requires the development of display capabilities similar to those presently used to display radar images in real time. A temporal history (*i.e.* a movie) of the lidar images together with auxiliary data superimposed over a GIS map displays relationships between a tremendous number of variables in a manner which is hard to convey to a non-technical audience in any other way. Detailed analysis of the relationships to derive causal effects will always require skilled personnel, but the job of explaining the results to the general public is greatly simplified with appropriate software. The lidar images are very

similar in concept and form to conventional radar images, and the general familiarity with radar data provides the basis for most explanations.

Commercially available Data Exploration (DX) software from IBM was used to render and help analyze the lidar images, as well as to import text and binary data files from the other sensors (traffic, PM, CO, and local weather data). A GIS base map was imported into the DX database along with GPS locations for the instruments. The DX software then interpolated a smoothed curve through the discrete lidar data points and superimposed the image over the GIS road grid. Icons with variable size, shape, and color were used to display the point sensor data at the proper locations. A sample of the Bunker Hills test data displayed in this fashion is shown in Fig. 54. This interface was very effective in communicating the relationship between the lidar images and the other environmental conditions to the general public at several transportation conferences.

The biggest limitation we encountered was that the current version of DX cannot be easily interfaced with the field instruments, and does not have real-time display capability. This may change in the future, depending on market demands for such capabilities in image acquisition and display programs, but it did hinder the evaluation test. Real-time data acquisition and display would provide feedback to the operators during the test and enable them to optimize the scans to best investigate the observed phenomena. The same display features which would enable the operators to quickly recognize and investigate particular relationships amongst the variables would also be needed to explain the data to a more general audience.

DX was originally developed for IBM's AIX operating system, and has been ported to run under the more commonly found UNIX operating system. We encountered several difficulties in getting the program to run on an SGI workstation operated under UNIX, but no problems using an IBM RISC-6000 computer operated under AIX. The difficulties with the SGI were eventually overcome with the help of IBM personnel. Since workstations operated under UNIX are more common that workstations operated under AIX, and since there seems to be no significant advantage of AIX over UNIX, this problem should be fixed to enable the widest possible use. We did not perform a comparison of the user-friendliness of DX versus other commercial visualization packages available on the different platforms.

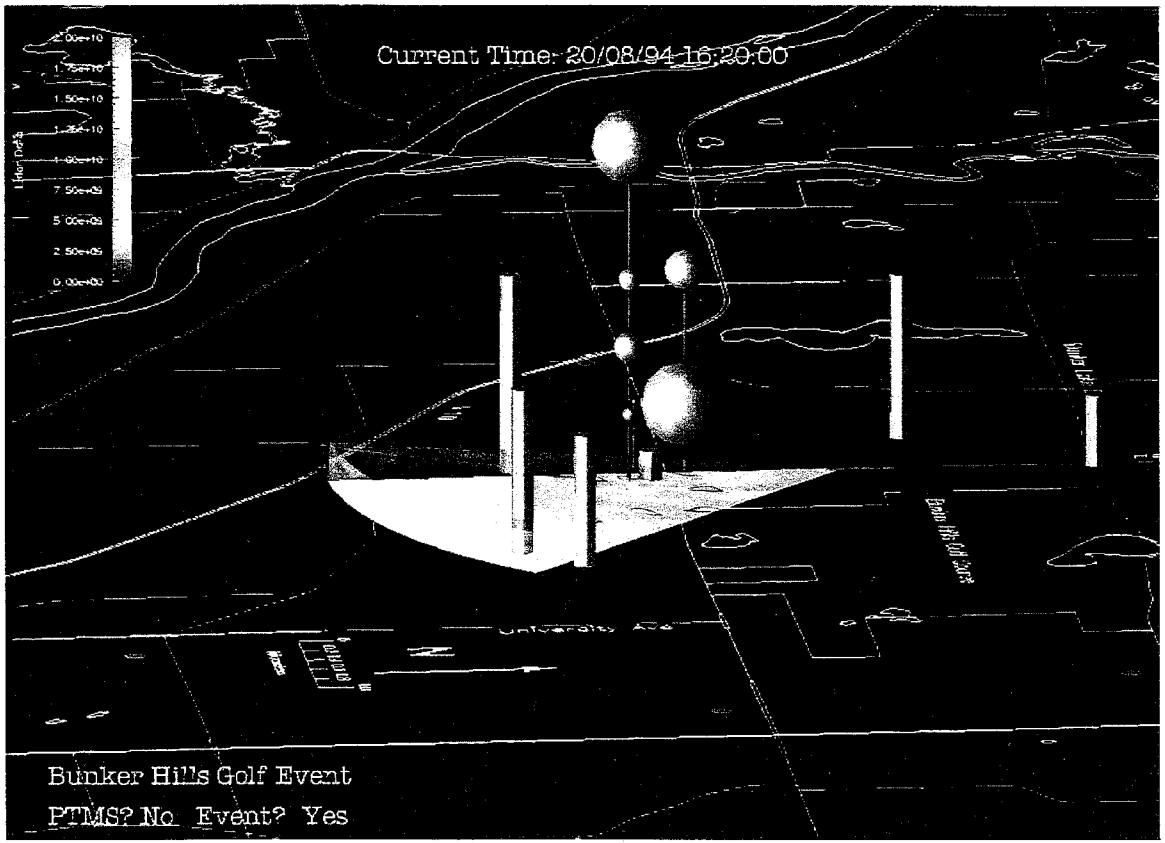

Fig. 54: Three-dimensional rendering of Bunker Hills lidar data together with point data from several Langan CO monitors (spheres) and several traffic counters.

The importation of both the lidar image files and text/binary files from auxiliary data sets currently requires a trained operator familiar with the file handling protocols observed by DX. Data importation libraries can be developed for specific instruments; for example, custom C programs were written by IBM personnel to import and display the lidar data and point sensor data. The fact that these programs had to be developed by skilled personnel at IBM in consultation with the lidar system operators at Los Alamos created a bottleneck in the analysis of the lidar images from the Minnesota tests. The bottleneck was particularly disappointing, since during the project conception stages, personnel from Santa Fe Technologies had indicated that the lidar images could be displayed in nearly real-time; what they were referring to was the ability to display the lidar signal along a given ray path versus time, such as those shown in Figs. 21, 31 and 32. However, real time display of the lidar data along with the auxiliary data overlaid on the GIS map was the capability which was needed, since this would enable the ability to observe and investigate relationships between various traffic flow and weather conditions and the aerosol signal distribution. With off-line data display, critical feedback paths for the lidar orientation and pollutant distributions were not available during the test, and hence the scan direction and scan resolution cannot be optimized to match the conditions present at the time.

Although the user must have some familiarity with the AIX or UNIX operating systems to be able to import data files into DX, the visual interface employed by DX facilitates image display. For example, standard features like 'zoom,' 'pan,' 'scroll,' and 'rotate' are accessible in this manner. Other features like changeable color maps and legends are also available. The interpolating curve used to display the discreet data as a more or less continuous image may be defined by the user, but the standard algorithms were sufficient for our purposes.

DX has standard image output capabilities, for example TIFF and PostScript formats, which may be printed out on suitable hard media. However, version 2.1 does not have many built-in functions for data analysis. User written modules written in a high level programming language like C can be executed from within DX, but writing such modules requires a highly-trained operator. A library of analysis tools would greatly enhance the power of the program, although a significant learning curve would still be faced in order to learn how to properly apply any analysis tools that were supplied. In an application for traffic control engineers, a better interface with statistical analysis packages would probably also be required.

SUMMARY, CONCLUSIONS, AND RECOMMENDATIONS

Summary of Evaluation Criteria and Lidar System Characteristics

The results of an operational test of a wide-area remote sensing lidar system used as an air quality monitoring device have been discussed. The goal was to analyze relationships between the lidar signal and roadside pollutant concentrations, specifically particulate matter and CO, and to identify variations in the response caused by changes in traffic levels or weather conditions.

The usefulness of elastic lidar technology for traffic-related pollution sensing applications was evaluated based on five criteria: 1) the ability to identify the source of particulate plumes, track their dispersion, and qualitatively indicate changes in particulate concentrations; 2) auxiliary measurements required to enable the lidar signal to be interpreted as a quantitative measure of pollutant concentrations; 3) ease of field deployment, *i.e.* field-of-view, range, operating requirements, portability, reliability, and safety; 4) versatility of lidar image display software for enabling acquisition and interpretation of images by an audience varying from public policy makers, regional planners, and air quality regulators to transportation engineers and atmospheric scientists; and 5) potential for providing useful data for development and validation of atmospheric models. The results of the evaluation are summarized for convenience in Table 8 on the following page (also shown as Table *i* in the Executive Summary). A brief discussion of the main factors affecting the evaluation under each criteria follows.

TABLE 8: EVALUATION CRITERIA AND SUMMARY OF RESULTS

Criteria	Evaluation Conclusions
Locate and track pollutant plumes, qualitative indication of particulate concentrations	Excellent spatial resolution provided line-of-site access exists. Temporal resolution is on the order of 1 sec. for a single point or a line, 2 min. for 2-D slices, and 10-15 min. for 3-D sectors. Can be used to identify conditions where high CO concentrations might exist, but will not provide a quantitative measure of CO.
Auxiliary measurements required for quantitative interpretation of signal	The lidar signal in near-ground applications near roadways is nominally proportional to the number concentration of particles with aerodynamic diameters of 1-5 μm. Linear correlation coefficients are typically 0.80-098 for short term (2-8 hour) periods. Correlation coefficients will decrease if particle compositions change, for instance if a large-scale sprinkler system turned on upwind, or if the lidar system gain is not periodically calibrated. Inertial impactors or related instruments are required to obtain quantitative particle mass concentrations, and may be combined with particle counters to provide information on effective particle material density. Humidity measurements would be needed to estimate scattering correction factors if measurements were made over a wide range of humidity levels.
Issues for field deployment: Field-of-view and range Operating requirements Portability Reliability Eye safety	 Measurable volume limited by line-of-sight access. Elevated site or portable platform required; wide-area resolution requires elevation over treetops & buildings. Maximum range of system tested was approx. 10 km. Two trained operators, 5 kW portable generator, ambient temps. between 32 and 110°F, no rain, wind limit depends on site location. Set up and check out requires approximately 1/2 day. Excellent; can be flown to city, transported to site in 12 ft. moving van, carried up to desired platform. Moderate; some down time caused by power supply or control circuitry failures; complete spares would be advisable for critical tests. Constraints on ambient conditions given above. The laser beam in this system was not eye safe to the unaided human eye within the first 1.2 km. This limits the near-field resolution in ground-level applications, which is important in urban environments where obstructions are common. FAA approval is required to ensure no interference with flight paths. The eye safety issue can be overcome by using a 1.5 μm wavelength or by increasing the diameter of the beam.
Image display and interpretation	Near real-time display of the data is needed, including time stamp and directional heading of the lidar beam. Ideally, the display would show the lidar data superimposed on the road grid. A fixed marker (a small target generating a repeatable lidar signal) would be useful in orienting the lidar images and monitoring system response. Ability to display traffic video in small inset within image would be useful, but not required.
Potential for model development and validation	Strong potential for evaluation and development of plume dispersion models for urban settings. Potential for coarse resolution of unobstructed wind fields provided aerosol plumes are present. Dial systems or fluorescence detection could be used for species specific detection, for example of NO_2, SO_2, volatile organic compounds, etc.

The first criteria, the ability to identify the source of particulate plumes, track their dispersion, and qualitatively indicate changes in particulate concentrations, represents some of the most useful data that can be acquired by an air quality monitoring tool. As an analogy, think of observing the plumes from several smokestacks by eye. The source and number of plumes, their dispersion, and estimations of opacity can be identified by the observer. The lidar system was able to locate hot spots associated with vehicle activity, track their evolution, and estimate peak concentrations of particulate matter within the plumes. The number and relative intensity of hot spots could be used as a measure of the air quality impacts associated with a given traffic control strategy. Moreover, spatial and temporal information available in a sequence of images could be used to develop more sophisticated pollutant dispersion models. The spatial resolution is an important advantage over traditional point-sensor air quality monitors. Rather than selecting point sampling sites by trial and error, data from representative distributions obtained by the lidar could be used to select more representative locations for point monitoring locations.

We note that the use of differential GPS measurements would greatly improve the positioning accuracy of the lidar images relative to the positions of known stationary objects, and is highly recommended in future deployments. In an advanced system, one would also have to develop a reliable means of determining changes in ground level elevation across the viewed region. Both of these factors have to do with the accuracy of the location of the pollutant plumes, and hence the ability to identify pollutant sources. However, since knowledge of the source may provide important clues as to the nature of the composition and size distributions of the aerosol particles, it may also have an indirect effect on concentration accuracies, which we discuss next.

The second criteria extends the first--is the signal an accurate measure of pollutant concentrations, or are additional auxiliary measurements required? We spent a good deal of effort determining how the lidar signal responded to changes in the particle size distribution. The correlation between the lidar signal and number concentrations of particles with aerodynamic diameters in the 1-5 μm range was quite good, ranging from 0.8-0.98 over relatively short intervals (2-8 hours) when unusual particle events were excluded and particle concentrations changed by a reasonable amount. "Unusual particle events" refers to concentrated plume sources which, when active, emit particles whose optical properties are significantly different from other particles in that region. In such cases, the lidar images would help to locate the plumes, but

auxiliary particle size and mass concentration measurements would be required to calibrate the lidar response.

Correlations to particle mass concentrations for particles with aerodynamic diameters in the 1-5 μm range, assuming the particle material density of these particles is constant at 2.2 g/cm^3, also range from 0.8-0.96, and follow nearly the same trends as the number concentrations. Correlations to ambient roadside CO concentrations, while evident to some degree under special circumstances, are not expected in general. A species-specific lidar system capable of directly imaging CO concentrations would have to be used to obtain quantitative measurements. However, there will be circumstances when, provided the wind and traffic conditions lie within certain bounds for a given area, the lidar signal could be used as an indicator of potentially high CO levels.

In viewing wide areas or in longer duration measurements, it would be advisable to collect calibration data on particulate matter at several points, so that spatial and temporal variations in the scattering properties and densities of the particles comprising the aerosol could be taken into account. With such calibrations, it would be possible to obtain reasonable estimates of the integrated exposures of individuals to particulate matter as they pass through the region. The only other way to obtain such information would be to equip many individuals with personal monitors to measure their exposure, and temporal resolution and sensitivity would be issues as well as the number of individuals needed to obtain a statistically significant result. Hence, lidar systems still appear to offer one of the best chances for monitoring the regional air quality impacts of ITS projects.

The third criteria deals with requirements for obtaining lidar images. Since the principal advantage offered by the lidar technology over traditional air quality monitoring methods is its ability to monitor time-varying pollutant concentrations over extended areas, the lidar unit must be relatively easy to site such that it has the desired field of view. Hence, it must be relatively compact and remotely locatable to enable line-of-sight access to the desired location(s). The farther the desired range, the higher the laser power requirement; larger powers imply not only a bigger laser, but also a larger power supply. However, as laser technology matures, system powers continue to increase while component footprints continue to decrease, so this should not represent a barrier to future deployments. The system we tested had a range of about 10 km.

This range could have been extended if greater system cost was acceptable, but modifications to ensure eye safety would also have been required to allow ground-level usage. Ensuring eye safety is a relatively straightforward design problem: the higher the laser power, the larger the beam diameter required to ensure that the beam can be viewed directly (purposely or inadvertently) by people (or animals) without eye damage. Care must be taken to allow for possible reflections off concave surfaces or focusing elements such as binoculars.

A more difficult limitation is posed by the requirement of line-of-sight access between the lidar unit and the monitored air volume. The air quality standards specify allowable pollutant concentrations at nominal breathing heights; therefore, it would be highly desirable for the lidar measurements to be obtained at heights as low as 10 feet. Unfortunately, buildings, trees, and hills impose rather severe restrictions on the field-of-view at these heights, and in general, the range is nowhere near 10 km for near-ground monitoring. Elevating the lidar on a portable jack stand or locating it on the roof of a nearby building helps significantly, but this also restricts the closest range which can be observed. Measurements above treetop / building levels would still be useful in identifying plume sources, but would have to be supplemented by portable ground level instruments to be most useful to the regulatory community. Measurements of the concentrations of submicron particles, ozone, or chemical precursors to ozone would be of much greater interest at treetop elevations, because variations in the concentrations of these pollutants are more gradual. Such measurements would require the development of new lidar systems using ultraviolet wavelengths.

Another critical piece pertains to the hardware and manpower needed to deploy the equipment. Presently, there are very few portable lidar systems available for making such measurements and a concomitantly small number of individuals trained to operate them; the system used in this test was supplied and operated by Los Alamos National Laboratory. It should be obvious that lidar measurements cannot be made on a whim. At the time of this writing, it is unknown whether a mass market for lidar measurements will develop, although new commercial systems are now being marketed. Regardless, as was done in this test, a lidar system can be shipped across the country, transported in a 14 foot moving van to the desired site, set up on a building or rented platform, and operated by two individuals. The on-site setup and check out, especially if the beam path were to be located accurately relative to a sampling location, requires

approximately a half-day. A portable 5 kW gasoline-powered generator was sufficient to supply all the necessary power requirements. This should be contrasted with 8 individuals required to operate traffic counters, CO monitors, particle sizing instruments, and traffic video equipment which were also part of the test.

The fourth criteria concerns ease of image acquisition and interpretation. Once the lidar data has been acquired, one must be able to summarize and interpret the tremendous volume of data quickly and easily. The lidar data are generally acquired in the form of two dimensional slices or three-dimensional sectors obtained by scanning the laser beam through a region of space. The return signals are converted into an image for visual inspection and further analysis. Some experience in interpreting the images is needed to avoid false conclusions caused by scattering off stationary objects, but these are generally fairly easy to recognize with a minimal amount of experience. The biggest limitation of the lidar technology that we tested was that the lidar images could not be displayed in real-time over the roadway grid . If such real time image display was available, then the appearance and development of aerosol plumes could be observed. Combining such capability with simultaneous real-time traffic video, traffic flow, and meteorological data, one could potentially discern cause and effect relationships between the traffic patterns and wind fields and the resultant pollutant distributions. Moreover, the real-time display capability would provide immediate feedback as to how to best optimize the lidar scan direction and resolution. This is analogous to how conventional radar images are now displayed.

If lidar is to become a widely accepted traffic management tool, the software used to do the image rendering must be made more user friendly. Numerous delays were encountered in properly orienting the lidar scan angles relative to the recorded GIS coordinates; this problem would be immediately obvious and rectified if a real-time display were available. In addition, the user would no longer have to deal with converting all of the data into a file format which can be readily viewed using the visualization software, as presumably this would be built in. This would eliminate another source of delays and further reduce training requirements.

Once the images are available in the proper format, the Data Explorer software package is a very powerful image visualization package. It is fairly transparent to install under IBM's AIX operating system, but installation on UNIX-based machines is fairly tricky and needs to be improved. A significant level of training would be required to familiarize users with the AIX or

UNIX-based operating system of the host computer as well as the various image display commands, but the visual interface facilitates recall of various operations and reduces learning time. Data Explorer is sophisticated enough that users could develop custom image and statistical analysis programs, but such development would require someone with knowledge of the C programming language as well as the mathematics of the desired analysis tools. Presumably, standard analysis packages could be developed and made available as one or more analysis libraries. In that event, users would have to be trained in the application and interpretation of such algorithms, but they would not have to be as familiar with the details of designing those routines. At the very least, input-output routines designed to interface directly between data displayed in DX and other commercially available image analysis and statistical analysis packages should be developed.

The fifth and final criteria pertains to the potential to provide data for developing and validating new pollutant dispersion models. The fact that the lidar signal corresponds linearly to the number concentration of relatively small aerosol particles makes it an excellent tool for validating dispersion sub-models in pollutant transport models. The particles will in general follow ambient air flows quite well with only a small settling velocity. A high speed, high resolution aerosol lidar system would be needed to gather enough detail on the motion of aerosol plumes to enable detailed analysis of the complex near-ground wind field, but there are very few other realizable alternatives which could produce comparable wide-area, high resolution, wind field data. Statistics derived from analyzing a variety of different terrains and environments could play a crucial role in the development of new near-ground air motion sub-models. The lidar signals also provide necessary information on the distribution of ambient aerosol source strengths. Together, the transport and source strength sub-models account for the majority of the uncertainty in model predictions of ground-level pollutant concentrations, and hence aerosol lidar data would be useful in developing and validating such models.

Conclusions Regarding Usefulness of Aerosol Lidar Measurements

Based on the results of this operational test, the following conclusions can be drawn with respect to the usefulness of elastic lidar signals for air quality monitoring:

1. The elastic lidar signal is an excellent qualitative indicator of particle number and mass concentrations, but cannot be used as a stand-alone quantitative measure due to variability in particle size and composition distributions. However, when augmented with auxiliary time-resolved measurements of particle size distributions and relative humidity at one or more points within the field-of-view, the signal can be effectively calibrated, and reasonably accurate measurements of particle number and mass concentrations are possible over extended regions. Lidar appears to be the only viable means of obtaining such wide-area information.

2. The elastic lidar signal is most sensitive to particles with diameters on the order of the wavelength of the laser beam. Hence, the response could be tailored to smaller particles if one was willing to address eye safety concerns associated with visible or ultraviolet lasers. This would be most effective for monitoring traffic related plumes. Eye-safe lasers near 2.5 μm would be more sensitive to larger particles than the current system.

3. Both particulate matter and CO concentrations vary with traffic conditions, but the lidar signal is not a strong indicator of CO concentrations. This was expected, since the concentrations of CO and particles whose aerodynamic diameters lie in the 1-5 μm range are not strongly linked. We did not observe any high CO concentration cases where CO levels exceeded ambient standards, so we cannot rule out the possibility of a threshold correlation, but we would anticipate that such a relationship would only exist under a few combinations of traffic flow, fleet composition, and wind direction, and false "hot" events could be triggered by other particulate sources. A species-specific lidar system (*e.g.* a DIAL system, which stands for Differential Absorption Lidar) would be better suited for quantitative CO measurements.

4. It may be possible to relate changes in local CO concentrations to changes in local concentrations of submicron particles, but doing so would require the ability to make time-resolved measurements of particle size distributions down to 0.1 μm and possibly below. This may work because fine and ultra-fine droplets of unburned hydrocarbons are formed under the

same conditions that CO is emitted, and these might generate a detectable elastic scattering signal if an ultraviolet lidar wavelength was used. However, the range of such a system incorporating a laser of similar power would be reduced by almost an order of magnitude due to atmospheric extinction. In addition, the correlation between the scattering signal and CO concentrations would be affected by the presence of soot particles emitted by Diesel vehicles.

5. Atmospheric conditions, particularly wind speed and direction, play important roles in determining local pollutant concentrations because of the complex mixing processes which occur in near-ground level urban environments. Mixing phenomena can be observed from two- and three-dimensional lidar scans. Only a few such scans were displayed here, but more effective visualizations can be produced using the three-dimensional rendering capabilities of the visualization software. Such information would be extremely valuable for the development and validation of more accurate dispersion models.

The point to keep in mind is that the lidar signal has both very good spatial resolution and very good time resolution. If individual plumes emanating from particular locations were visible, then the lidar signal would give an indication of the dispersion of that plume, and associated health impacts could be assessed based on knowledge of the particle source and the distribution of the plume. At that time, additional size and composition measurements could be taken to obtain more quantitatively accurate data, if such data were needed to determine appropriate actions to take. The data on size distributions and compositions could be built up into a data base, which could in turn be used to interpret subsequent lidar images. In the vast majority of cases, however, the identification of particle sources and an indication of how they disperse is the critical factor, and the lidar system is ideally suited for that role. As an example, the wide area sensing capability of the lidar system should enable one to estimate the impact of ITS technologies on particulate concentrations based on scans made before and after the technology is implemented.

Recommendations

Many of the difficulties encountered in this operational test arose out of the tight time schedules under which both the experimental plan and test schedules were carried out. Future operational tests should be planned by persons qualified in experimental design and familiar with

the subject areas involved, but need not necessarily be done by the project evaluators. The design should then sent out for peer review. This would require significant lead time. The hypotheses to be tested, the equipment required, and the evaluation criteria would be explicitly defined in the design, and then operational teams and evaluation teams could compete for the right to carry out the project. Some advantage would lie with the original experimental design planners, but the test would be more scientifically sound if carried out in this fashion.

Lidar systems used for future ground-level tests must have eye-safe beams at the exit of the laser. Sites should then be selected well in advance which enable both wide area scans of the desired transportation corridor(s) and line-of-sight access to positions where ground-based sampling stations could be located. The best plan would be to carefully select a suitable location, and then analyze variations observed at that location over an extended period of time. A single sampling station with real-time particle size resolution capabilities would enable quantitative calibration of the lidar signal at that point. If several sampling stations were used, the variability of the calibration across the entire lidar field-of-view could be evaluated. If staffing and equipment for multiple sampling sites were too costly, then it would be possible to use mobile sampling equipment to check the correlation at different locations at different times. The tradeoff would be in the test duration required to obtain statistically significant indications of spatial variability in the presence of time-varying phenomena.

Real-time display of the lidar scans similar to the display of conventional radar scans should be implemented. The data should be superimposed on a GIS map of the area such that orientations can be verified. Targets with known return signals should be located at known positions within the field of view of the lidar to verify directional data. An example of a suitable target might be a retroreflector with a very small entrance aperture mounted on a telescoping pole. The location of the target on the image would provide a ground truth position determination, and the signal would improve the ability to correct for beam extinction through the atmosphere. Auxiliary data from other point sensors should also be displayed in real-time either in separate windows or superimposed as time-varying icons on the image. Examples might include a traffic video window, a graphical window displaying a short but continuously updated time history of the output from a selected sensor, or the time varying column heights, color maps, or icon sizes such as those developed for the CO sensors in this test.

Time synchronization of all the deployed instruments must be maintained during the experiment to better than a minute. This would necessarily be addressed if all data were acquired and displayed by a single computer. Some form of telemetry system would likely be required to transmit the data to a single point for recording and display.

Time-resolved particle size distribution measurements are crucial for calibrating the lidar signal. If inertial particle counting instruments are used, then additional information regarding the average effective density and particle composition can be inferred. Chemical analyses of the MOUDI samples would provide a means of determining time-averaged compositions of the non-volatile materials comprising the particles in each size range. Again, such information could provide clues as to the source of the particulate matter, its associated health impact, and variations in the lidar correlation.

The Langan L15 CO monitors with 0.5 ppm lower resolution limit were inadequate for ambient roadside sampling. Instruments with 0.05 ppm lower resolution limit should be used in future tests. Moreover, on-site calibrations with known trace gas concentrations must be carried out to ensure the validity of the recorded data, or at least to enable correction factors to be derived.

REFERENCES

Allen, D. and Hering, S. (1990). "Size Distribution of Aerosol Sulfate, Nitrate Carbonyl, and Aliphatic Carbon During the SCAQS Period," *Proc. - 82nd A&WMA Annual Mtg.,* Air and Waste Management Assoc., Pittsburgh, PA.

Armbruster, L. (1987). "New Generation of Light-Scattering Instruments for Respirable Dust Measurement," *Annals of Occupational Hygiene*, vol. 31, pp. 181-193.

Bohren, C. F., and Huffman, D. R. (1983). *Absorption and Scattering of Light by Small Particles*, John Wiley and Sons, New York.

Braverman, T. N. (1995). "CO and PM-10 Intersection and Roadway Air Quality Modeling," presented at Vehicle Emissions and Air Quality Symposium, July 26-28, 1995, Minneapolis, MN. Braverman can be reached at US-EPA Office of Air Quality Planning and Standards, Research Triangle Park, NC.

Buttler, W. T., Eichinger, W. E., Lebeda, C. F., Cooper, D. I. and Moses, J., (1993). "Barcelona Air Quality Initiative," Los Alamos National Laboratory Preprint LA-UR-93-3672.

Chakravarty, S. and Hofeldt, D. L. (1994a). "First Milestone Report on the Evaluation of Lidar System for Area Sensing of Vehicle Emissions: Initial Results and Recommendations for Future Tests," (available from Minnesota Department of Transportation).

Chakravarty, S. and Hofeldt, D.L. (1994b). "Second Milestone Report on the Evaluation of Lidar System for Area Sensing of Vehicle Emissions: Initial Statistical Modeling and Recommendations for Future Tests," (available from Minnesota Department of Transportation).

Chakravarty, S. and Hofeldt, D.L. (1995a). "Third Milestone Report on the Evaluation of Lidar System for Area Sensing of Vehicle Emissions: Description of the Rosedale Test" (available from Minnesota Department of Transportation).

Cheng, Y. S., Chen, B. T., and Yeh, H. C. (1990). "Behavior of Isometric Nonspherical Aerosol Particles in the Aerodynamic Particle Sizer," *J. of Aerosol Science*, vol. 21, pp. 701-710.

Chylek, P., Ramaswamy, V., Cheng, R., and Pinnick, R. G. (1981). "Optical Properties and Mass Concentration of Carbonaceous Smokes," *Appl. Opt.*, vol. 20, p. 2980.

Cornille, P., Maenhaut, W., Pacyna, J. M. (1990). "Sources and Characteristics of the Atmospheric Aerosol Near Damascus, Syria," *Atmospheric Environment,* vol. 24A, pp. 1083-1093.

Cottingame, W. B. (1995). Private communication. Dr. Cottingame is with the Earth and Environmental Sciences Division of Los Alamos National Laboratory, Los Alamos, NM.

Dabbert, W. F. (1973). "Validation and Applications of an Urban Diffusion Model for Vehicular Emission," *Atmospheric Environment*, vol. 7, pp. 603-618.

deLeeuw, G., Kunz, G. J., and Lamberts, C. W. (1986). "Humidity Effects on the Backscatter/ Extinction Ratio," *Appl. Opt.*, vol. 25, pp. 3971-3974.

deLeeuw, G. and Lamberts, C. W. (1987). "Influence of Refractive Index and Particle Size Interval on Mie Calculated Backscatter and Extinction," *J. Aerosol Sci.*, vol. 18, pp. 131-138.

Eichinger, W. E. (1995). Comments on contents of Los Alamos National Laboratory Report by W. T. Butler *et al.*, "El Paso Demonstration: Wind Speed Measurements with a Scanning Elastic-Backscatter Lidar."

Grams, G. W., Blifford, I. H. Jr., Gillette, D. A., and Russell, P. B. (1974). "Complex Index of Refraction of Airborne Soil Particles," *J. Appl. Metrology*, vol. 13, pp. 459-471.

Hanel, G. (1976) "The Properties of Atmospheric Aerosol Particles as Functions of the Relative Humidity at Thermodynamic Equilibrium with the Surrounding Moist Air," *Adv. Geophys.*, vol. 19, p. 73.

Hänel, G. and Thudium, J. (1977). "Mean Bulk Densities of Samples of Dry Atmospheric Aerosol Particles: A Summary of Measured Data," *Pure Appl. Geophys.*, vol. 115, p. 799.

Hanel, G. (1988). "Single Scattering Albedo, Asymmetry Parameter, Apparent Refractive Index, and Apparent Soot Content of Dry Atmospheric Particles," *Appl. Opt.*, vol. 27, pp. 2287-2295.

Hanna, S. R. (1982). *Handbook on Atmospheric Diffusion*, DOE-TIC/11223, Technical Information Center, U. S. Department of Energy.

Harris, F. S. (1982). "Tropospheric Aerosols: Reviews of Current Data on Physical and Optical Properties," in *World Climate Research Program*, WCP-43, H. E. Gerber, ed., International Council of Scientific Union, World Meteorological Organization, Geneva.

Harris, F. S., Mathur, S. L., and Philbrick, C. R. (1995). "Optical Properties and Distribution of Stratospheric Aerosols," *Proc. of the 2nd Topical Symposium on Combined Optical-Microwave Earth and Atmosphere Sensing*, IEEE, Piscataway, NJ, pp. 167-169.

Heinz, S, Knoche, R., and Schaefer, K. (1994). "Optimization and Management of Ambient Pollutant Concentration Measurements by Dispersion Modeling," *Proc. of the 2nd International Conf. on Air Pollution, Part 1*, Barcelona, Spain, Computational Mechanics Publ., Southampton, Engl., pp. 531-536.

Hering, S. V. and McMurry, P. H. (1991). "Optical Counter Response to Monodisperse Atmospheric Aerosols," *Atmospheric Environment*, vol. 25A, pp. 463-468.

Hinds, W. C. (1982). *Aerosol Technology*, Wiley-Interscience, New York.

Ji, X., Jiang, D., Fei, S., Yuan, H., He, P., Ye, B., Lei, Z. Feng, C. (1993). "Road Dust Emission Inventory for the Metropolitan Area of Shanghai City", *Atmospheric Environment*, vol. 27A, pp. 1735-1741.

Klett, J. D. (1981). "Stable Analytical Inversion Solution for Processing Lidar Signal Returns," *Appl. Opt.*, vol. 20, pp. 211-220.

Kovalev, V. A. (1993). "Lidar Measurement of the Vertical Aerosol Extinction Profiles with Range-Dependent Backscatter-to-Extinction Ratios," *Appl. Opt.*, vol. 32, pp. 6053-6065.

Kolev, I., Savov, P., and Parvanov, O. (1996). "Lidar Investigation of Air Quality Over Complex Terrain," *Proc. 1996 Conf. on Lasers and Electro-Optics Europe*, Hamburg, Germany.

Leonelli, J. (1995). "LIDAR Technology Measuring the Atmosphere," *Phot. Spectra*, vol. 29, #6.

Lilienfeld, P. (1996). "Nephelometry Applied to Continuous Monitoring of Ambient Fine Particulate Matter," *Proc. of the 1995 Specialty Conf. on Optical Remote Sensing for Environmental and Process Monitoring*, San Francisco, CA, Air and Waste Management Assoc., Pittsburgh, PA, pp. 484-504.

McMurry, P. H. and Anderson, M. (1990a). "Organic and Elemental Carbon Size Distributions of Los Angeles Aerosols Measured During SCAQS," *Proc. - 82nd A&WMA Annual Mtg.*, Air and Waste Management Assoc., Pittsburgh, PA.

McMurry, P. H. and Stolzenburg, M. R. (1990b). "On the Sensitivity of Particle Size to Relative Humidity for Los Angeles Aerosols," *Proc. - 82nd A&WMA Annual Mtg.*, Air and Waste Management Assoc., Pittsburgh, PA.

Measures, R. M., 1984. *Laser Remote Sensing: Fundamentals and Applications*, Wiley-Interscience, New York.

Overbeck, J. A., Salisbury, M. S., and Richmond, R. (1996). "Airborne Lidar System Profiles Wind Speeds," *Laser Focus World*, April, 1996, pp. 89-92.

Pandithurai, G., Devara, P. C. S., Raj, P. E., and Sharma, S. (1996). "Aerosol Size Distribution and Refractive Index from Bistatic Lidar Angular Scattering Measurements in the Surface Layer," *Remote Sensing of the Environment*, vol. 56, pp. 87-96.

Pope, C. A. III, Thun, M. J., Namboodiri, M. M., Dockery, D. W., Evans, J. S., Speizer, F. E., and Heathe, C. W., Jr., (1995). "Particulate Air Pollution as a Predictor of Mortality in a Prospective Study of U.S. Adults," *Am. J. Respir. Crit. Care Med.*, vol. 151, pp. 669-674.

Sasano, Y. and Browell, E. V. (1989). "Light Scattering Characteristics of Various Aerosol Types Derived from Multiple Wavelength Lidar Observations," *Appl. Opt.*, vol. 28, pp. 1670-1679.

Seinfeld, J. H., 1986. *Atmospheric Chemistry and Physics of Air Pollution,* Wiley, New York.

Sheridan, P. J., Schnell, R. C., Kahl, J. D., Boatman, J. F., and Garvey, D. M. (1993). "Microanalysis of the Aerosol Collected Over South-Central New Mexico During the ALIVE Field Experiment, May-December, 1989," *Atmospheric Environment*, vol 27A, pp. 1169-1183.

Shettle, E. P. and Fenn, R. W. (1979). "Models of Aerosols of the Lower Atmosphere and the Effect of Humidity Variations on their Optical Properties," Report AFGL-TR-79-0214,U.S. Air Force Geophysical Laboratory, Hanscom Air Force Base, MA.

Sloane, C. S. (1984). "Optical Properties of Aerosols of Mixed Composition," *Atmos. Environment*, vol. 18, p. 871.

Stein, S. W., Turpin, B. J., Cai, X., Huang, P.-F., and McMurry, P. H. (1994). "Measurements of Relative Humidity-Dependent Bounce and Density for Atmospheric Particles Using the DMA-Impactor Technique," *Atmospheric Environment*, vol. 28, pp. 1739-1746.

Sutton, S., and Bennett, M. (1994). "Measurement of Wind Speed Using a Rapid-Scanning Lidar," *International Journal of Remote Sensing,* vol. 15, pp. 375-380.

Wilson, W. E., "Differentiating Fine and Coarse Atmospheric Aerosols: Rationale and Techniques," seminar presented to the Dept. of Mechanical Engineering, University of Minnesota, Apr. 19, 1995 (available on videotape). (Dr. Wilson is a Senior Science Advisor at the Atmospheric Research and Exposure Assessment Laboratory, U.S. Environmental Protection Agency, Research Triangle Park, NC 27711).

Wolf, J. P., Kölsch, H. J., Rairoux, P., and Wöste, L. (1990). "Remote Detection of Atmospheric Pollutants Using Differential Absorption Lidar Techniques," in *Applied Laser Spectroscopy*, W. Demtröder and M Ingusico, eds., Plenum Press, New York.

APPENDIX A: LIDAR SIGNAL RESPONSE

This appendix contains a somewhat simplified discussion of the lidar signal dependence. The main points should be accessible to both technical and non-technical readers. More detailed discussions abound in the literature (*e.g.* Klett, 1981; Measures, 1984; Kovalev, 1993).

Fig. A1 shows the basic geometry of the lidar system (repeated here for convenience).

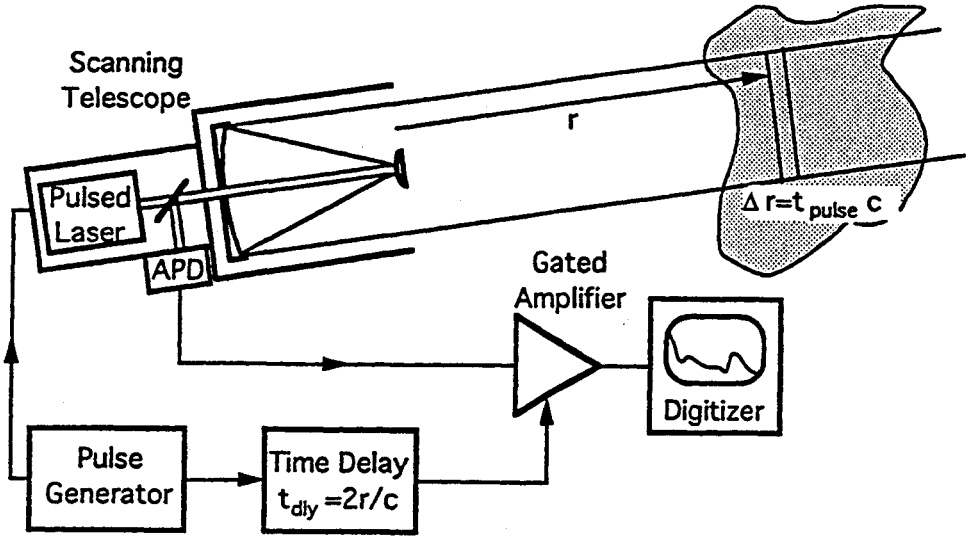

Fig. A1: Schematic of a lidar system.

Lidar Signal Dependence

We start by examining how much light is scattered to the detector by a group of particles located a distance r from the source of a pulsed laser beam which illuminates them. To simplify the notation, appropriate average values for the laser beam intensity and particle composition will be used in lieu of the writing out the integrals across the beam profile and particle distribution, respectively. Then, the optical signal generated by the illuminated particles at distance r from the laser can be written as

$$P_{det}(r) = \sum_{particles} n_p(r, D_p)\, I(r)\, \overline{\sigma}_{sca}(r, D_p, m)\, \Omega_{coll}(r) \left[\begin{array}{c} \text{fraction of scattered light} \\ \text{which returns to detector} \\ \text{after being scattered} \end{array} \right] \qquad \text{(A 1)}$$

where P_{det} is the power [W] of the light which returns to the detector after being scattered by the particles at location r (sampled at time $t = 2r/c$ after the laser pulse is emitted), n is the number of particles of diameter D_p illuminated by the laser pulse at a distance r from the colocated laser / detector unit, $I(r)$ is the average laser beam intensity [W/cm^2] at location r, $\overline{\sigma}_{sca}$ is the scattering cross section per unit steradian [cm^2/sr] associated with particles of this size (averaged over variations in composition and morphology which might occur across particles of the same size), m is the effective complex refractive index which accounts for the average composition and morphology of the particles of this size class, Ω_{coll} is the solid angle [sr] subtended by the telescope which collects the backscattered light, and the fraction results from the fact that some of the scattered light which initially starts back toward the detector is lost due to absorption and scattering (*a.k.a.* extinction) by molecules and other aerosol particles located between the particles at r and the detector. The summation is over all the particles of different sizes which are illuminated by the laser pulse at position r.

We now expand this equation to introduce quantities which we can either measure or we want to determine. The number of particles illuminated by the laser pulse at position r can be written in terms of the volume, V_{mv}, [m^3] occupied by the laser pulse at position r and the number density, N_p, [m^{-3}] of the particles there: $n = NV_{mv}$. The illuminated volume is just the product of the beam cross section, A_b, [m^2] at r times the length, Δr, [m] of the light pulse, $V_{mv} = A_b \Delta r$, where Δr is fixed by the pulse duration, τ_{pulse} [s]: $\Delta r = c\,\tau_{pulse}$ (c is the speed of light [m/s]). The cross-sectional area of the beam at position r cancels out if we further expand the laser beam intensity in terms of the beam power, P_b, [W] and beam area at r, *i.e.* $I(r) = P_b / A_b$. Thus, the divergence of the laser beam as it propagates doesn't affect the signal strength, but rather only determines the spatial resolution of the measurements.

We can also introduce the extinction coefficient, α_{ext}, [m^{-1}] to keep track of the attenuation of the scattered light caused by the presence of intervening particles which reside between the detector and the particles at location r. These intervening particles can either absorb the scattered light or scatter it in a different direction away from the detector. The extinction coefficient accounts for the net decrease in the signal. The definition of the local extinction coefficient is

$$\overline{\alpha}_{ext}(r, D_p, m) = N_p(r, D_p)\left[\overline{C}_{sca}(r, D_p, m) + \overline{C}_{abs}(r, D_p, m)\right] \quad \text{(A 2)}$$

where $\overline{C}_{abs}$ [m^2] is the effective absorption cross section of the particles and $\overline{C}_{sca}$ [m^2] is the total scattering cross section for the particles, which assumes that scattering in all directions removes power from the beam. (Again, both of the cross sections are averaged over any variations in composition or morphology.) The extinction coefficient is a function of particle size because both the number concentration and the cross section vary with size, and it also varies with r because the particle concentrations and effective refractive index are functions of r. This complicates the situation, because the fraction of the scattered light which returns to the detector depends on the losses caused by all particles integrated along the entire beam path. In order to keep things simple for now, we'll just write the loss of signal in terms of a spatially averaged extinction coefficient, $\overline{\overline{\alpha}}_{ext}$, in which the double bar serves as a reminder of the combined composition and spatial average. One must keep in mind that the average extinction coefficient, $\overline{\overline{\alpha}}_{ext}$, generally varies slowly with r. Thus, equation (A-1) can be rewritten as

$$P_{det}(r) = \sum_{particles} P_b(r)\,\Delta r\, N_p(r, D_p)\,\overline{\sigma}_{sca}(r, D_p, m)\,\Omega_{coll}(r)\exp\left[-\overline{\overline{\alpha}}_{ext}(r)\ r\right] \quad \text{(A 3)}$$

Finally, we notice that the laser beam itself undergoes the same attenuation as it propagates to position r that the scattered light undergoes as it returns to the detector. The result is that we can use the power leaving the laser, P_0, instead of P_b (r), if we simply double the distance used to account for the extinction. Making the necessary substitutions, we arrive at

$$P_{det}(r) = \sum_{particles} P_0 \exp\left[-2\overline{\overline{\alpha}}_{ext} r\right]\Delta r\, N_p(r, D_p)\,\overline{\sigma}_{sca}(r, D_p, m)\Omega_{coll}(r) \quad \text{(A 4)}$$

Although equation (A4) may look somewhat complicated to non-technical readers, the interpretation is relatively straightforward: the amount of light scattered back to the detector increases linearly with the laser power, particle concentration, scattering cross section of the particles, and the solid angle subtended by the collection optics. All of these make intuitive sense. Note that the product of the particle number density and the scattering cross section appears, so we can't easily separate whether an increased signal is due to an increase in the concentration of

particles or their effective cross section. However, if the size distribution and the average scattering cross section remained nominally constant, then to first order, the change in the signal with distance would reflect changes in particle concentration. A small perturbation would be caused because the average extinction coefficient would change to reflect the change in the local particle concentration, but the magnitude of the change would be relatively small owing to the smoothing caused by the spatial averaging. Some readers are puzzled by the appearance of the pulse length in (A4); simply put, more particles are illuminated by longer segments of light. Other authors sometimes define the product of number density and scattering cross section as a scattering efficiency, which in our development would have units of [m^{-1} / sr]; such a quantity is not very useful for the discussion here, although one can see from the units that a larger value for Δr would result in a larger signal.

If extinction is negligible and particle concentrations are fairly uniform, equation (A4) predicts that the detected signal should drop off nominally with r^2 because the solid angle collected by the telescope is equal to the lens area (which is constant) divided by r^2. Since the distance to the particles is known from the time required for the scattered light to return to the detector (the distance and ranging part of lidar), the recorded signal can be scaled by r^2 to correct for the decreasing solid angle. Extinction increases the rate at which the signal decays with distance, so it causes the signal to decay more rapidly than r^2. The average extinction coefficient over any portion of the beam path can then be determined from the change in the signal. Since the extinction cross section can also be estimated from information on the particle size distribution and the composition of the particles, the plausibility of various combinations of size distributions and particle compositions can be checked. Time-resolved measurements of the size distribution for several points along the beam path would greatly enhance the information which could be obtained.

In aerosol lidar systems, the laser wavelength is generally chosen such that scattering and absorption by particles dominates the change in the signal between two adjacent positions, r_1 and r_2. Measurements using multiple wavelengths, polarization properties, or angular distribution of the scattered light are sometimes used to extract further information about particle morphology or composition, but such variations are still difficult to separate from variations in particle size and concentration. Equation (A4) can also be used to describe species-specific differential absorption

lidar (DIAL) measurements made with tunable laser systems. In these systems, lidar measurements are recorded at two nearby wavelengths, one of which is strongly absorbed by a particular molecular species in the atmosphere, and the other of which is not. The particle scattering and extinction is nearly identical because of the proximity of the wavelengths; hence, a comparison of the extinction losses between r_1 to r_2 at these two wavelengths allows one to determine the average concentration of the molecular species-of interest over the distance $r_2 - r_1$ independent of variations in the particle distribution. The detection limit is once again determined by the product of the concentration of the species and its absorption cross section such that the additional absorption caused by the molecular species results in a measurable change in the signal level over what is caused by aerosol particles alone. (Wolf *et al.*, 1990)

Spatial and Temporal Resolution

In order to resolve spatial variations in the concentration field, the scattered power level must be recorded as a function of time. The electrical signal, $S(r)$, generated by the detector electronics is proportional to the power which reaches the detector:

$$S(r) = S\left(t = 2r/c\right) = G(t)\,R(t)\,P_{\text{det}}(r) \qquad \text{(A 5)}$$

where $t = 2r/c$ is the time elapsed between when the laser pulse was emitted and when it is digitized (corresponding to the round-trip time required for the light to propagate to and return from the measurement volume at r), $G(t)$ is the amplifier gain [V/A], and $R(t)$ is the detector responsivity [A/W] In general both the amplifier and detector must be temperature and humidity stabilized such that they remain constant over time. The time variation of the signal thus corresponds to spatial changes in $P_{det}(r)$; as the beam is scanned, the signal can be displayed as an image similar to a conventional radar image. Since $P_{det}(r)$ is proportional to the particle concentration at r, the image contains information about the spatial distribution of the particles.

The spatial resolution of the lidar system is determined by several factors: the pulse width of the laser beam and the digitization rate of the signal processing equipment control the resolution along the beam (radial) direction, while the diameter of the beam at position r and the minimum angular increments in the scanning hardware determine the resolution in the transverse (azimuthal) and elevation directions. The former limit arises because light travels at a speed of

approximately one foot per nanosecond (1 ns = 10^{-9} sec.). Hence, a laser pulse of 10 ns duration would have a length of 10 ft, and the signal digitization rate determines the spacing between consecutive 10 foot samples along the beam path. Because the light must make a round trip between the laser and the particles, if we wanted the centers of the sampled volumes to be spaced by 10 ft, we would want to digitize the return signal every 20 ns. The divergence of the beam determines the diameter of the 10 ft. long cylinder of particles illuminated by the pulse at position r (and hence the sample volume), while the angular increments of the scanning hardware determines the spacing between adjacent sample volumes.

The temporal resolution depends on the number of pulses which are averaged together to improve the statistical accuracy of the lidar data, and the volume included in the scan. For example, if the laser repetition rate is 50 Hz, then a 1 second average would improve the signal-to-noise level of all the points along a particular laser direction by about a factor of $\sqrt{50} \approx 7$. After the 1 second interval, the scanning hardware would increment the beam direction and obtain another 1 second average of the aerosol distribution along the new direction. When the entire scan was completed, a new scan could be undertaken. Thus, the scan time varies depending on the amount of averaging required, the spatial resolution, and field-of-view that were selected.

Effects of Size and Composition Distributions

As noted above, typical beam diameters in lidar applications are on the order of a meter, and typical pulse durations are on the order of 10 ns. Thus, illuminated volumes are on the order of 1-10 cubic meters. Such volumes contain a large number of particles, each of which contributes scattered light to the signal received at the detector. Since the number is quite large, the summations indicated above are often taken over a continuous distribution of particles sizes rather than a discreet number of particles. Mathematically, this means the summations in equations (A1-A4) are replaced by integrals over a particle size distribution function. To do this properly, we must expand both the scattering and extinction factors in equation (A3), because both depend on the particle size distribution:

$$P_{det}(r) = P_0\ \Delta r\ \Omega_{coll}(r) \exp\left[- \int_{r'=0}^{r} 2\,\overline{\alpha}_{ext}\left(r', D_p, m\right)\ dr' \right] \int_{D_p=0}^{\infty} f_r\left(r, D_p\right) N_{tot}(r)\ \sigma_{sca}\left(r, D_p, m\right)\ dD_p \qquad \text{(A 6a)}$$

$$P_{det}(r) = P_0\ \Delta r\ \Omega_{coll}(r) \exp\left[- \int_{r'=0}^{r} 2 \int_{D_p=0}^{\infty} f_r\left(r', D_p\right) N_{tot}(r') \left[\overline{C}_{sca}\left(r', D_p, m\right) + \overline{C}_{sca}\left(r', D_p, m\right)\right] dD_p\ dr' \right] \int_{D_p=0}^{\infty} f_r\left(r, D_p\right) N_{tot}(r)\ \sigma_{sca}\left(r, D_p, m\right)\ dD_p \qquad \text{(A 6b)}$$

Here $f_r(r,D_p)$ is the normalized particle size distribution function at position r, and N_{tot} is the total particle number concentration across all size ranges. The product $f_r(r,D_p)\ N_{tot}\ dD_p$ represents the number concentration of particles in the size range D_p to $D_p + dD_p$, and plays the role of $N_p(D_p)$ in equations (A2-A4). Notice that what was formerly described as the average extinction coefficient is actually a fairly complicated integral, because the size distribution function can vary with position.

In this analysis, we have neglected any contributions from multiple scattering, *i.e.* instances in which light reaches the detector after more than one scattering event. Because of the signal gating and field of view of the telescope, we would primarily be concerned with two possibilities: 1) back scattering by particles at r followed by a shallow angle scattering event by an intervening particles, or 2) forward scattering by an intervening particle followed by near back scattering from a particle at r. In either case, the multiply scattered light may still be collected by the receiving telescope. The result is that the extinction used above is a slight overestimate. In general, this effect is negligible as long as $\left(\overline{\overline{\alpha}}_{ext}\ r\right)$ remains less than 0.1, but becomes increasingly important as $\left(\overline{\overline{\alpha}}_{ext}\ r\right)$ approaches 1 or higher It will have an effect in hazy conditions where visibility is on the order of the clear-day range of the lidar system.

Equation (A-6b) is messy enough, but in reality, there would be other distribution integrals describing the range of particle morphologies and compositions for each size range at each position. We have simplified matters somewhat by lumping this distribution into an effective

refractive index, m, which in the most general case is a function of both r, D_p, and time. Time is a factor because particle characteristics at any position may vary with time, for example as particle sources turn on or off, or if the relative humidity changes (*e.g.* Hanel, 1977; Shettle, 1979; deLeeuw, 1986; McMurry, 1990b). The variation of the extinction coefficient with r contains information about how m is varying, but it still involves size distributions at all positions. If the latter are reasonably well known, then the extinction data can be inverted to yield information about effective refractive indices; however, if neither the size nor the composition distributions are known, then it is likely that a large number of possible combinations of size and composition distributions could give rise to both the observed scattering signal and the observed extinction.

In other words, since distributions of particle size, morphology, and composition (*i.e.* m) can vary across the lidar field of view, both could lead to changes in the lidar signal without corresponding changes in the total particle concentration. Hence, in order to recover the particle number concentration at r, one must account for variations in these integrals. Variations in the size distribution function were expected to be important because of the respective functional shapes of the size distribution function, $f(r,D_p)$, and the scattering cross section, $\sigma_{sca}(D_p)$, which are described in more detail below. The purpose of the simultaneous, time-resolved measurements of particle size distributions acquired during the Albuquerque tests was to measure the impact of such changes. Since the effective refractive index is difficult and expensive to measure, we estimated the refractive index from previously published results (*e.g.* Grams, 1974; Shettle, 1979; Harris, 1982; Sloane, 1984; de Leeuw, 1987; Sasano, 1989; Allen, 1990; Cornille, 1990; Hering, 1991; Ji, 1993; Harris, 1995; Pandithurai, 1996) as well as from observations of the source(s) of the aerosol particles at the test sites.

Fig. A2 depicts what might be a typical particulate matter distribution in a horizontal scan and the resultant lidar signal versus position along a particular beam direction. Color-coded images can be used to display the time history of the spatial profile along the beam (see App. E). To recover quantitative measurements of particle concentrations from the lidar signals, one then needs to invert a measured quantity which represents the integral across a distribution of particles of unknown size, shape, and composition. In addition, a calibration measurement is often required to reduce uncertainties associated with beam power, pulse length, detector response, and amplifier gain (see equations A4 and A5); these values should be monitored or the calibration

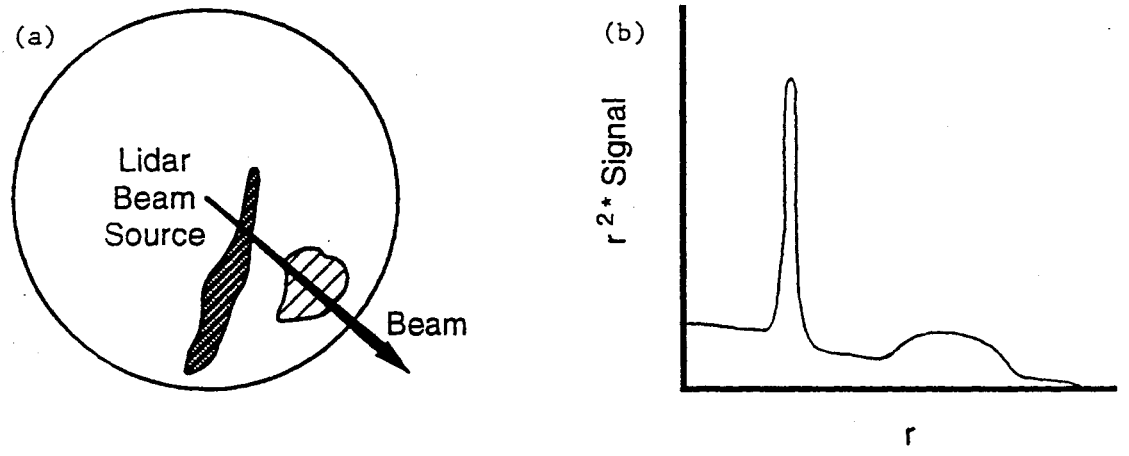

Fig. A2: Illustration of lidar signal distribution. (a) Hypothetical aerosol concentration distribution seen in a complete 360° horizontal lidar scan, drawn in this fashion for analogy to conventional storm radar images. The darker the shading, the higher the aerosol concentration. (b) Signal distribution as a function of distance along the beam, corrected for varying solid angle. A small amount of extinction is indicated by the decay in the signal level with distance.

repeated periodically to guard against drifts over time. Then, realistic estimates of the scattering and extinction cross sections of the particles must be made, using data on characteristic sizes, morphologies, and compositions appropriate for particles in the area of interest. Factors known to significantly influence the response include local soil composition and terrain, local industry and vehicle fleet makeup, proximity to large bodies of saltwater, and humidity; these should be kept in mind when using data from different regions. Finally, an estimate of the particle size distribution over the region must be made. The first guess usually assumes constant composition and size distribution along the beam path, and an average value for the extinction coefficient (obtained by fitting the signal decay) which is also uniform over space. Then, the spatial distribution of the total number density can be estimated from the measured signal variation using equation (A6b).

This description requires some elaboration to more clearly spell out uncertainties in the estimates which are used. Without going into detail, one can say that the particle cross sections are complicated functions of particle size, morphology, composition, and scattering angle. For conventional lidar systems, a backscattering geometry is used, so the scattering angle is fixed by the system geometry, but the other factors still influence the magnitude of the signal scattered

back to the detector. Lorenz-Mie scattering theory, which is applicable to homogeneous spherical particles, is generally used to predict trends caused by variations in particle size or composition [see Bohren and Huffman, 1983]. Effects of particle morphology and composition (*i.e.* most naturally occurring non-liquid particles are neither spherical nor homogeneous) are often taken into account together through the use of an effective refractive index based on fits to experimental data from real particles (Hanel, 1988). Experimental data on extinction and backscattering cross-sections are most relevant to lidar measurements, and abound in the literature.

Fig. A3 shows theoretical backscattering cross sections per unit solid angle and extinction cross sections as a function of particle size. There are actually three curves shown in each plot, showing the effect of varying the average carbon content in the particles. One sees that the backscattering cross section of spherical particles is a highly oscillatory function of particle size and spans many orders of magnitude over the particle size range shown. The impact of varying the average carbon content is not apparent until one gets to particles in excess of 10 μm. The total extinction cross section is smoother because it effectively integrates the scattering over all angles, but the range of values still spans many orders of magnitude.

The curves shown would be applicable to scattering or extinction by single homogeneous spherical particles; however, because the lidar signal is generated by scattering from a multitude of particles comprised of a range of sizes, morphologies, and compositions, it is more appropriate to

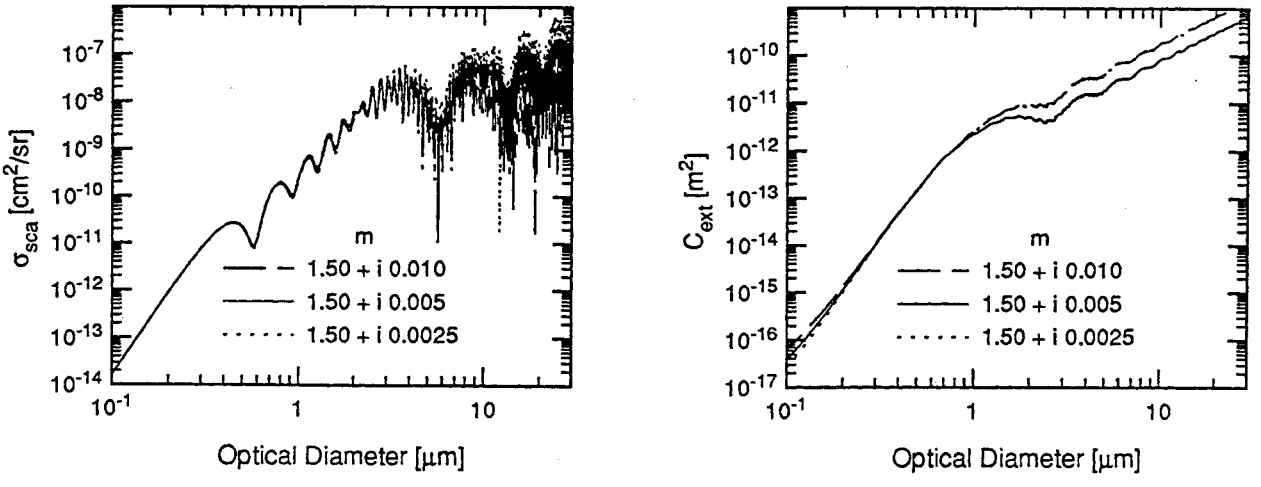

Fig. A3: Scattering cross sections as a function of particle size for spherical particles with representative refractive indices.

think in terms of a running average through the cross sections as being representative of the average particle cross section. In other words, to estimate the power scattered by particles at location *r*, one would finding the average cross section appropriate for the range of compositions, morphologies, and orientations of particles in a given particle size class, multiply by the relative number density of particles in that size class, and sum over all size classes (refer to equation A6).

Interpretation of the lidar signal thus relies on the fact that a very large number of particles are illuminated at each position along the beam, such that for any position, use of an effective refractive index is valid. Changes in the particle size distribution or particle composition (and hence *m*) which might occur from location to location across the lidar field of view would change the average cross section of the illuminated particles, and could lead to changes in the magnitude of the lidar signal without a corresponding change in the total particle concentration. However, since extinction is integrated along the entire beam path, in general it will not vary as quickly as might the backscattering cross section in response to variations in particle sources. Because the scattering cross sections are so strongly dependent on particle size, we were concerned that variations in the size distribution function would be most important.

As discussed in the section describing the results of the Albuquerque tests, assuming a nominally constant size distribution along a short section (approximately 400 m) of the lidar beam running parallel to a major urban thoroughfare at a constant elevation was appropriate. The constancy of the size distribution was attributed to the stirring action of vehicle wakes and the dominance of entrained road dust, and the lack of other particulate sources. In such a case, an extinction coefficient can be determined from the attenuation of the lidar signal, and henceforth an effective refractive index (average composition) can be determined. In general roadside tests, one would expect size distributions to shift toward smaller sizes with increasing elevation or distance from the roadway due to particle settling, although the change might be fairly slow due to the vigorous vehicle wake turbulence and the thermal energy in the vehicle exhausts. A reduction in particle concentrations in the size range of 1-5 μm would cause the lidar signal to fall off more rapidly that the particle number concentration. Hence, knowledge of changes in size distribution would be important if accurate number concentrations were to be recovered.. For example, a set of size distribution measurements could be taken as a function height, and the time average values at each elevation could be used to arrive at a vertical size distribution factor. It would be

necessary to do this at several locations to check the generality of the vertical distribution, as things such as vehicle-generated turbulence, thermal energy from vehicle exhaust, and thermal updrafts from pavement could easily affect the vertical distribution. However, if such measurements were taken, not only could they be used to analyze lidar signals in a current test, but assuming they were published, they would become part of the research data base which might be useful in predicting distributions at other sites.

It is also important to realize that if large temporal fluctuations are present, they can affect both the lidar signal and particle concentration measurements. For example, consider aerosol distributions near a major intersection when a signal light switches from red to green: the change in thermal energy in the vehicle exhausts as they accelerate as well as the change in the turbulence associated with vehicle wakes would probably result in larger particles being periodically lifted to higher elevations. The temporal variations might have a short enough time scale that the lidar image would pick them up, but aerosol distribution measurements might average them out, unless taken using bag samplers. Similar effects could be associated with changes in wind velocity or direction or variations in particle sources (construction activity, lawn mowing, industrial emissions, etc.). This is not to say the either set of data is inaccurate, only that the finite time resolutions must be kept in mind when analyzing the data.

Mass Concentrations

Thus far, the discussion has focused on particle number concentrations; in order to relate the lidar signal to particulate mass concentrations which appear in air quality standards, one needs to multiply the number density by the mass per particle to obtain the particle mass concentration, $M_p = \left(\frac{\pi}{6}\rho D_p^3\right)\left(N_p\right)$, where ρ is the density of the material which comprises the particle. Referring back to equation (A4), if we multiply the number density by the mass per particle and divide the cross section by the mass per particle, the equation is unchanged, but the latter quotient shows up as a mass specific cross section. The new relation is then

$$P_{det}(r) = \sum_{particles} P_0 \exp[-2\overline{\overline{\alpha}}_{ext} r]\, \Delta r\, M_p\left(r, D_p, \rho\right) \overline{R}_{sca}\left(r, D_p, m, \rho\right) \Omega_{coll}(r) \qquad \text{(A 7)}$$

The density of the material comprising the particle now shows up as an additional parameter affecting the mass specific cross section. Including it adds somewhat to the uncertainty associated with the cross section estimate; however, since the density tends to be correlated with particle size and effective refractive index, the increase in uncertainty is not as high as might be anticipated. Again, information on typical particle densities is available in the literature [Hänel and Thudium, 1977; Chylek *et. al.*, 1981; Harris, 1982; Shah *et al.*, 1986; Armbruster, 1987; Cheng *et al.*, 1990; McMurry, 1990a; Stein *et al.*, 1994] as are bulk soil and mineral properties. Typical variations of M_p and $\overline{R}_{sca}$ alongside cumulative fractions for the lidar signal and various mass concentrations, are shown in Fig. A4. As before, the highly oscillatory nature of the mass-specific scattering cross section would be averaged out when integrated over a distribution of real particles.

Since $\overline{R}_{sca}$ is not independent of size, the mass concentrations of particles whose specific scattering cross sections are large will be preferentially weighted relative to the mass concentration of particles which have smaller mass specific scattering cross sections when the

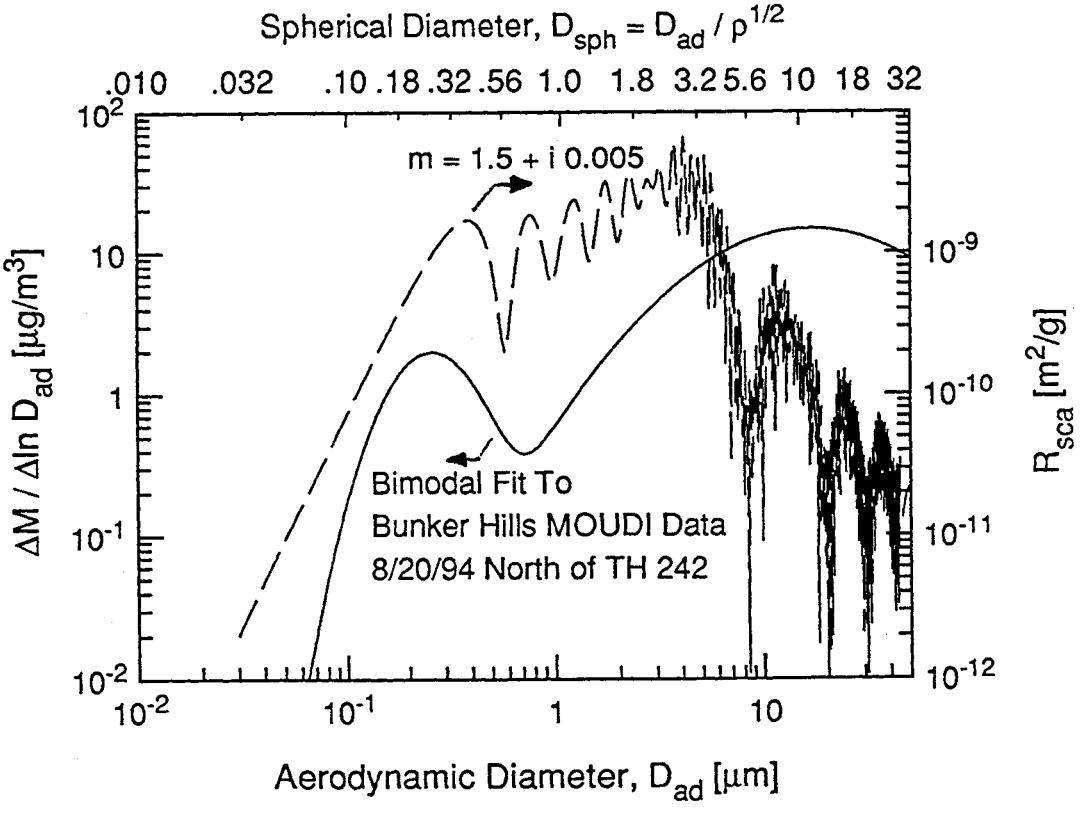

Fig. A4: Typical distribution of particle mass concentration and mass-specific scattering cross sections versus particle size. Equivalent spherical diameters are indicated to reflect a linear increase in particle material density from 1 to 2.2 g/cm^3 between D_{ad} of 0.8 to 2.5 µm.

summation indicated in equation (A7) is taken. It turns out that for particles whose material densities are on the order of 1-2 g/cm^3, the mass specific cross section peaks for particles whose equivalent spherical diameters are on the same order as the wavelength of the laser light. The net effect can be visualized as in Fig. A5 by plotting cumulative fractions which indicate the fraction of the total aerosol mass or the fraction of the total lidar signal contributed by each particle size range.

Fig. A5 plots cumulative fractions for several air quality particulate standards. The PM-10 standard is the one currently used in regulations, and accounts for particles whose aerodynamic diameters are less than 10 μm. The respirable mass fraction shown has an additional factor which accounts for the fact that the upper regions of the bronchial tract filter out many of the larger particles and prevent them from reaching the alveoli sacs in the lungs. If the lidar were to be an ideal indicator of aerosol mass concentrations, it would accumulate at the same rate as the mass concentration we are interested in. As can be seen in Fig. A5, this is not exactly the case, but the signal does accumulate at a similar rate to the respirable mass fraction. We should point out that

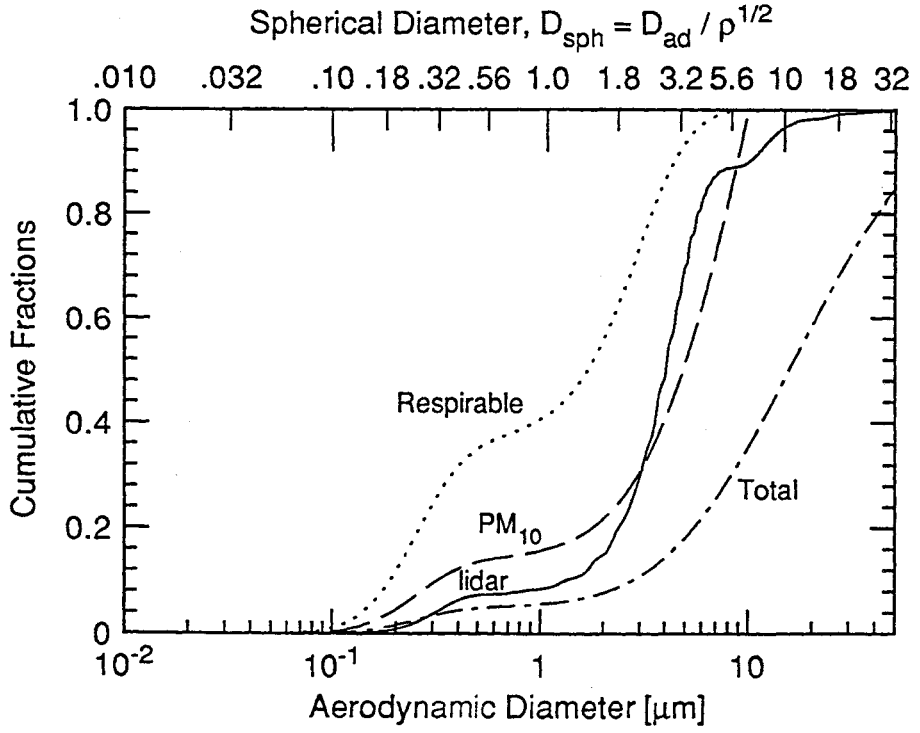

Fig. A5: Cumulative fractions comparing the increase in the lidar signal with the increase in various mass concentrations associated with different particle size ranges. The equivalent spherical diameters shown assume a linear increase in particle material density from 1 to 2.2 g/cm^3 between D_{ad} of 0.8 to 2.5 μm.

the PM-10 standard is currently under review. At issue is the relative importance of health effects associated with mass concentrations of coarse particles compared to the health effects of the more numerous but lighter submicron (fine) particles, which can penetrate farther into the lungs. There is growing evidence that the larger number concentration of submicron particles may have an important role in the ultimate health impact, and a new small particle standard may soon be put into place. In this event, concern would probably shift back toward the number concentration of small particles, and the mass concentration and hence material density may become less important.

Because the mass specific scattering cross section peaks at a particle size near that of the laser wavelength, one would need to shorter wavelength laser to increase the sensitivity to smaller particles. Thus, if a small particle standard is implemented, one might want to use a visible or ultraviolet lidar system. Visible systems would be problematic due to inherent driver distraction, so an eye-safe ultraviolet system would be desirable. It would be possible to make such a system, but the range would be significantly less than the current system (on the order of 1-2 km), because ultraviolet wavelengths are attenuated more strongly as they propagate through the atmosphere.

Summary

In conclusion, the factors listed above make quantitative determination of absolute concentrations based solely upon inversion of the lidar signal subject to considerable uncertainty; however, just as radar scans display relative raindrop concentrations over space but not necessarily absolute raindrop concentrations, the lidar images display relative aerosol concentrations over space. The change in the relative concentration is less sensitive to the absolute accuracy of the parameters, and hence lidar scans display useful information on the spatial distribution of the aerosols. Such information enables one to locate and identify particle sources, thereby improving the accuracy of the estimates one needs to make for the particle characteristics.

The relative concentrations are affected by particle size, morphology, and composition distributions. Local aerosol sampling measurements should be obtained simultaneously as was done in the Albuquerque test to assist in calibrating the lidar signal such that it can be inverted into an indication of the number concentration vs position. The potential for reasonable accuracies with excellent spatial and temporal resolution was demonstrated by the Albuquerque

data. In addition, it would be beneficial to obtain sampling measurements in regions or under conditions in which unusual lidar signals were observed. Details of the sampled particulate characteristics could then be compiled alongside the corresponding lidar data to establish a database useful for improving the accuracy of the lidar signal inversion in subsequent tests. Combining lidar data with several particle sampling measurements appears to be the only currently viable means by which accurate information on the magnitude and spatial distribution of particle concentrations can be measured with time resolutions adequate to resolve the dynamic variations in ambient particulate concentrations.

APPENDIX B: TEST SITE MAPS

The maps shown on the following pages show the road grid and the location of various sensors at the different test sites.

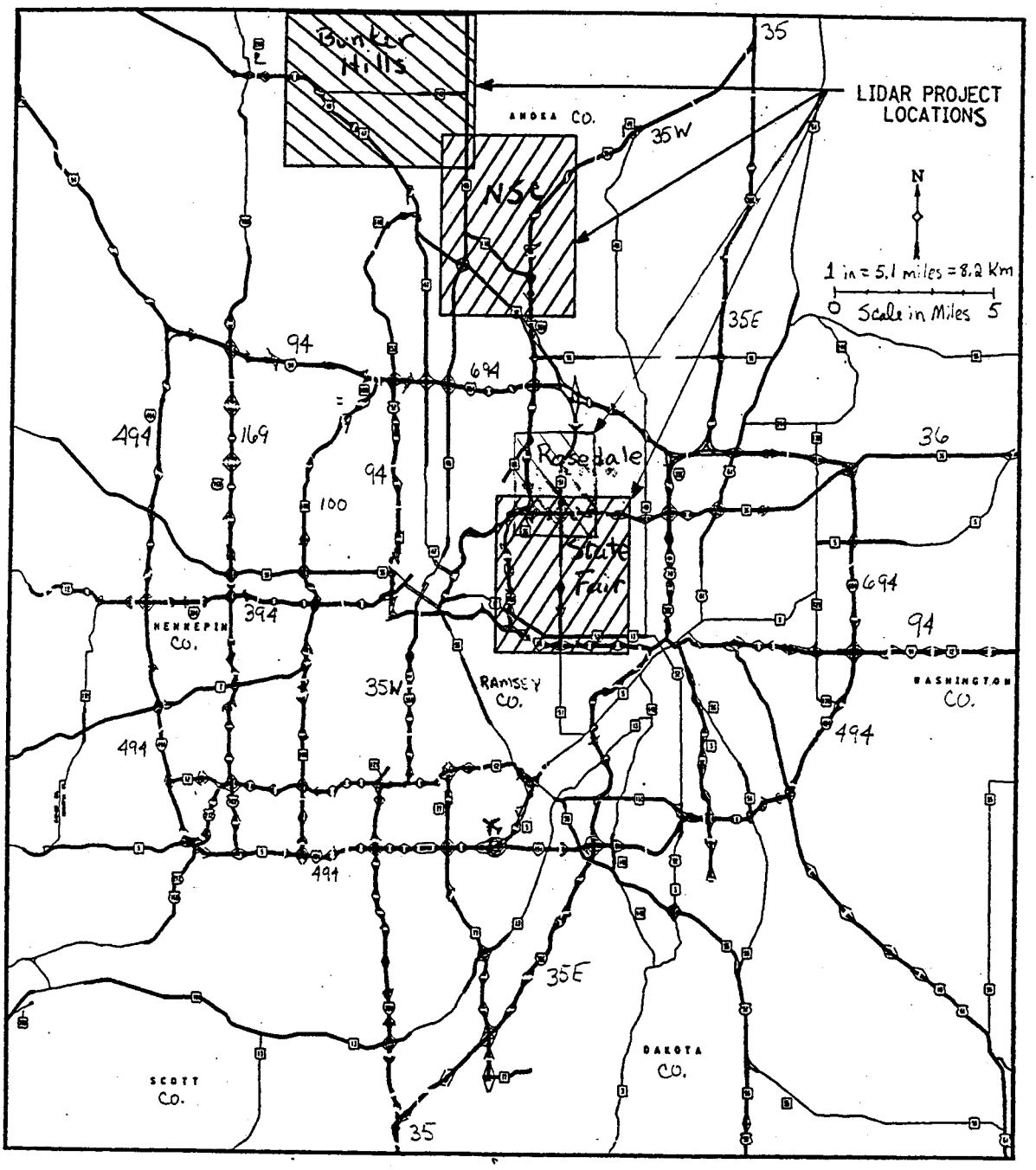

Fig. B1: Map of greater Minneapolis - St. Paul metropolitan area showing regions covered by four lidar tests carried out in Minnesota. In chronological order, these were National Sport Center (NSC) in Blaine, Bunker Hills Golf Course in Coon Rapids, the State Fair in St. Paul, and Rosedale Shopping Center in Roseville. Major highway numbers have been re-labelled for clarity.

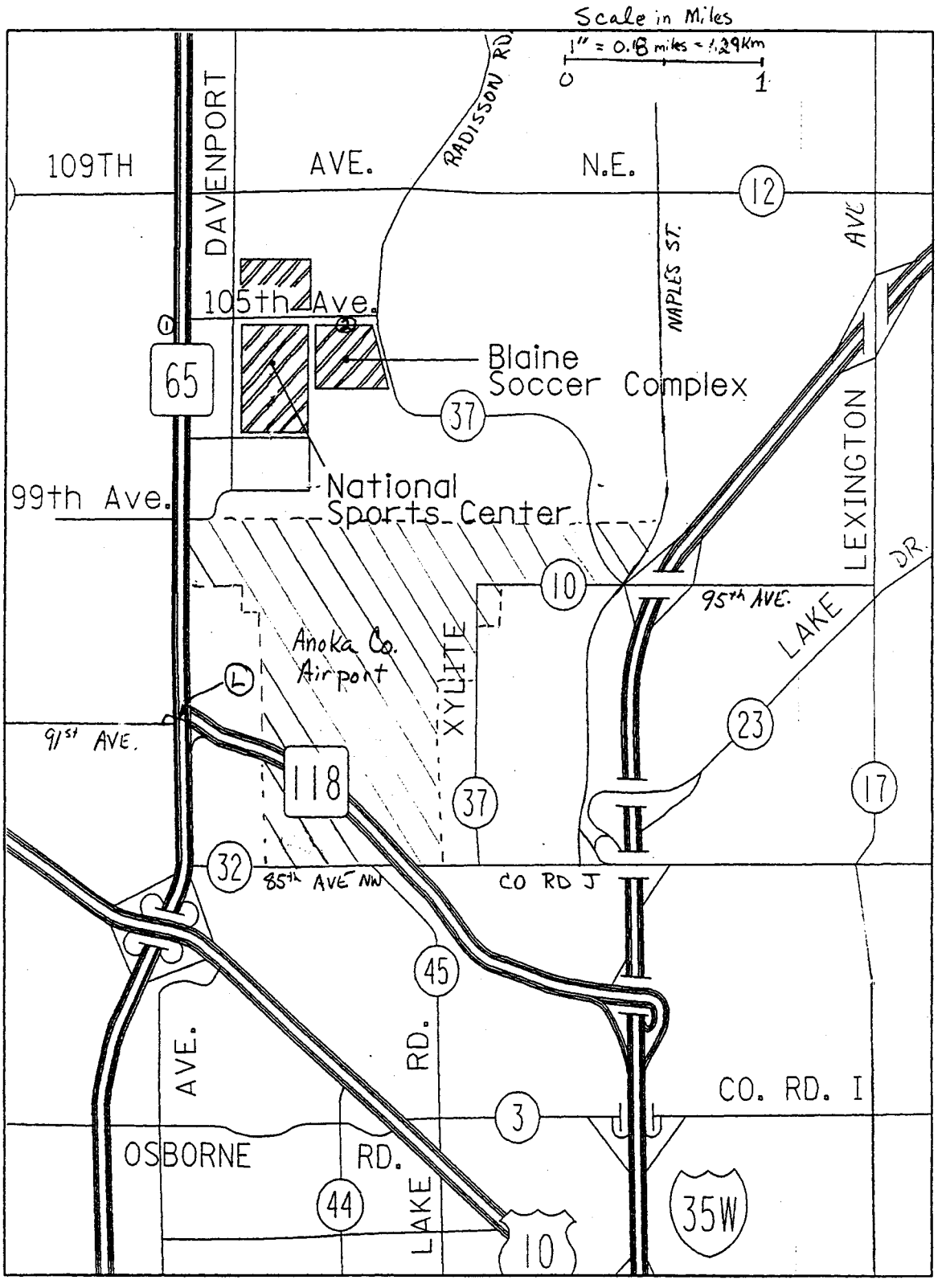

Fig. B2(a): Map showing streets, lidar (L), and sampling station locations (1) and (2) at the National Sports Center test site, Blaine, MN. Fig. B2(b) gives detail of instrumentation at sampling sites.

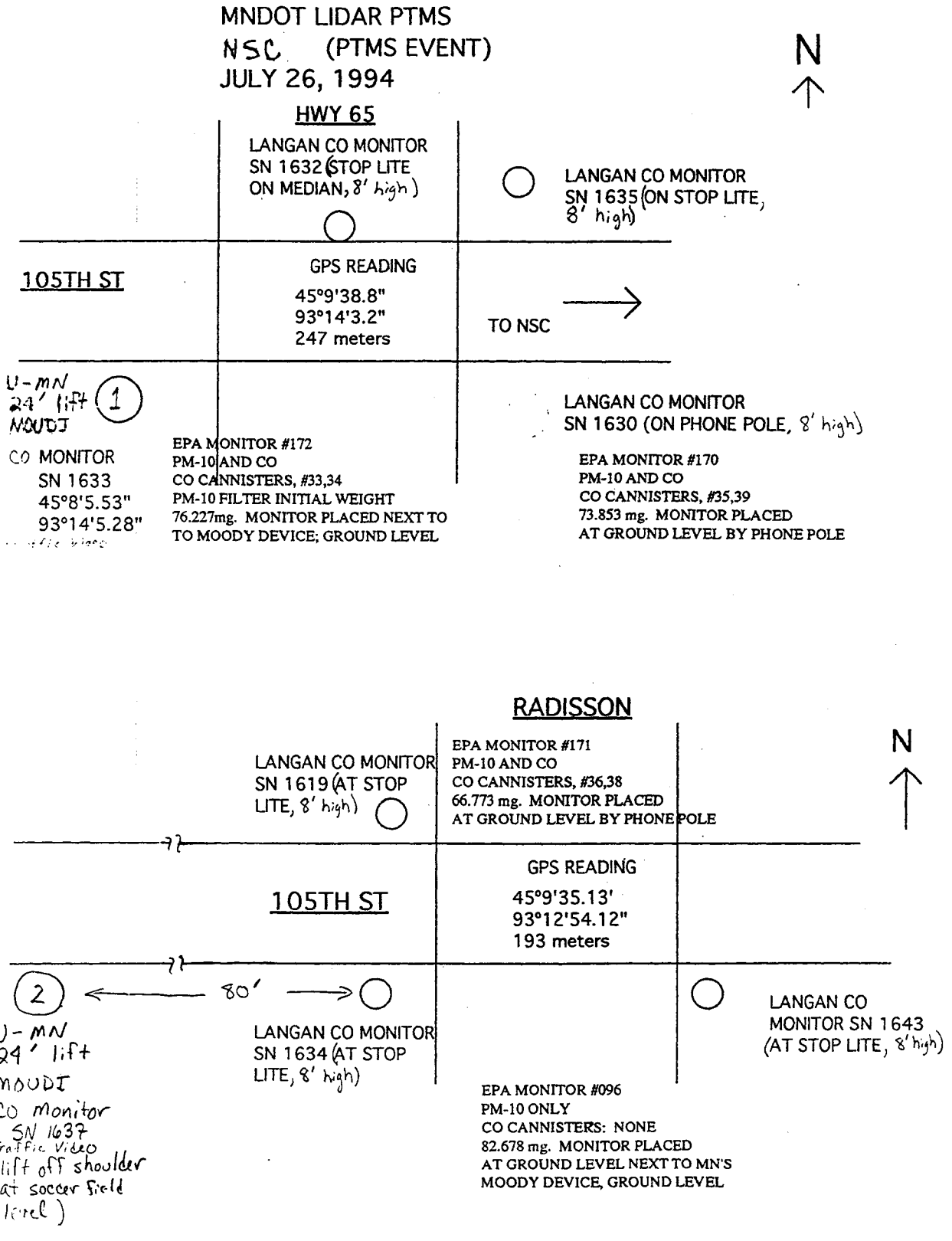

Fig. B2(b): Detailed layout of instumentation at sampling stations (1) (upper drawing) and (2) (lower drawing) at NSC test site. Refer to Table 1 in body of report for description of instrumentation. GPS readings are indicated to specify locations relative to lidar data.

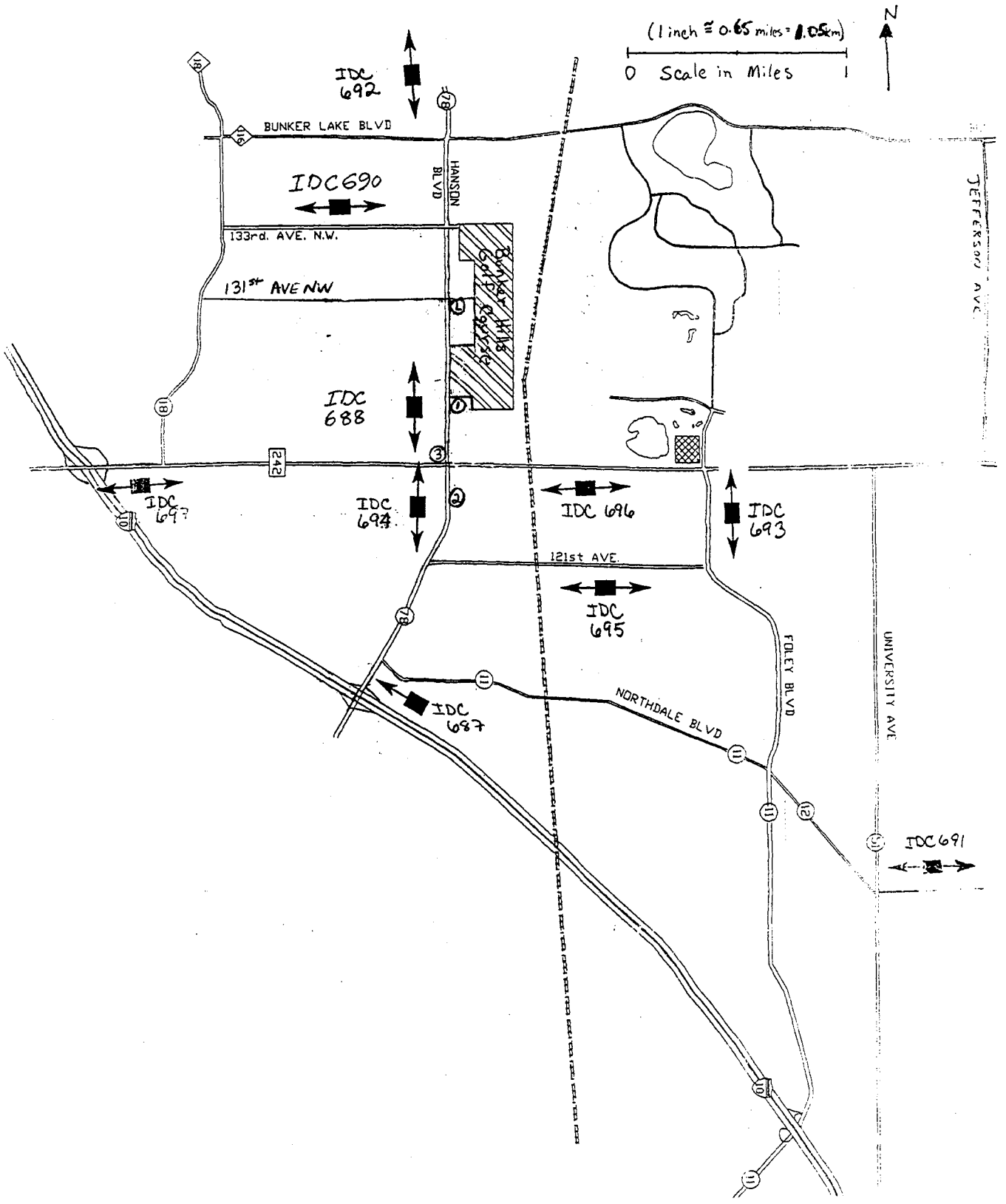

Fig. B3(a): Map showing streets, the locations of the lidar unit (L) and sampling stations (1) and (2), and the locations of traffic counting tubes at the Bunker Hills Golf Course test site, Coon Rapids, MN. A double arrow indicates a traffic counter which counts vehicles crossing in each direction. Fig. B3(b) gives detail of instrumentation at sampling sites.

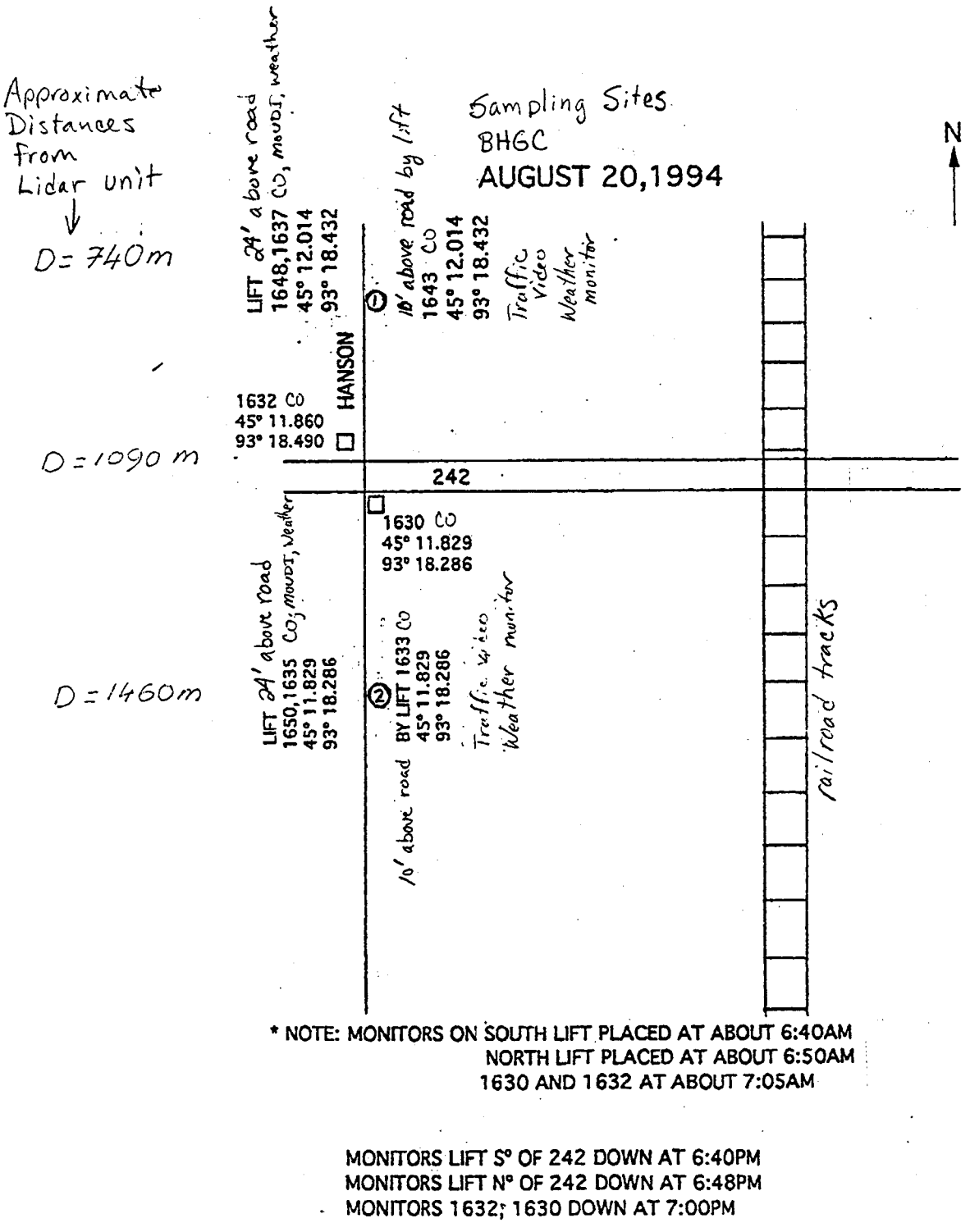

Fig. B3(b): Sketch showing locations of sampling stations and CO monitors at the Bunker Hills Golf Course test site, Coon Rapids, MN, including GPS data.

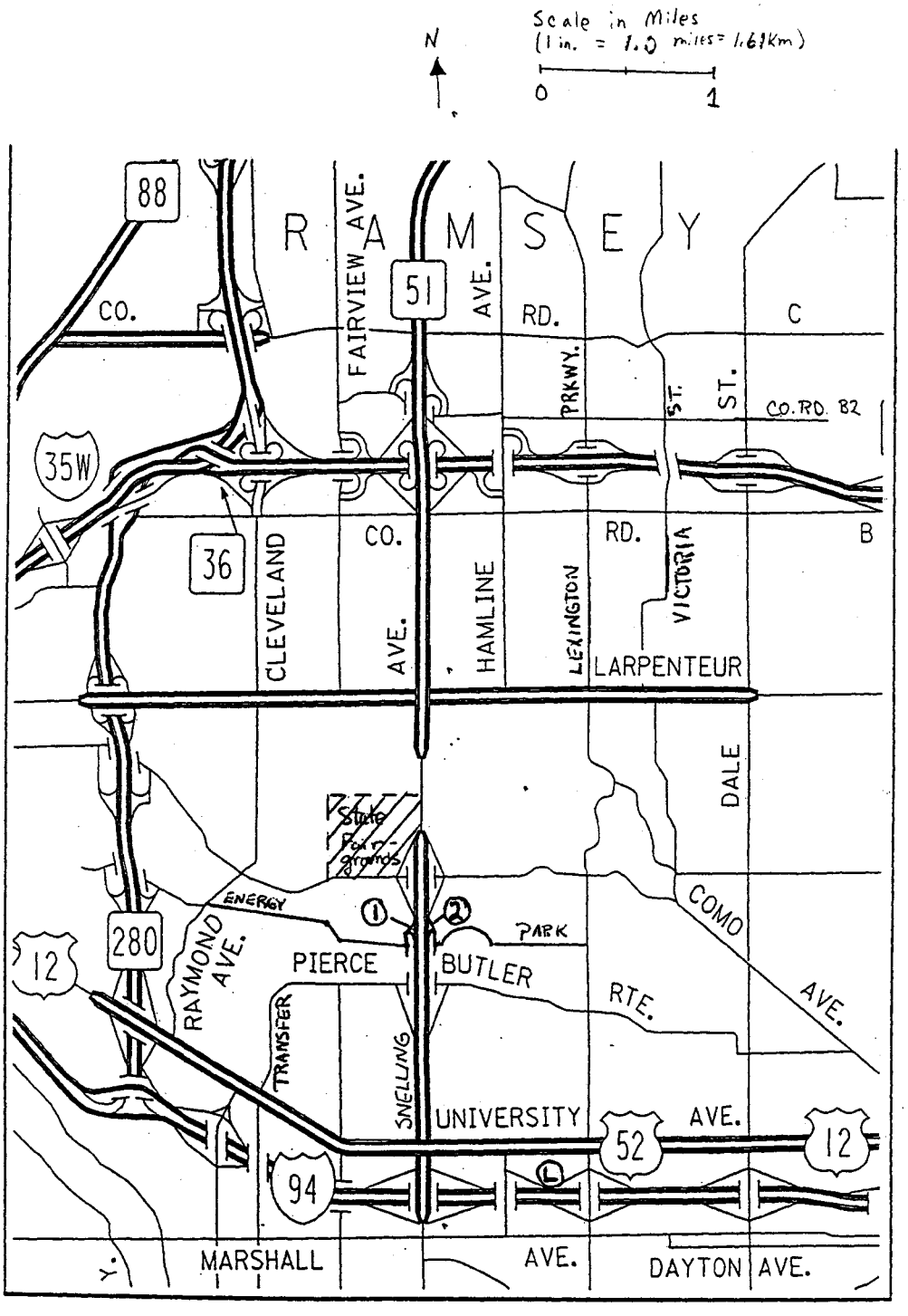

Fig. B4(a): Map showing the area surrounding the State Fair test site, including lidar (L) and sampling station locations (1) and (2), St. Paul, MN. Fig. B4(b) gives detail of instrumentation at sampling sites.

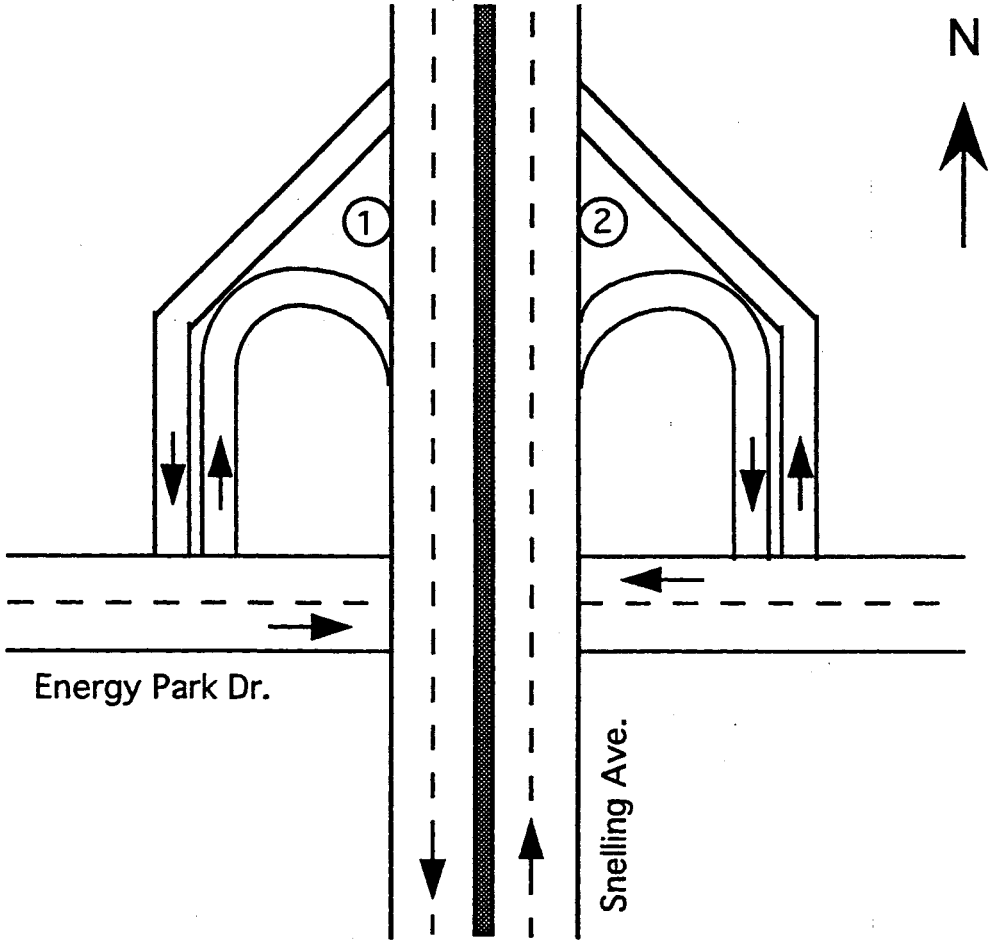

Fig. B4(b): Shetch of sampling site instrumentation at State Fair test. Lidar unit was located roughly 2.5 km from sampling sites on the rooftop of a 24 story apartment building at 1247 St. Anthony Dr. (just north of I-94 between Hamline and Lexington).

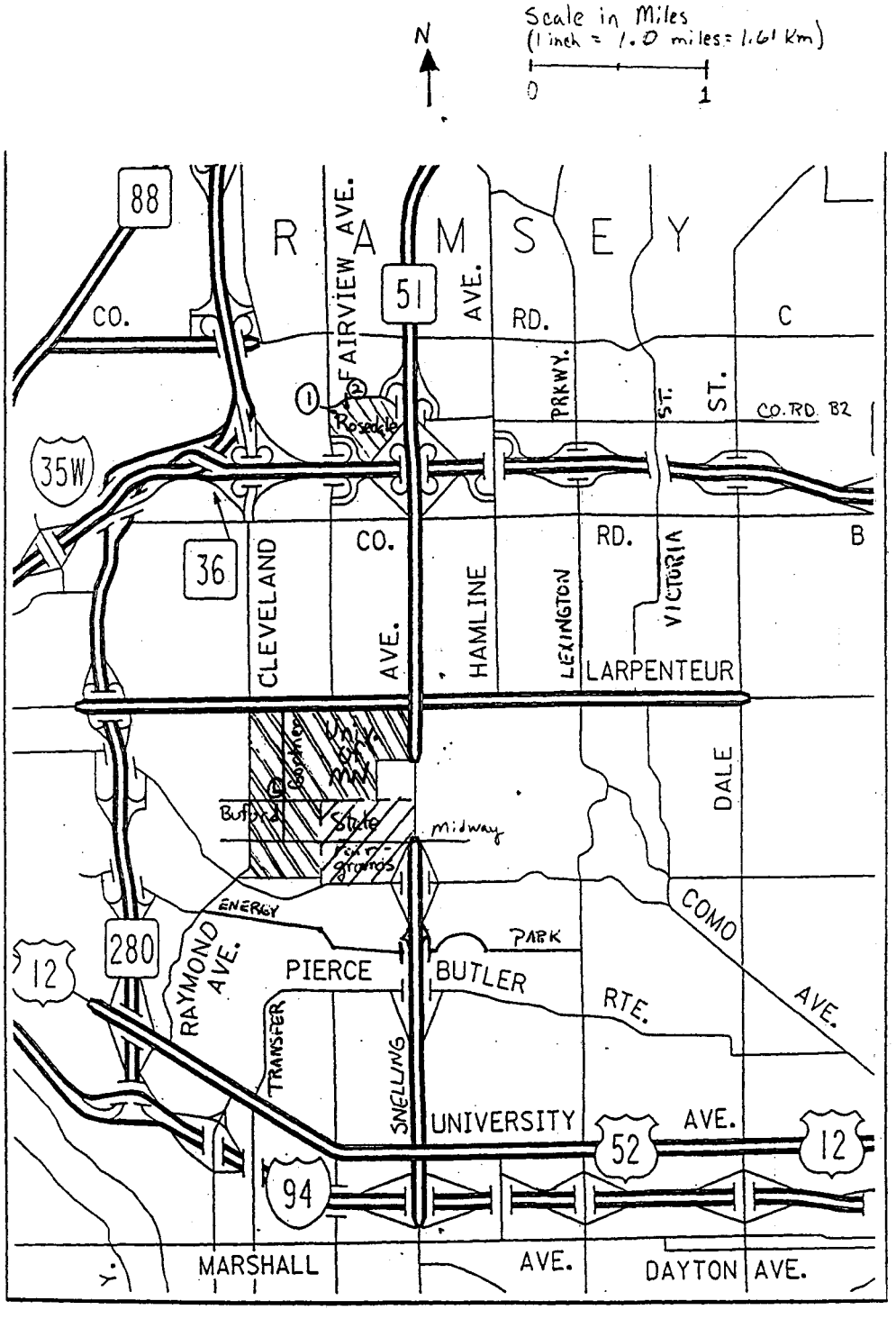

Fig. B5(a): Map showing streets and locations of lidar unit (L) and sampling stations (1) and (2) for the Rosedale Shopping Center test site, Roseville, MN. Fig. B5(b) gives detail of instrumentation at sampling sites.

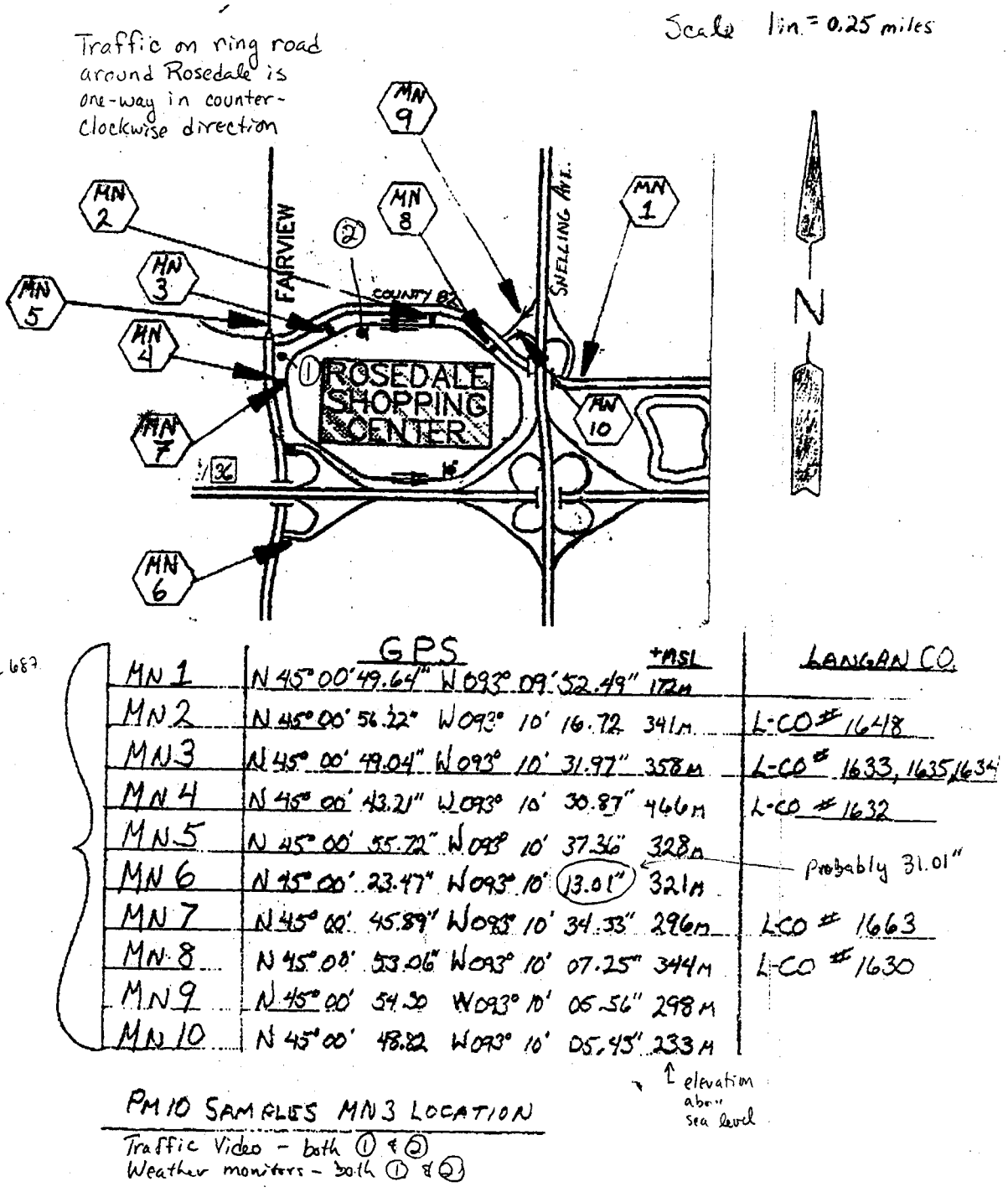

Fig. B5(b): Detail of traffic flow and sensor locations (lifts located at (1) and (2)) at the Rosedale site, Roseville, MN. GPS data given for numerous sensor positions.

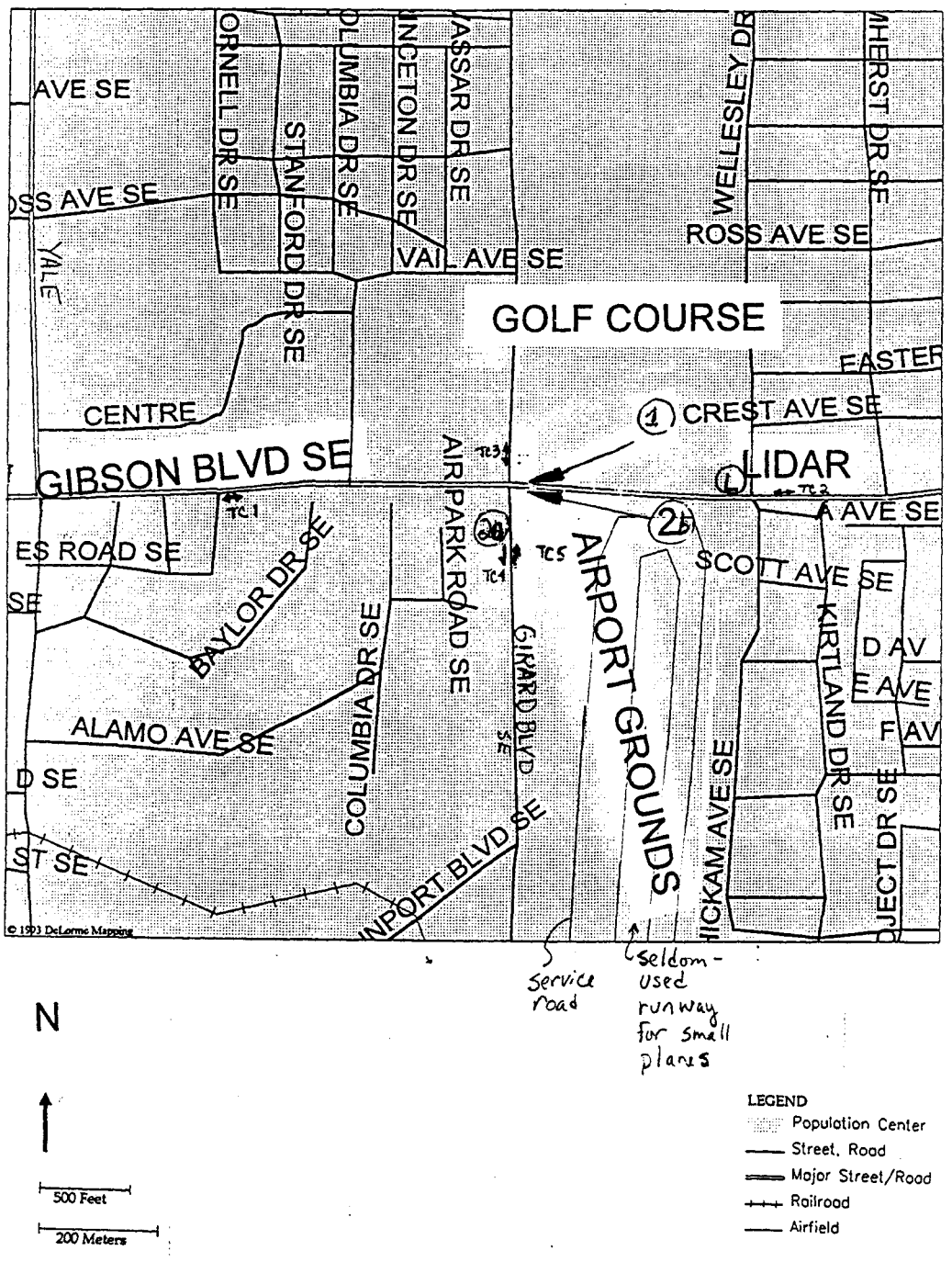

Fig. B6: Detail map of the Albuquerque, NM, site near the international airport. Lidar source (L) was 390 m from sampling station (1), which was 65' from Girard and 10' from Gibson; sampling station (2) was about 200 ft. south of Gibson at (2a) on Thurs., 6/22, and across the street from station (1) at (2b) on Friday, 6/23. Data was recorded along a line roughly parallel to Gibson Blvd, 13.5 ± 1 ft. (4.1 ± 0.3 m) above the ground and 17 ± 1 ft. (5.2 ± 0.3 m) north of the northernmost curb of Gibson Blvd. at sampling station (1) (*i.e.* 3.5 ± 1 ft. above and 7 ± 1 ft. to the north of the inlet of station (1)). Traffic counter (TC) positions are indicated with arrows.

APPENDIX C: TIME-AVERAGED PARTICLE MASS CONCENTRATION DISTRIBUTIONS FROM MOUDI INSTRUMENTS

Particle mass distribution data obtained using the micro-orifice uniform deposition impactors (MOUDI) instruments are grouped together in this appendix for ease of comparison. The data is presented in chronological order for those test in which there was lidar data to compare with (NSC and Bunker Hills in Minnesota, and Albuquerque, New Mexico). The MOUDIs record time-integrated size distributions resolved into ten different aerodynamic diameter size ranges. The MOUDIs were elevated on lifts such that their sampling inlets were located at an elevation of approximately 24 feet above the roadway during all of the Minnesota tests. During the Albuquerque test, a single MOUDI sampled from the same 10 ft. high inlet as did the time-resolved aerosol instruments to provide a check on the time-resolved data.

The MOUDI instruments operate as described below. A vacuum pump draws air into the sampling inlet at a rate of 30 liters/min. Particles are separated into a number of size classes by a series of inertial impaction stages. The flow rate is carefully controlled such that particles of a given aerodynamic diameter always impact on the same stage. The cut sizes have been verified in a laboratory calibration procedure, and are a function only of the sampling flow rate. The flow rate combined with typical ambient aerosol mass concentration distributions requires that the aerosol particles be collected over a time period approaching 8 hours or longer in order to obtain sufficient particulate mass for accurate weighing. The mass concentration in each size range is gotten by measuring the increase in mass of each stage due to the collected particle mass and dividing by the total volume of air which passes through the instrument during the collection interval. Each stage is therefore weighed before and after the collection interval, and the weighing is done in a humidity-controlled environment to neutralize the impact of ambient humidity during collection.

The sampling inlet of each MOUDI contains a cyclone designed to cut off particles whose aerodynamic diameter exceeds 18 μm. Thus, all particles larger than 18 μm are separated out of the aerosol stream by the cyclone, and are collected on a filter for subsequent weighing. After the inlet, the aerosol stream is directed at a cascaded series of impactor stages which separate the aerosol particles into sequentially smaller size ranges. The first impactor stage has a cutoff diameter of 10 μm, such that it collects particles whose aerodynamic diameters lie in the range of

10-18 μm. Particles less than 10 μm pass around the first impactor plate and head to the next stage. The next impactor stage has a cut size of 5.62 μm, so it collects particles whose aerodynamic diameters lie in the range of 5.62 - 10.0 μm. The process is repeated at each subsequent impactor stage, with cut sizes getting progressively smaller; the final impactor cut size is at an aerodynamic diameter of 0.10 μm. Particles smaller than 0.1 μm are collected on a filter which can be also be weighed. The impactor cut sizes are logarithmically-spaced such that each collects a range of particles whose width is equivalent in log-space to the width of the other bins. The resolution is 4 bins per decade, *i.e.* the bins cover aerodynamic size ranges of 0.10-0.18, 0.18-0.32, 0.32-0.56, 0.56-1.00, 1.00-1.78, 1.78-3.16, 3.16-5.62, 5.62-10.0, and 10.0-18 μm. Thus, the bins have equal width in log space, *i.e.* the difference between the logarithms of the upper and lower size limits is 0.25 regardless of which bin we consider. Particles smaller than 0.1 μm are collected on the exit filter, while particles larger than 18 μm are collected by the cyclone.

The following plots show histograms of the raw time-integrated data for each aerodynamic size bin. The ordinate gives the time-averaged mass concentration ($\mu g/m^3$) per unit log interval of the size range over which the particles are collected; the number is gotten by taking the mass collected on the appropriate stage, dividing by the total sampled volume (30 lpm flow rate times length of test), and then normalizing by the logarithmic width of the bin (0.25 for the bins between 0.1 and 18 μm). Bimodal log-normal distribution functions have been used to fit the mass concentration data. The mass median diameter (*a.k.a.* the geometric mean diameter) and geometric standard deviation for each fitted mode are shown in the legend, along with mass concentration information. The tails of the fits at the lowermost and uppermost particle sizes should be regarded with caution, because they are affected by where one draws the limit on the particle sizes assumed to contribute to each mode, and because the sampled distributions may not follow the bimodal log-normal distribution very well in these ranges. This is especially true of the largest particle range, since the mass can be grossly skewed by a single very large particle.. Thus, the geometric standard deviations should be regarded as representative for comparisons amongst similar data, but not an absolute quantity.

The first four plots show data from the NSC test. Data from the lowest filter range was not collected, so the geometric standard deviation of the fine mode is smaller than in plots from

subsequent tests. In general, the mass concentrations measured in the NSC tests were significantly higher than those measured in other tests, especially for the fine modes. The plots for July 25 at 65 and 105th and July 26 at Radisson and 105th also show unusually high concentrations for the large particles. We suspect that large particles were generated by vehicles parking in gravel and grass parking lots, and that "particle bounce" also affected the smaller size bins. Particle bounce refers to a large particle impacting on an impactor plate, but rebounding back off to slip down to the next plate. Because mass varies with the diameter cubed, particle bounce can greatly skew test results. Hence, after the NSC tests, we took care to coat each impactor plate with a very thin grease film so that bounce was minimized in subsequent tests.

The next six plots give the distributions measured on August 20, 21, and 22 at each of the two sampling sites at the Bunker Hills Golf Course event. Note the scale change on both axes from the previous plots. These plots also show the uncertainty associated with the weigh scale accuracy, and these error bars are applicable to all of the MOUDI data. The coarse mode was seen to be dominant in these tests, with total mass concentrations generally in the range of 30-50 $\mu g/m^3$. This was typical of subsequent observations as well. The overflow parking lot was a grassy field which did see some use during the event; however, in comparison to the NSC tests, the fine mode was much smaller. We concluded from the consistency of these results that particle bounce probably was a factor which skewed the NSC test results.

Data was not reduced for the State Fair or Rosedale test because of the lack of Lidar data for these tests.

The final two plots show the size distributions measured at the 10 ft. sampling height at sampling station 1 (the north side of Gibson Blvd.) on June 22 and 23 in Albuquerque, NM. The results are similar to those measured in the Bunker Hills test in the 1-5 μm aerodynamic size range, despite the difference in sampling elevations at the two sites. Data for particles whose aerodynamic diameters exceed 7.5 μm should be ignored, as particle losses in the sampling line leading to the MOUDI were found to be quite large depending on the details of the sampling line arrangement. In other words, bends in the sampling tubes and tubing connectors can cause the larger particles to impact out of the air stream prior to reaching the MOUDI. This may explain the low concentrations found in the larger size ranges in the 6/23 test. The fact that there are still large particles which reach the MOUDI may be indicative of a very large particle being dislodged

from the sampling tube walls and being carried to the MOUDI inlet. Because of both of these effects, the coarse mode concentration and width are probably underestimated in the 6/23 data.

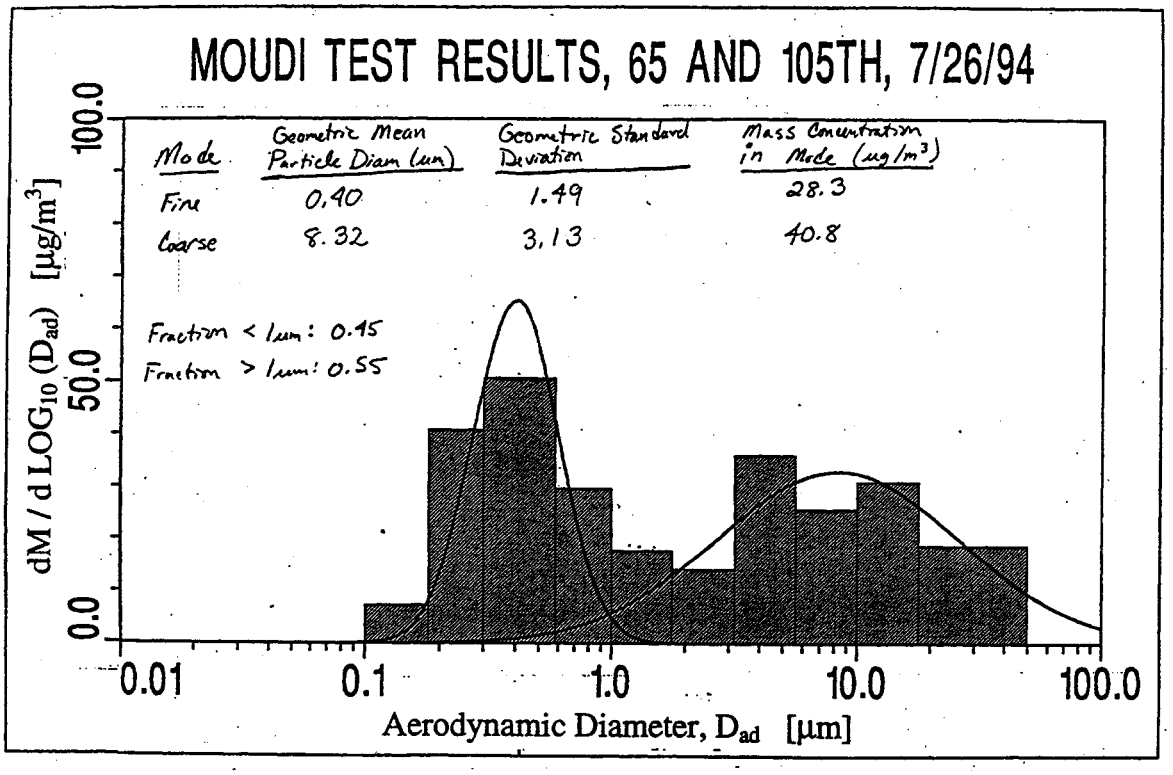

Fig. C1: Time-integrated mass concentration distribution from the NSC test on **July 26** at **sampling station 1** (located at the intersection of Trunk Hwy. 65 and 105th streets, Blaine, MN -- see also Figs. B2a and B2b).

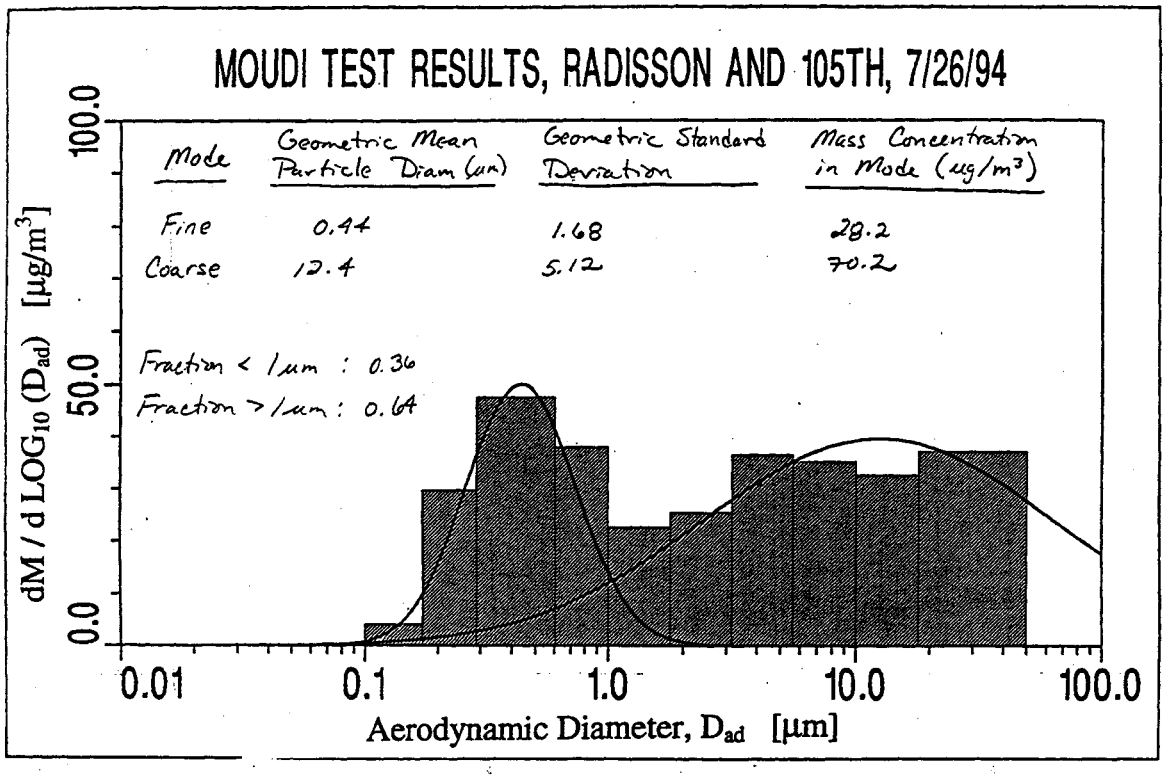

Fig. C2: Time-integrated mass concentration distribution from the NSC test on **July 26** at **sampling station 2** (located alongside 105th street, near the intersection with Radisson Ave., Blaine, MN -- see also Figs. B2a and B2b).

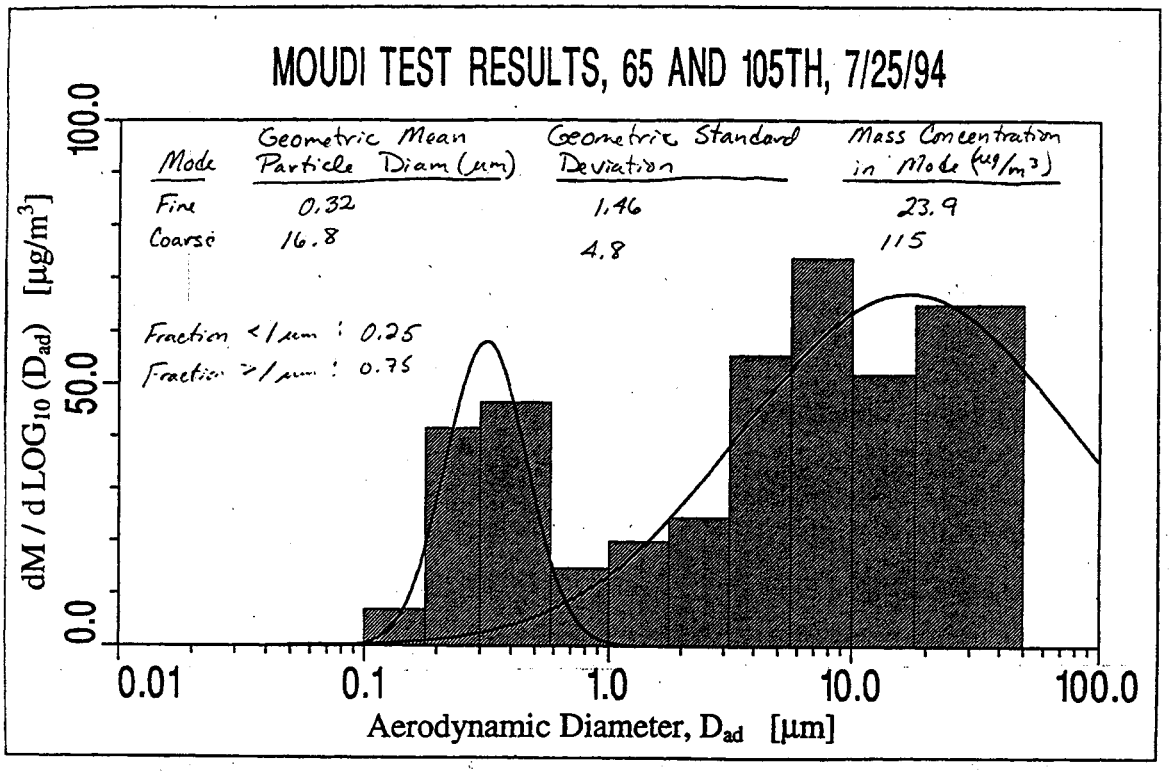

Fig. C3: Time-integrated mass concentration distribution from the NSC test on **July 25** at **sampling station 1** (located at the intersection of Trunk Hwy. 65 and 105th streets, Blaine, MN -- see also Figs. B2a and B2b).

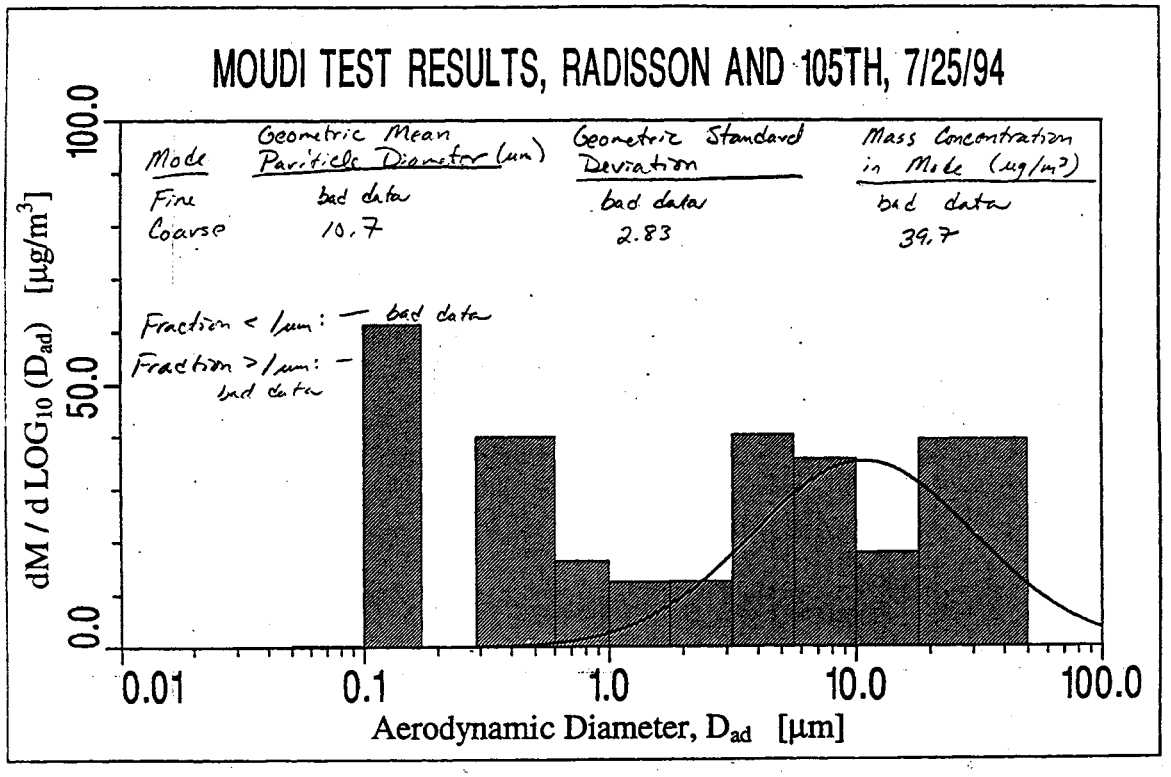

Fig. C4: Time-integrated mass concentration distribution from the NSC test on **July 25** at **sampling station 2** (located on the south side of 105th street, near the intersection with Radisson Ave., Blaine, MN -- see also Figs. B2a and B2b).

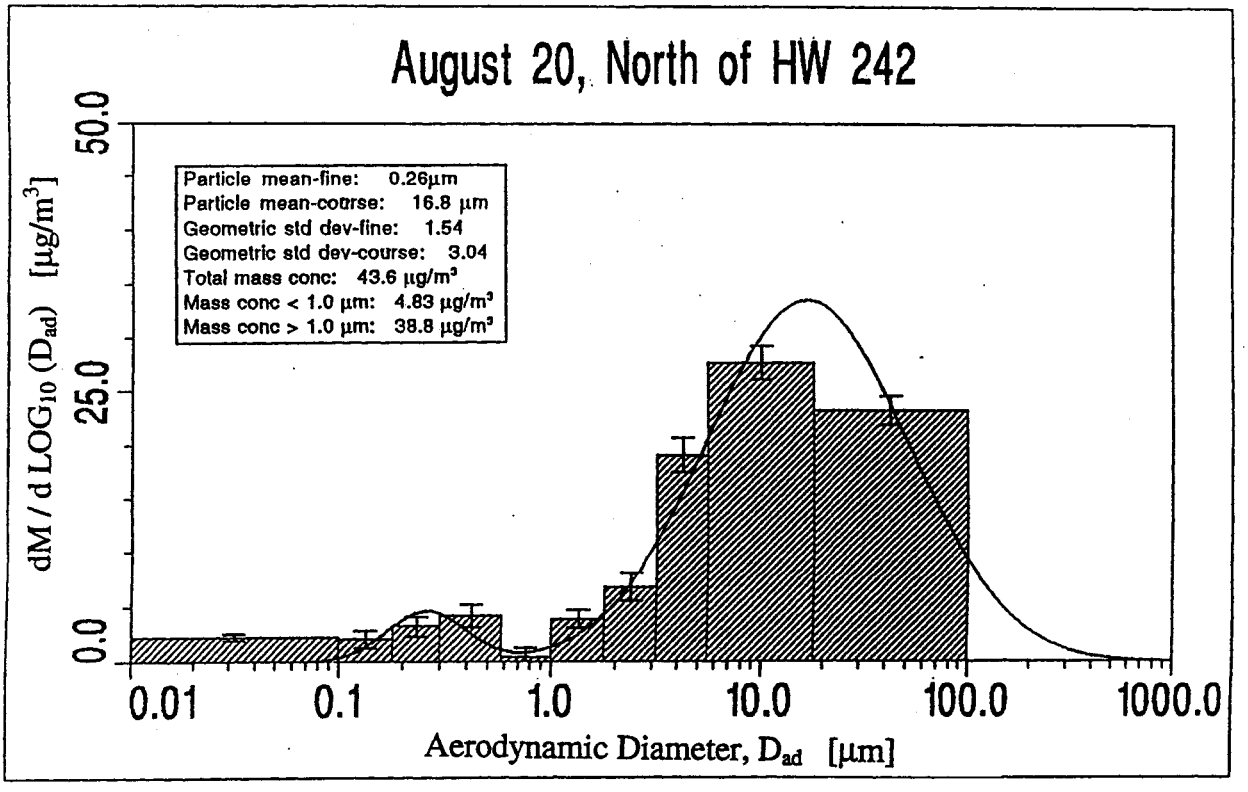

Fig. C5: Time-integrated mass concentration distribution from the **Bunker Hills** test on **August 20** at **sampling station 1** (located on the east side of Hanson Blvd. north of Trunk Hwy. 242, Coon Rapids, MN -- see also Figs. B3a and B3b).

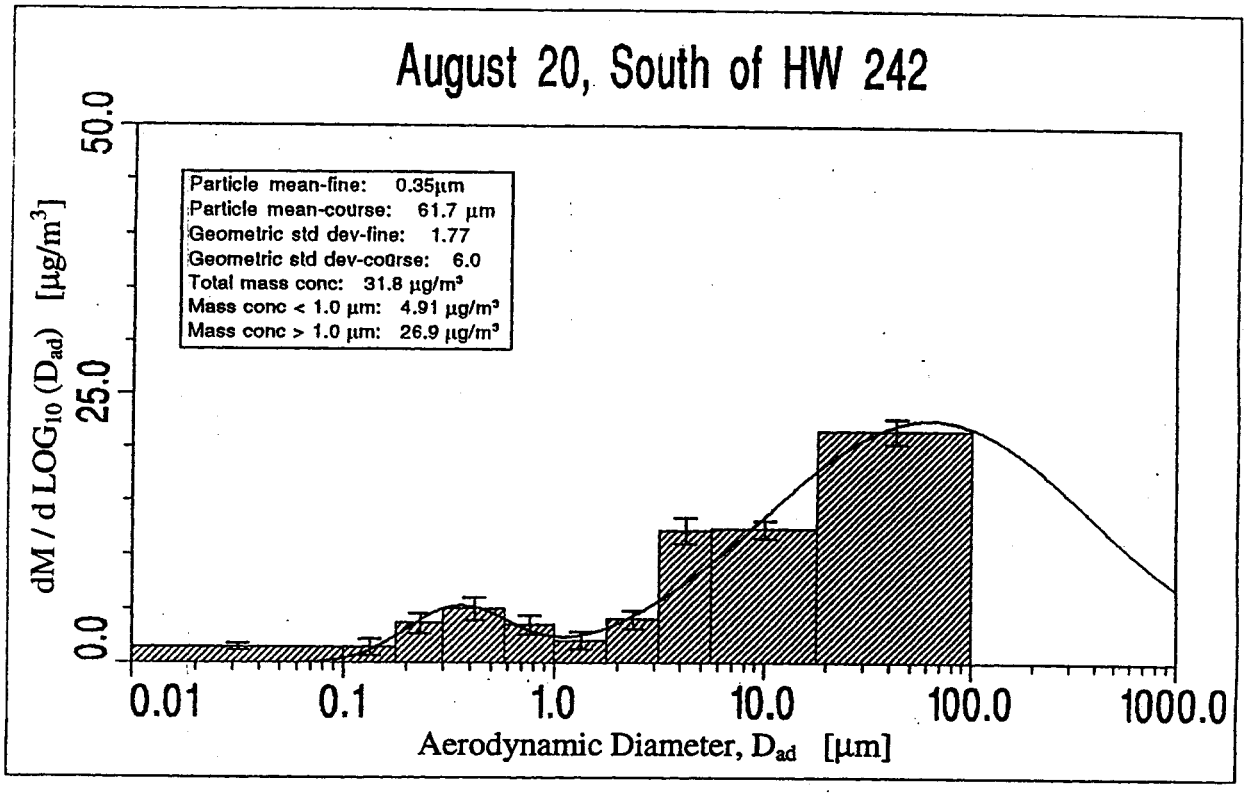

Fig. C6: Time-integrated mass concentration distribution from the **Bunker Hills** test on **August 20** at **sampling station 2** (located on the east side of Hanson Blvd. south of Trunk Hwy. 242, Coon Rapids, MN -- see also Figs. B3a and B3b).

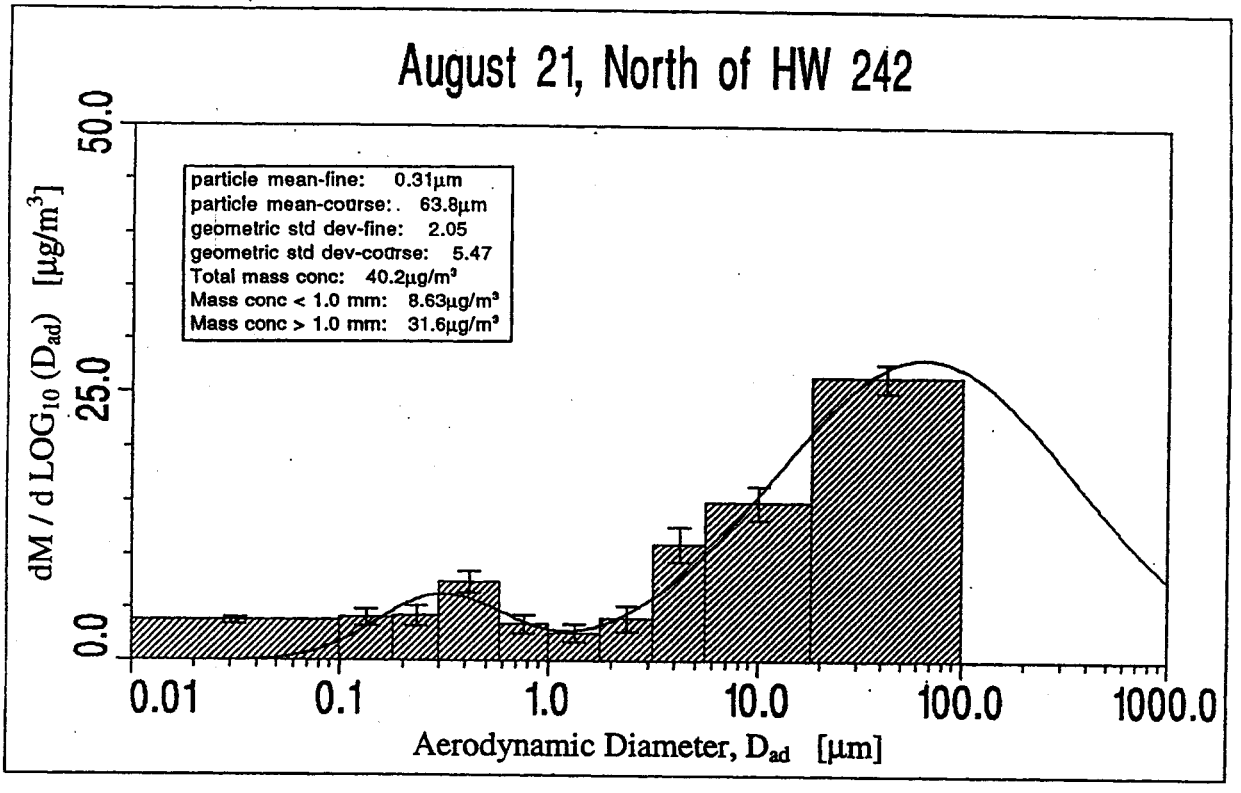

Fig. C7: Time-integrated mass concentration distribution from the **Bunker Hills** test on **August 21** at **sampling station 1** (located on the east side of Hanson Blvd. north of Trunk Hwy. 242, Coon Rapids, MN -- see also Figs. B3a and B3b).

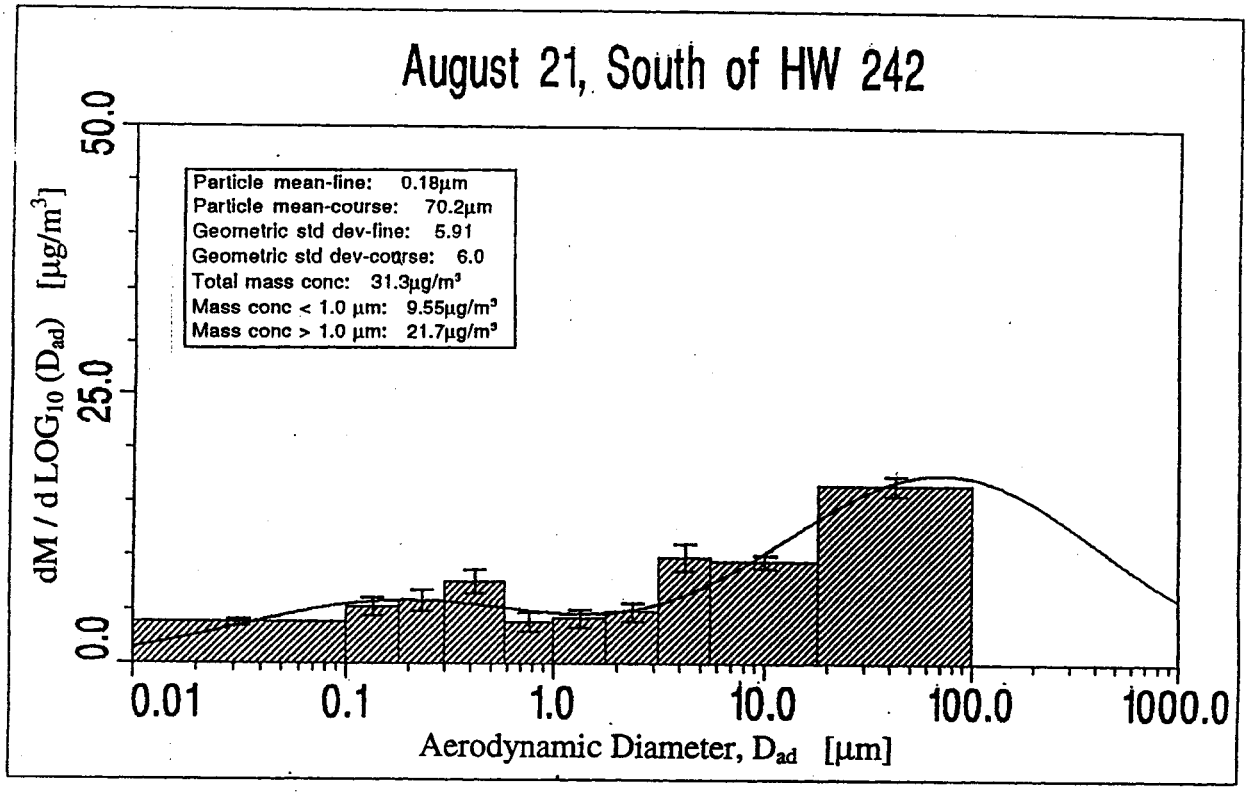

Fig. C8: Time-integrated mass concentration distribution from the **Bunker Hills** test on **August 21** at **sampling station 2** (located on the east side of Hanson Blvd. south of Trunk Hwy. 242, Coon Rapids, MN -- see also Figs. B3a and B3b).

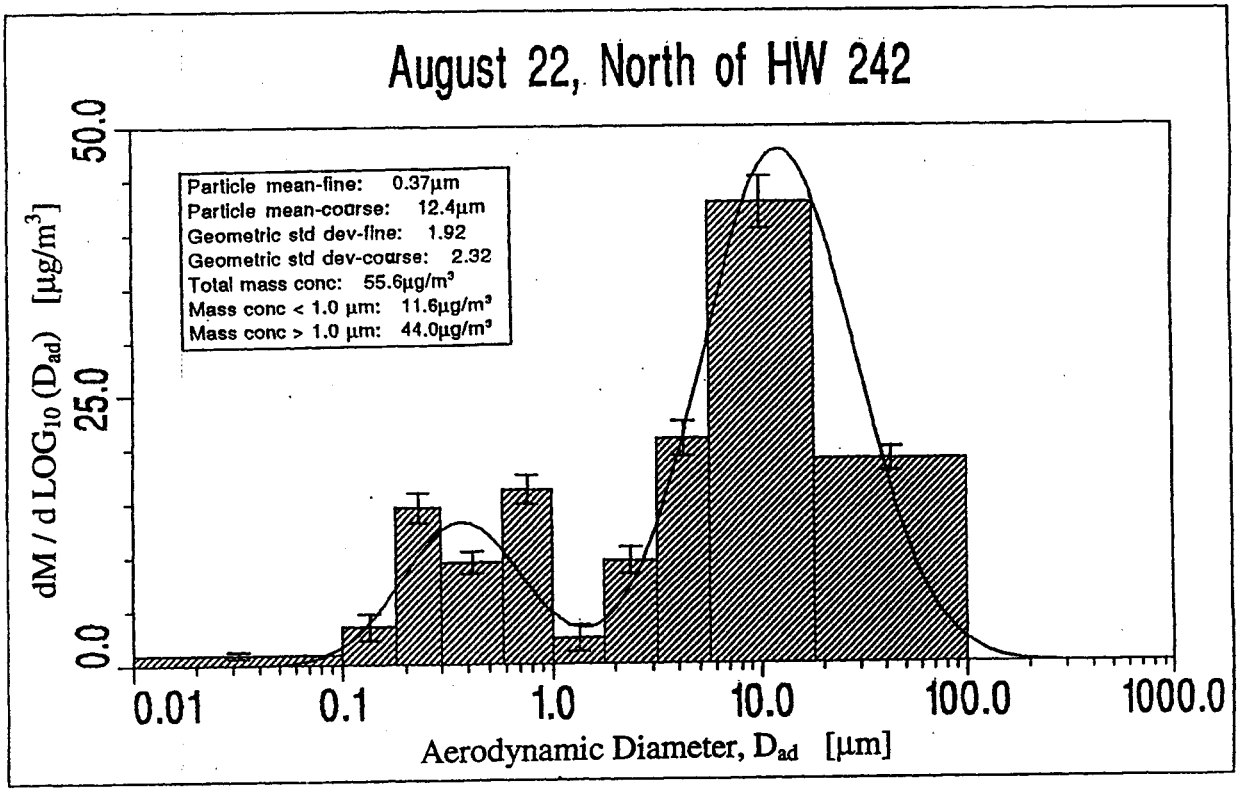

Fig. C9: Time-integrated mass concentration distribution from the **Bunker Hills** test on **August 22** at **sampling station 1** (located on the east side of Hanson Blvd. north of Trunk Hwy. 242, Coon Rapids, MN -- see also Figs. B3a and B3b).

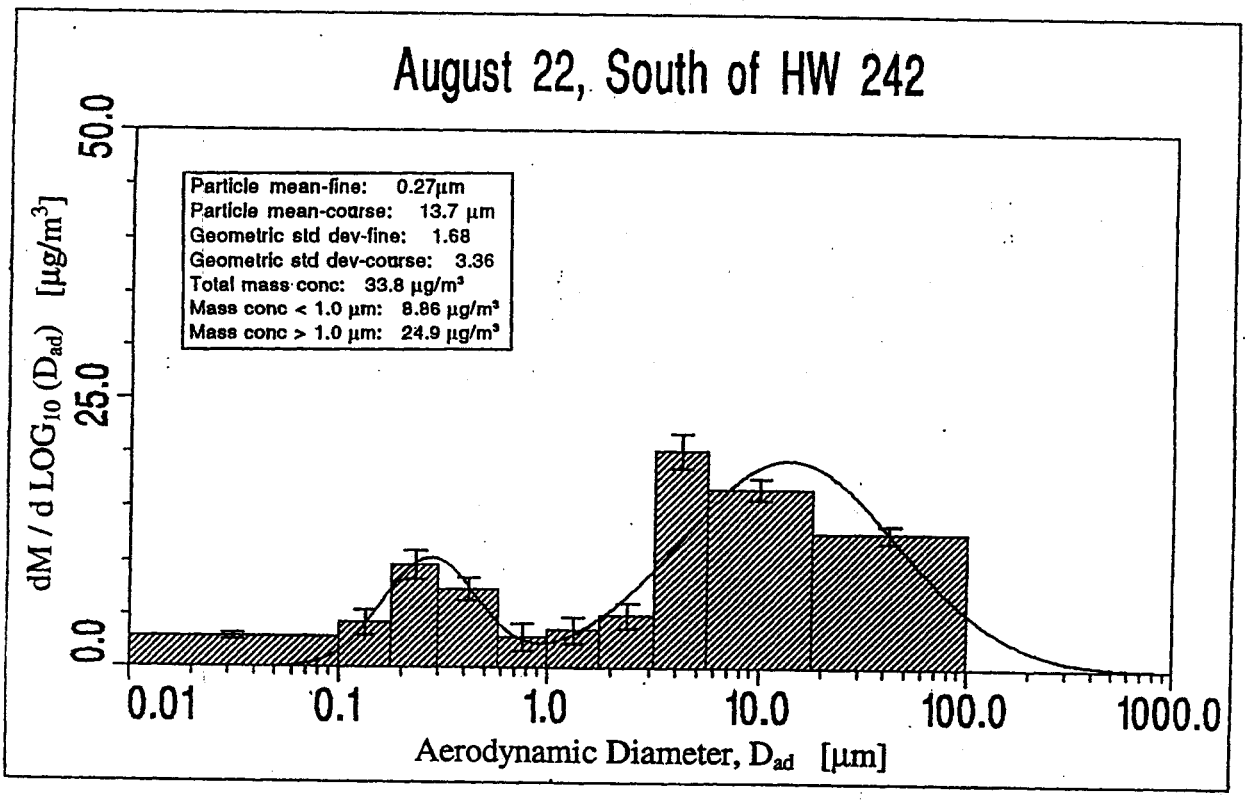

Fig. C10: Time-integrated mass concentration distribution from the **Bunker Hills** test on **August 22** at **sampling station 2** (located on the east side of Hanson Blvd. south of Trunk Hwy. 242, Coon Rapids, MN -- see also Figs. B3a and B3b).

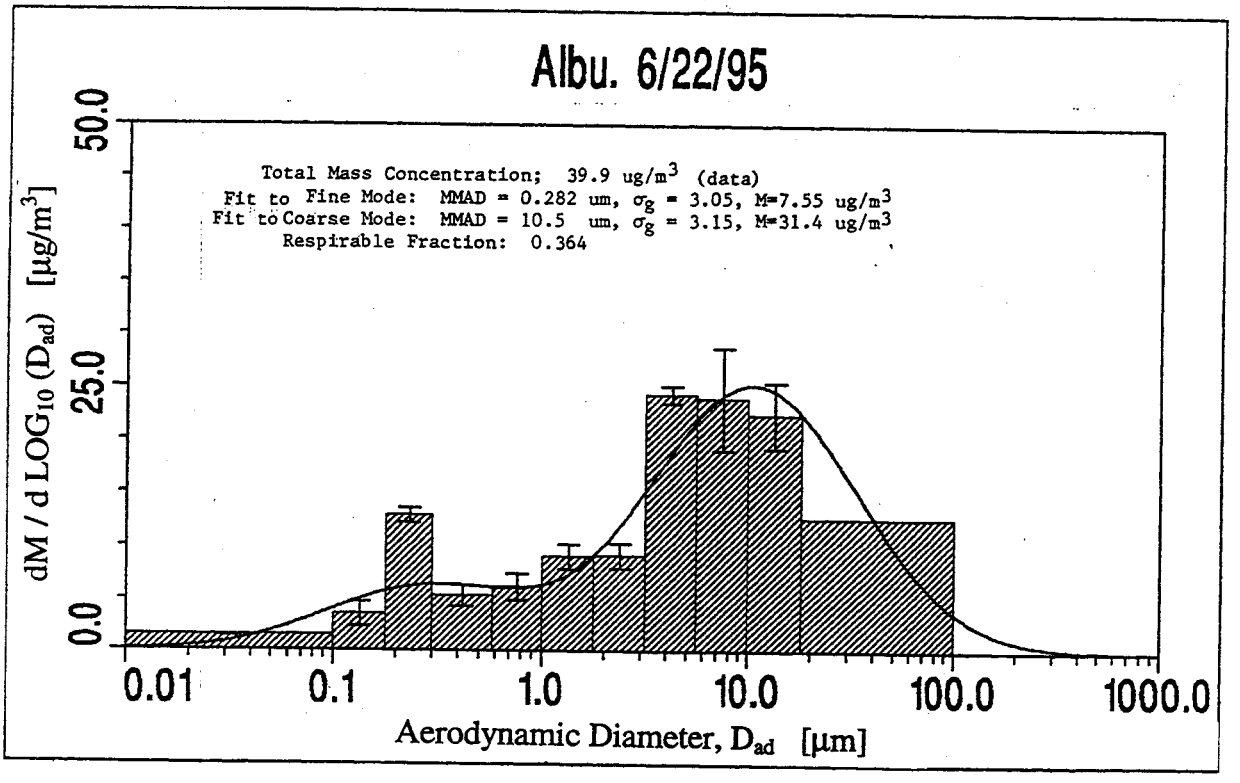

Fig. C11: Time-integrated mass concentration distribution from the **Albuquerque** test on **June 22** at **sampling station 1** (located on the north side of Gibson Blvd. just east of the intersection with Girard, Albuquereque, NM -- see also Fig. B6).

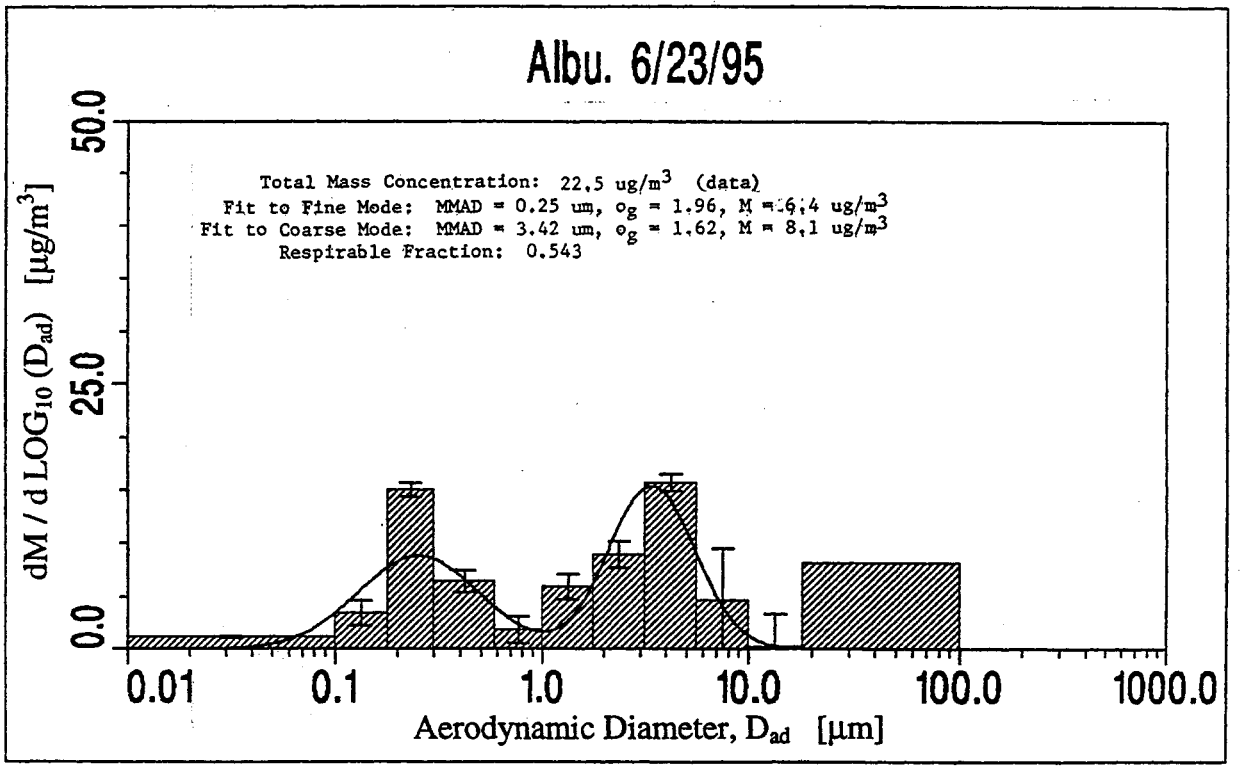

Fig. C12: Time-integrated mass concentration distribution from the **Albuquerque** test on **June 23** at **sampling station 1** (located on the north side of Gibson Blvd. just east of the intersection with Girard, Albuquereque, NM -- see also Fig. B6).

APPENDIX D: ALBUQUERQUE LANGAN CO DATA PLOTS

The purpose of this appendix is to document the Langan L-15 portable CO sensor data pertaining to the Albuquerque test. The graphical printouts included here are copies of the originals received from Santa Fe Technologies. The format is that which is output by the Data Bear™ software supplied with the Langan sensors, which Santa Fe personnel used to process the CO data. Hence, although the scales chosen by Santa Fe do not always have the desired resolution to enable direct comparison to the other data sets, the plots are adequate to document the performance of the Langan L-15 sensors, which satisfies our purpose here.

Although the graphical data is an accurate representation of the output of the sensors, the ASCII data files which were supposed to correspond to the plots were replete with errors. Of the 34 files received from Santa Fe Technologies, only 7 contained useful data. It is unclear whether the integrity of the original raw data files was lost. Each file had to be examined individually for correct data, as some of them were misnamed, indicating that they had data from a different sensor than was actually the case. Most of the problems appear to result from improper use of the Data Bear™ software by Santa Fe Technology personnel--for example, not selecting useful time periods to save. Another problem apparently occurred because the Data Bear software doesn't use a fixed number of places for each data quantity it outputs--hence, the data can get misaligned if it is simply imported into a spreadsheet without care. This mistake apparently was made in the case of several files. A list of the files received along with the errors is given below.

Table D1: Langan CO Data Files from Albuquerque Test as Supplied by Santa Fe Technologies

Sensor	Filename	Comments	Size (kB)	Disk #	Beg. Date	Beg. Time	End Date	End Time
1630	950622 ppm 1630.1	early end date	295	2	6/13	13:18:35	6/22	17:57:35
(on sign	950622 temp 1630.2	no data in file	1	3	6/22	18:02:35	6/22	18:02:35
next to	*950626 ppm 1630_1 #4*	*CO & temp both days*	*331*	*4*	*6/15*	*18:40:35*	*6/26*	*10:39:35*
road,	*950626 temp 1630.2 #5*	*CO & temp both days*	*346*	*4*	*6/15*	*18:50:41*	*6/26*	*10:49:41*
10 ft	950626 temp 1630.2 #3	same data as above, different end date	93	3	6/15	18:36:35	6/18	15:09:35
high	950706 ppm 1630.1	garbage data-fields messed up?	563	5	-	-	-	-
	950622 temp 1633.2	misnamed-data is for sensor 1630, not 1633	298	2	6/13	13:18:35	6/22	18:02:35
1632	ppm1632.1-6/22/95	only a couple minutes	2	1	6/13	13:21:54	6/13	13:39:54
(on	*ppm1663.1-6/22/95*	*CO data for 6/22*	*285*	*1*	*6/13*	*13:21:54*	*6/22*	*17:27:54*
table								
3 ft	temp1633.2-6/22/95	data ends on 6/21	254	1	6/13	13:21:54	6/21	8:38:54
high)	950626 ppm 1632.1 #2	garbage data-fields messed up?	77	4	-	-	-	-

1633 (sample inlet, 10 ft high	950619 ppm 1633.1	ends too early	183	2	6/13	13:06:38	6/19	10:24:38
	950619 temp 1633.2	ends too early	191	2	6/13	13:06:38	6/19	10:32:38
	950622 ppm 1633.1	ends too early	83	2	6/13	13:06:38	6/16	5:01:38
	950622 temp 1633.2	misnamed--times match data from 1630	298	2	6/13	13:18:35	6/22	18:02:35
	950619 temp 1633.2	ends too early	191	3	6/13	13:06:38	6/19	10:32:38
1635 (on table 3 ft high	950619 ppm 1635.1 #1	1 data point	1	4	6/26	10:57:34	6/26	10:57:34
	950626 temp 1635.2 #2	1 data point	1	4	6/26	11:18:34	6/26	11:18:34
	950626 ppm 1635.1 #3	no data	0	4	-	-	-	-
1648 (sample inlet 10 ft high	950619 ppm 1648.1	ends too early	187	2	6/13	13:18:40	6/19	10:48:40
	950619 temp 1648.2	ends too early	196	2	6/13	13:18:41	6/19	10:59:41
	950622 temp 1648.2	ends too early	0.5	2	6/13	13:18:45	6/13	13:36:45
	950622 temp 1648.2	*temp data for 6/22*	*305*	*3*	*6/13*	*13:18:45*	*6/22*	*17:38:45*
	950626 ppm 1648.1 #1	misnamed-duplicate of temp data	305	3	6/13	13:18:45	6/22	17:38:45
	950619 temp 1648.2 #2	garbage-fields not properly separated?	120	3	-	-	-	-
	950706 ppm 1648.1	garbage-fields not properly separated?	508	5	-	-	-	-

1663 (on sign by road, 10 ft high)	1663-6/22/95	ends too early	2	1	6/13	13:18:42	6/13	13:36:42
	ppm 1663.1	*CO data for 6.22*	*285*	*1*	*6/13*	*13:18:42*	*6/22*	*17:11:42*
	1663.2	data incorrect -- fields scrambled in middle of file?	297	1	6/13	-	-	-
	1663.2-6/22/95	*temp data for 6/22*	*297*	*1*	*6/13*	*13:18:42*	*6/22*	*17:12:42*
	950622 ppm 1663.1	only 1 min of data	1	3	6/22	18:06:42	6/22	18:06:42
	950622 temp1663.2	even though times are different, data is identical to temp data in 1663.2-6/22/95	298	3	6/13	13:18:47	6/22	18:10:47
	950622 temp 1663.2a	garbage-fields messed up?	236	3	-	-	-	-
	950626 ppm 1663.1	only 1 min of data	1	5	6/26	10:10:47	6/26	10:10:47
	950626 temp 1663.2	*temp data both days*	*346*	*5*	*6/15*	*18:11:47*	*6/26*	*10:10:47*

Because of the lack of valid computer data, it was essentially impossible to establish the correlation between Langan monitors and the Dasibi 3003 device. However, it is obvious from the first graph of the data from sensor 1630 on 6/23 (generated by the author to ease comparison of temperature and CO plots) that there is a substantial baseline drift correlated to the sensor temperature curve. Similar CO concentration profiles were recorded by the other sensors. The large spikes on the CO plots on this day correspond to the times when the sensor was spanned using 20.3 ppm calibration gas. Immediately prior to this, the sensor was fed with zero grade gas containing 0 ppm CO. Both the zero and calibration gas inputs were fed into the sensor for over three minutes in order to ensure that the slow sampling flow rate did not affect the instrument response. As can be seen from the figure, the baseline zero drifts with temperature, but the span calibration stays roughly 20 ppm above the baseline. This implies that the offsets of the amplifiers used to output the signals from the Langan sensors drifted with temperature, but that the gains remained relatively constant at the values set during indoor calibrations conducted prior to the test.

Langan CO and Temp. Histories, 6-23-95

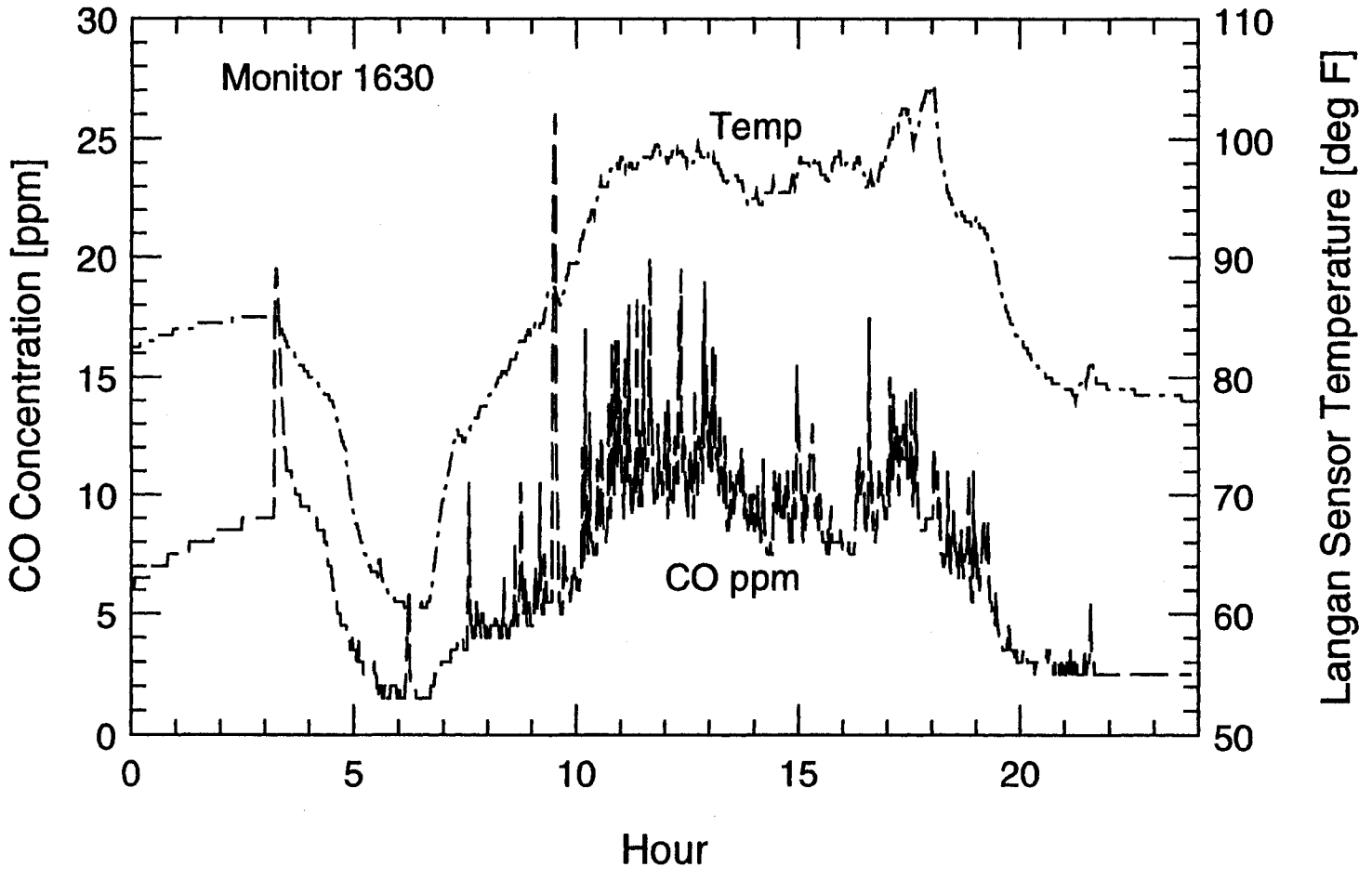

Title:

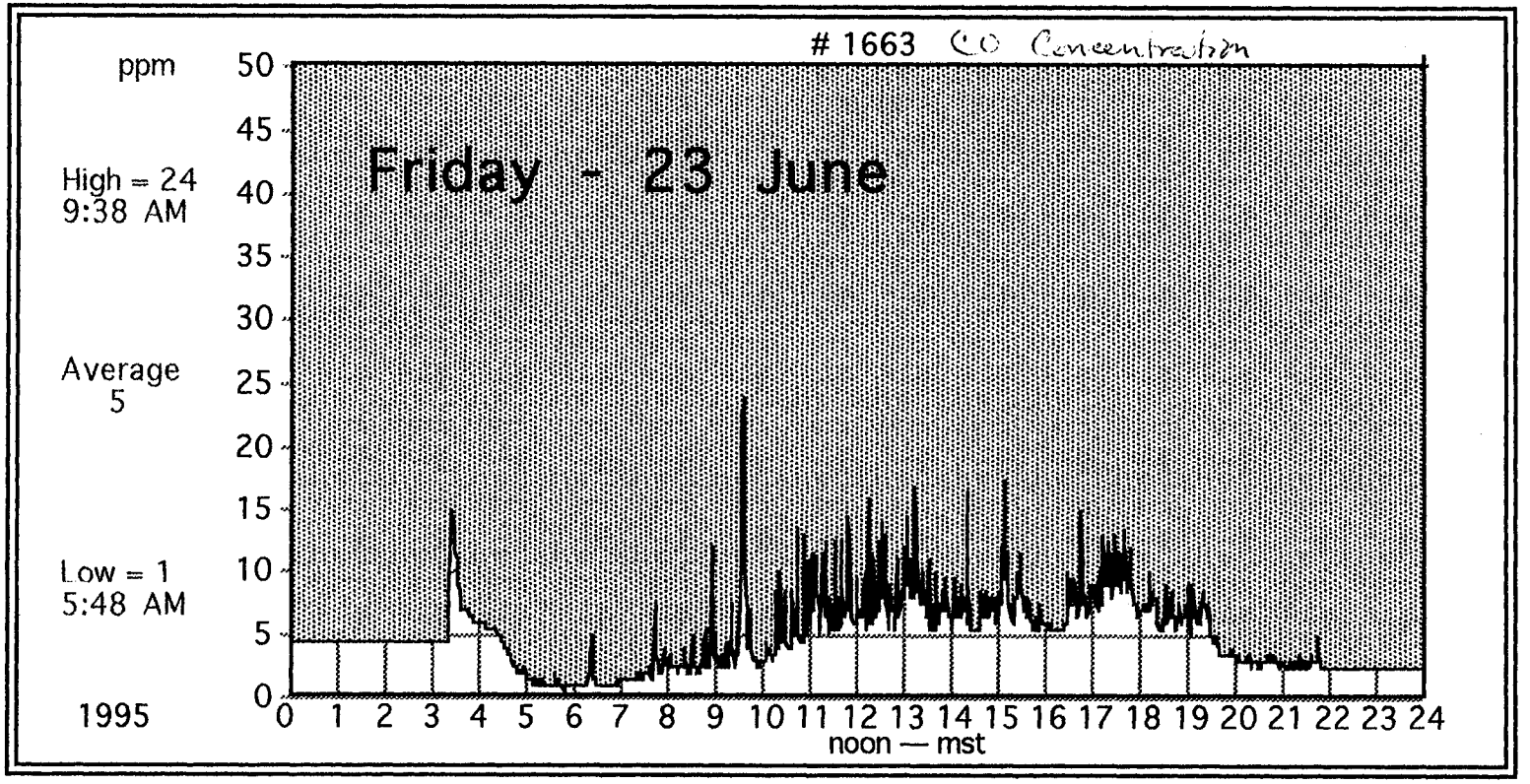

DataBear™ Measurer
Langan Products, Inc.

Title:

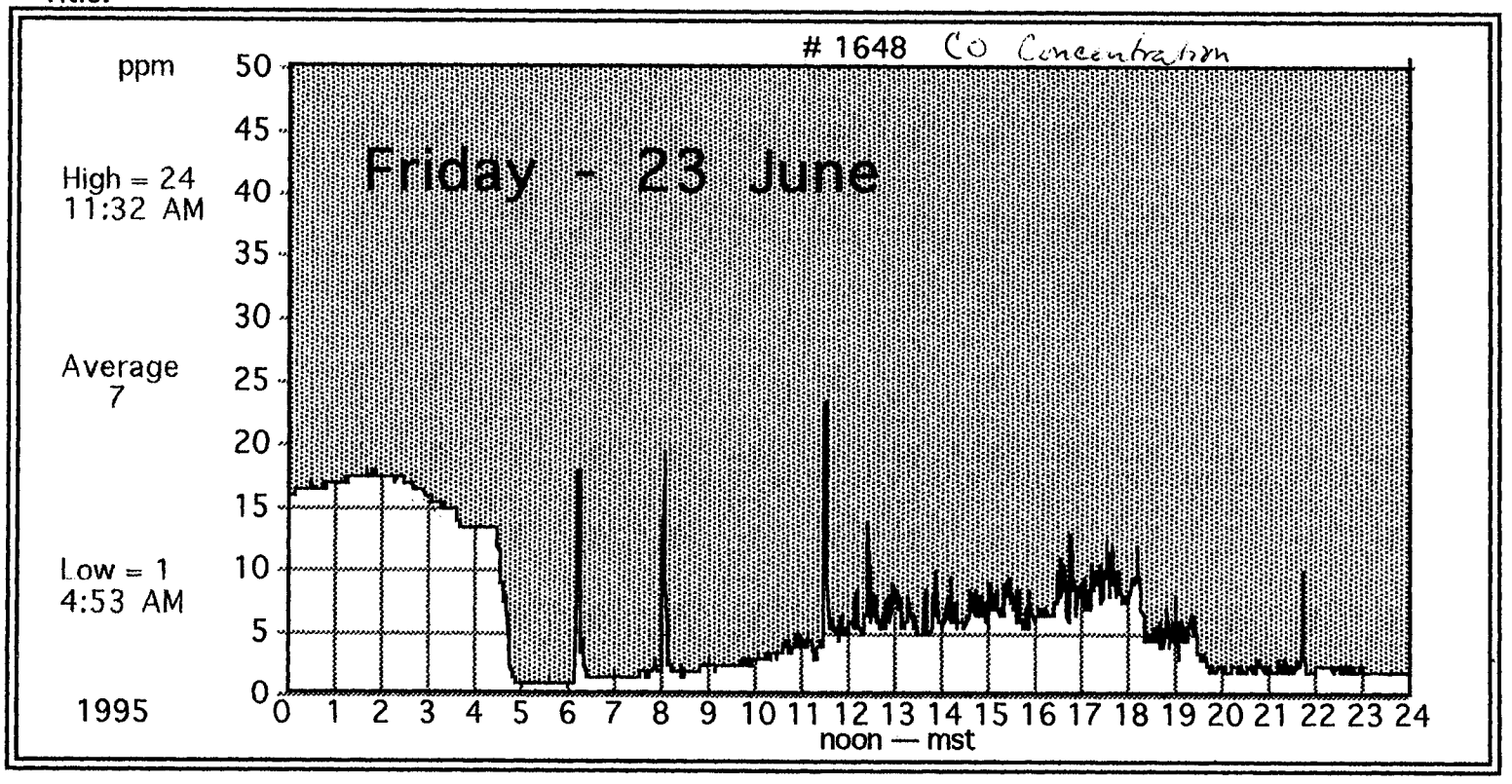

DataBear™ Measurer
Langan Products, Inc.

Title:

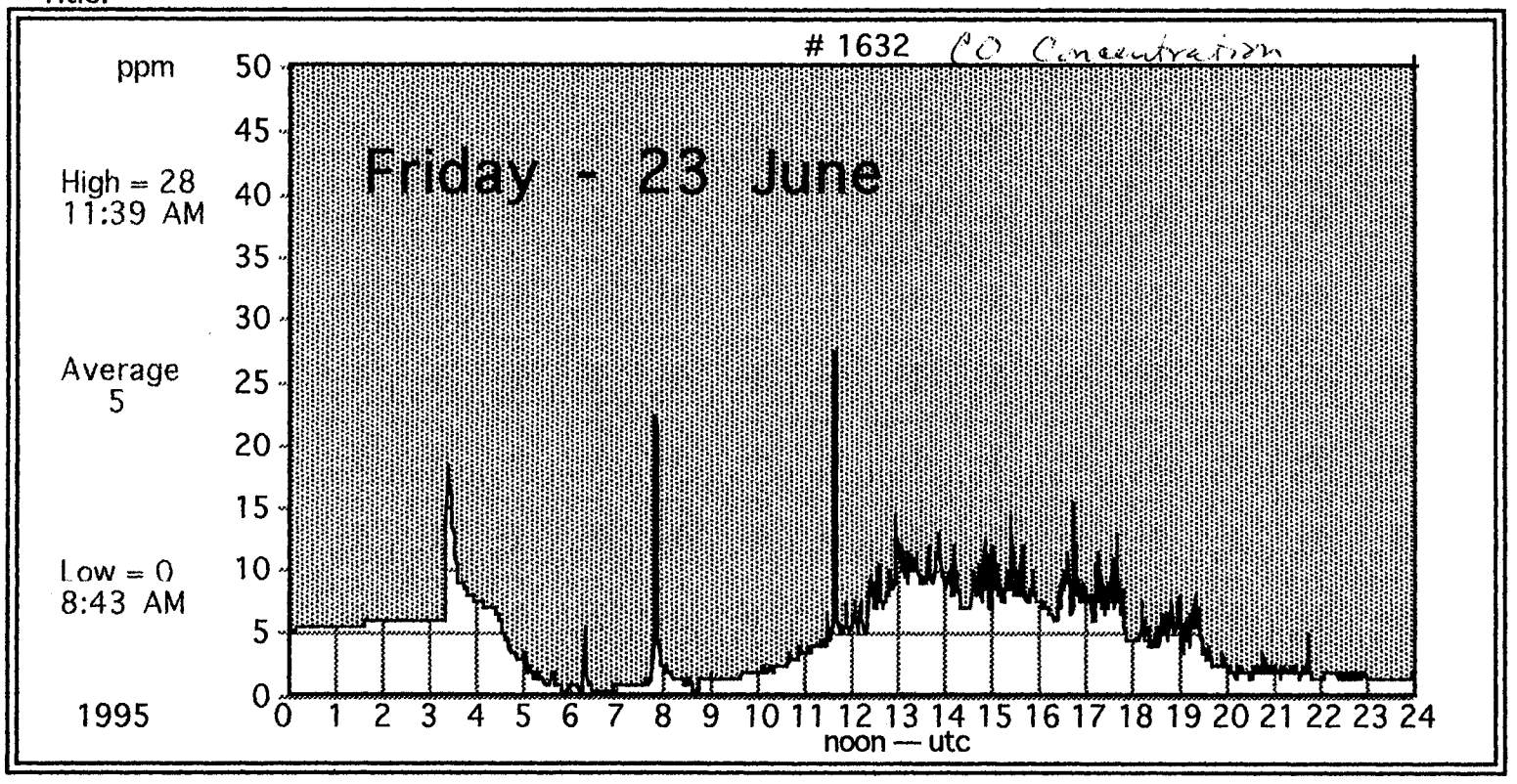

DataBear™ Measurer
Langan Products, Inc.

Title:

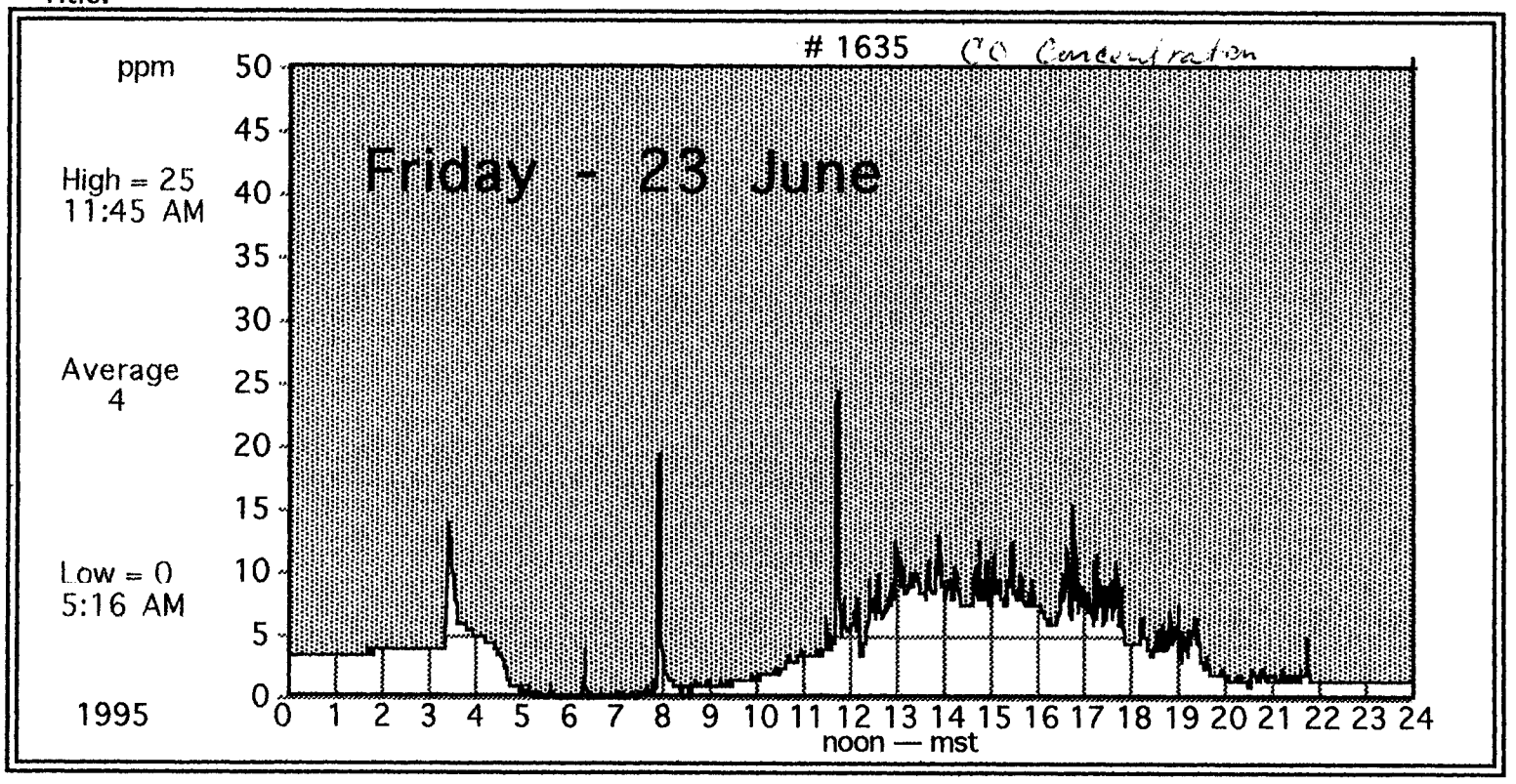

DataBear™ Measurer
Langan Products, Inc.

Title:

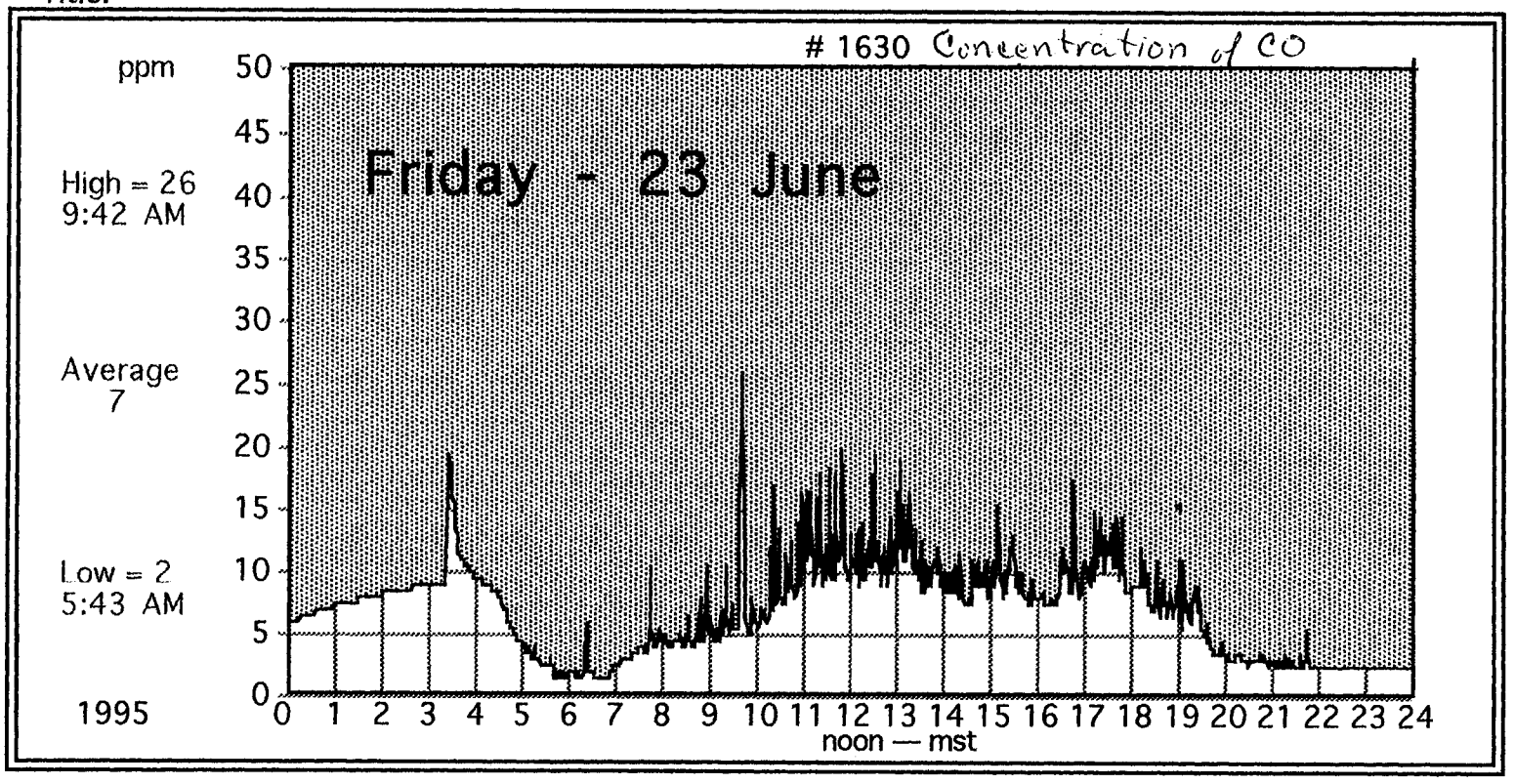

DataBear™ Measurer
Langan Products, Inc.

Similar correlations between instrument temperature and CO baseline drift can be seen on the Thursday data, but the effect is less obvious because abnormally high CO readings during the early morning hours make it difficult to pick out the calibration times. In fact, calibrations were only done at the beginning and end of the day on Thursday. When the Dasibi instrument came on-line at about 9:00 a.m., it showed similar large fluctuations in the ambient CO concentration correlated with the passage of lawnmowers and utility vehicles on the adjacent golf course. The wind was also very calm early Thursday morning, so it is possible that some of the early CO spikes around 6:00 came from dirty vehicles on the roadway. However, this seems unlikely, because we are certain that spikes clustered around 9:00 were caused by the operation of the golf course vehicles, and if anything, we would have expected to see an increasing frequency of CO spikes corresponding to the increase in traffic volume had the spikes been vehicle-related.

Title:

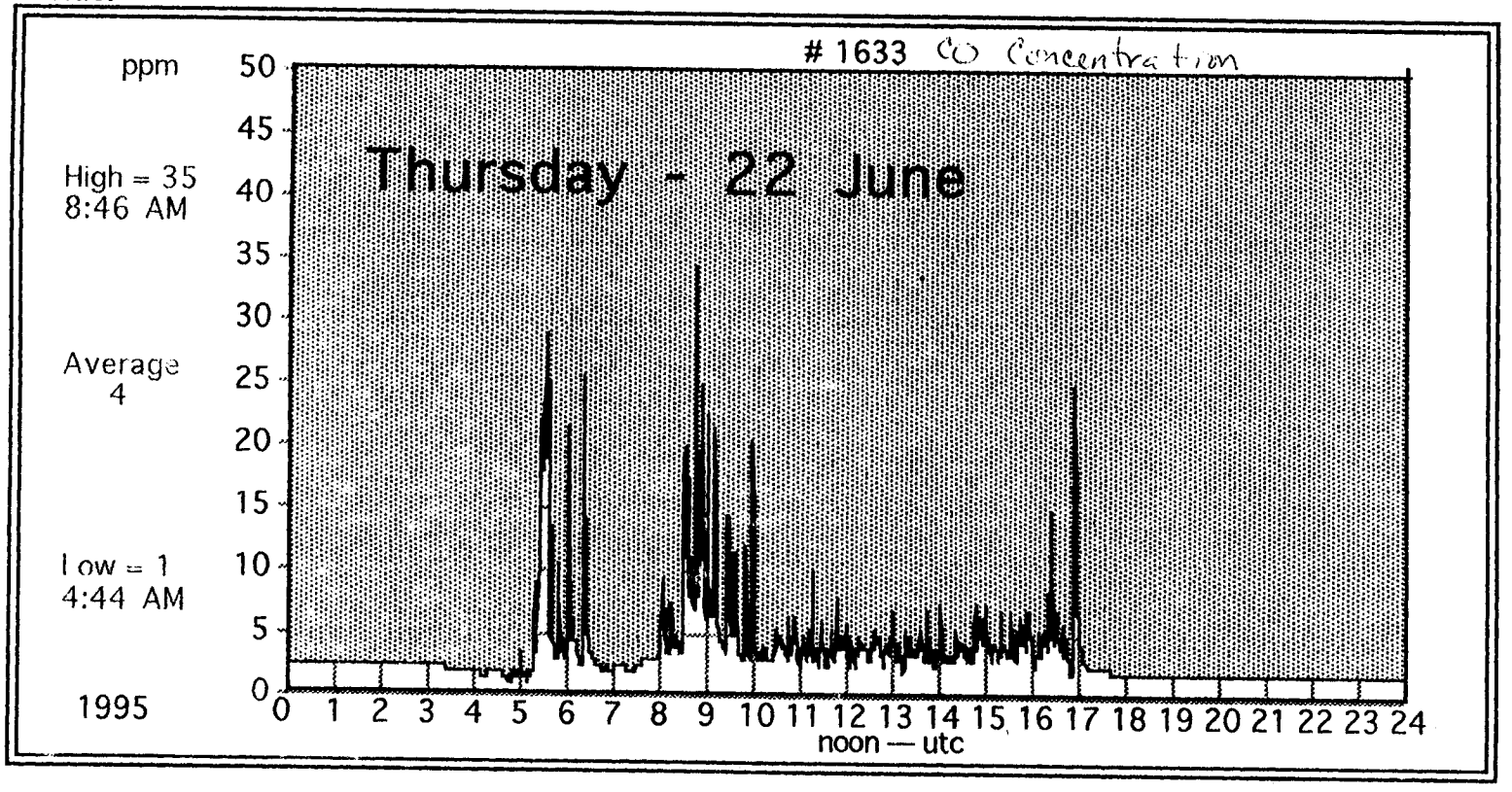

)ataBear™ Measurer
angan Products, Inc.

Title:

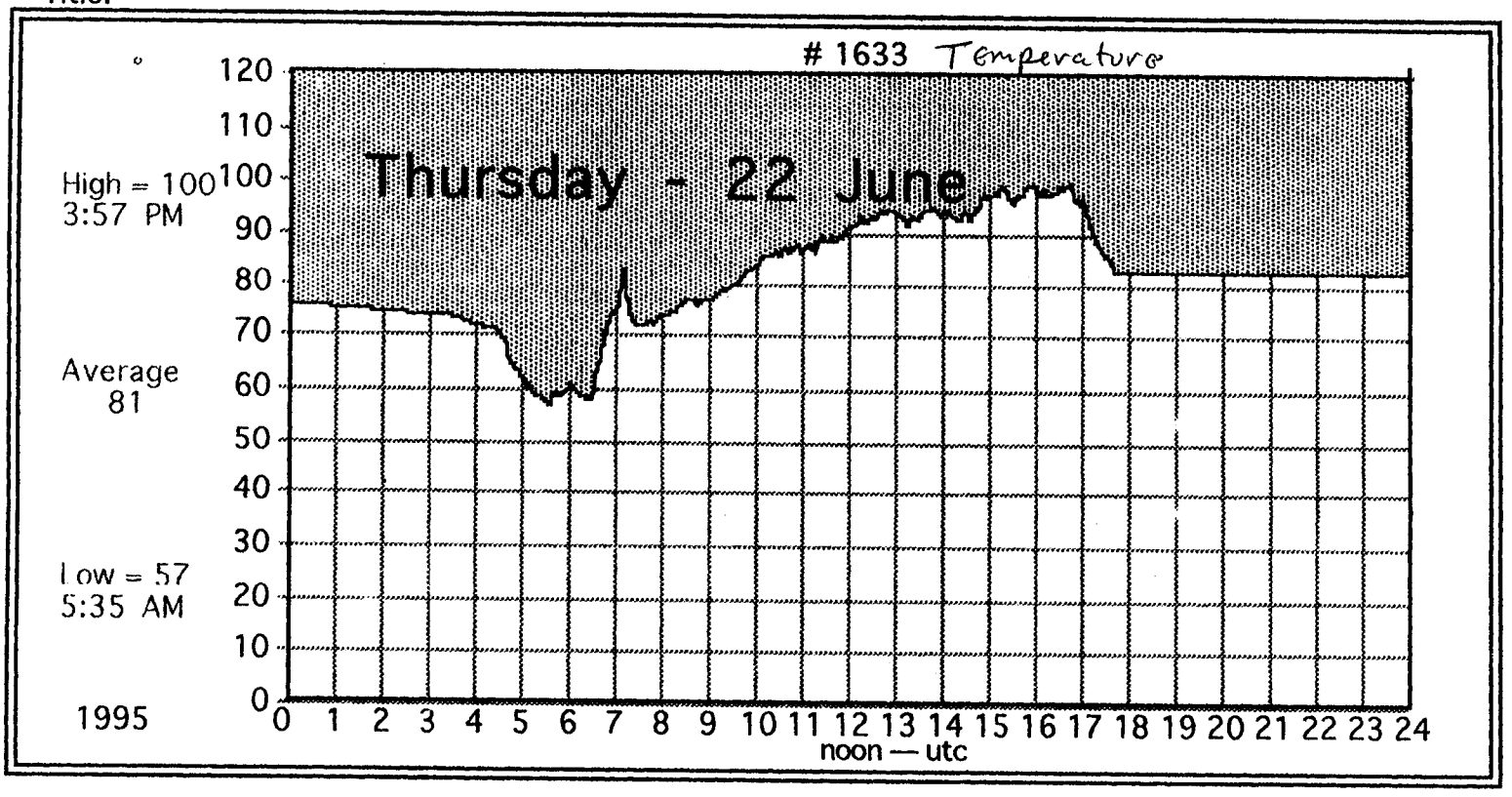

)ataBear™ Measurer
.angan Products, Inc.

Title:

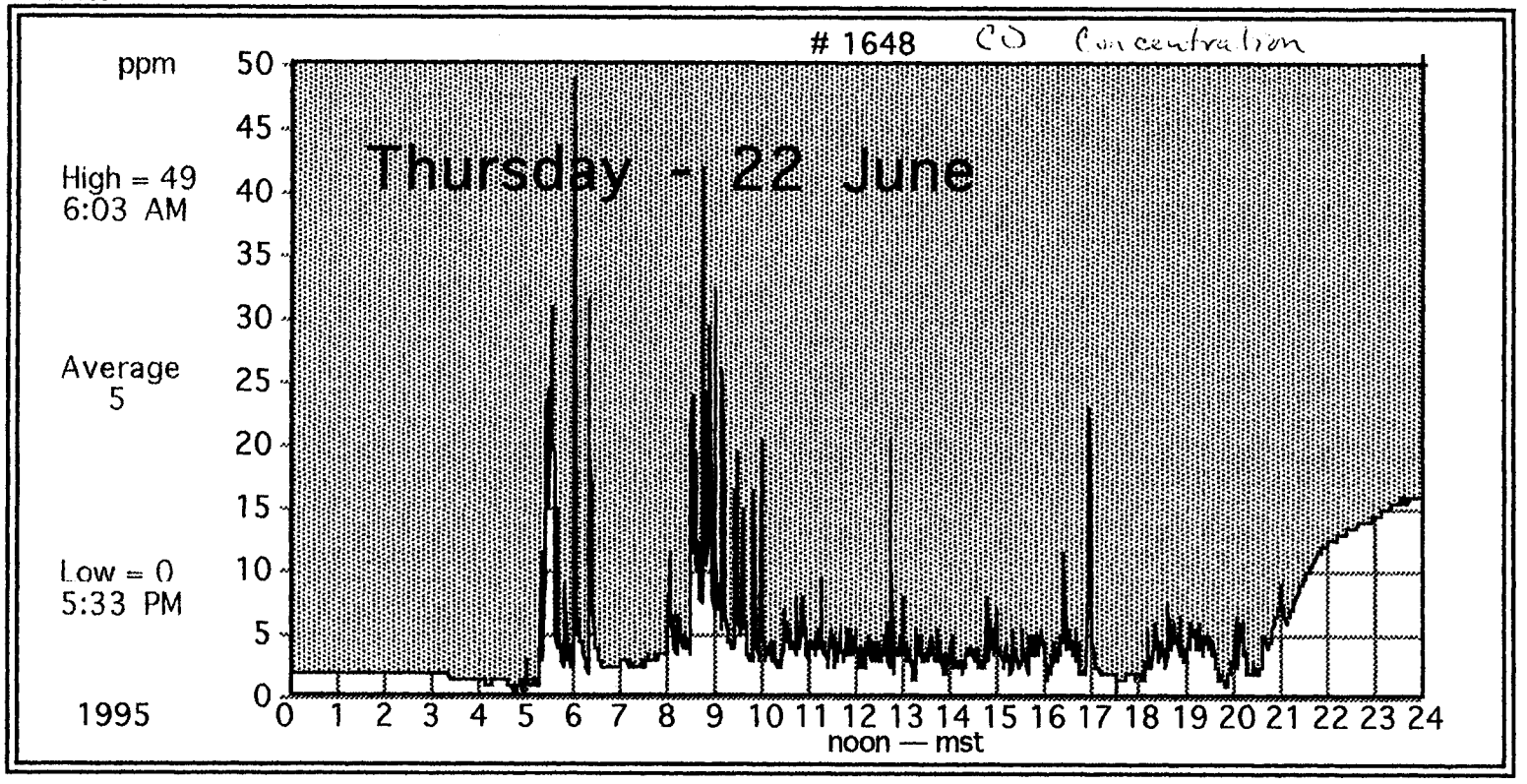

DataBear™ Measurer
Langan Products, Inc.

Title:

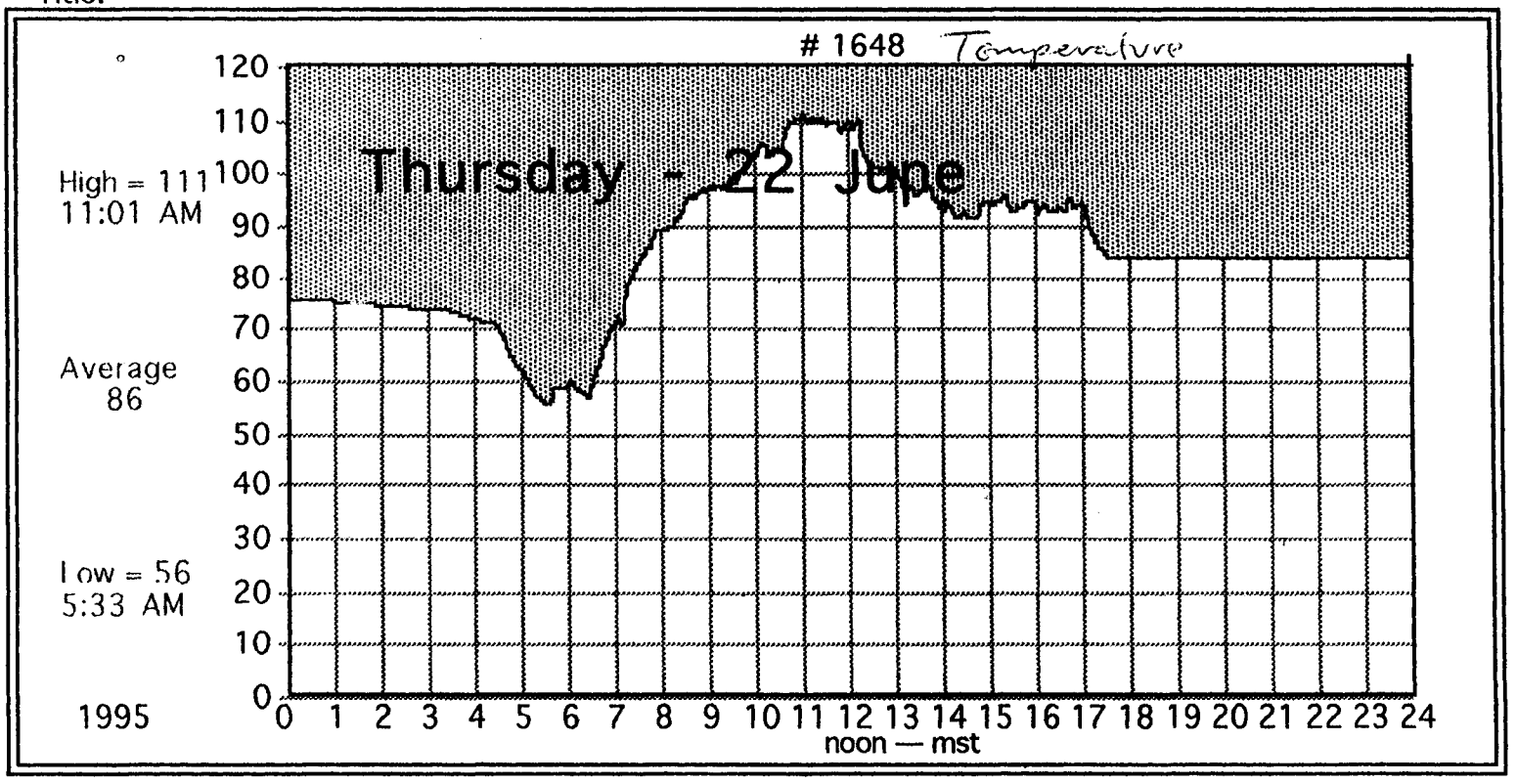

)ataBear™ Measurer
.angan Products, Inc.

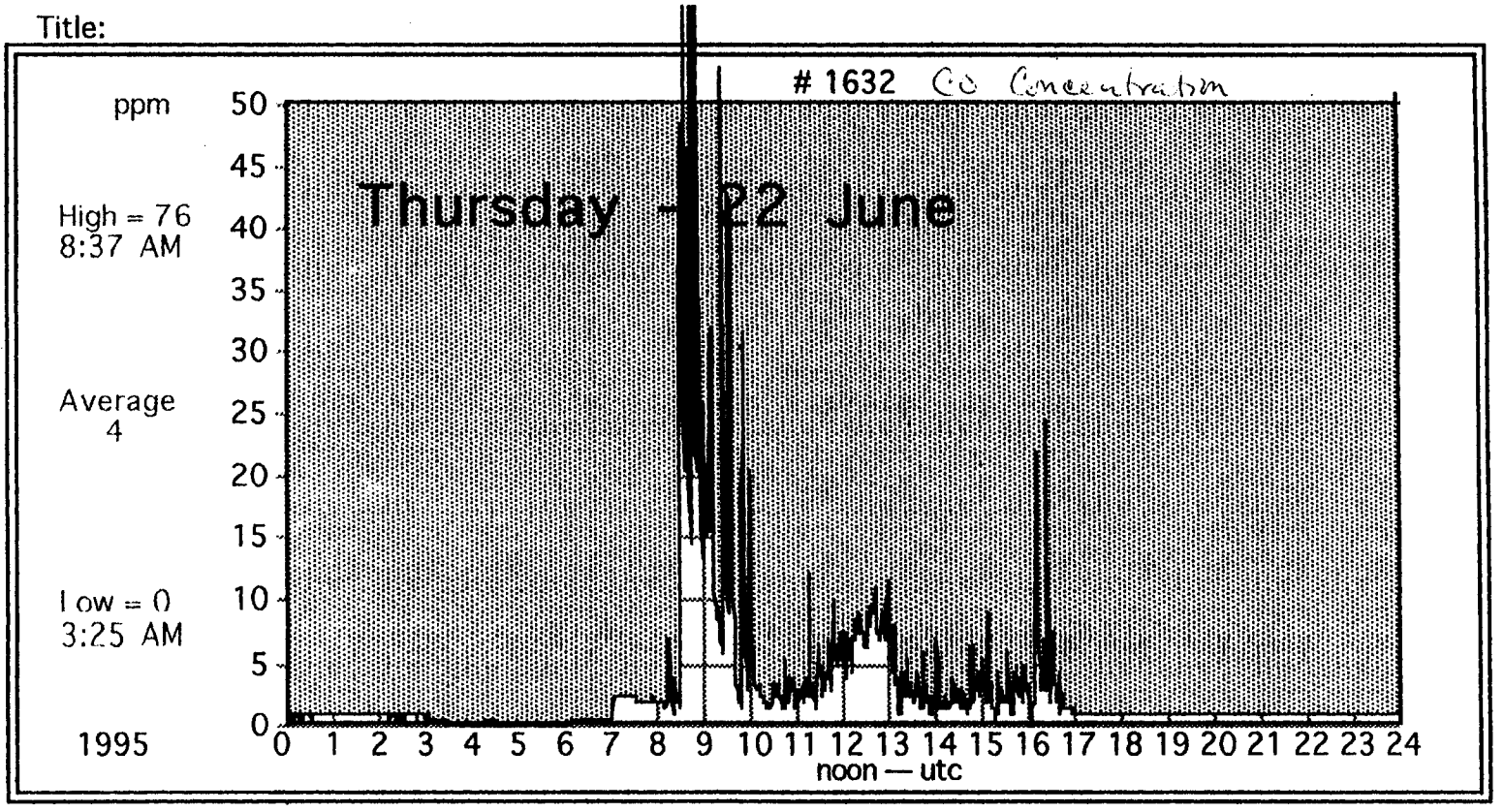

DataBear™ Measurer
Mangan Products, Inc.

Title:

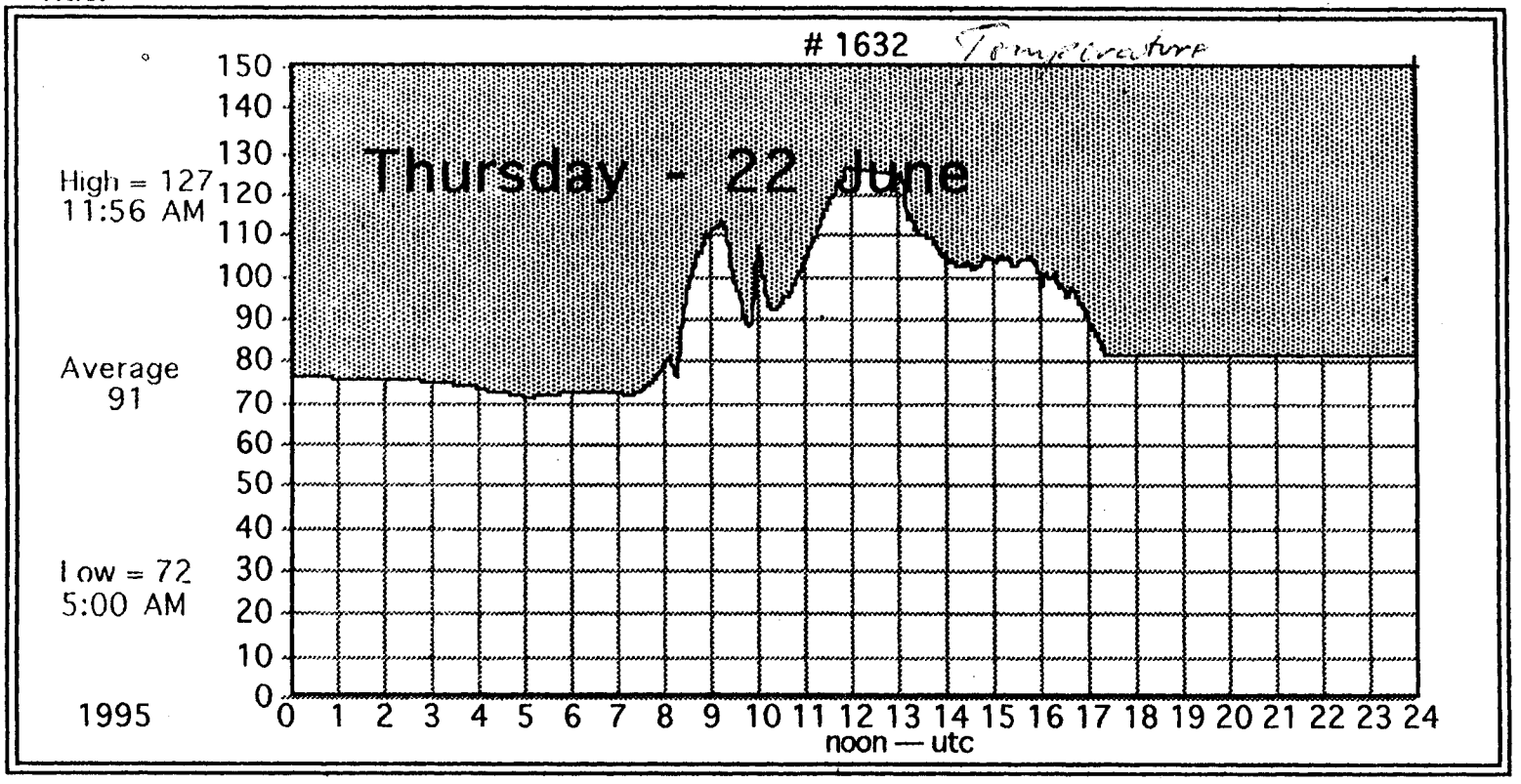

)ataBear™ Measurer
.angan Products, Inc.

Title:

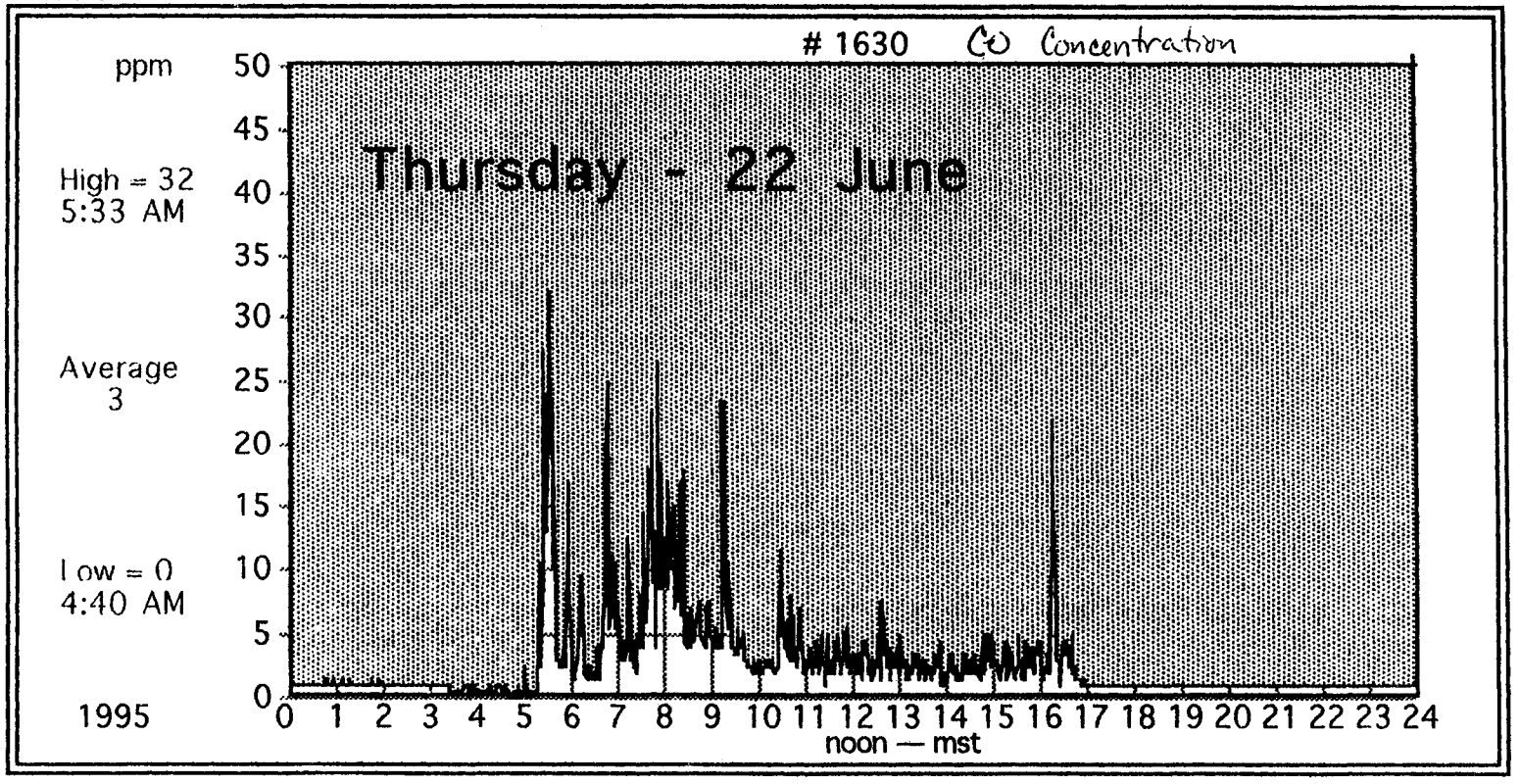

)ataBear™ Measurer
.angan Products, Inc.

Title:

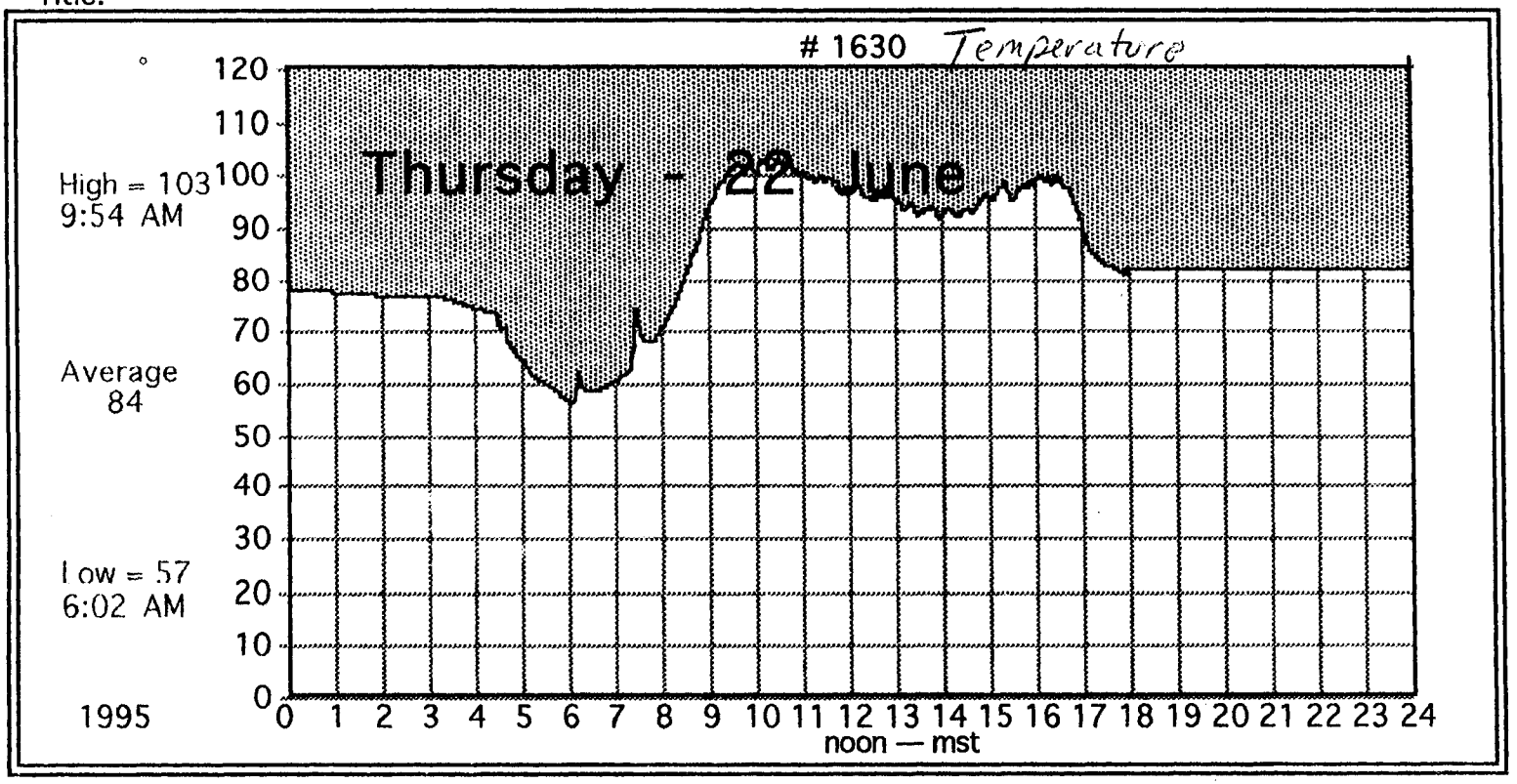

DataBear™ Measurer
Langan Products, Inc.

Title:

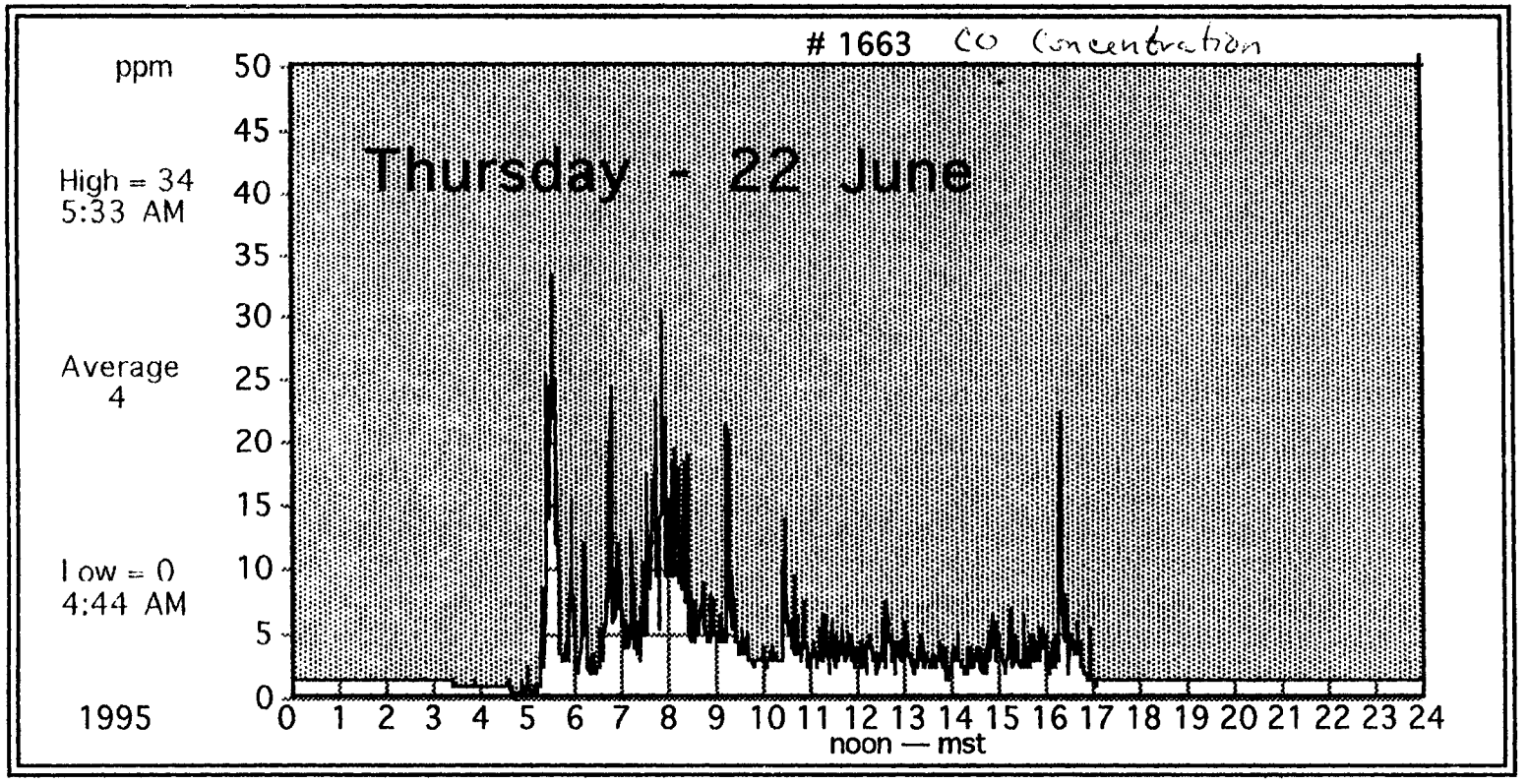

)ataBear™ Measurer
angan Products, Inc.

Title:

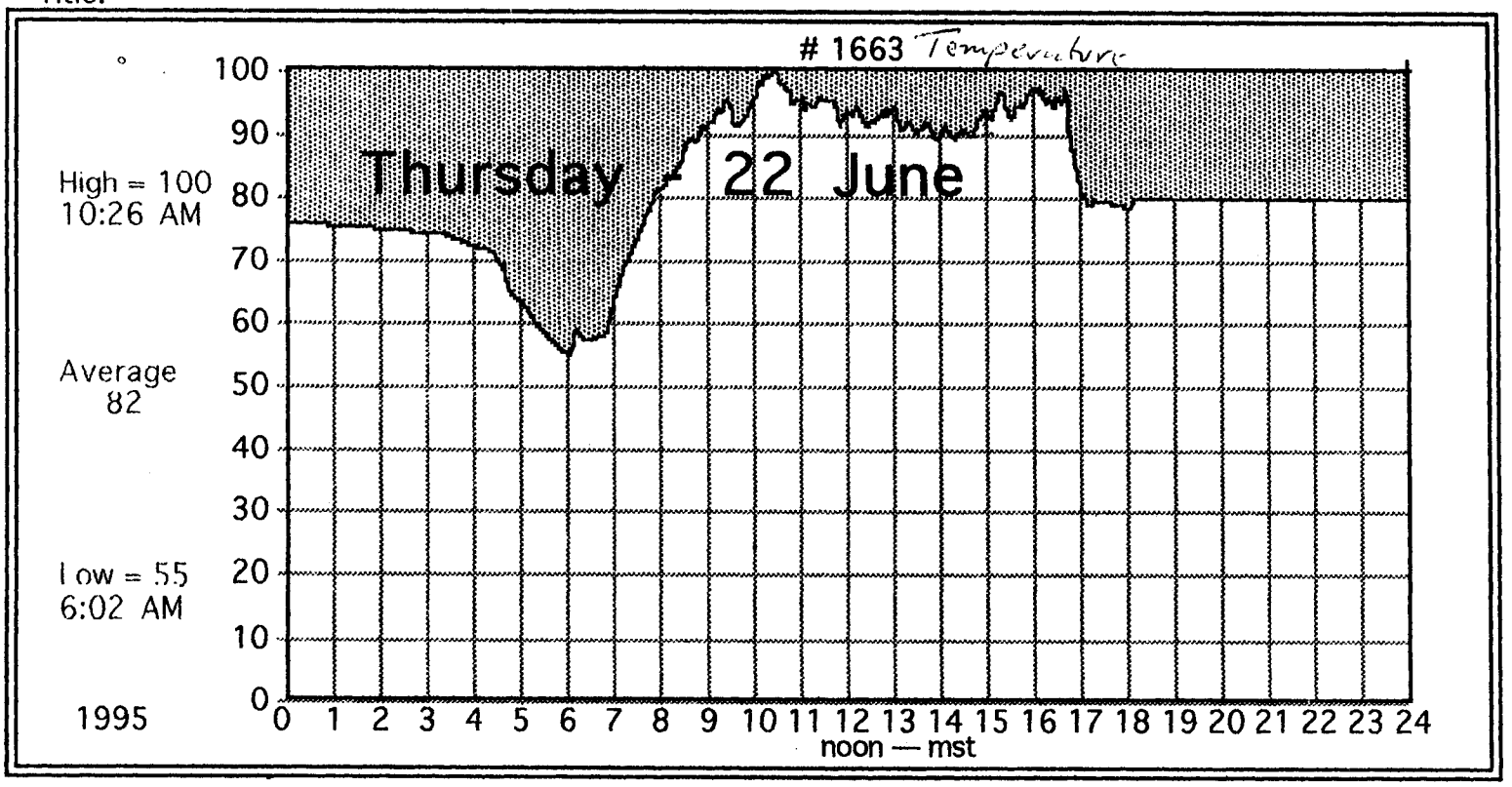

DataBear™ Measurer
Langan Products, Inc.

A copy of the original Dasibi 3003 strip chart data is also included here to document the "true" (*i.e.* most accurate) roadside CO concentrations measured during the test. The Dasibi sampled from the same 10 ft high inlet as the particle sampling instruments. Span and zero calibrations were taken regularly on both days, and both the zero and span readings remained stable regardless of temperature. The Dasibi did exhibit some short periods of high frequency noise randomly spaced in time, the source of which we could not ascertain; however, these were not very frequent, and they were easily recognized as unreal because of the high temporal frequency. These are indicated as erratic behavior on the strip chart recording. We knew these are unreal, because the sample flow rate of the instrument together with the volume of the sensor chamber combined to give an instrument response time of about 15 seconds or so, whereas the random fluctuations in voltage resulted in almost vertical lines on the chart at the maximum slew rate of the recorder.

Note: the pages of the strip charts proceed backward in time. The numbers at the bottom correspond to the panels of the accordion folds of the strip chart paper, not to any specific time scale. Times have been written in along the top to aid the reader in scanning the data, because there is significant overlap from page to page. The reader is advised to flip to the first panel of a strip and proceed to higher panel numbers in order to view the data in chronological order. One final note: there are several gaps in the time record on Thursday due to generator outages. The Friday data stops just after 2:15 p.m. because the equipment had to be returned to New Mexico Environmental Health Dept. (local air quality agency) personnel.

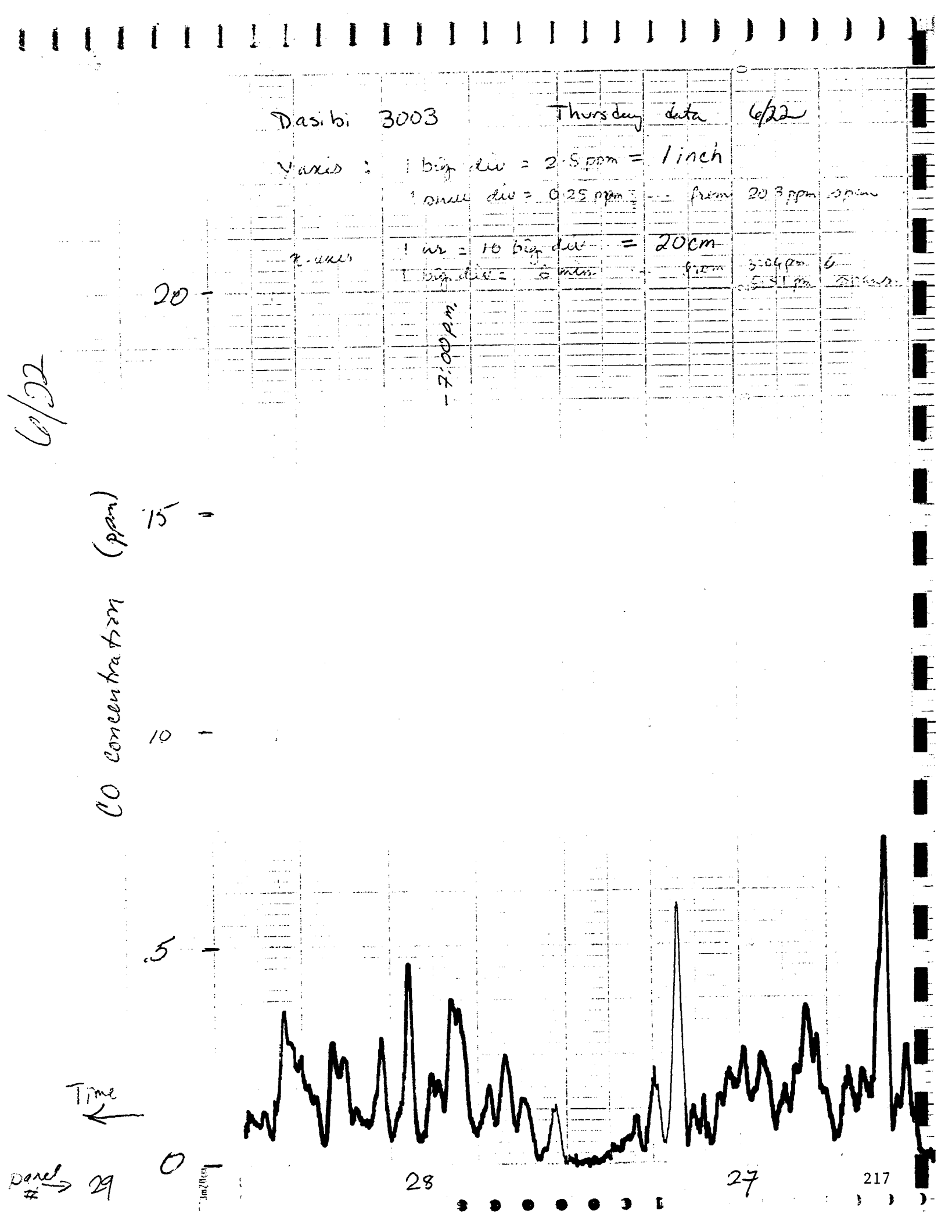
Dasibi 3003
Thursday data 6/22
Y axis : 1 big div = 2.5 ppm = 1 inch
1 small div = 0.25 ppm
X-axis
1 hr = 10 big div = 20 cm
1 big div = 2 cm
6/22
20
15
10
5
0
CO concentration (ppm)
7:00 p.m.
Time
Panel # 29
28
27
217

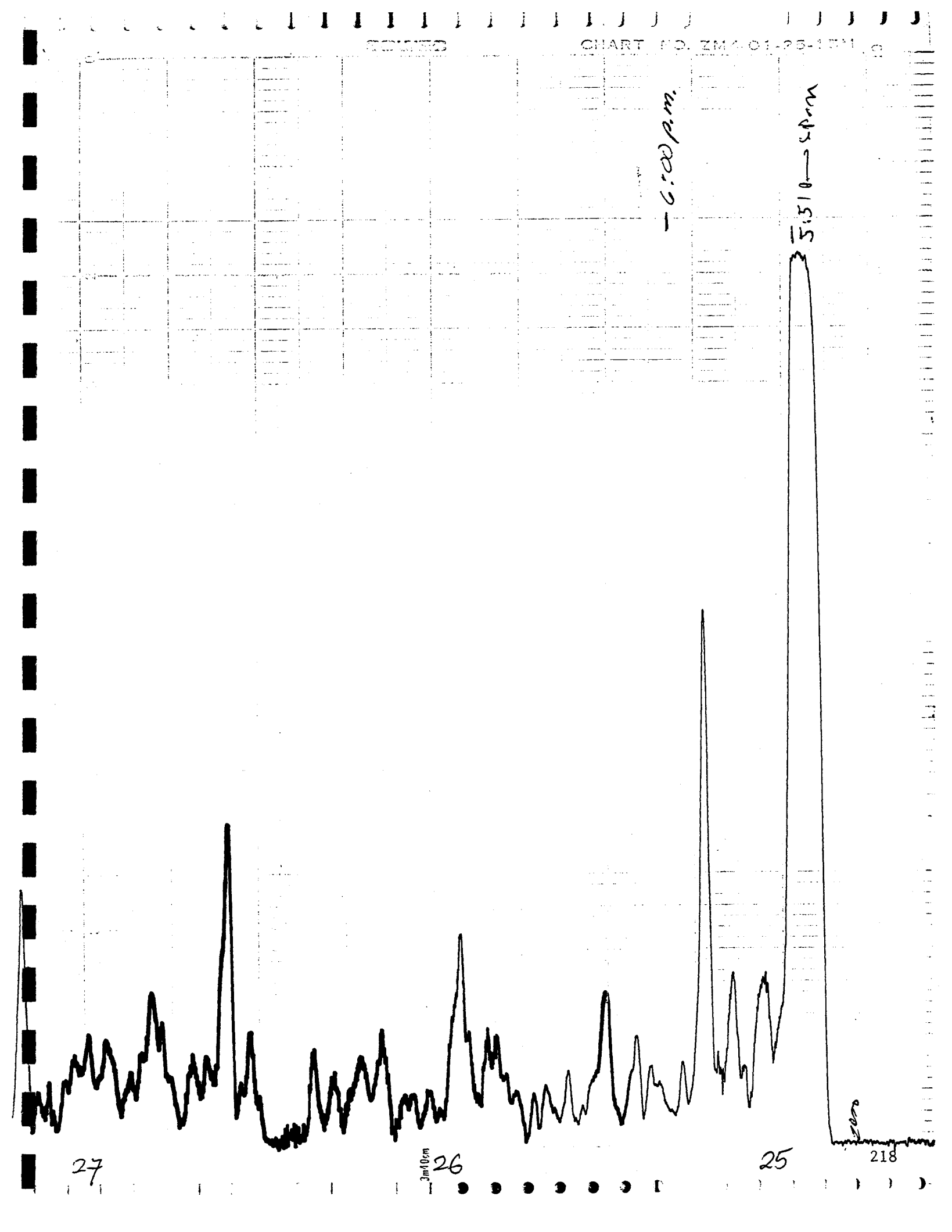
CHART NO. ZM4-01-93-1
5:51 — 5 min
w.d. 0.7 —
27
26
25
218

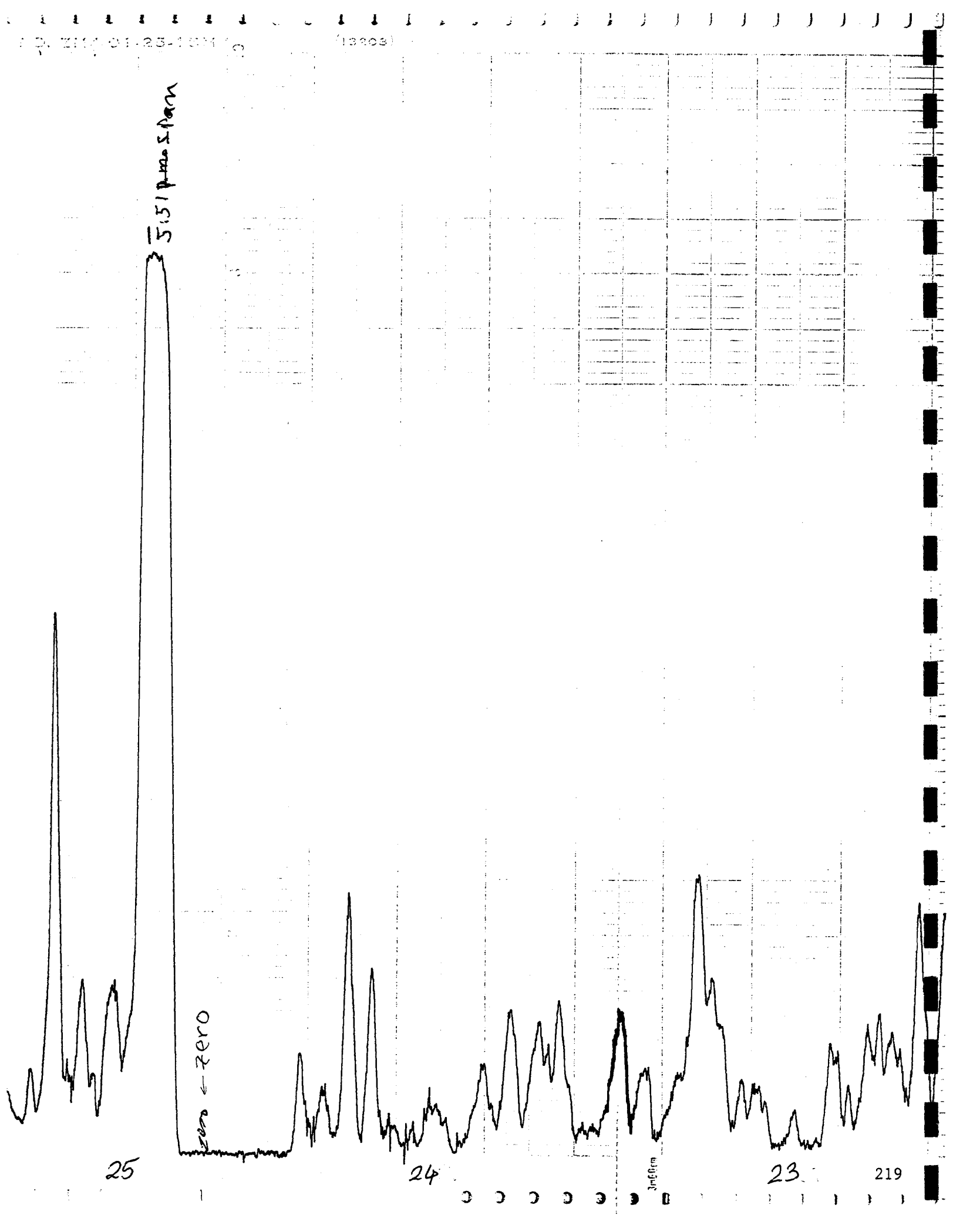
5151 Pmax Sparm
zero ← zero
25
24
23

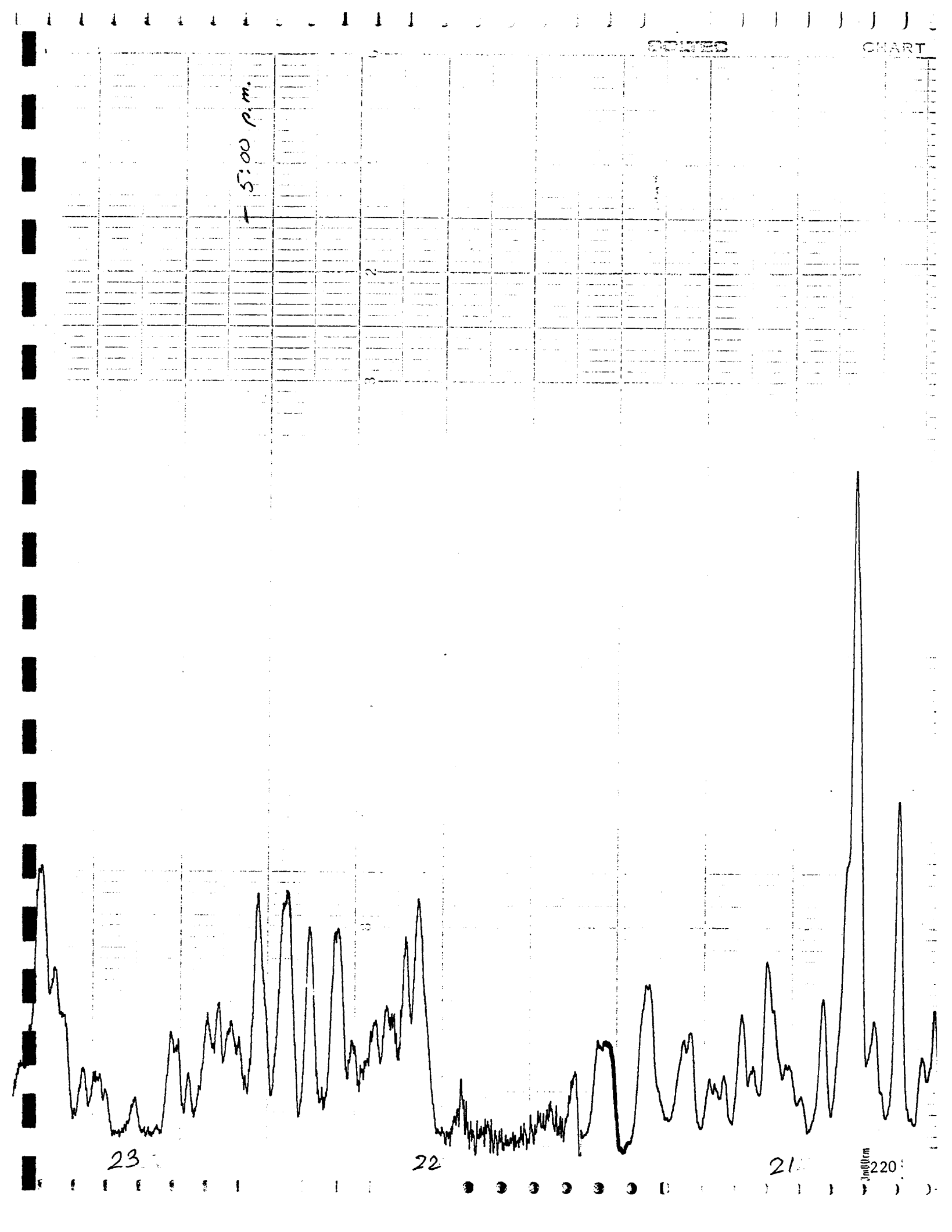
CHART
+ 5:00 p.m.
23
22
21
220

JEC CHART NO. ZM4-01-25-15M (13208)

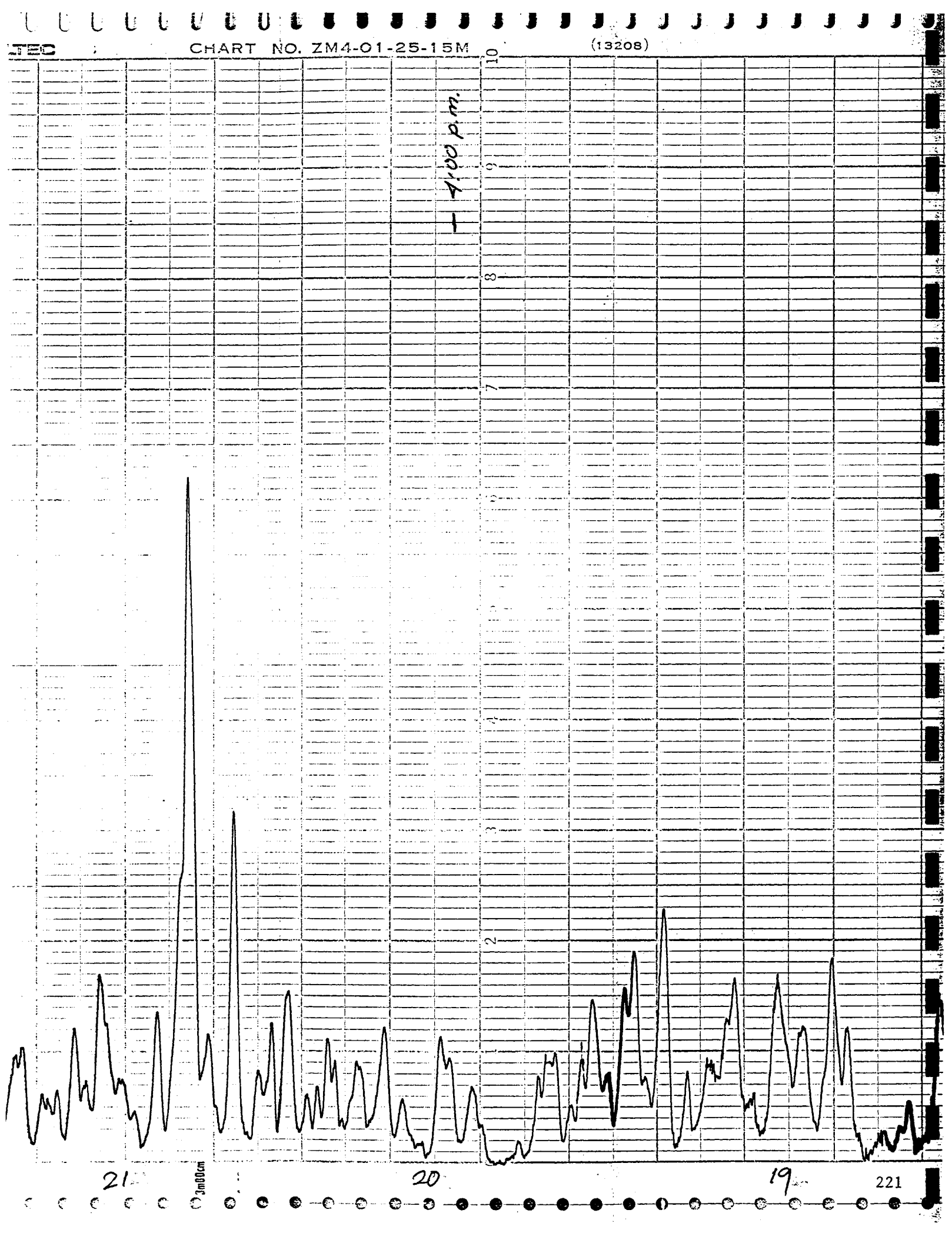

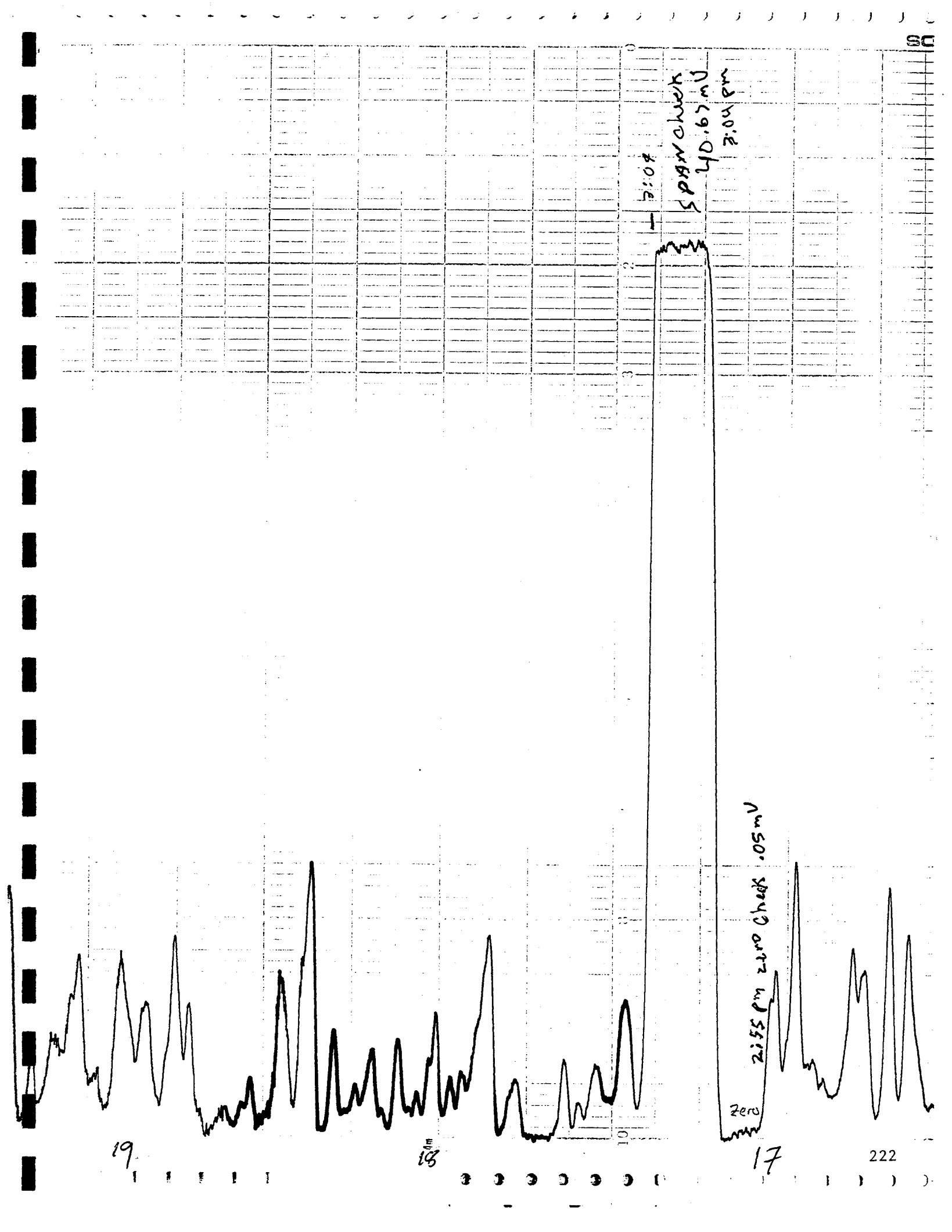
Span check 40.67 mV
3:04 pm
3:04
2:55 pm zero check .05 mV
Zero
19
18
17
222

SOLTEC CHART NO. ZM4-01-25-15M (13208)

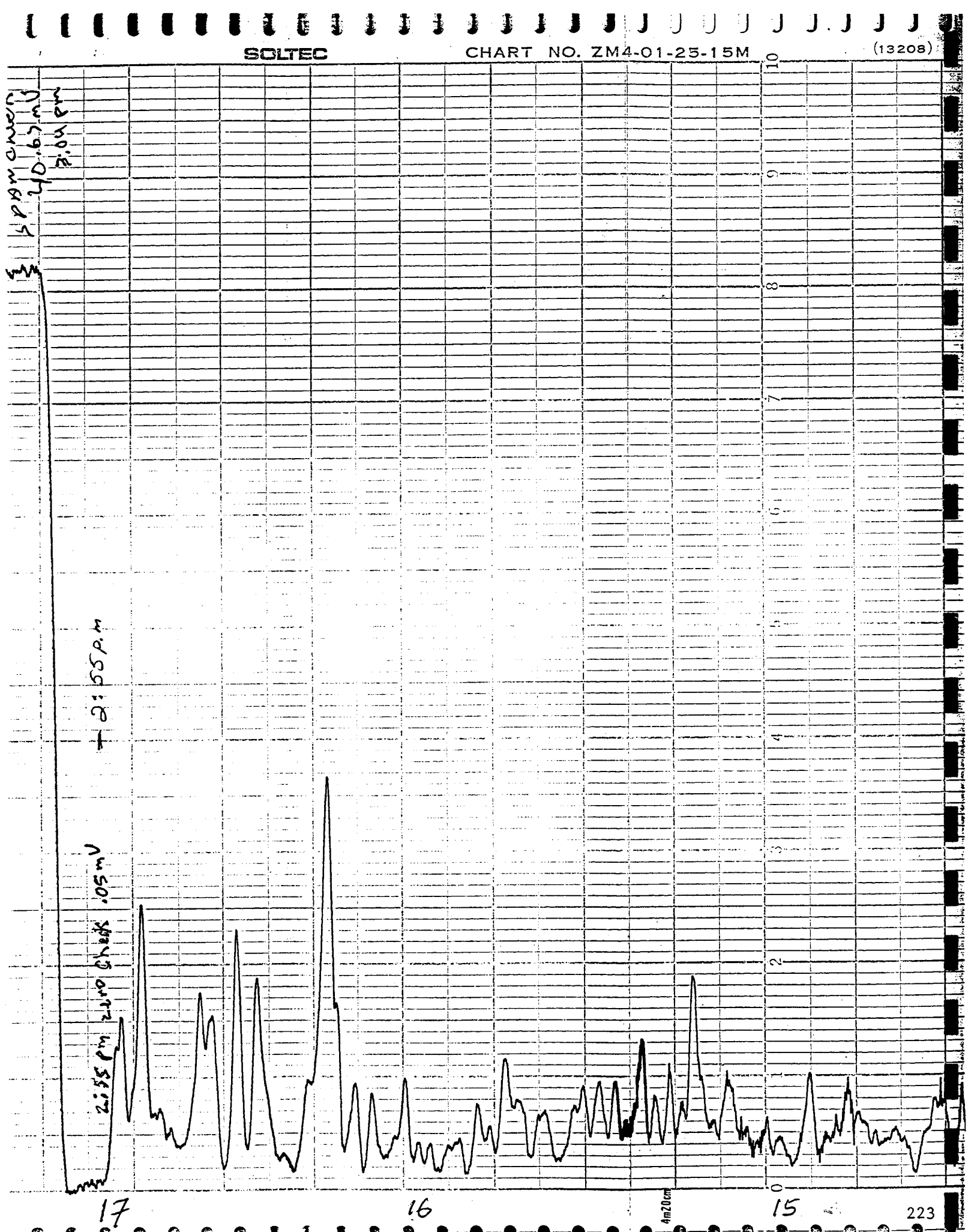

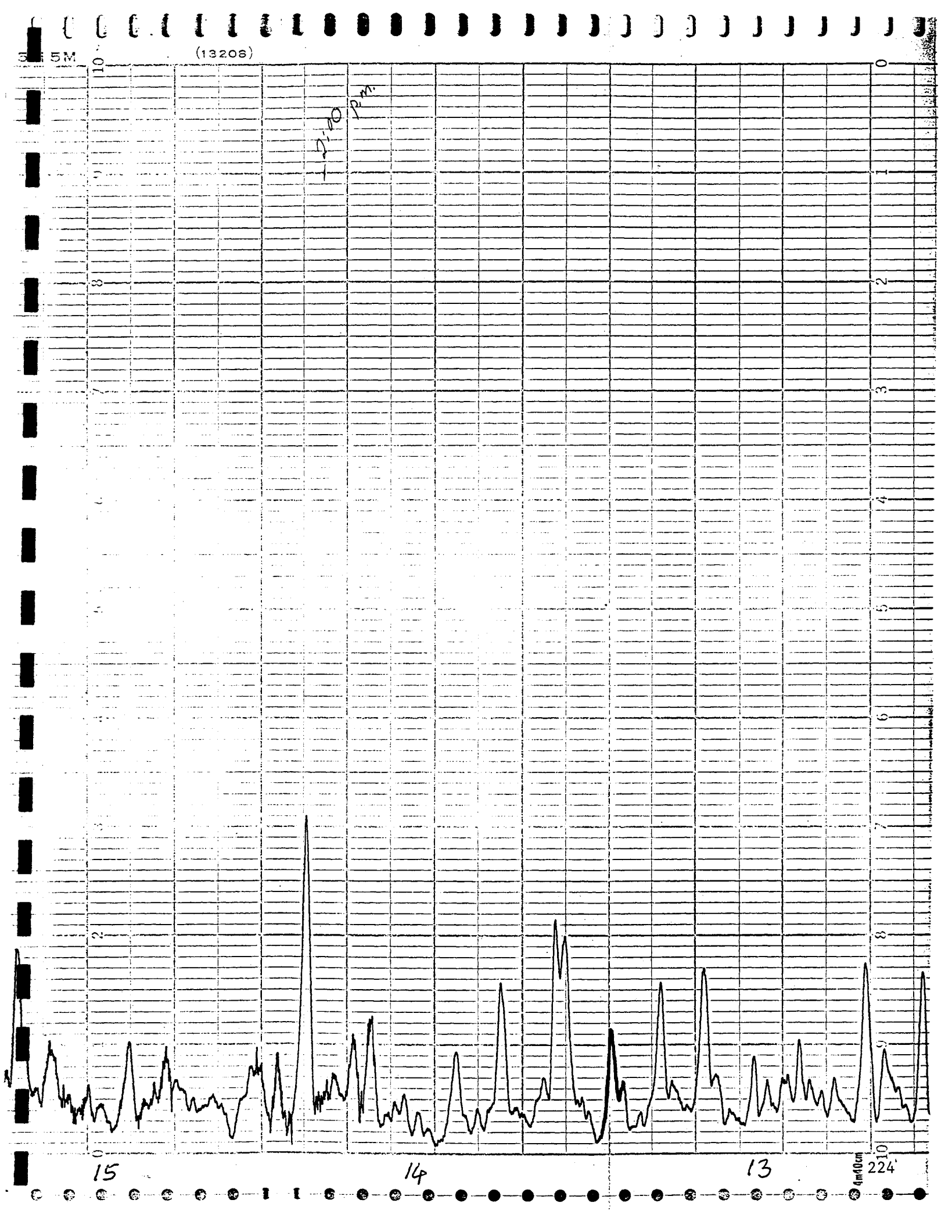
5M
(13208)
1-2:10 p.m.
15
14
13
224
4m10cm

SOLTEC

CHART NO. ZM4-01

11:00 p.m.

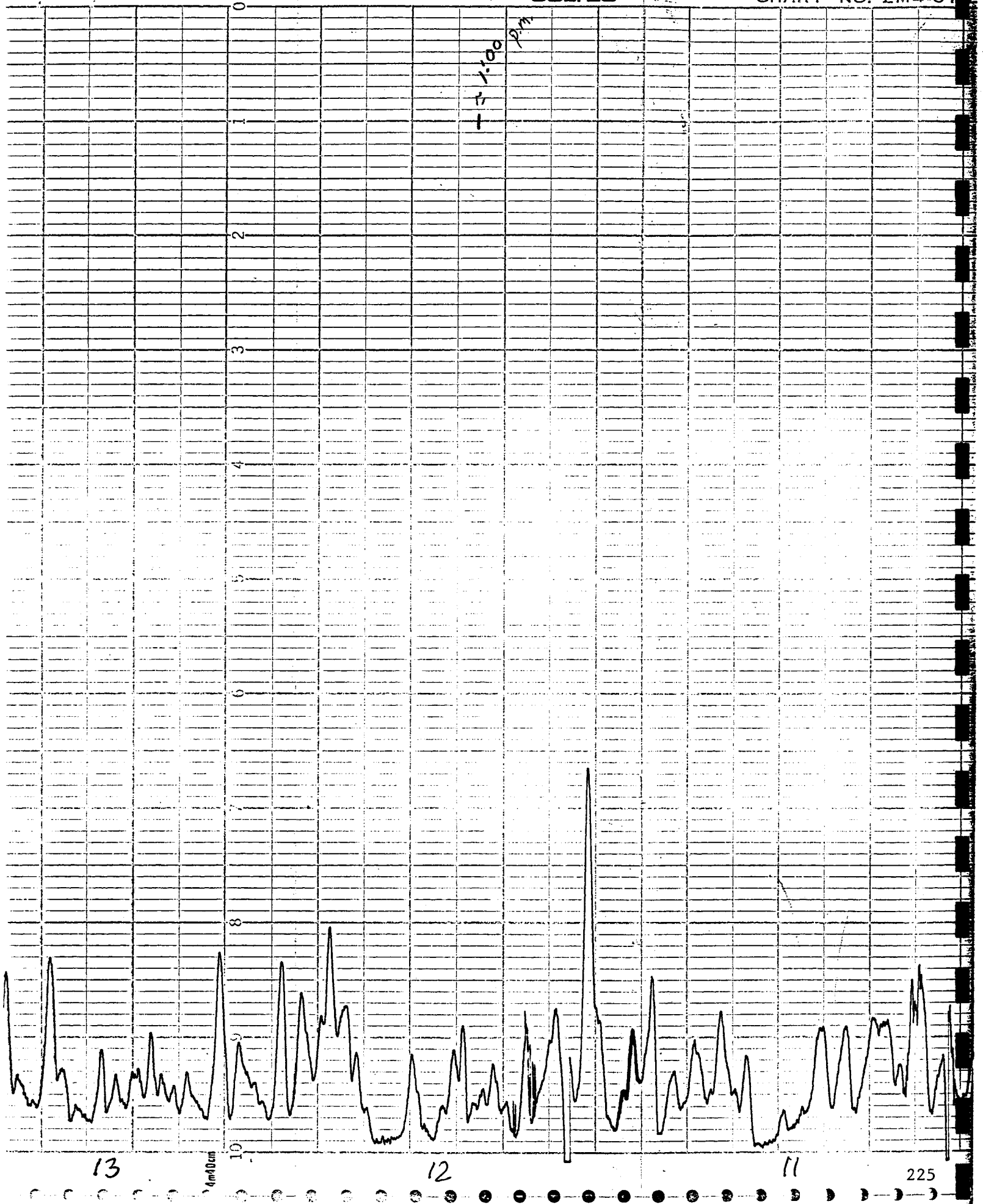

CHART NO. ZM4-01-25-15M (13208)

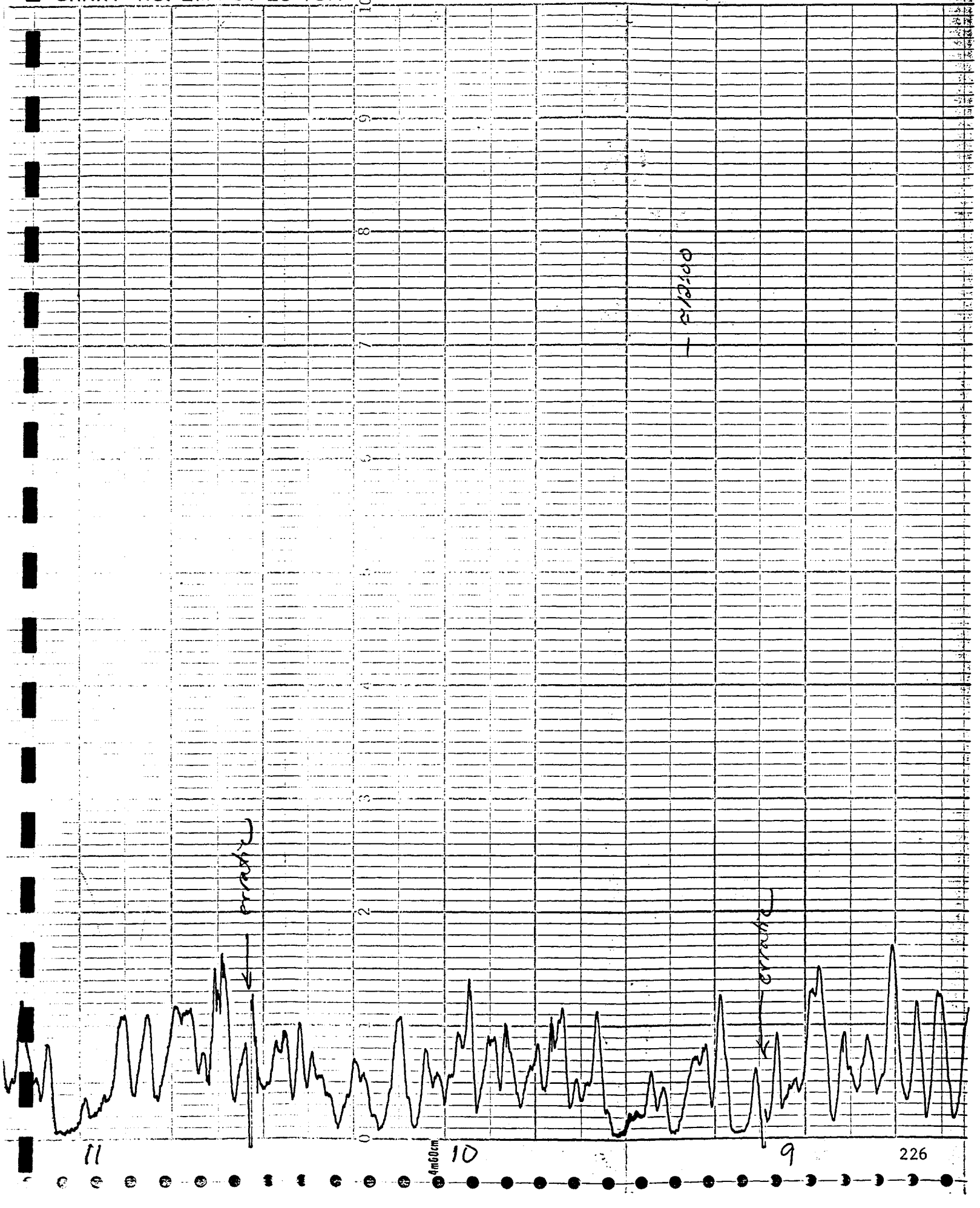

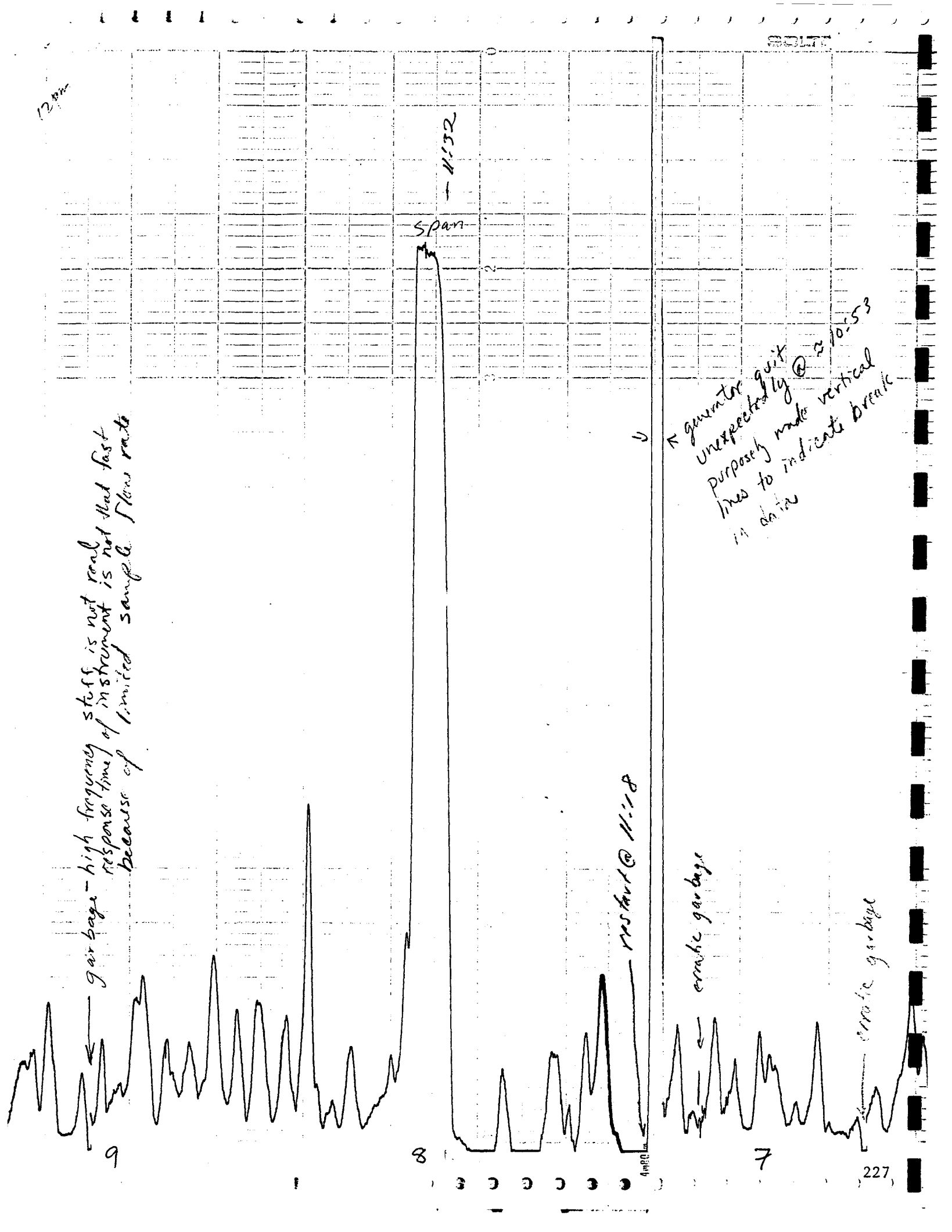
12pm
span
- 11:32
9
8
7
gas bags - high frequency stuff is not real
response time of instrument is not that fast
because of limited sample flow rate
generator quit unexpectedly @ ~ 10:53
purposely made vertical lines to indicate break in data
erratic gas bags
erratic gas bags
227

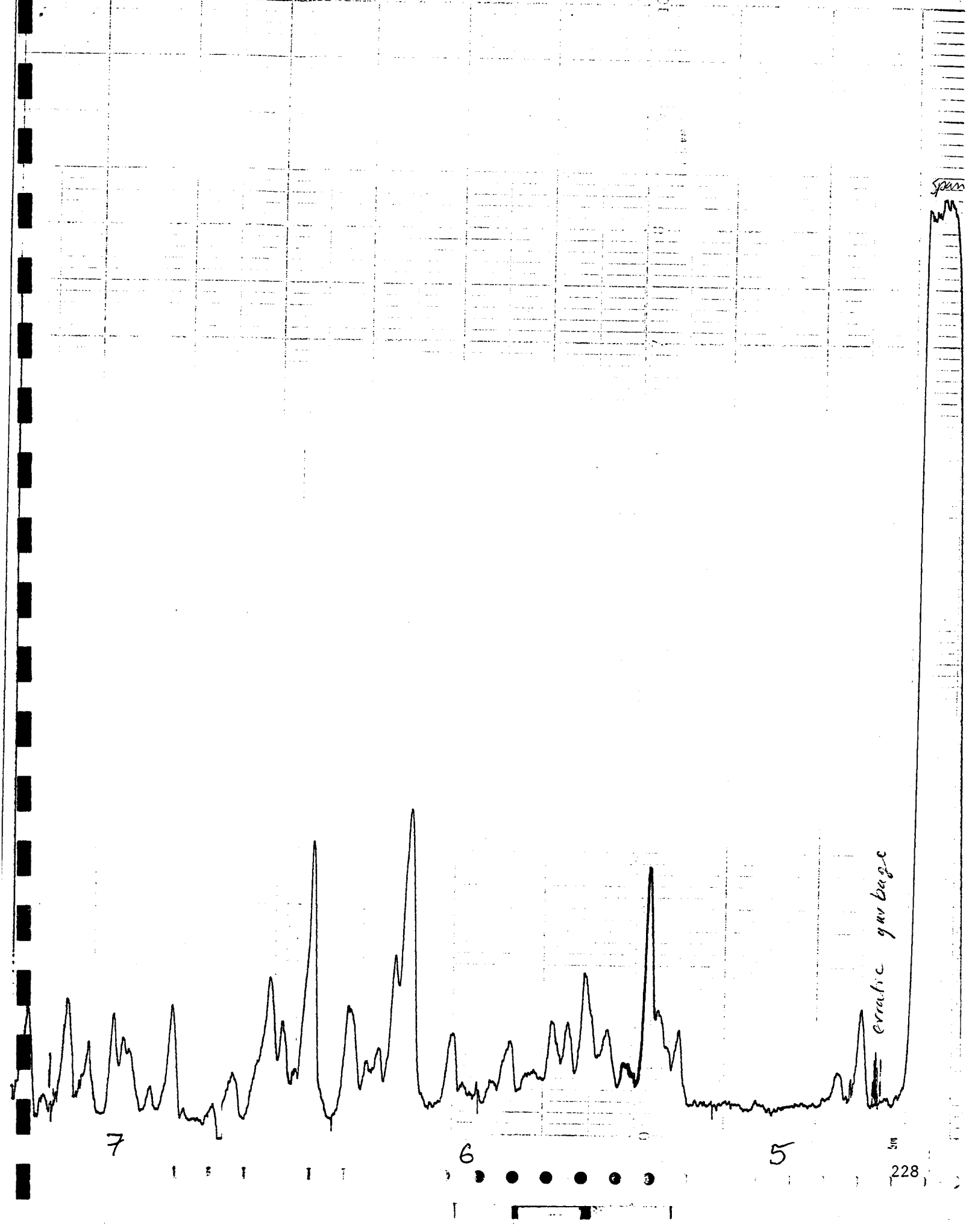
span
erratic gain change
7
6
5
228

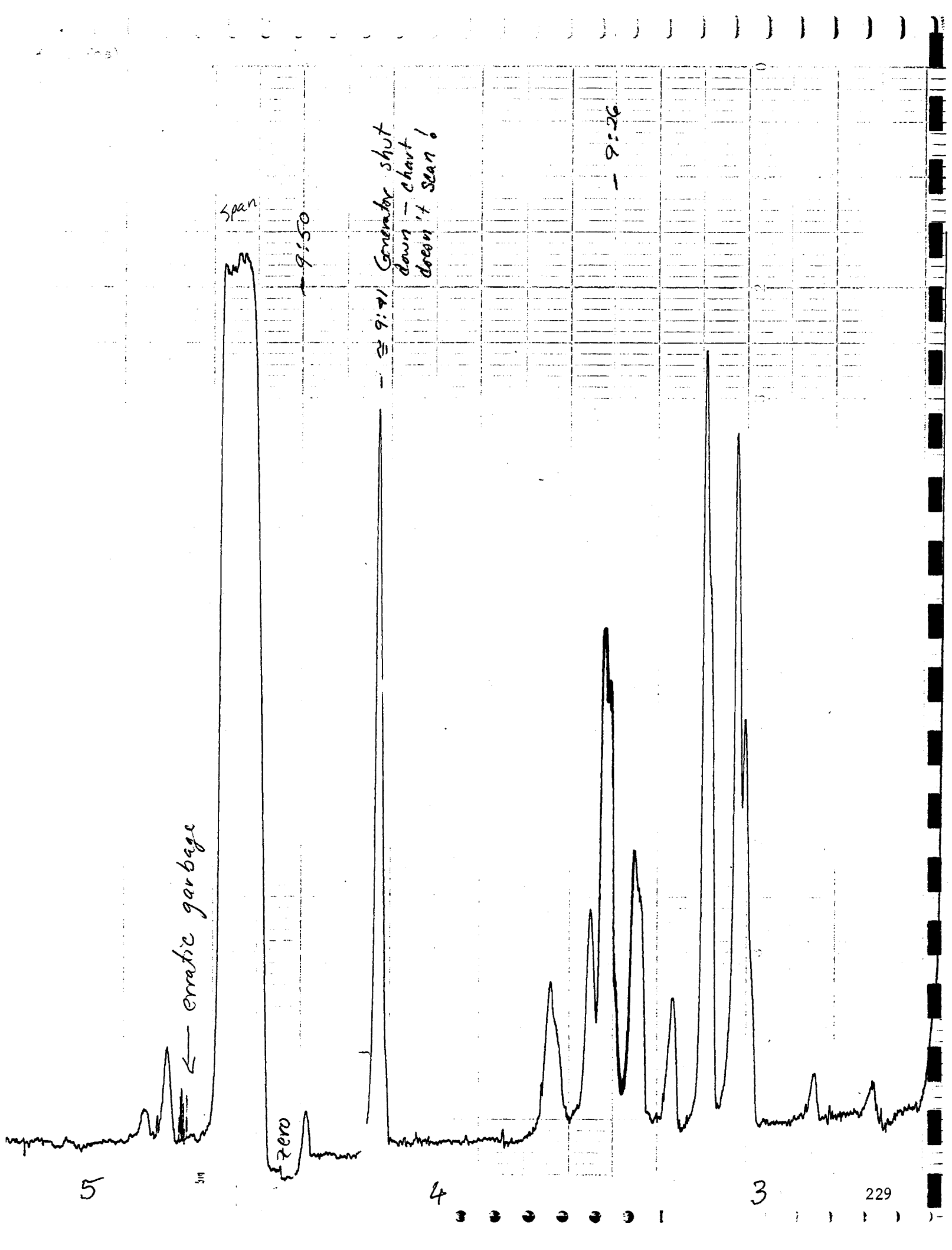
span
9:50
≅ 9:41 Generator shut down - chart drew 1/4 scan!
9:56
← erratic garbage
zero
5
4
3

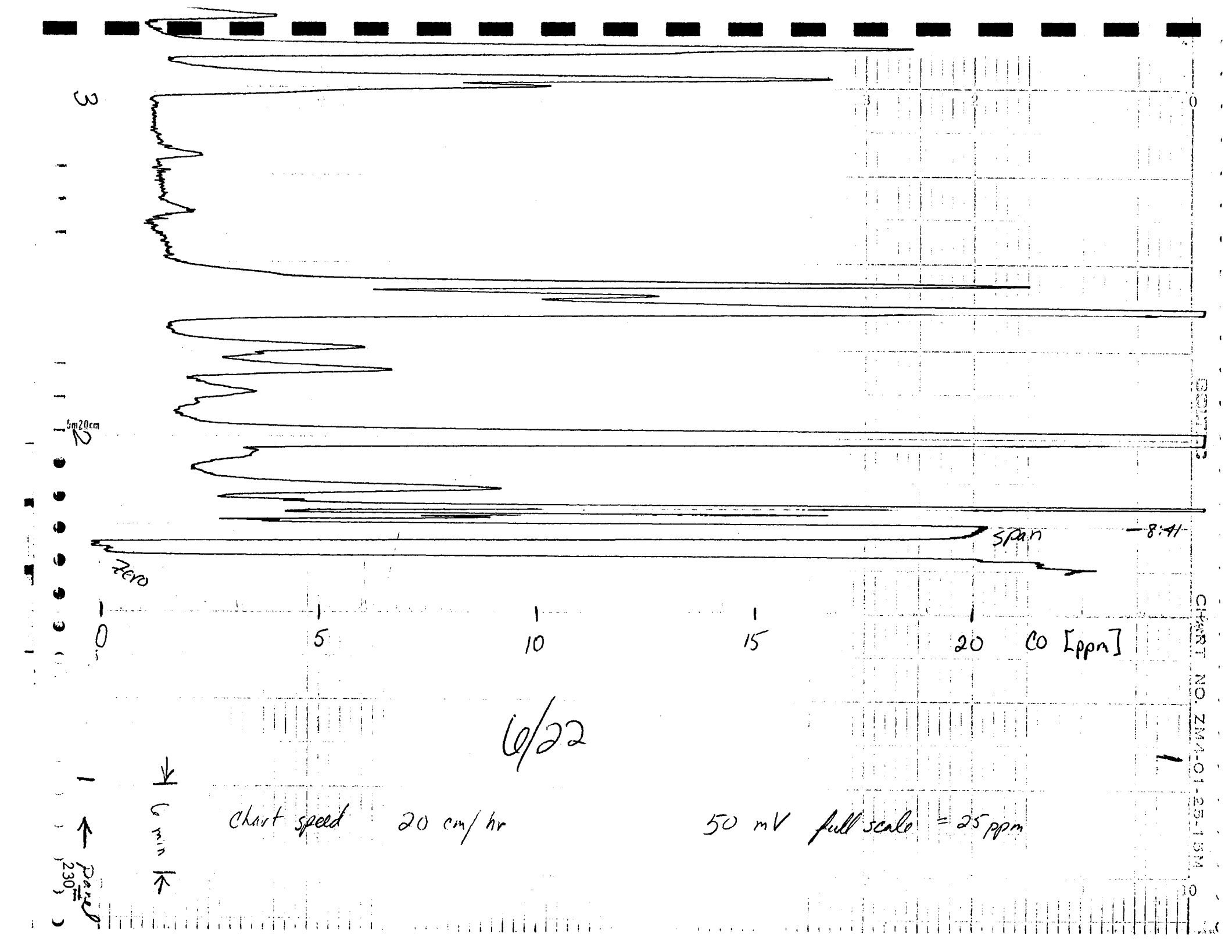
zero
span
8:41
0
5
10
15
20
CO [ppm]
6/22
chart speed 20 cm/hr
50 mV full scale = 25 ppm
6 min
Panel 230
CHART NO. ZM4-01-25-1SM

DASIBI 3003
Friday data 6/23

y-axis : 2.5 ppm / inch

x-axis : 1 hr / 20 cm
(i.e. chart speed
= 20 cm/hr)

CO Monitoring Station here (Equipment are Taken by Local EPA) (6/23/1995)

CO Concentration (ppm)

15 –

10 –

5 –

0 –

← Time

Start 2:10 p.m.

Peak 2:40 p.m.

Panel # → 25 24 23

1m 20cm

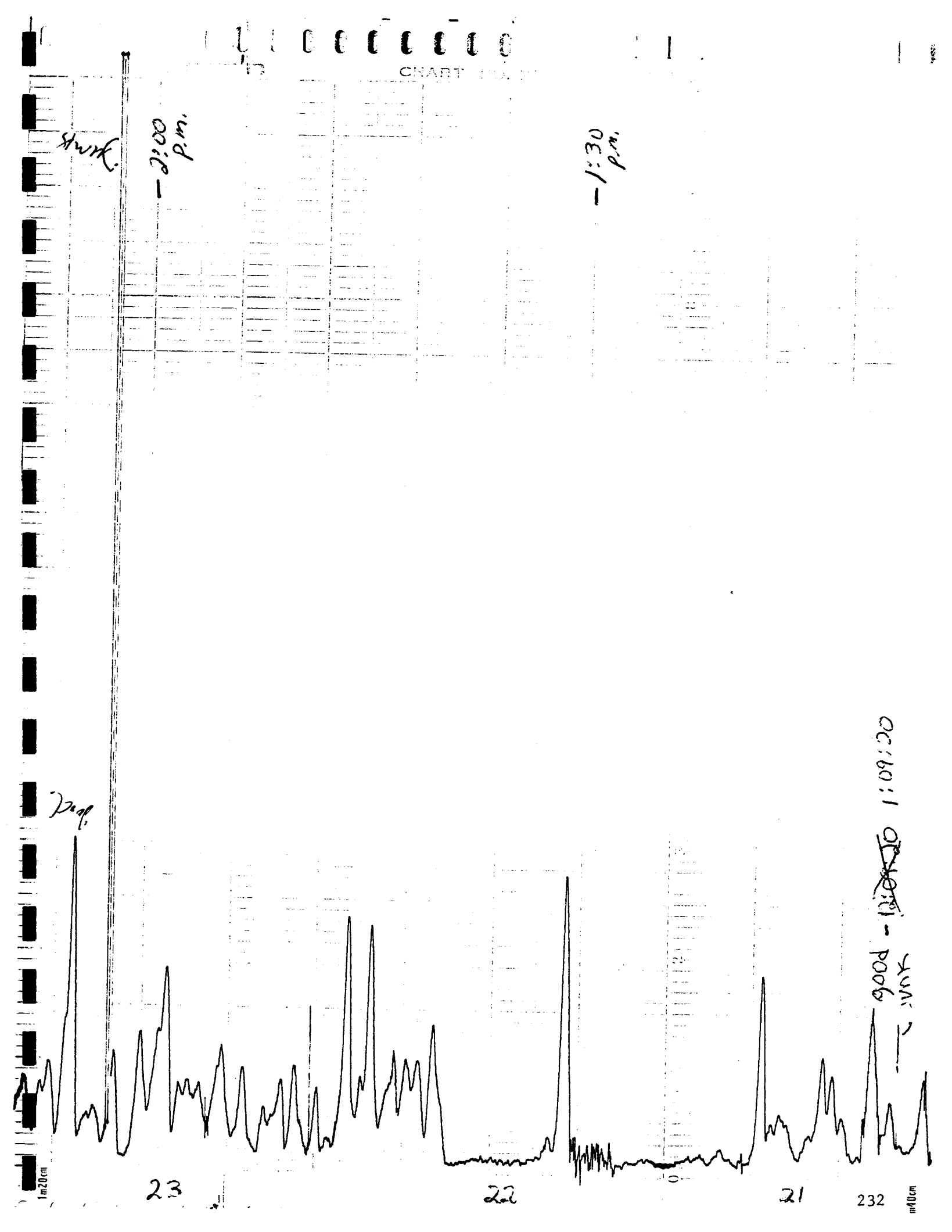
Start. - 2:00 p.m.
- 1:30 p.m.
Dep.
good - [illegible] 1:09:20
23
22
21
232

(12208)

End 08:11

Junk

Junk

Good - 12:08:30

12:23

12:32

12 N 30 p.m.

21

20

19

1m=40cm

233

SOLTEC CHART NO. ZM1-01-25-15M

12:30 p.m.

1:00 p.m.

12:32 p.m.

Erratic

Erratic

Erratic

Erratic

Erratic

Erratic

19 18 17

1mGOcm

234

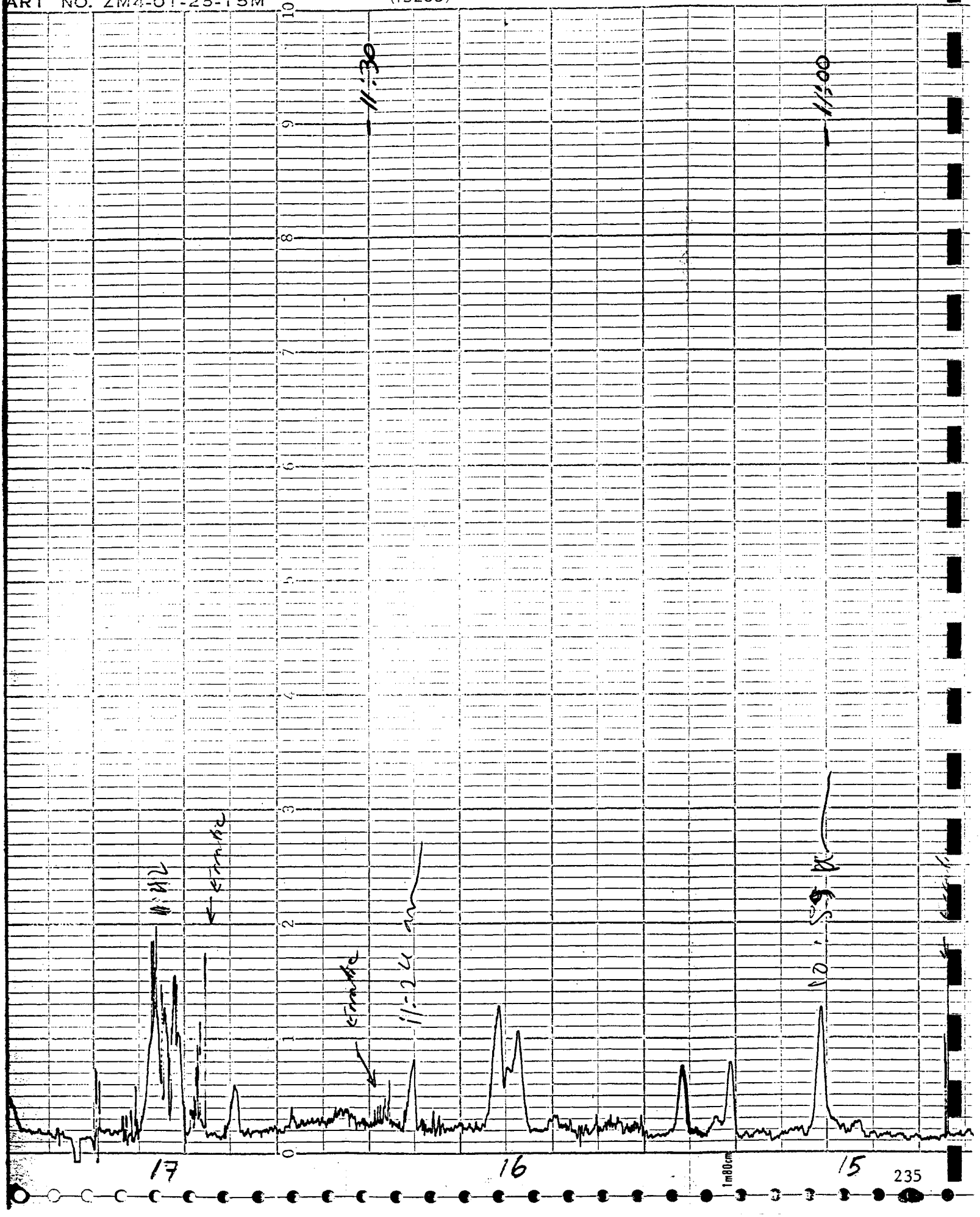
11:30
11:00
11:27 mm
17
16
15
1m80cm
235

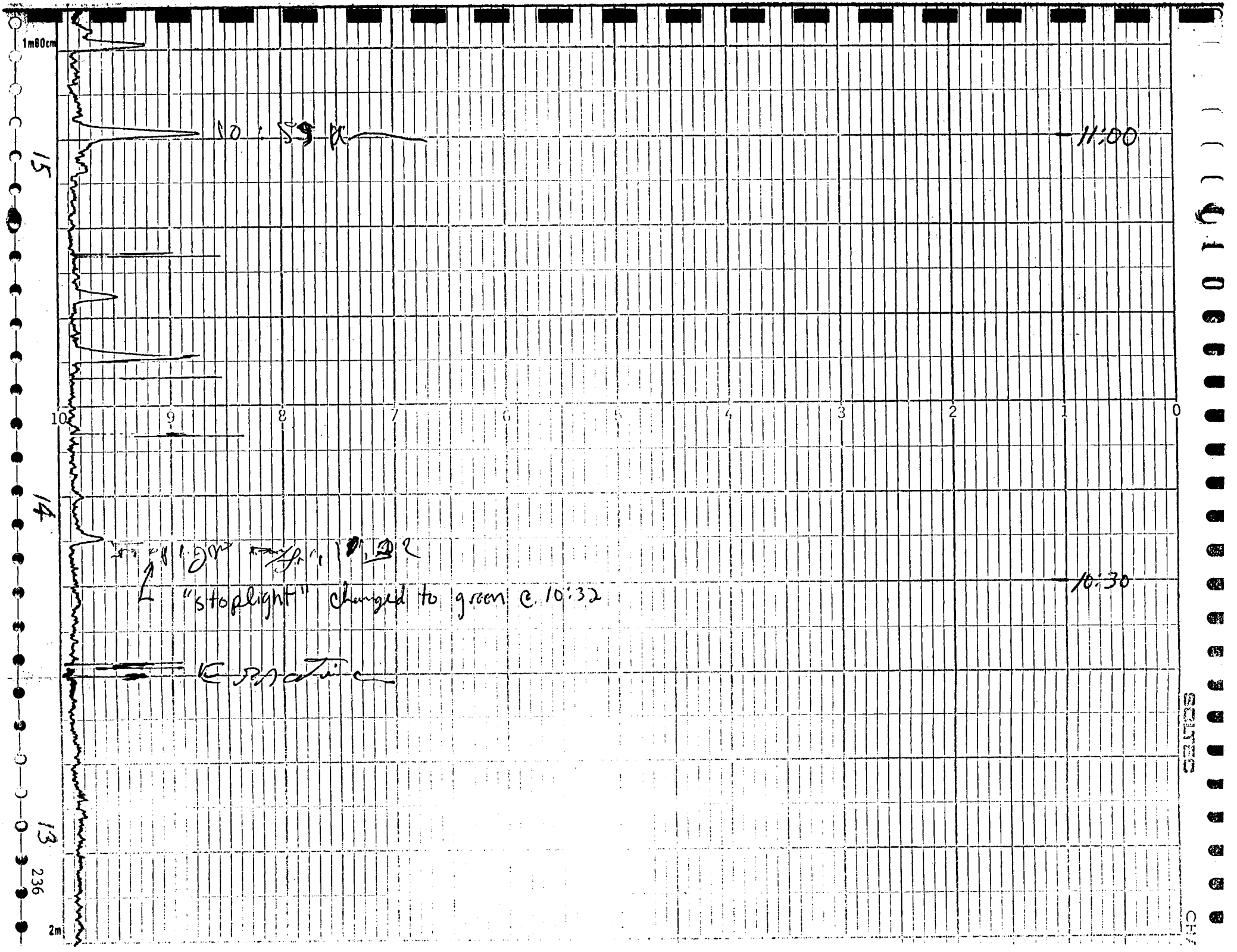
1m80cm
15
14
13
2m
236
10
9
8
7
6
5
4
3
2
1
0
11:00
10:30
"stoplight" changed to green @ 10:32
CH

SOLTEC CHART NO. ZM4-01-25-15M (13208)

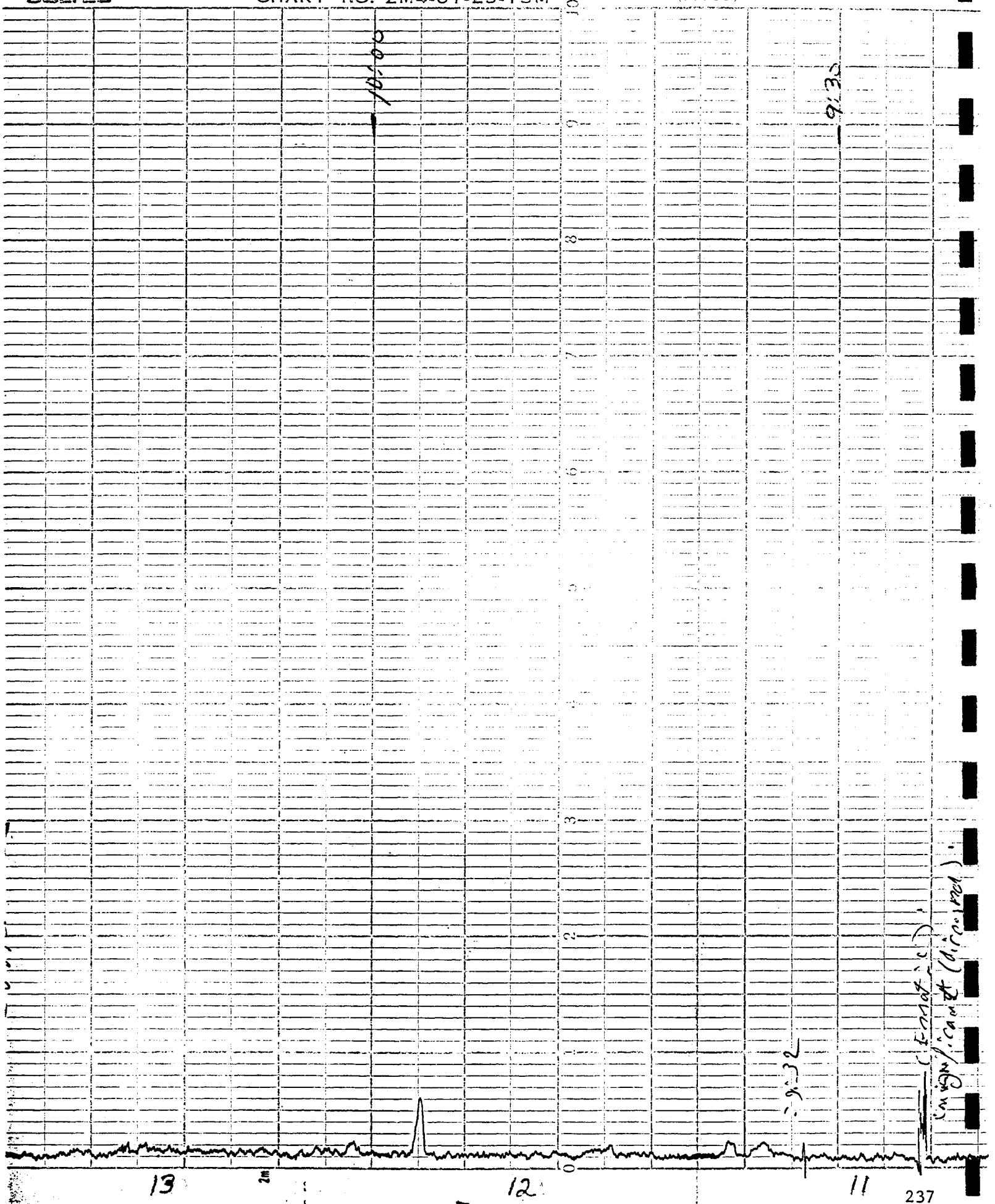

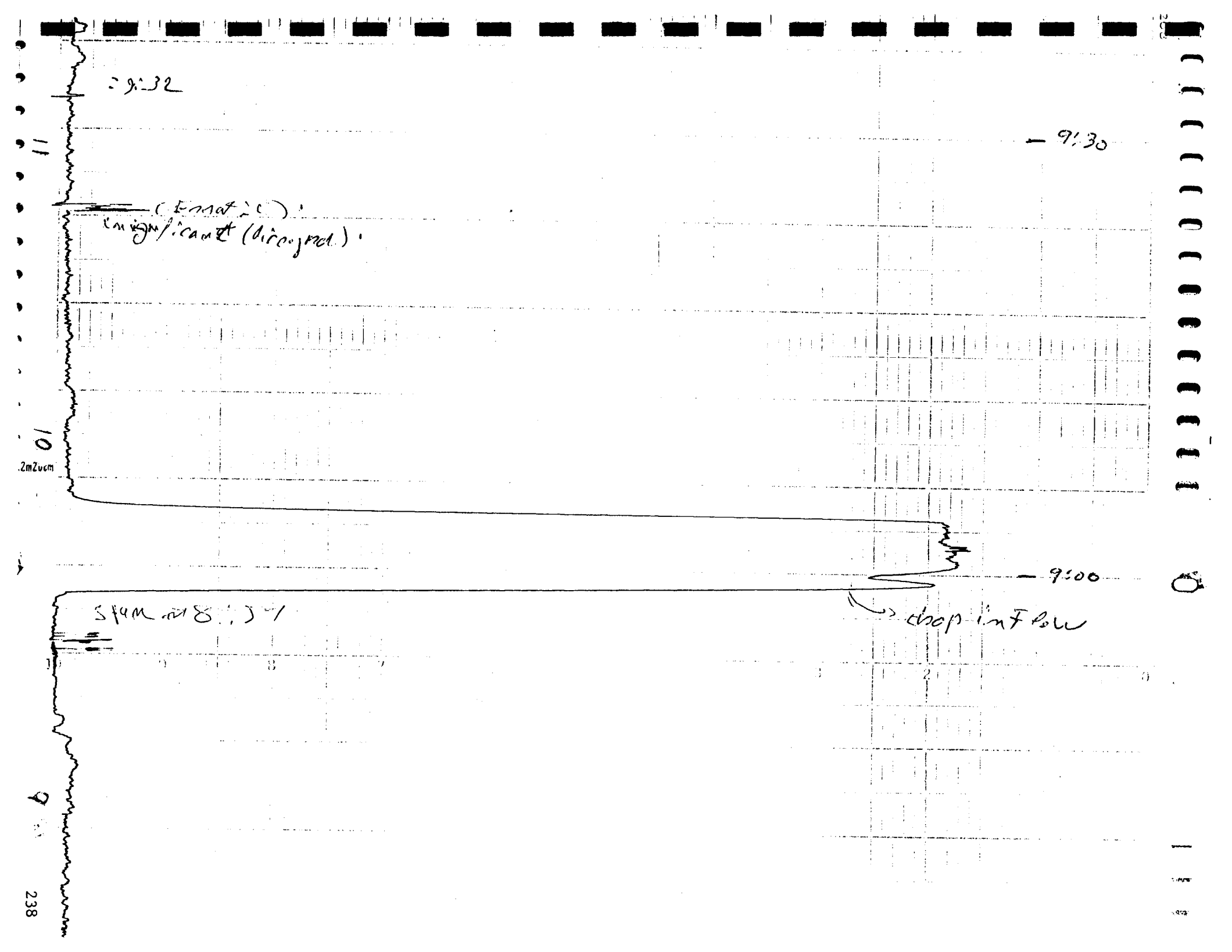
9:32
9:30
(transient)
insignificant (diverged)
9:00
drop in flow

8:30

8:00

Médiane déviation ed Ce segment. (8:35)

9

8

7

2mV/0cm

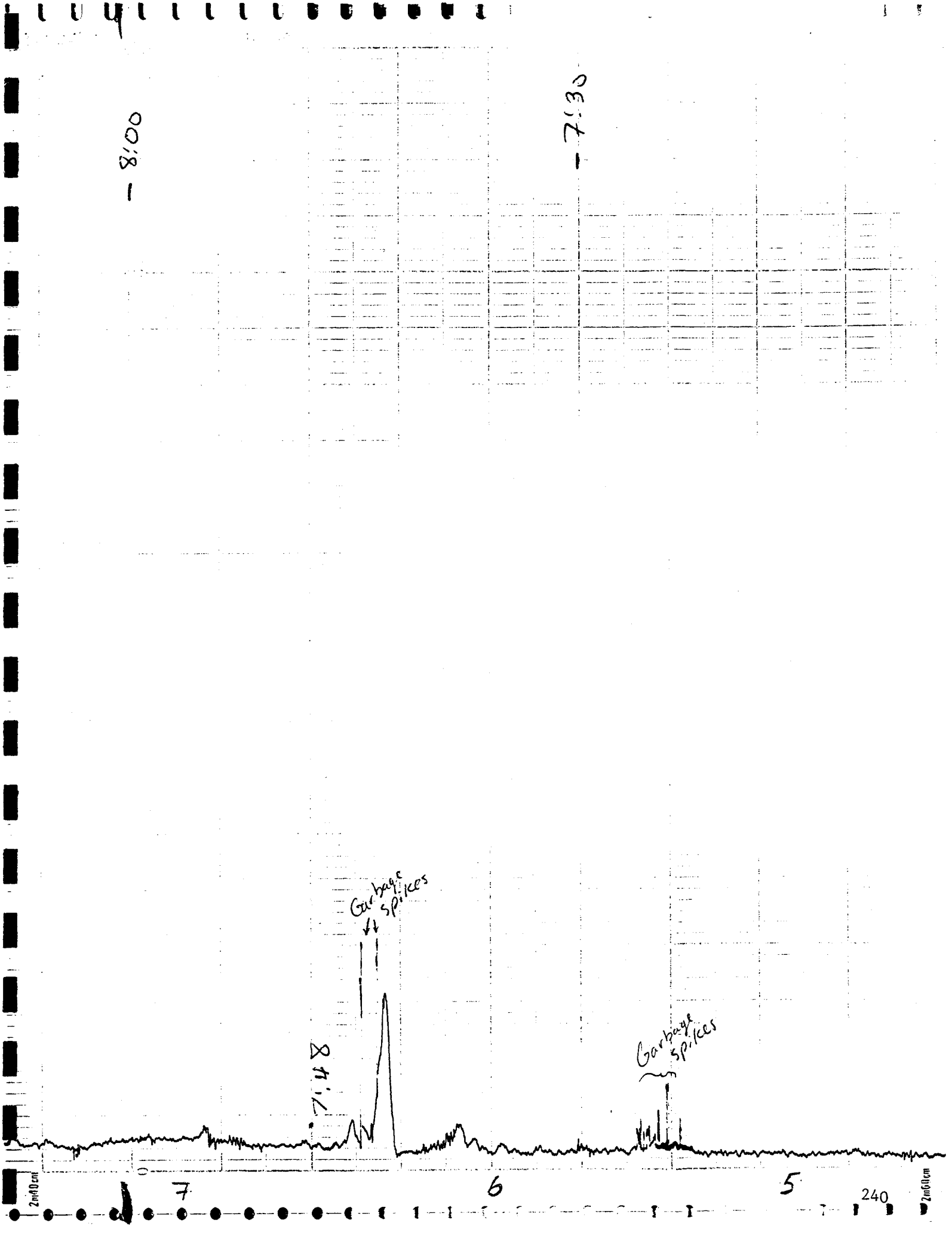
8:00
7:30
Garbage spikes
8:11
Garbage spikes
7
6
5
240

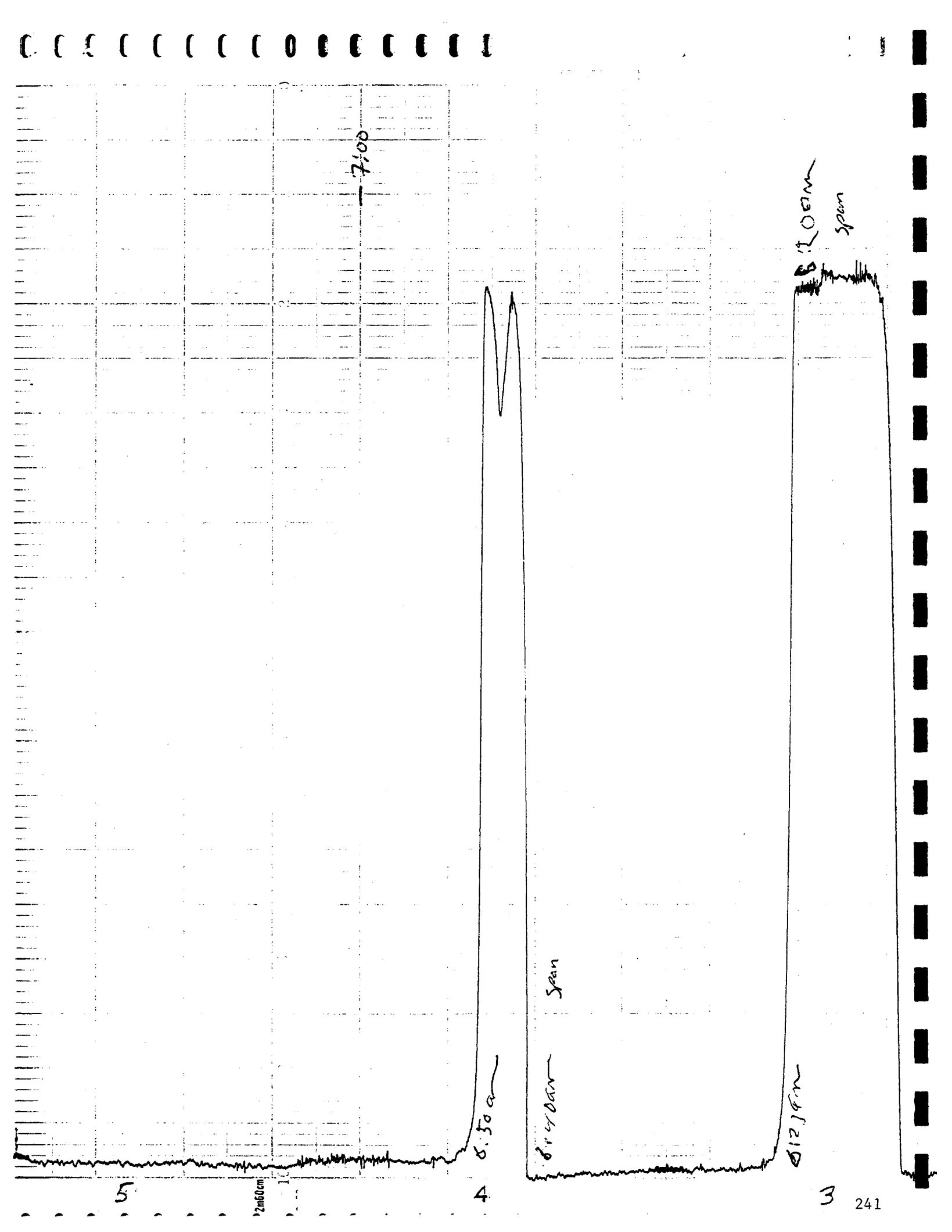
7:00
8:50 a
Span
8:49 am
8:12 am
9:10 am
Span
5
4
3
2m60cm

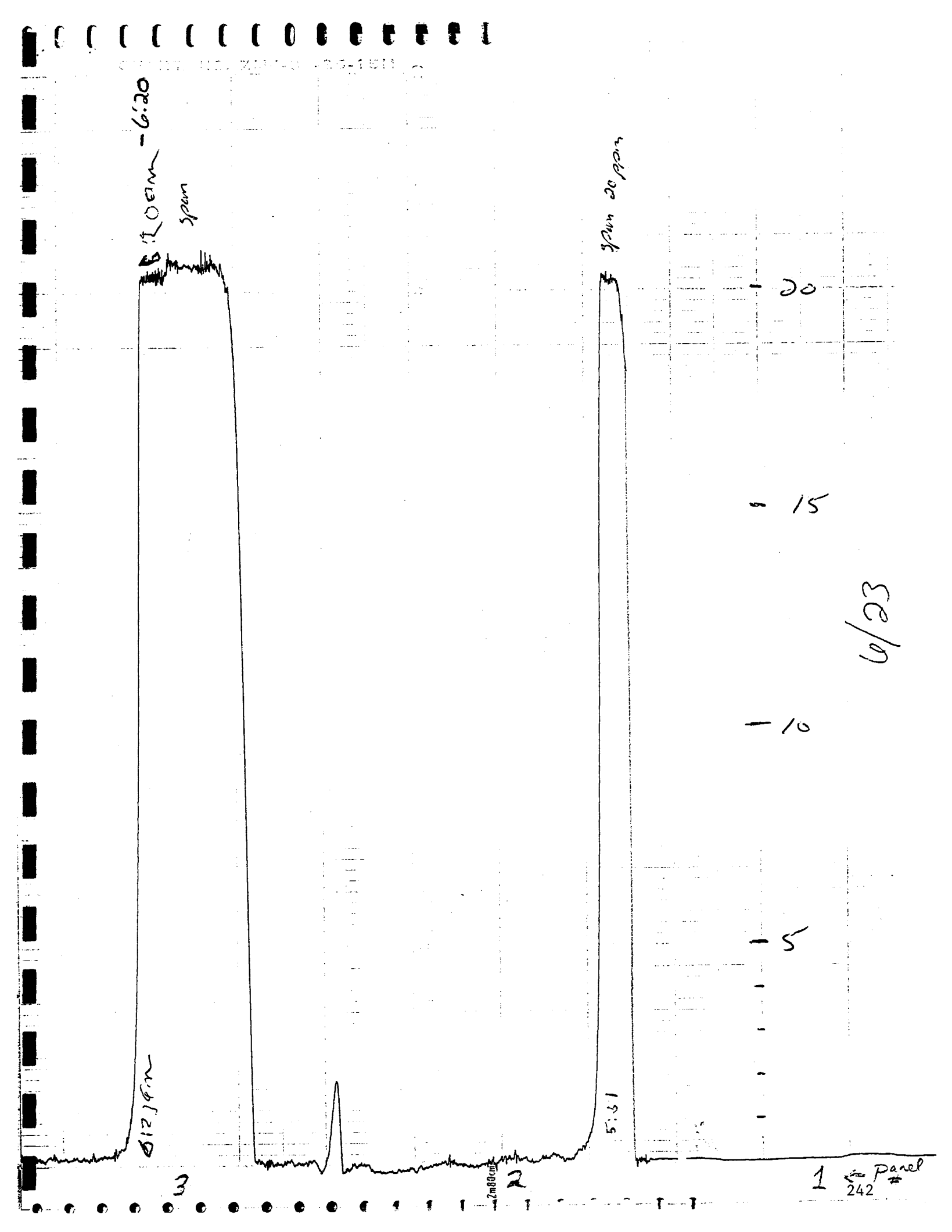
6:20
span
span 20 span
20
15
10
5
6/23
3
2
1
Panel
242

APPENDIX E: DISTANCE-TIME IMAGES OF ALBUQUERQUE LIDAR SIGNAL

Much additional information is available if the lidar signal along the entire beam path is plotted as a function of time, rather than just the lidar signal at a single point. An illustration of this can be seen by comparing the impressions one gets from Fig. 21 versus Fig. 18, as well as Figs. 31-33 versus Fig. 28. In fact, the spatio-temporal distribution helped us to recognize the sprinkler and tire spinning events discussed in the text. The false color plots in this appendix were prepared by Bill Eichinger from the lidar data taken on Friday, 6/23/95, in Albuquerque, NM. They were referred to as time domain, or TD plots, by the lidar operators. Similar images were available on the lidar system computer during the test.

The absolute magnitude of the lidar signal is an arbitrary scale, so one can ignore the exponents and concentrate on the relative changes in signal level. The time axis shows elapsed time (in seconds) after the starting time stamp (24 hour format) shown in the upper right of each plot. The range profile plotted for each time represents the average of 100 individual laser pulses, each of which is about 10 ns long and occur at a repetition frequency of 50 Hz. Thus, the lidar data plotted is really a 2 second average range profile stepped in time over a total elapsed time of approximately 20 minutes. The data starts at a distance of 50 m from the laser as determined by the minimum digitizer delay after the laser fires. The signal saturates at a distance of about 400 m where the beam hits a tree (purposely used as a beam stop).

The azimuth and elevation angles are also indicated in the legend at the upper left. These document the direction of the laser beam relative to a fixed axis of the laser mount. The laser beam direction was changed very slightly just after 11:00 a.m. in order to bring it slightly closer to the aerosol sampling inlet. The change in beam direction is so small that it has negligible effect over the short range of distance spanned by the data.

The raw data have been corrected using the standard r-squared correction factor as indicated in the color bar. This correction is used to account for the decreasing solid angle collected by the receiver as the distance increases (see App. A). Barring local changes in aerosol concentrations, one would expect to see regions of the plot wherein little variation in color (*i.e.* particle concentrations) occurred with increasing range. In fact, however, the r-squared correction appears to have over-corrected the data, as the images uniformly show corrected signal

levels which generally increase with range. The explanation is that this data was acquired from distances very close to the laser. This is a non-standard operating mode, and in fact an additional correction factor would be required to account for how the telescope and laser beam axes intersect. This is a difficult correction factor to predict analytically, and so the data was left as shown. An estimate could be obtained by using a sequence of profiles which show very little change over periods of several minutes. These most likely correspond to instances of relatively uniform particle concentration, or else we would expect the profiles to change with the motion of the wind.

Concentrated local sources of particle emissions generate plumes which disperse in the wind. These plumes are visible on the plots as local maxima which may progress to shorter or longer ranges as time increases depending on whether the wind has a component blowing toward or away from the laser, respectively. In fact, the progression of the plume gives an idea of the magnitude of the component of the wind in the direction of the beam path. One must keep in mind that the data is one-dimensional in space, and represents only a single line profile through the plume at a constant elevation above the roadway in a particular direction. Hence, one is far from assured that the data plotted includes the local maximum concentration of the plume, but one can at least get a general sense for the strength of the plume and its dispersion rate. However, from these images, one can imagine how the method could be extended to determine wind velocities and dispersion rates if one were to have three-dimensional lidar data taken over time. The caveat is that the wind data would only be available with a resolution corresponding to the presence of discernible plume features.

The golf course sprinkler event appears as the very widespread and long duration signal saturation which begins at about 7:20 a.m. This is discussed at some length in the text. There is also apparently some interference from tree branches swaying in the wind which appears around 1:35 p.m. (13:35) at a distance of about 100 m, and again several times later. The give away is that the position of the signal does not change with time, and there is no indication of plume dispersion. Data for distances beyond obstructions, as well as for times shortly after the obstruction appears, should be disregarded, since the amplifier requires time to recover after the overrange signal condition occurs.

The one-dimensional time domain plots shown here were used by the Los Alamos scientists to monitor the performance of the system during the tests. The increase in information content relative to time histories of data from individual points should be obvious after reading the text. Still greater advantages could be obtained if the two- and three-dimensional scan renderings could be generated in real time during the test. These would allow much greater confidence in the accuracy of the data to be established while there was still time to make positioning corrections, if necessary. An overlay of such data onto a GPS grid would complete the picture. This represents the best, albeit fairly costly, way of establishing ground-truth locations during the test, as needed for comparison with other measurements.

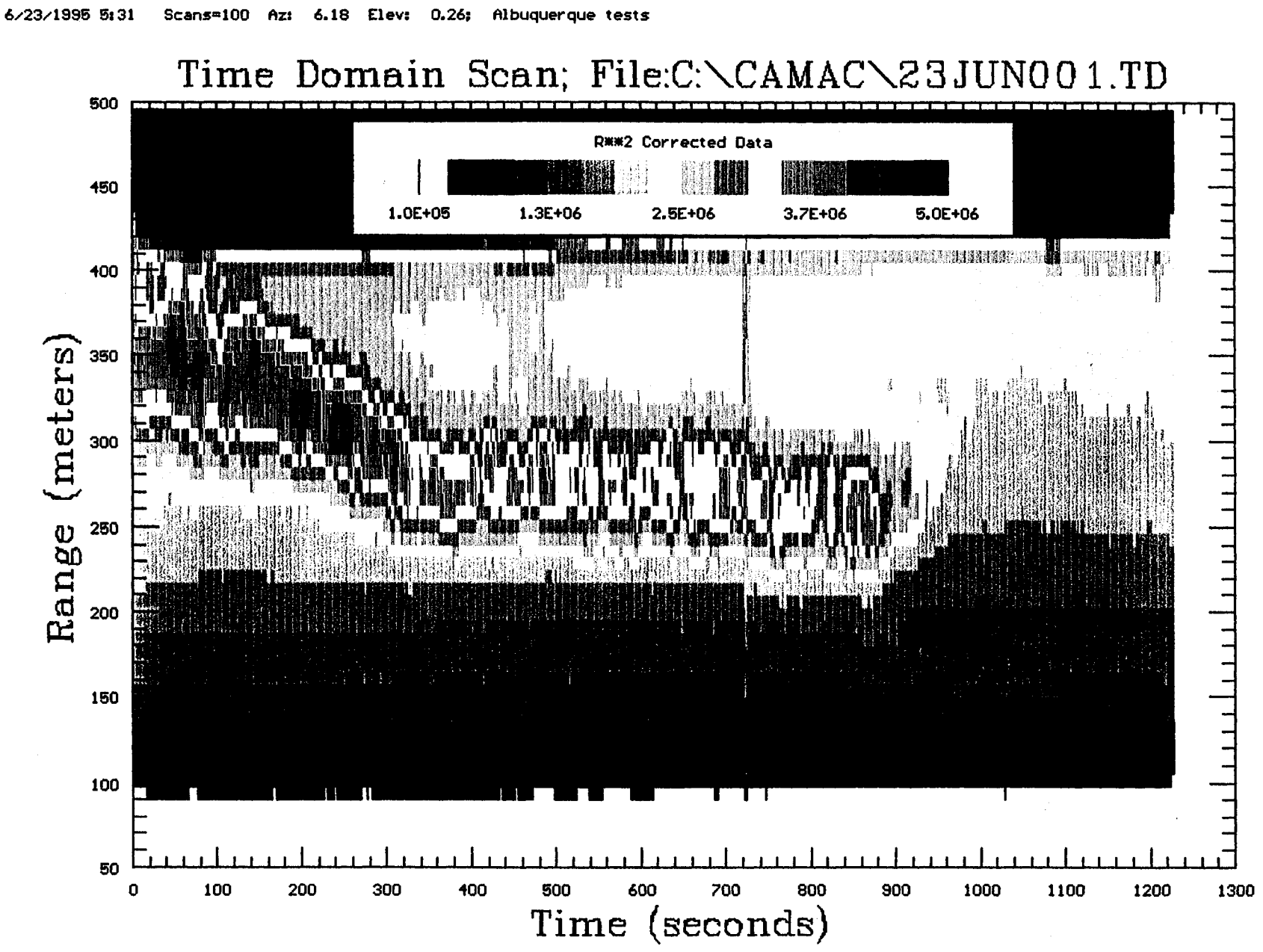
6/23/1995 5:31 Scans=100 Az: 6.18 Elev: 0.26; Albuquerque tests
Time Domain Scan; File:C:\CAMAC\23JUN001.TD
R**2 Corrected Data
1.0E+05
1.3E+06
2.5E+06
3.7E+06
5.0E+06
Range (meters)
500
450
400
350
300
250
200
150
100
50
0
100
200
300
400
500
600
700
800
900
1000
1100
1200
1300
Time (seconds)

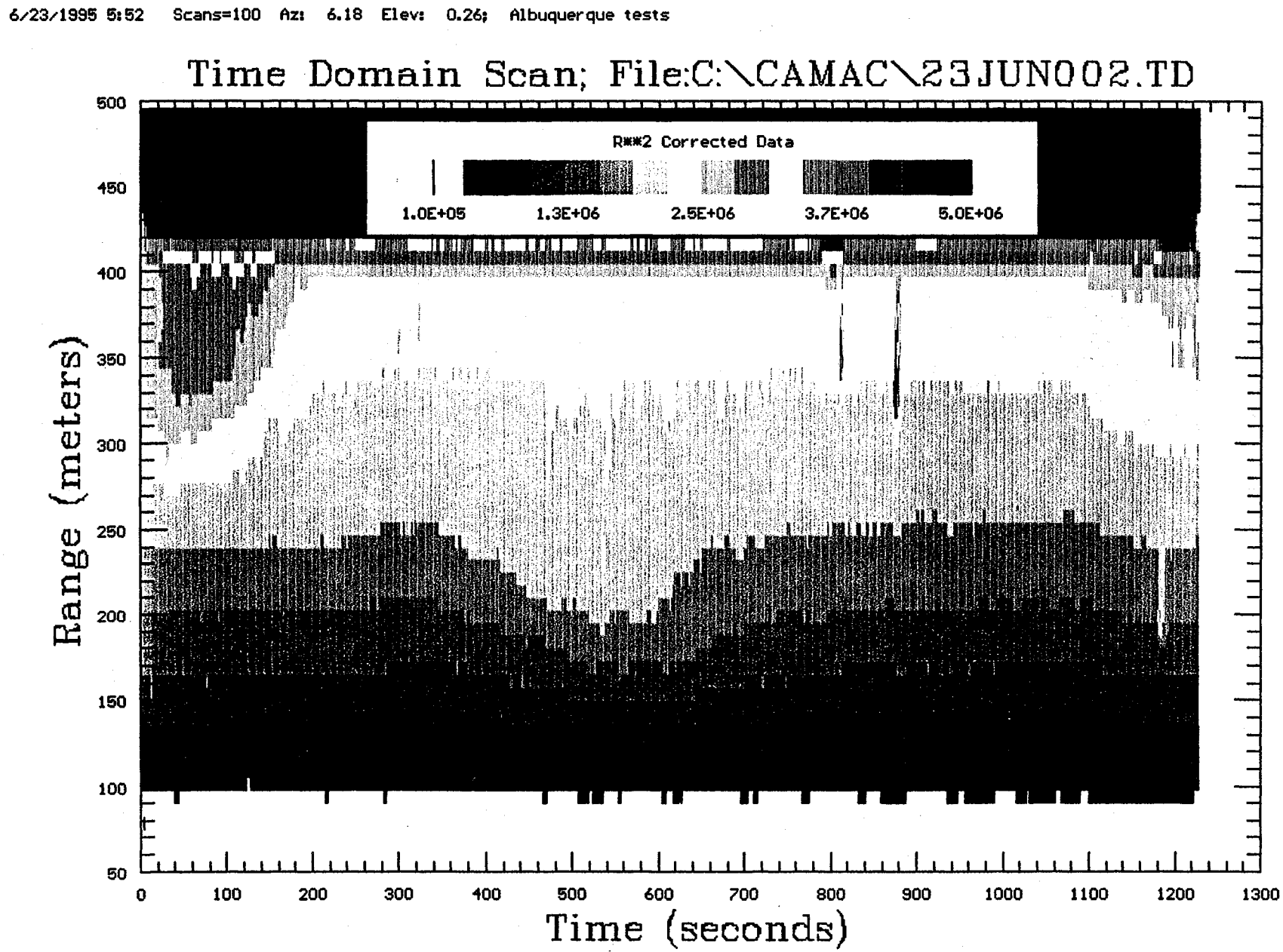
6/23/1995 5:52 Scans=100 Az: 6.18 Elev: 0.26; Albuquerque tests
Time Domain Scan; File:C:\CAMAC\23JUN002.TD
R**2 Corrected Data
1.0E+05
1.3E+06
2.5E+06
3.7E+06
5.0E+06
Range (meters)
Time (seconds)
500
450
400
350
300
250
200
150
100
50
0
100
200
300
400
500
600
700
800
900
1000
1100
1200
1300

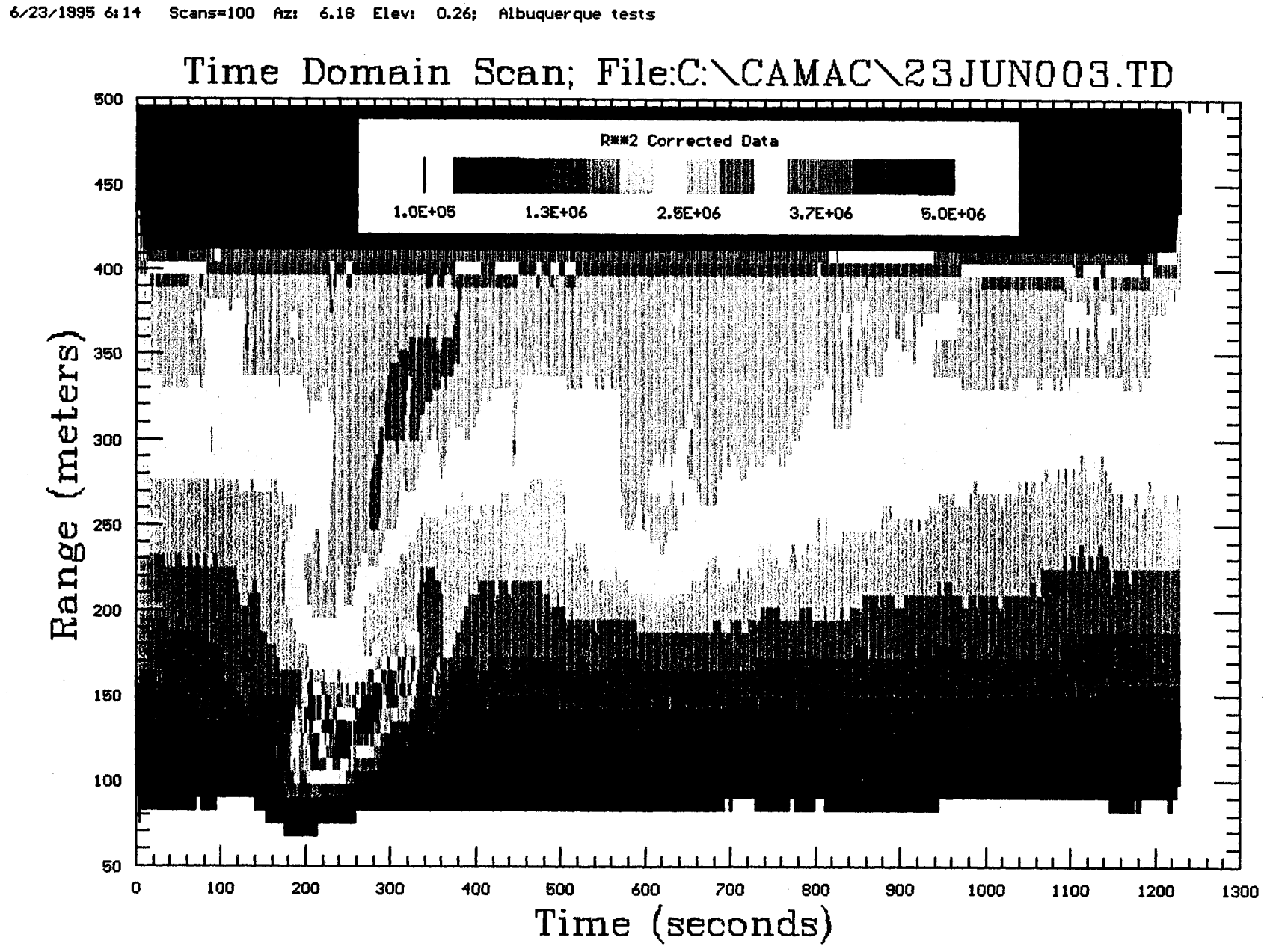
6/23/1995 6:14 Scans=100 Az: 6.18 Elev: 0.26; Albuquerque tests
Time Domain Scan; File:C:\CAMAC\23JUN003.TD
R**2 Corrected Data
1.0E+05
1.3E+06
2.5E+06
3.7E+06
5.0E+06
Range (meters)
500
450
400
350
300
250
200
150
100
50
0
100
200
300
400
500
600
700
800
900
1000
1100
1200
1300
Time (seconds)

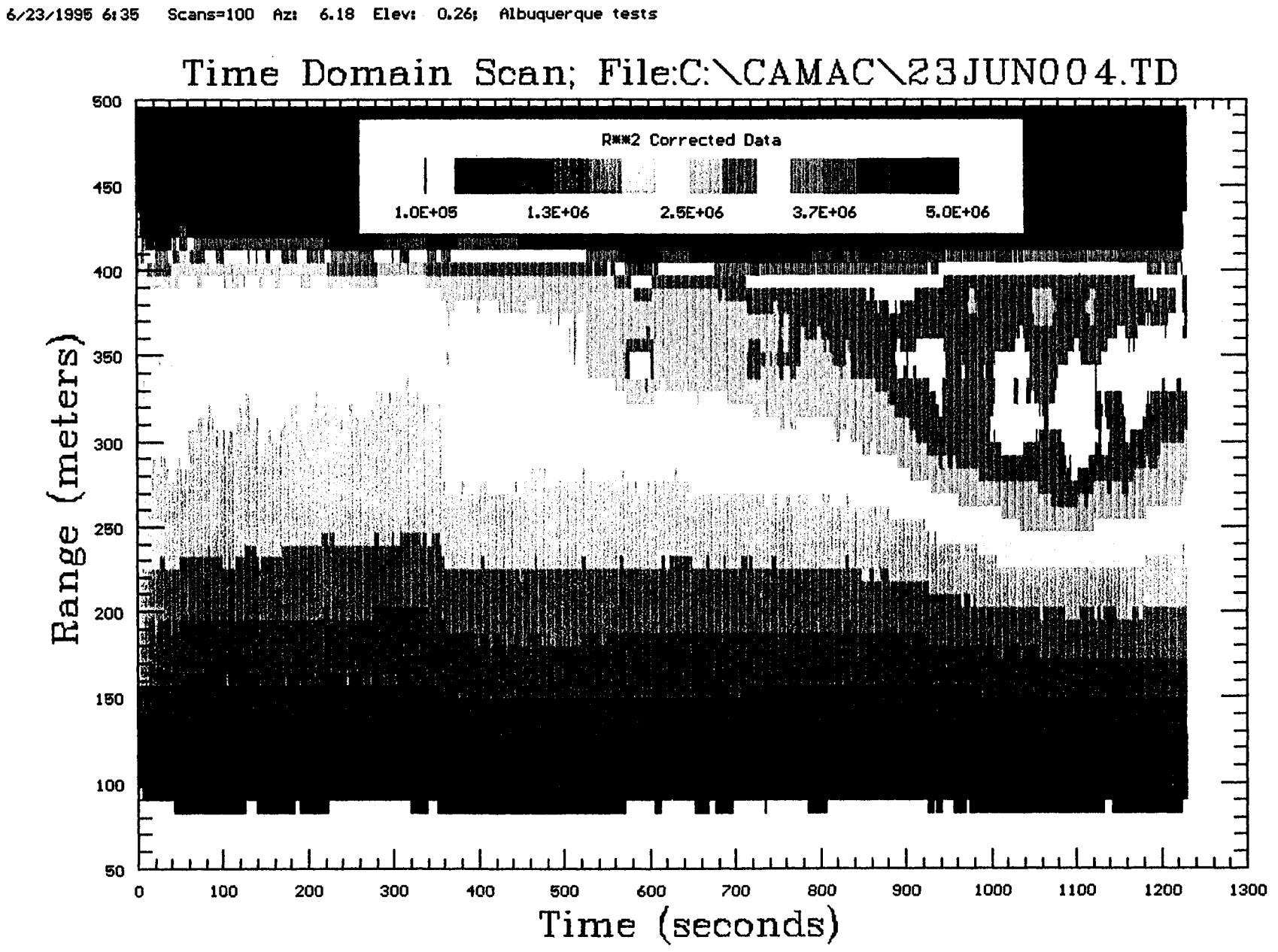
6/23/1995 6:35 Scans=100 Az: 6.18 Elev: 0.26; Albuquerque tests
Time Domain Scan; File:C:\CAMAC\23JUN004.TD
R**2 Corrected Data
1.0E+05
1.3E+06
2.5E+06
3.7E+06
5.0E+06
Range (meters)
500
450
400
350
300
250
200
150
100
50
0
100
200
300
400
500
600
700
800
900
1000
1100
1200
1300
Time (seconds)

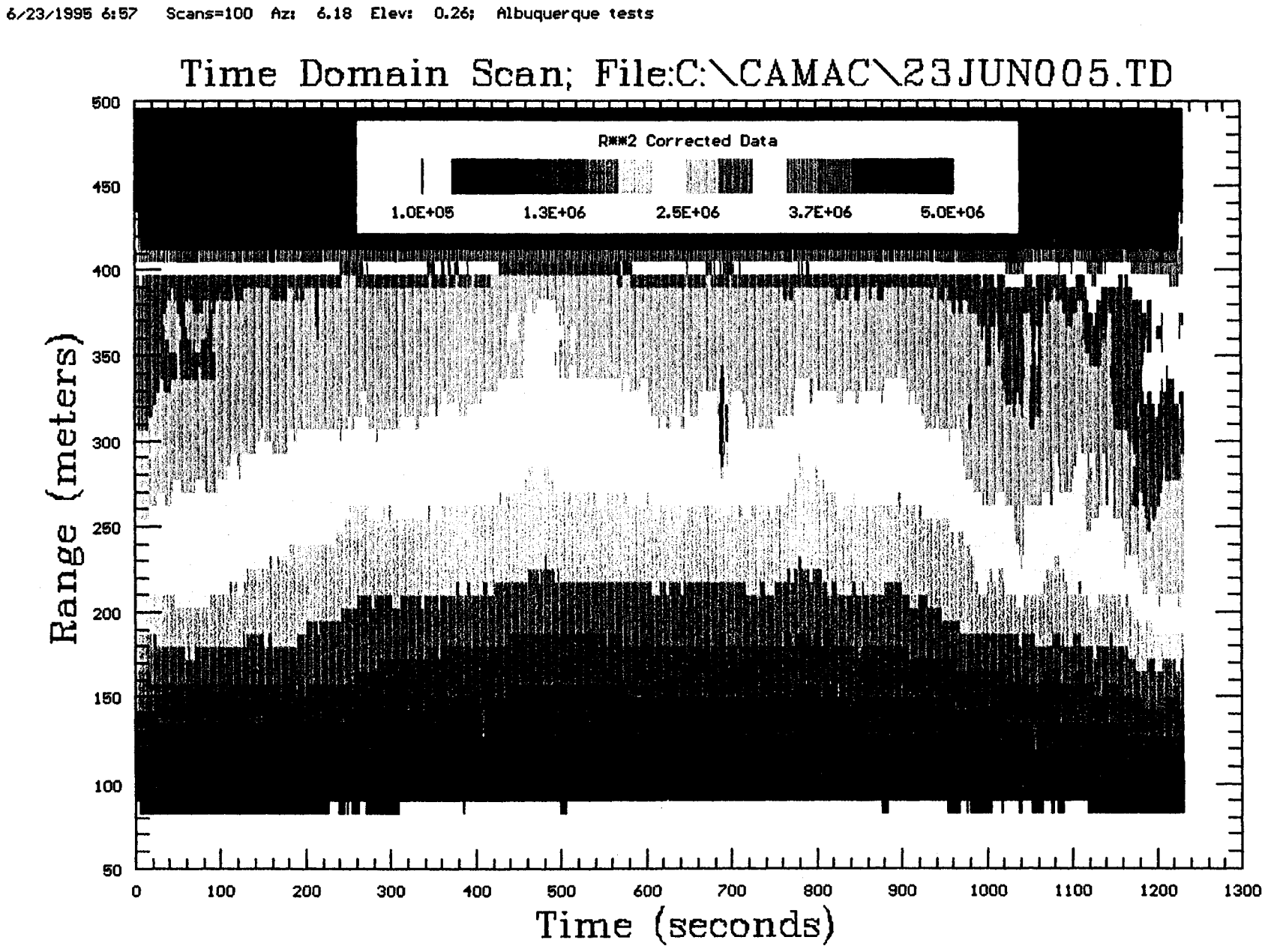
6/23/1995 6:57 Scans=100 Az: 6.18 Elev: 0.26; Albuquerque tests
Time Domain Scan; File:C:\CAMAC\23JUN005.TD
R**2 Corrected Data
1.0E+05
1.3E+06
2.5E+06
3.7E+06
5.0E+06
Range (meters)
500
450
400
350
300
250
200
150
100
50
0
100
200
300
400
500
600
700
800
900
1000
1100
1200
1300
Time (seconds)

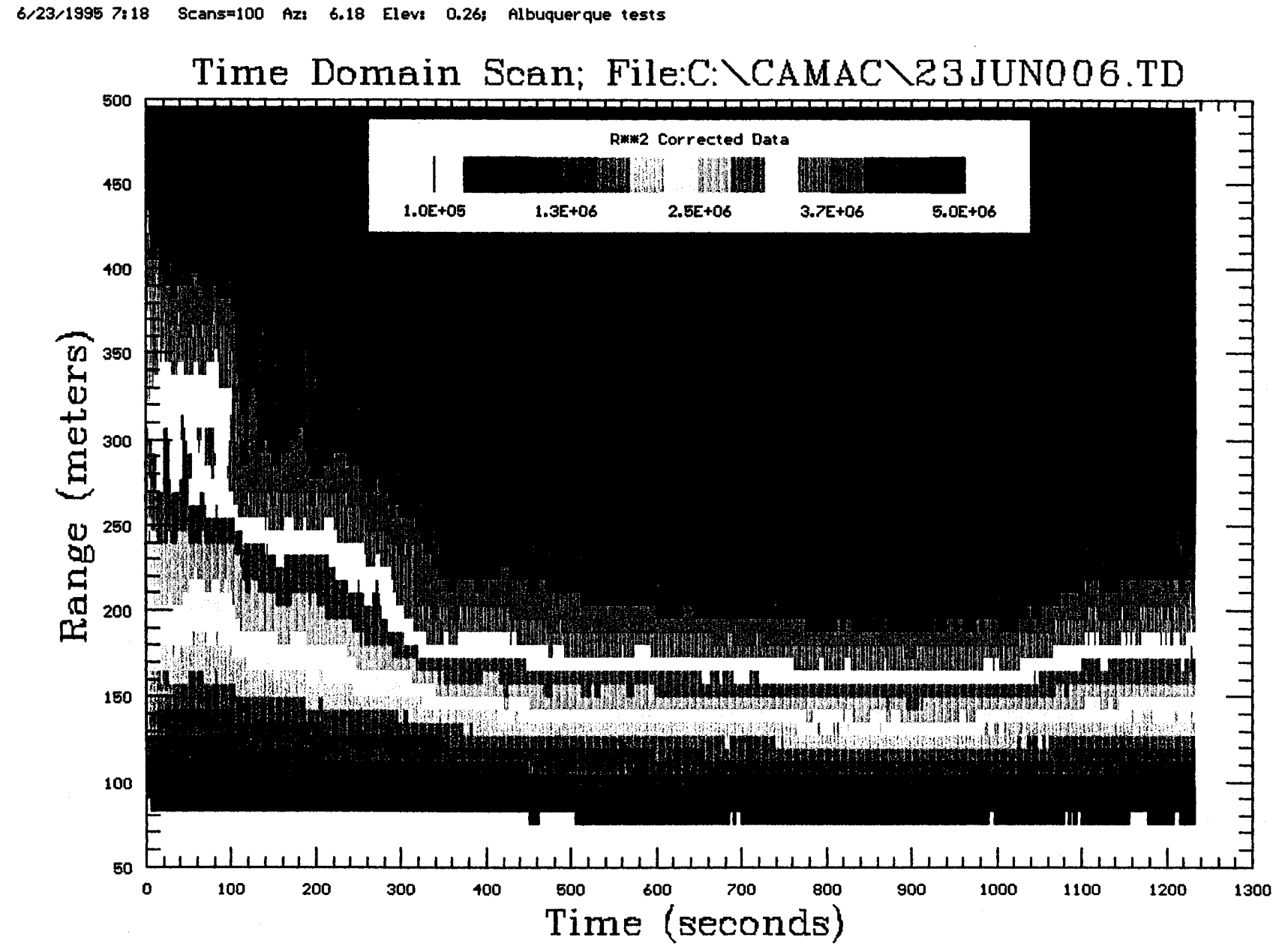
6/23/1995 7:18 Scans=100 Az: 6.18 Elev: 0.26; Albuquerque tests
Time Domain Scan; File:C:\CAMAC\23JUN006.TD
R**2 Corrected Data
1.0E+05
1.3E+06
2.5E+06
3.7E+06
5.0E+06
Range (meters)
500
450
400
350
300
250
200
150
100
50
0
100
200
300
400
500
600
700
800
900
1000
1100
1200
1300
Time (seconds)

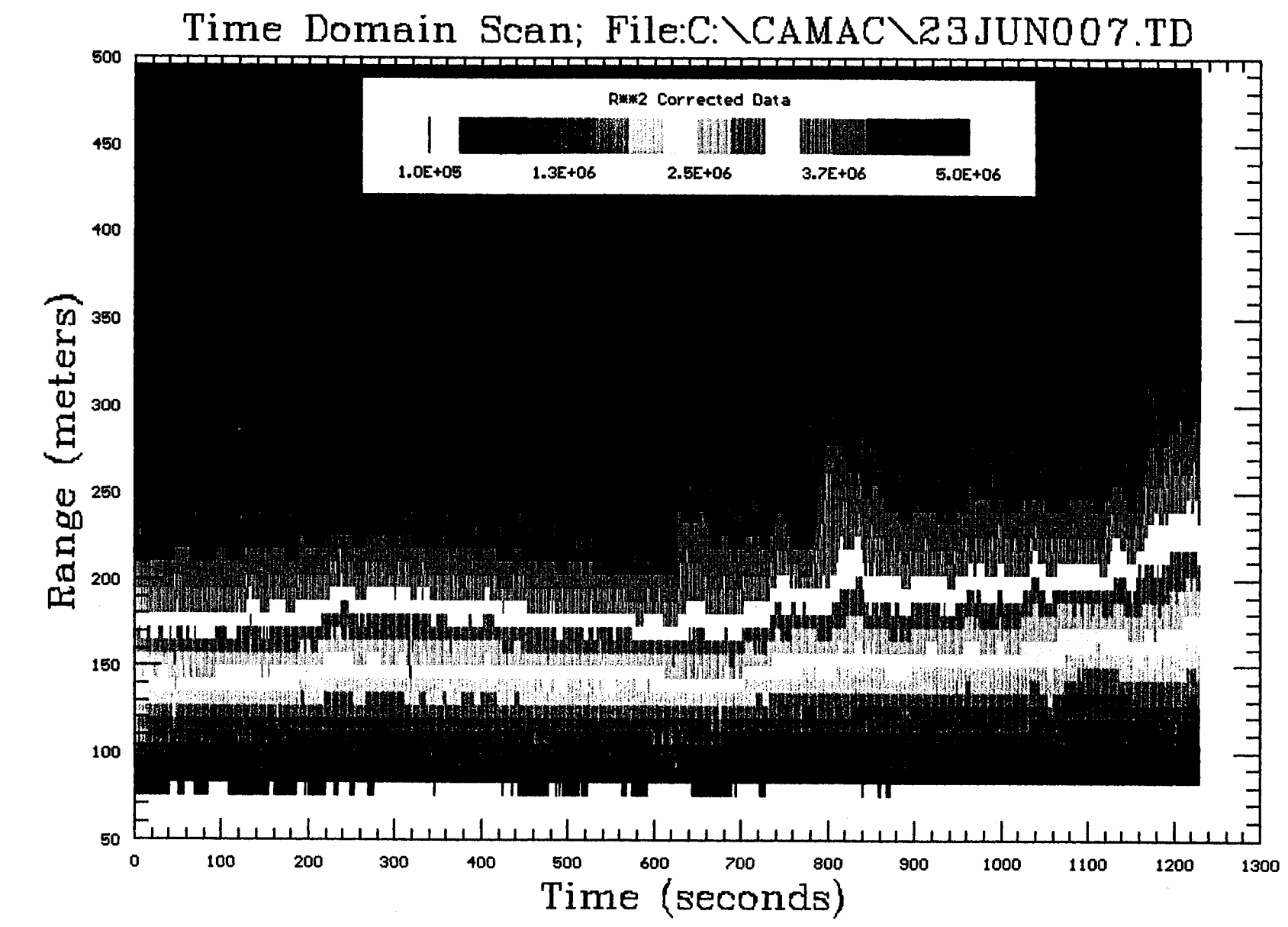
6/23/1995 7:39 Scans=100 Az: 6.18 Elev: 0.26; Albuquerque tests
Time Domain Scan; File:C:\CAMAC\23JUN007.TD
R**2 Corrected Data
1.0E+05
1.3E+06
2.5E+06
3.7E+06
5.0E+06
Range (meters)
500
450
400
350
300
250
200
150
100
50
0
100
200
300
400
500
600
700
800
900
1000
1100
1200
1300
Time (seconds)

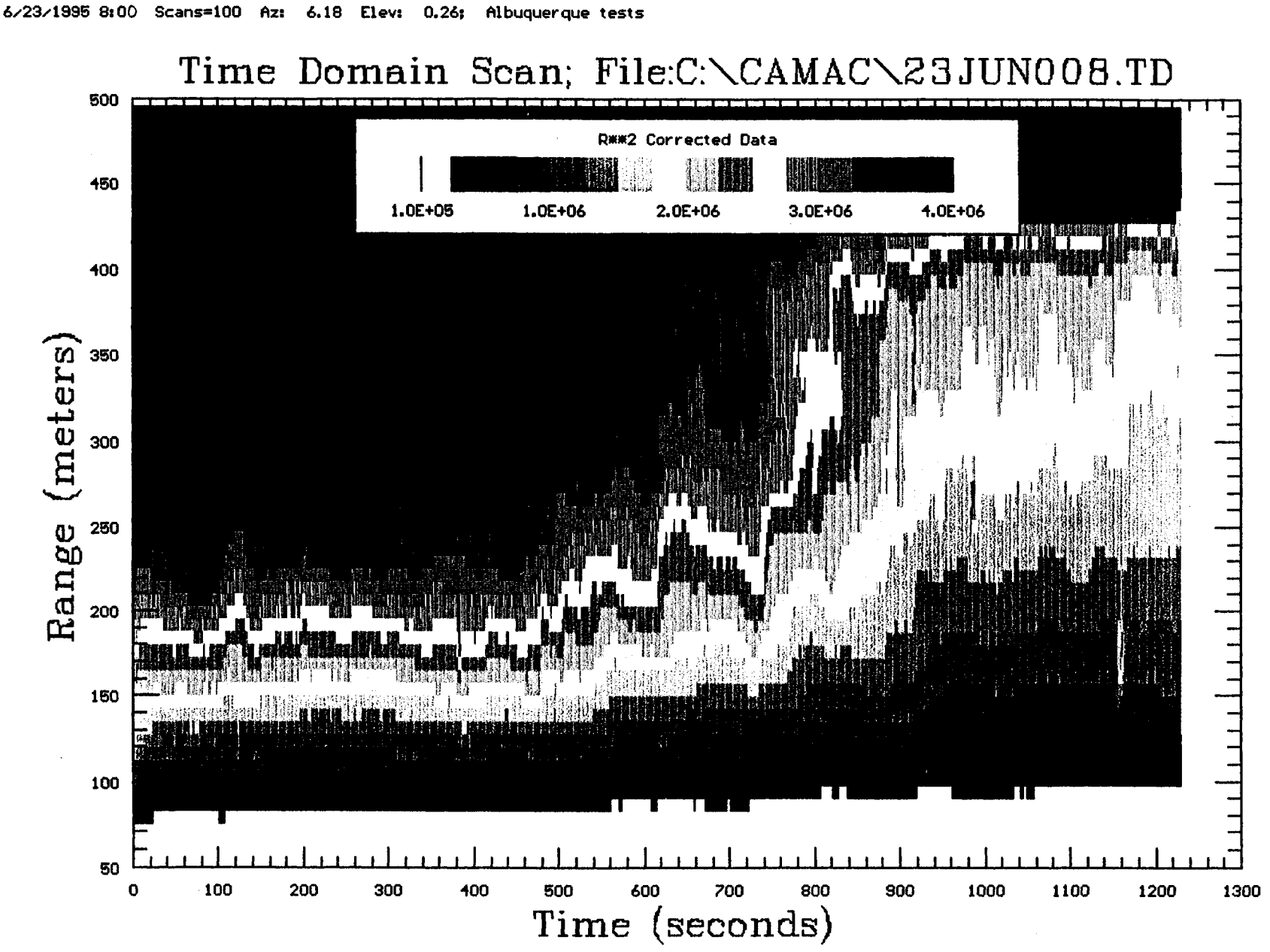
6/23/1995 8:00 Scans=100 Az: 6.18 Elev: 0.26; Albuquerque tests
Time Domain Scan; File:C:\CAMAC\23JUN008.TD
R**2 Corrected Data
1.0E+05
1.0E+06
2.0E+06
3.0E+06
4.0E+06
Range (meters)
500
450
400
350
300
250
200
150
100
50
0
100
200
300
400
500
600
700
800
900
1000
1100
1200
1300
Time (seconds)

6/23/1995 8:20 Scans=100 Az: 6.18 Elev: 0.26; Albuquerque tests

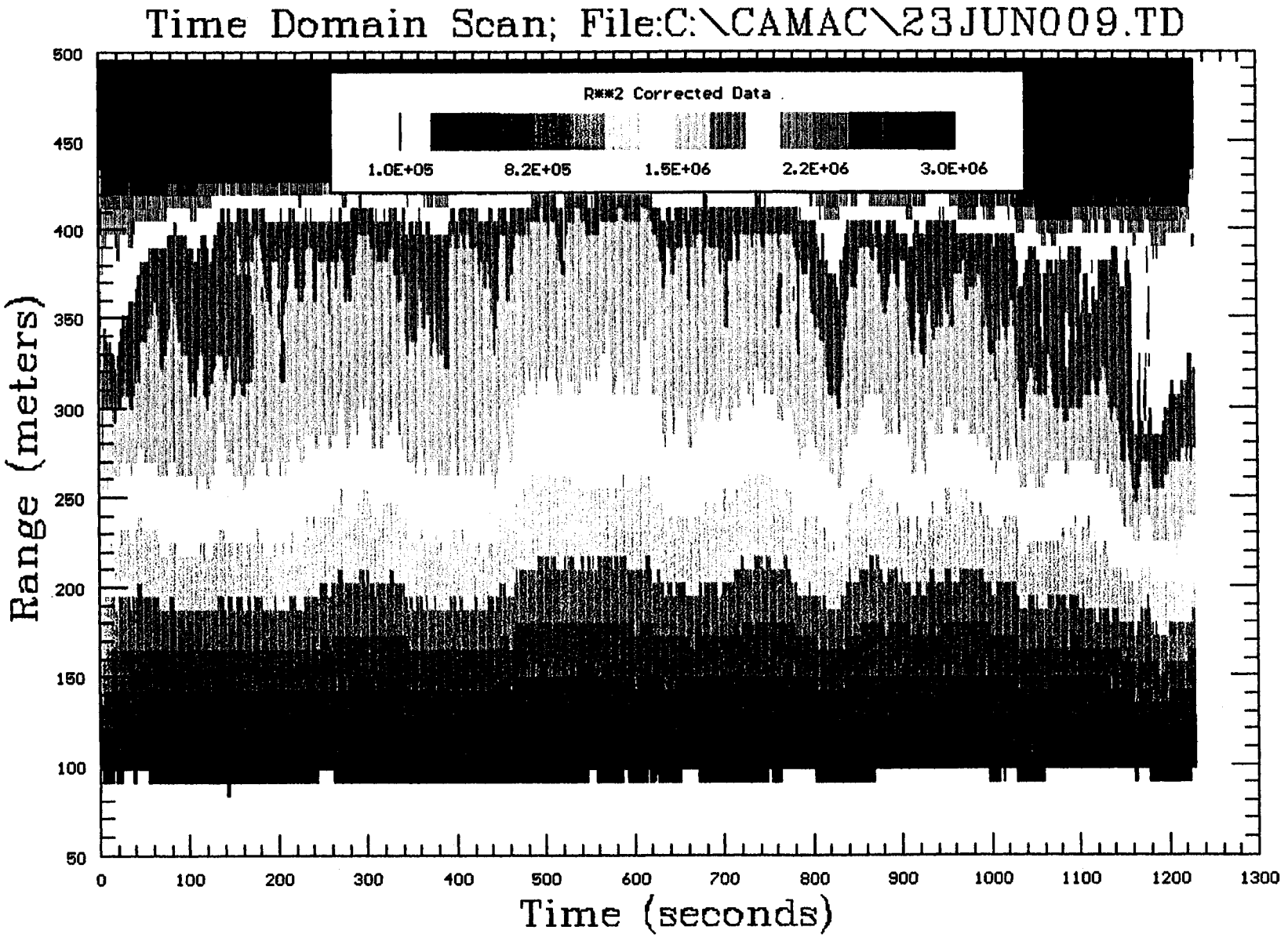

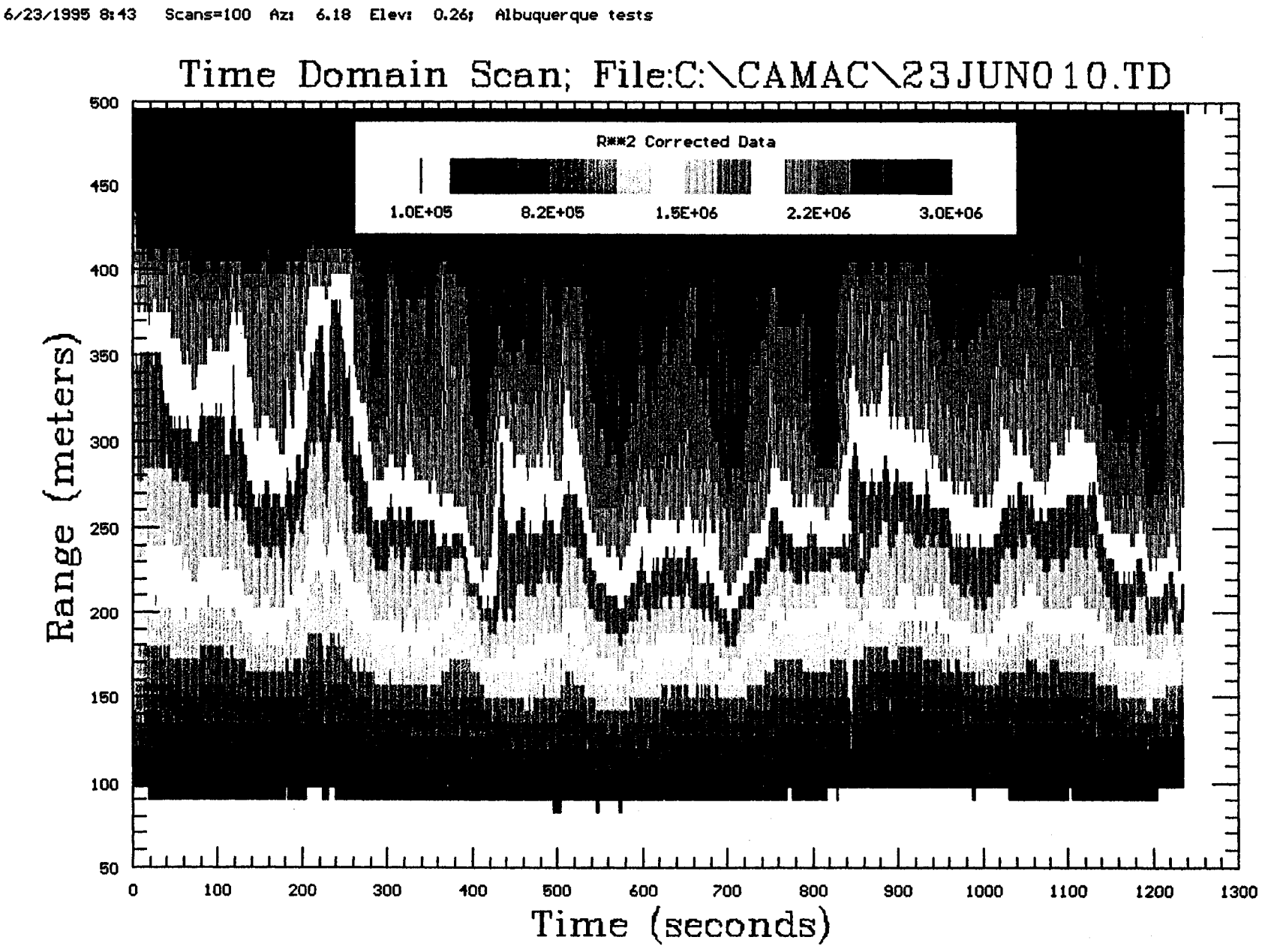
6/23/1995 8:43 Scans=100 Az: 6.18 Elev: 0.26; Albuquerque tests
Time Domain Scan; File:C:\CAMAC\23JUN010.TD
R**2 Corrected Data
1.0E+05
8.2E+05
1.5E+06
2.2E+06
3.0E+06
Range (meters)
500
450
400
350
300
250
200
150
100
50
0
100
200
300
400
500
600
700
800
900
1000
1100
1200
1300
Time (seconds)

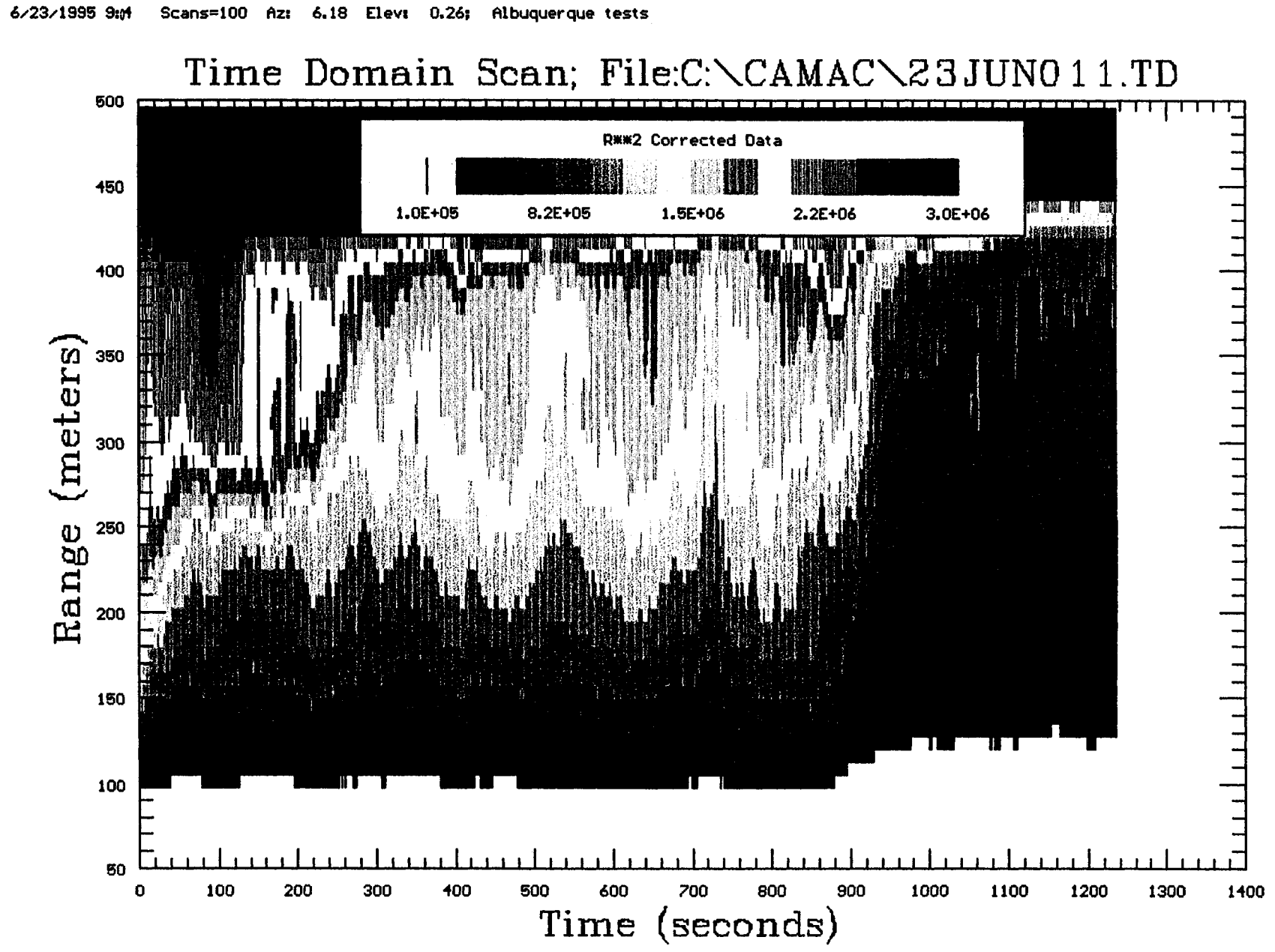
6/23/1995 9:04 Scans=100 Az: 6.18 Elev: 0.26; Albuquerque tests
Time Domain Scan; File:C:\CAMAC\23JUN011.TD
R**2 Corrected Data
1.0E+05
8.2E+05
1.5E+06
2.2E+06
3.0E+06
Range (meters)
500
450
400
350
300
250
200
150
100
50
0
100
200
300
400
500
600
700
800
900
1000
1100
1200
1300
1400
Time (seconds)

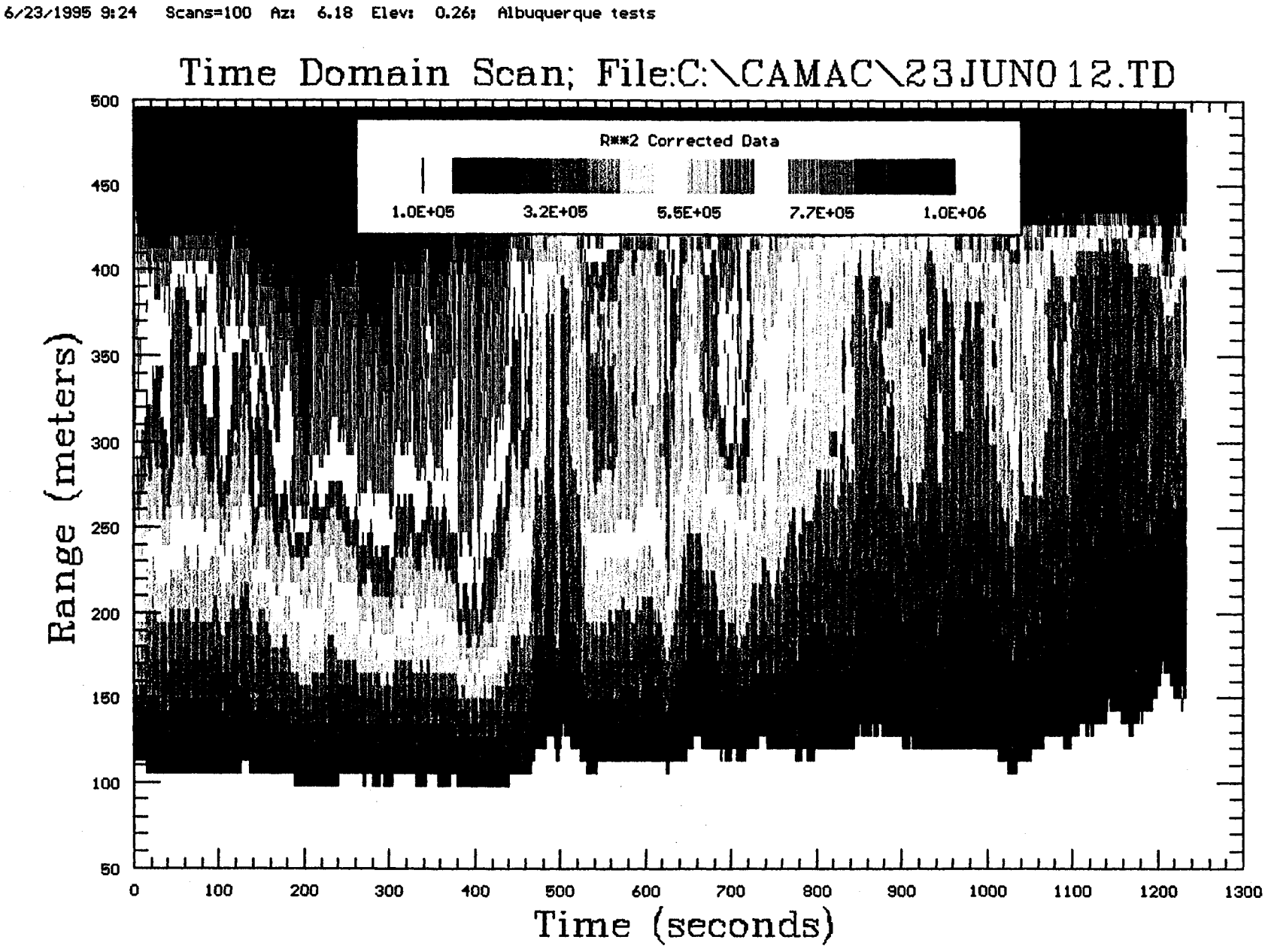
6/23/1995 9:24 Scans=100 Az: 6.18 Elev: 0.26; Albuquerque tests
Time Domain Scan; File:C:\CAMAC\23JUN012.TD
R**2 Corrected Data
1.0E+05
3.2E+05
5.5E+05
7.7E+05
1.0E+06
Range (meters)
500
450
400
350
300
250
200
150
100
50
0
100
200
300
400
500
600
700
800
900
1000
1100
1200
1300
Time (seconds)

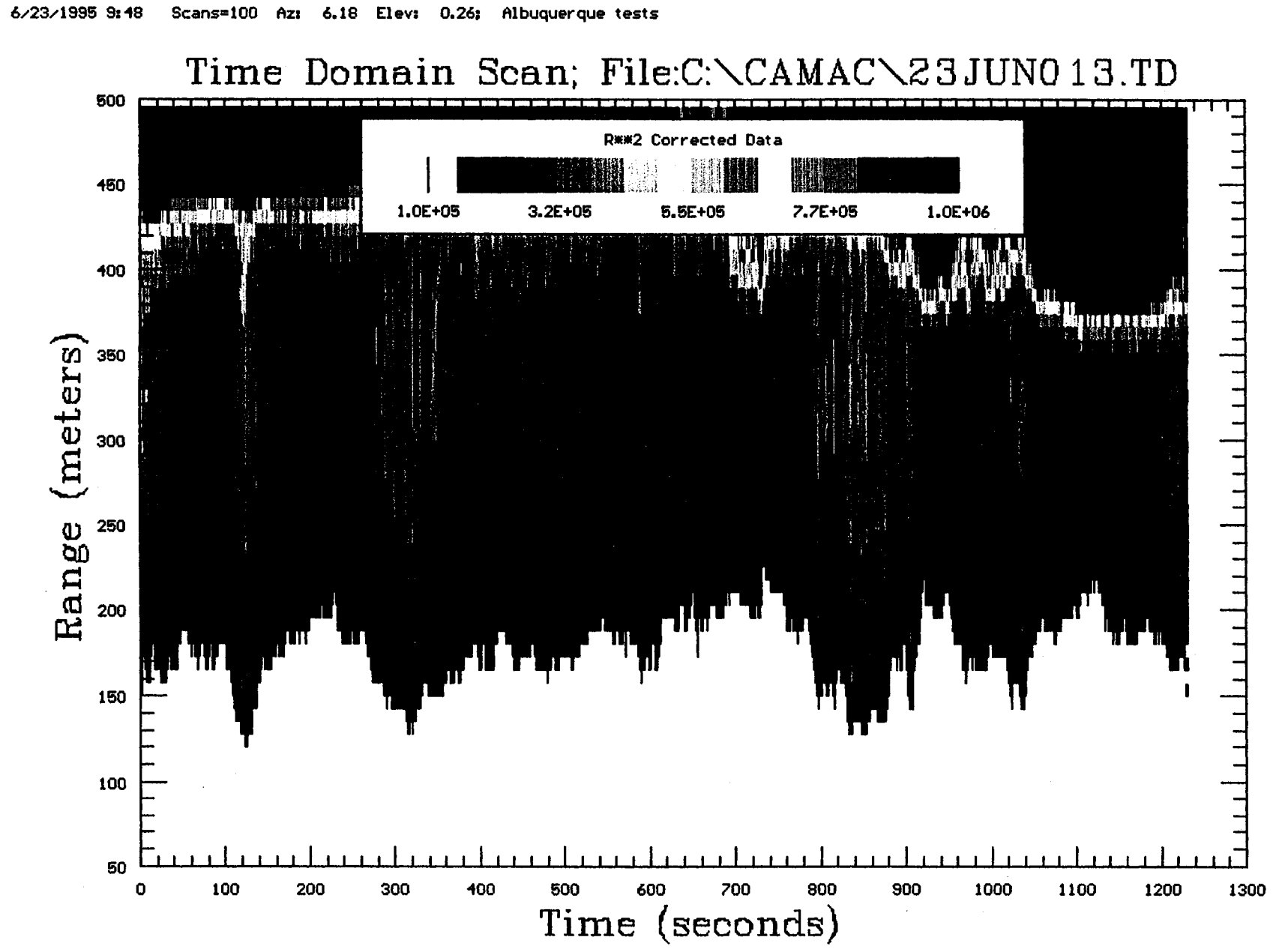
6/23/1995 9:48 Scans=100 Az: 6.18 Elev: 0.26; Albuquerque tests
Time Domain Scan; File:C:\CAMAC\23JUN013.TD
R**2 Corrected Data
1.0E+05
3.2E+05
5.5E+05
7.7E+05
1.0E+06
Range (meters)
500
450
400
350
300
250
200
150
100
50
0
100
200
300
400
500
600
700
800
900
1000
1100
1200
1300
Time (seconds)

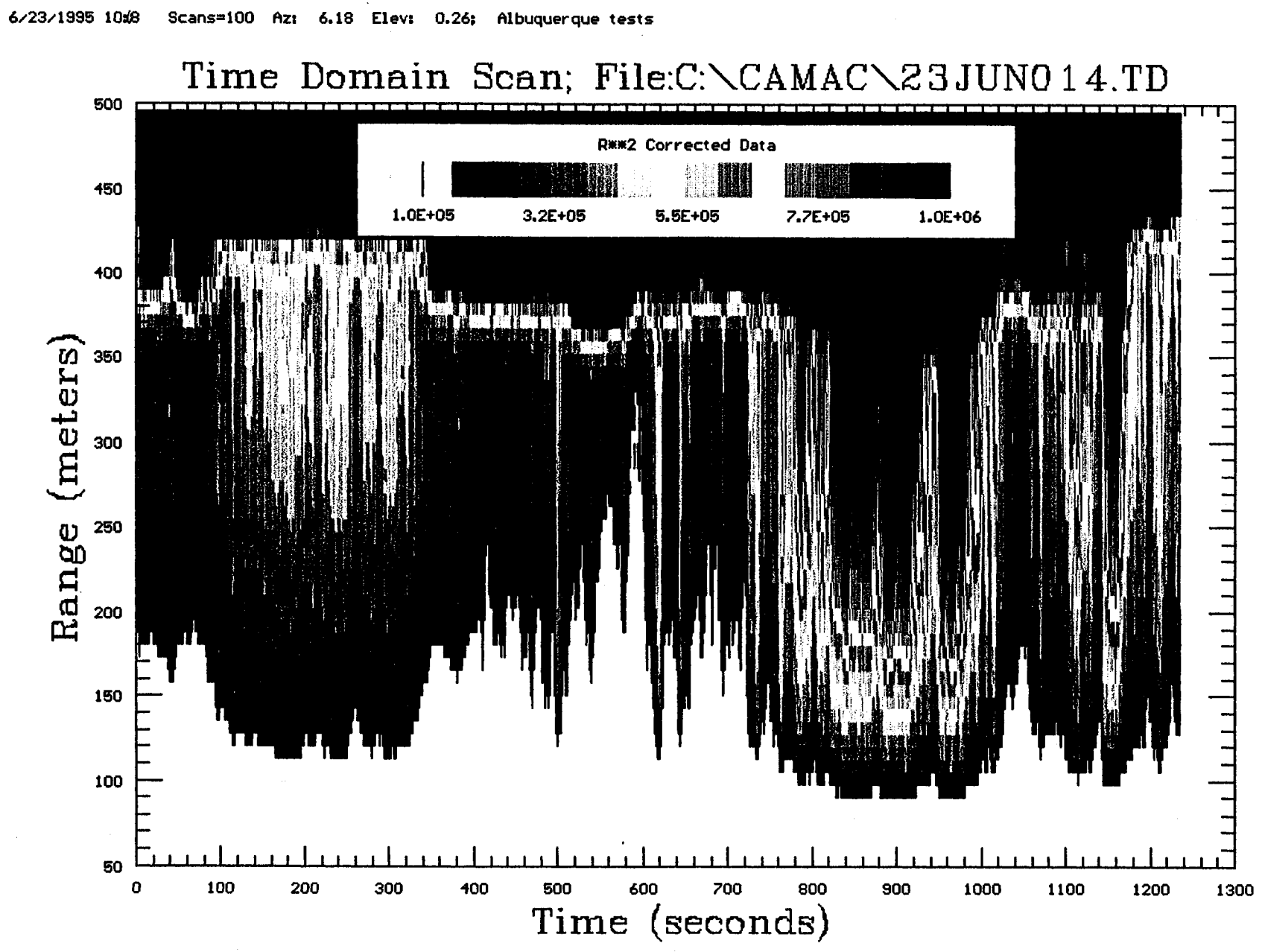
6/23/1995 10:8 Scans=100 Az: 6.18 Elev: 0.26; Albuquerque tests
Time Domain Scan; File:C:\CAMAC\23JUN014.TD
R**2 Corrected Data
1.0E+05
3.2E+05
5.5E+05
7.7E+05
1.0E+06
Range (meters)
500
450
400
350
300
250
200
150
100
50
0
100
200
300
400
500
600
700
800
900
1000
1100
1200
1300
Time (seconds)

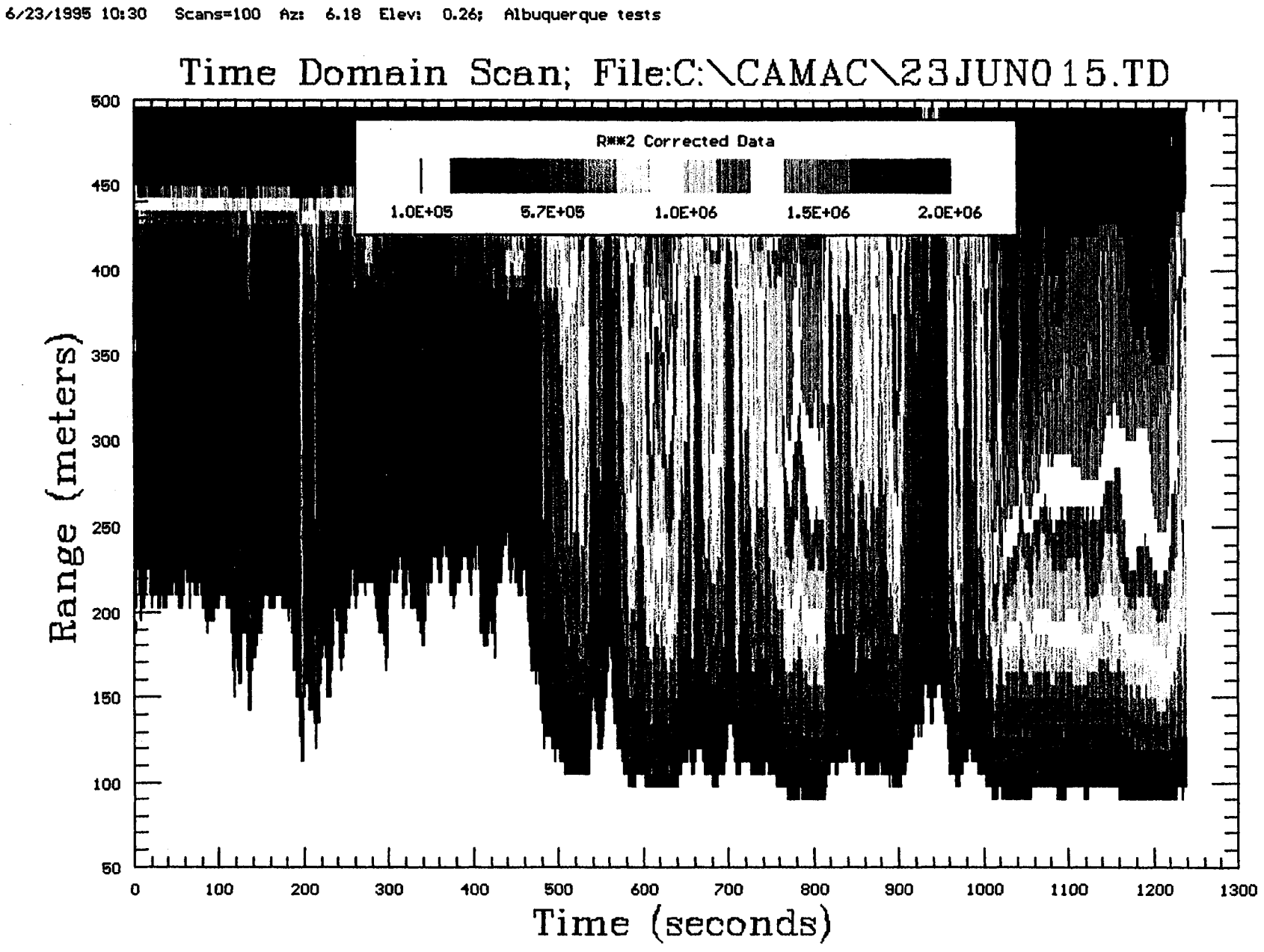
6/23/1995 10:30 Scans=100 Az: 6.18 Elev: 0.26; Albuquerque tests
Time Domain Scan; File:C:\CAMAC\23JUN015.TD
R**2 Corrected Data
1.0E+05
5.7E+05
1.0E+06
1.5E+06
2.0E+06
Range (meters)
500
450
400
350
300
250
200
150
100
50
0
100
200
300
400
500
600
700
800
900
1000
1100
1200
1300
Time (seconds)

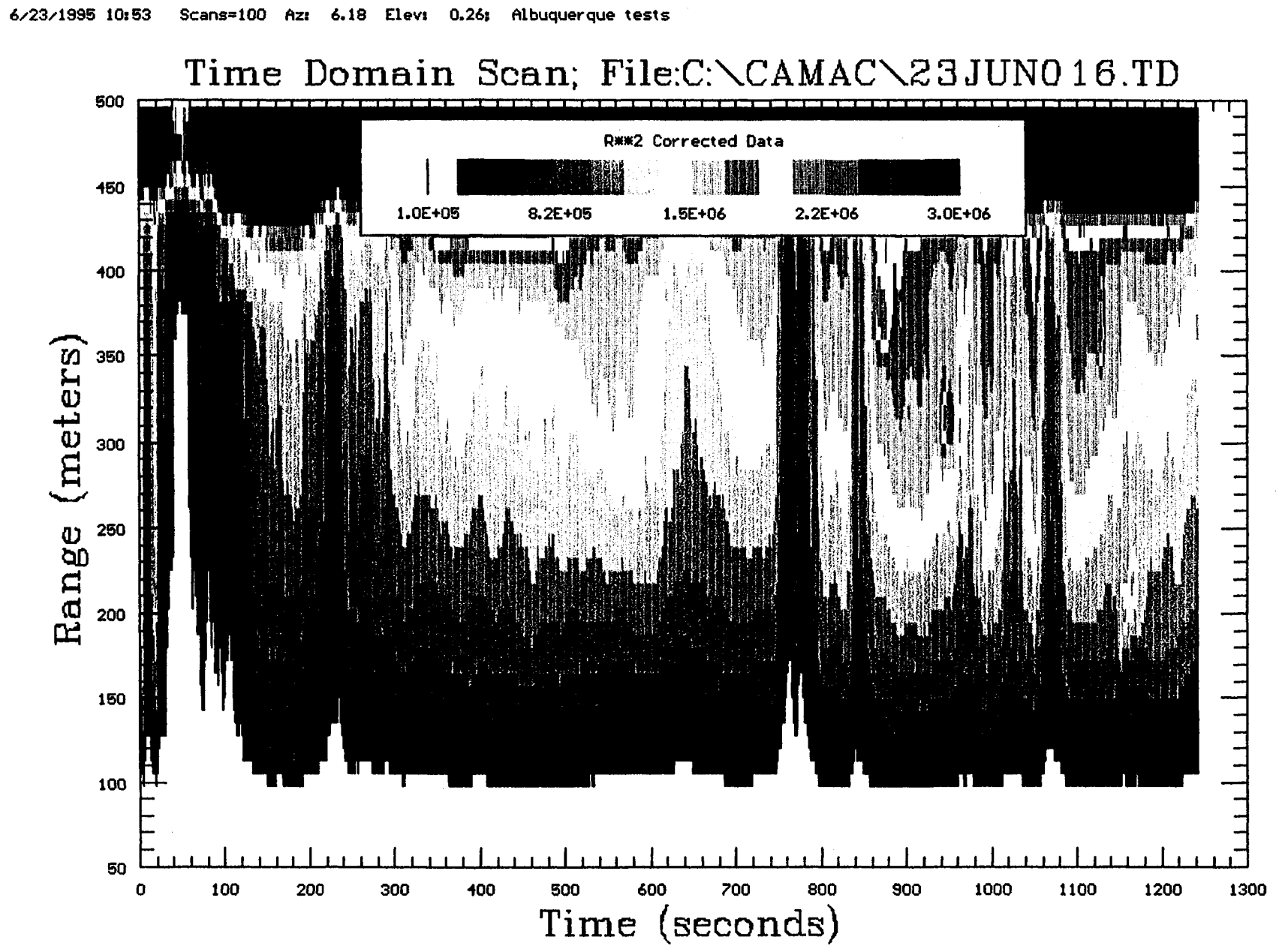
6/23/1995 10:53 Scans=100 Az: 6.18 Elev: 0.26; Albuquerque tests
Time Domain Scan; File:C:\CAMAC\23JUN016.TD
R**2 Corrected Data
1.0E+05
8.2E+05
1.5E+06
2.2E+06
3.0E+06
Range (meters)
500
450
400
350
300
250
200
150
100
50
0
100
200
300
400
500
600
700
800
900
1000
1100
1200
1300
Time (seconds)

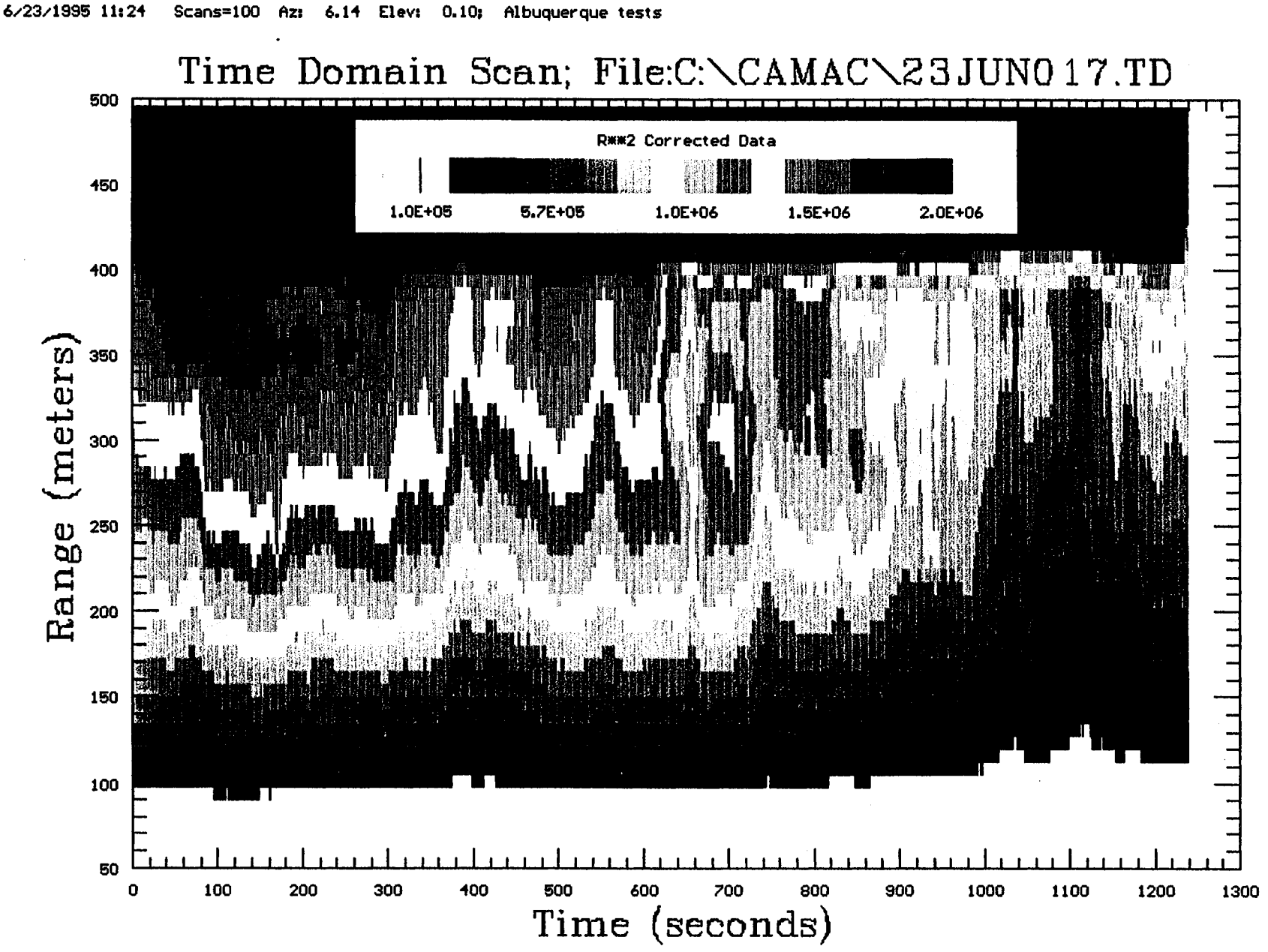
6/23/1995 11:24 Scans=100 Az: 6.14 Elev: 0.10; Albuquerque tests
Time Domain Scan; File:C:\CAMAC\23JUN017.TD
R**2 Corrected Data
1.0E+05
5.7E+05
1.0E+06
1.5E+06
2.0E+06
Range (meters)
500
450
400
350
300
250
200
150
100
50
0
100
200
300
400
500
600
700
800
900
1000
1100
1200
1300
Time (seconds)

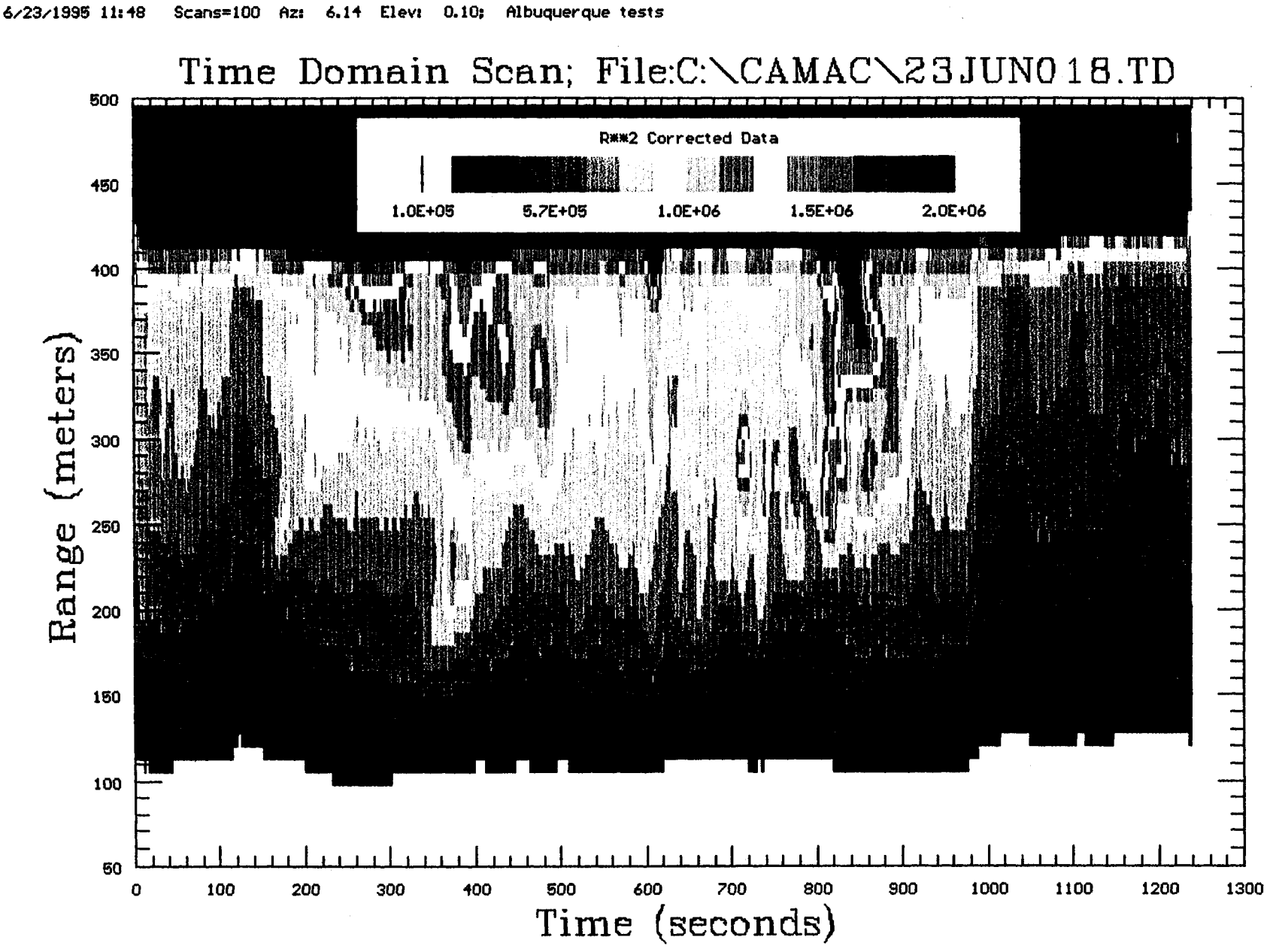
6/23/1995 11:48 Scans=100 Az: 6.14 Elev: 0.10; Albuquerque tests
Time Domain Scan; File:C:\CAMAC\23JUN018.TD
R**2 Corrected Data
1.0E+05
5.7E+05
1.0E+06
1.5E+06
2.0E+06
Range (meters)
500
450
400
350
300
250
200
150
100
50
0
100
200
300
400
500
600
700
800
900
1000
1100
1200
1300
Time (seconds)

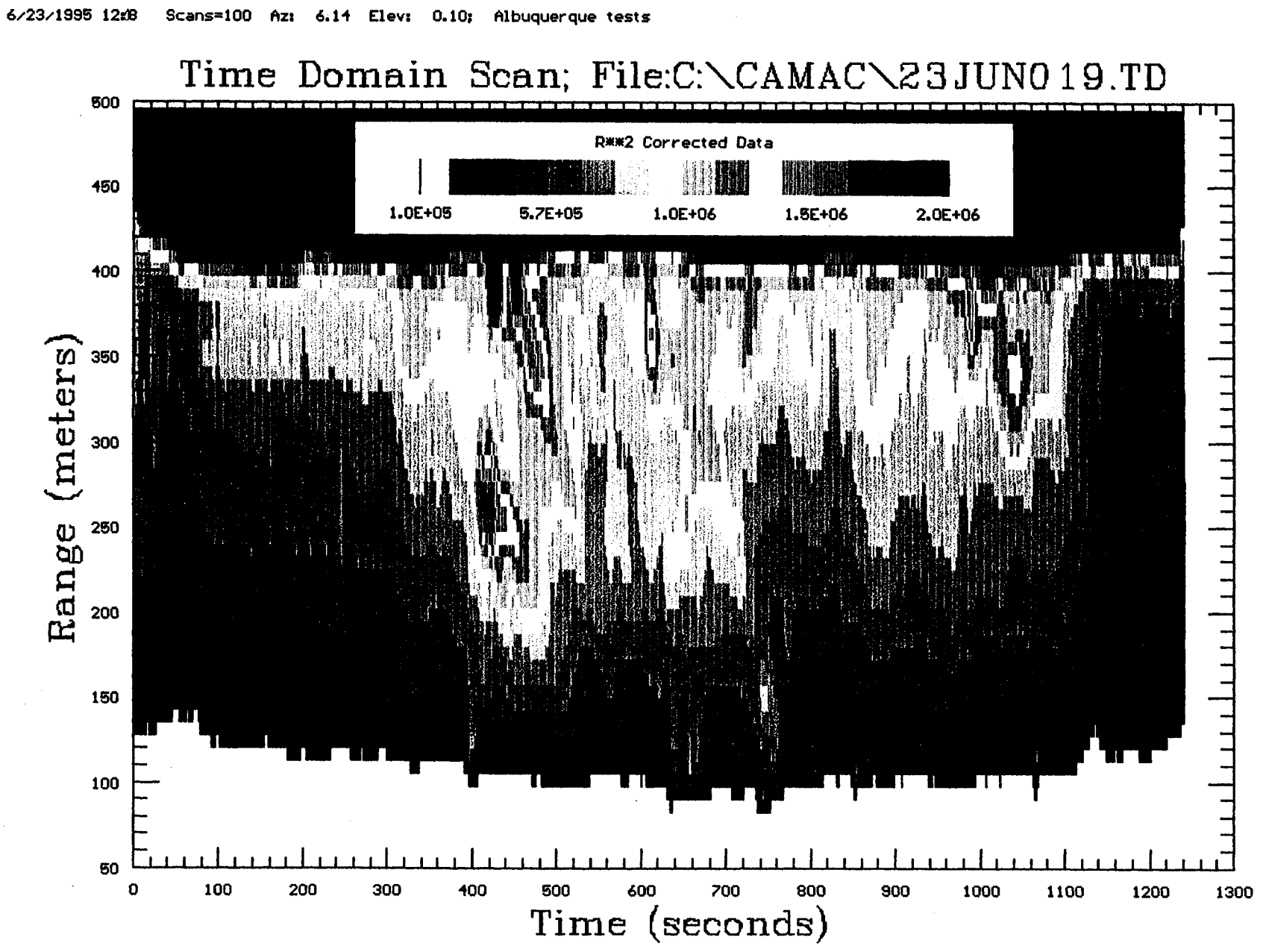
6/23/1995 12:08 Scans=100 Az: 6.14 Elev: 0.10; Albuquerque tests
Time Domain Scan; File:C:\CAMAC\23JUN019.TD
R**2 Corrected Data
1.0E+05
5.7E+05
1.0E+06
1.5E+06
2.0E+06
Range (meters)
500
450
400
350
300
250
200
150
100
50
0
100
200
300
400
500
600
700
800
900
1000
1100
1200
1300
Time (seconds)

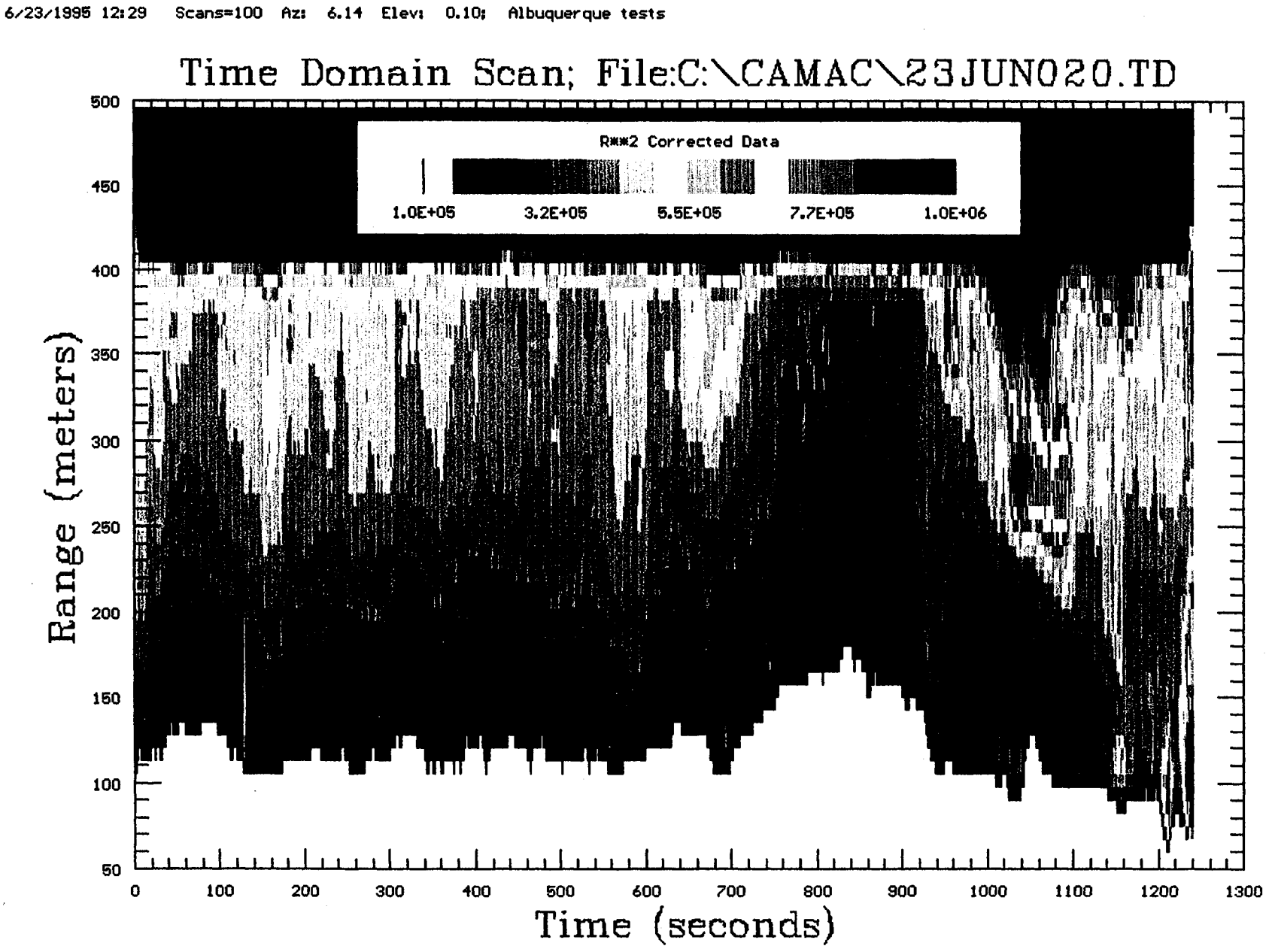
6/23/1995 12:29 Scans=100 Az: 6.14 Elev: 0.10; Albuquerque tests
Time Domain Scan; File:C:\CAMAC\23JUN020.TD
R**2 Corrected Data
1.0E+05
3.2E+05
5.5E+05
7.7E+05
1.0E+06
Range (meters)
500
450
400
350
300
250
200
150
100
50
0
100
200
300
400
500
600
700
800
900
1000
1100
1200
1300
Time (seconds)

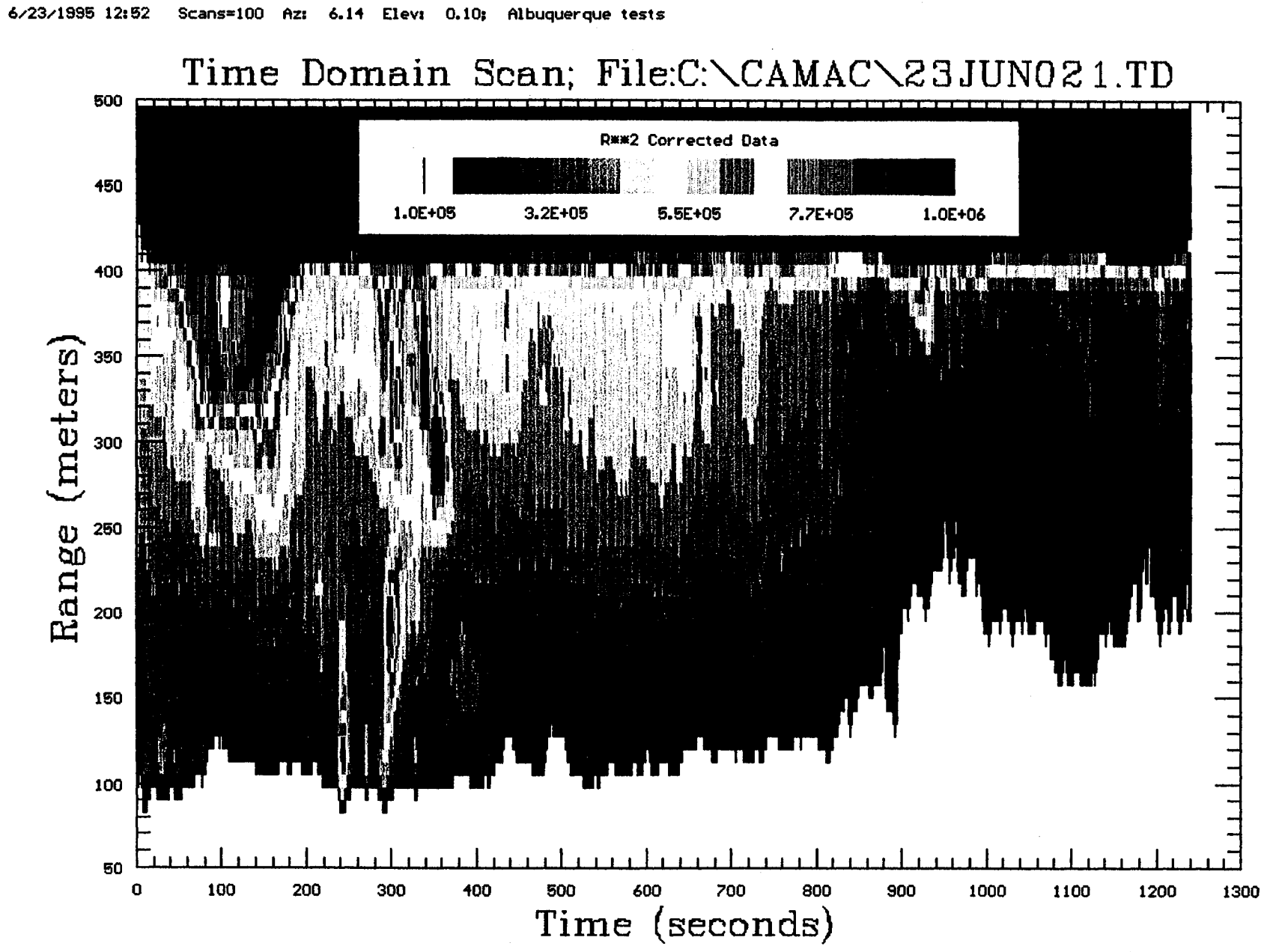
6/23/1995 12:52 Scans=100 Az: 6.14 Elev: 0.10; Albuquerque tests
Time Domain Scan; File:C:\CAMAC\23JUN021.TD
R**2 Corrected Data
1.0E+05
3.2E+05
5.5E+05
7.7E+05
1.0E+06
Range (meters)
500
450
400
350
300
250
200
150
100
50
0
100
200
300
400
500
600
700
800
900
1000
1100
1200
1300
Time (seconds)

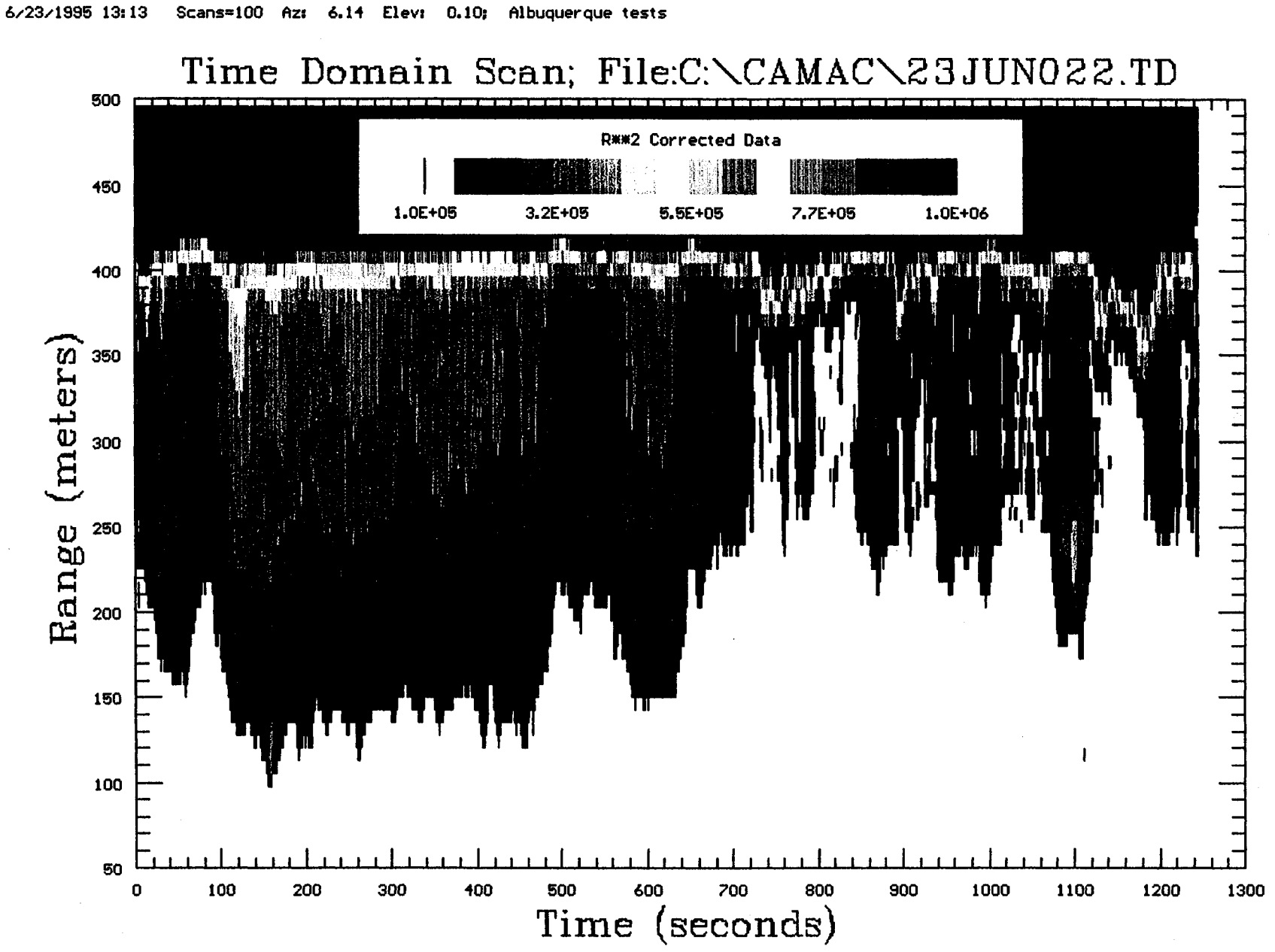
6/23/1995 13:13 Scans=100 Az: 6.14 Elev: 0.10; Albuquerque tests
Time Domain Scan; File:C:\CAMAC\23JUN022.TD
R**2 Corrected Data
1.0E+05
3.2E+05
5.5E+05
7.7E+05
1.0E+06
Range (meters)
500
450
400
350
300
250
200
150
100
50
0
100
200
300
400
500
600
700
800
900
1000
1100
1200
1300
Time (seconds)

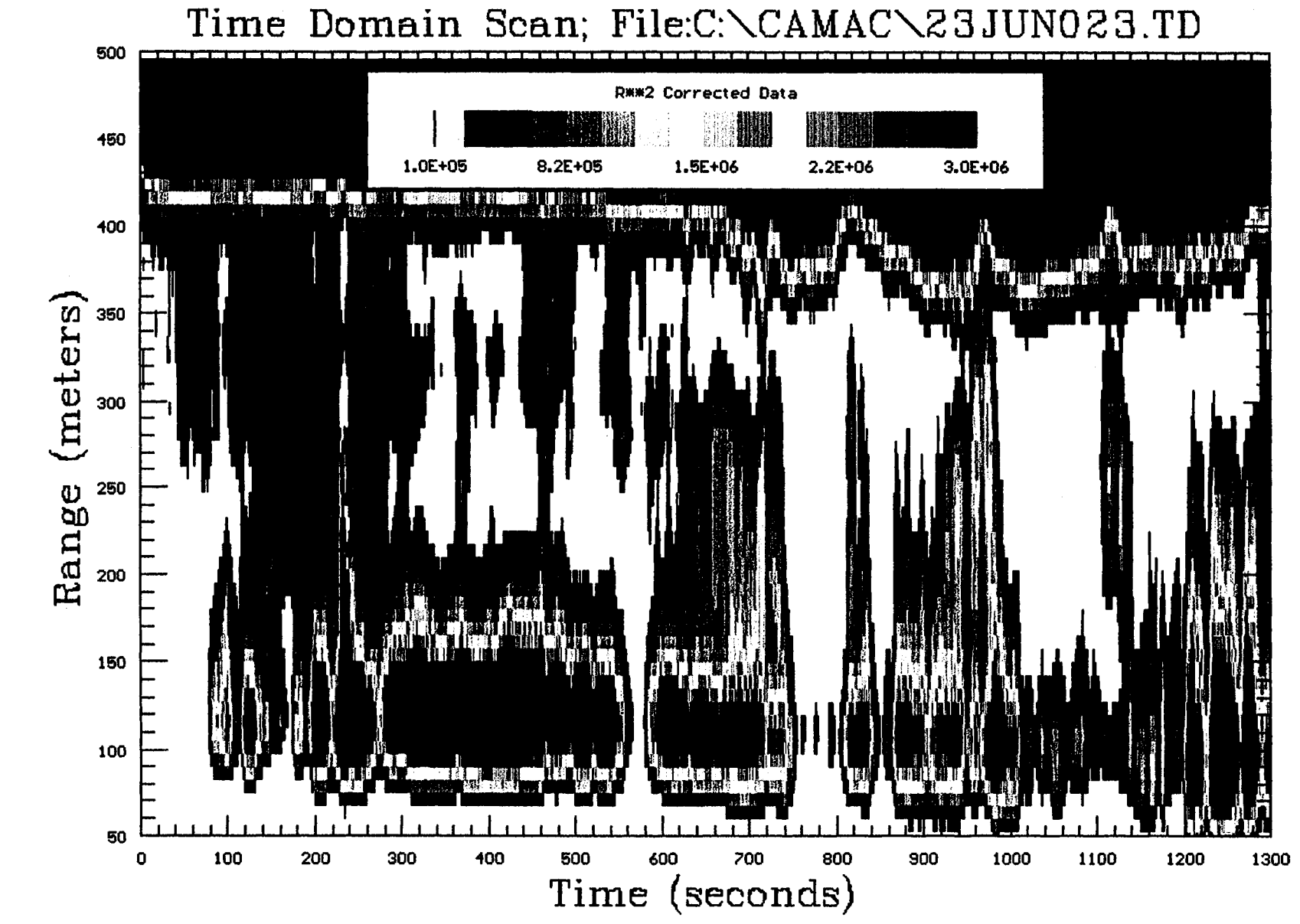
6/23/1995 13:34 Scans=100 Az: 6.14 Elev: 0.10; Albuquerque tests
Time Domain Scan; File:C:\CAMAC\23JUN023.TD
R**2 Corrected Data
1.0E+05
8.2E+05
1.5E+06
2.2E+06
3.0E+06
Range (meters)
500
450
400
350
300
250
200
150
100
50
0
100
200
300
400
500
600
700
800
900
1000
1100
1200
1300
Time (seconds)

6/23/1995 14:33 Scans=100 Az: 6.14 Elev: 0.10; Albuquerque Tests

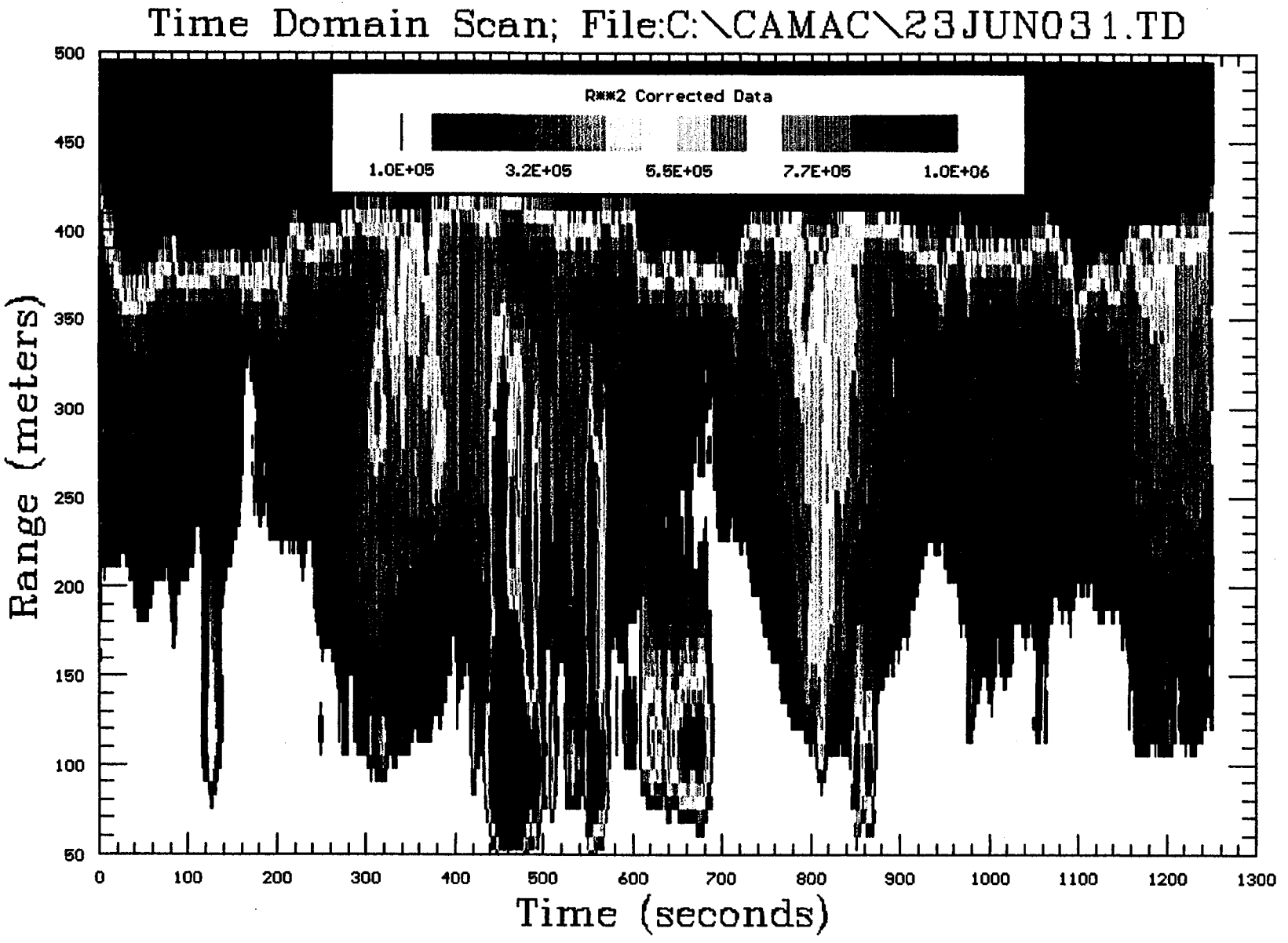

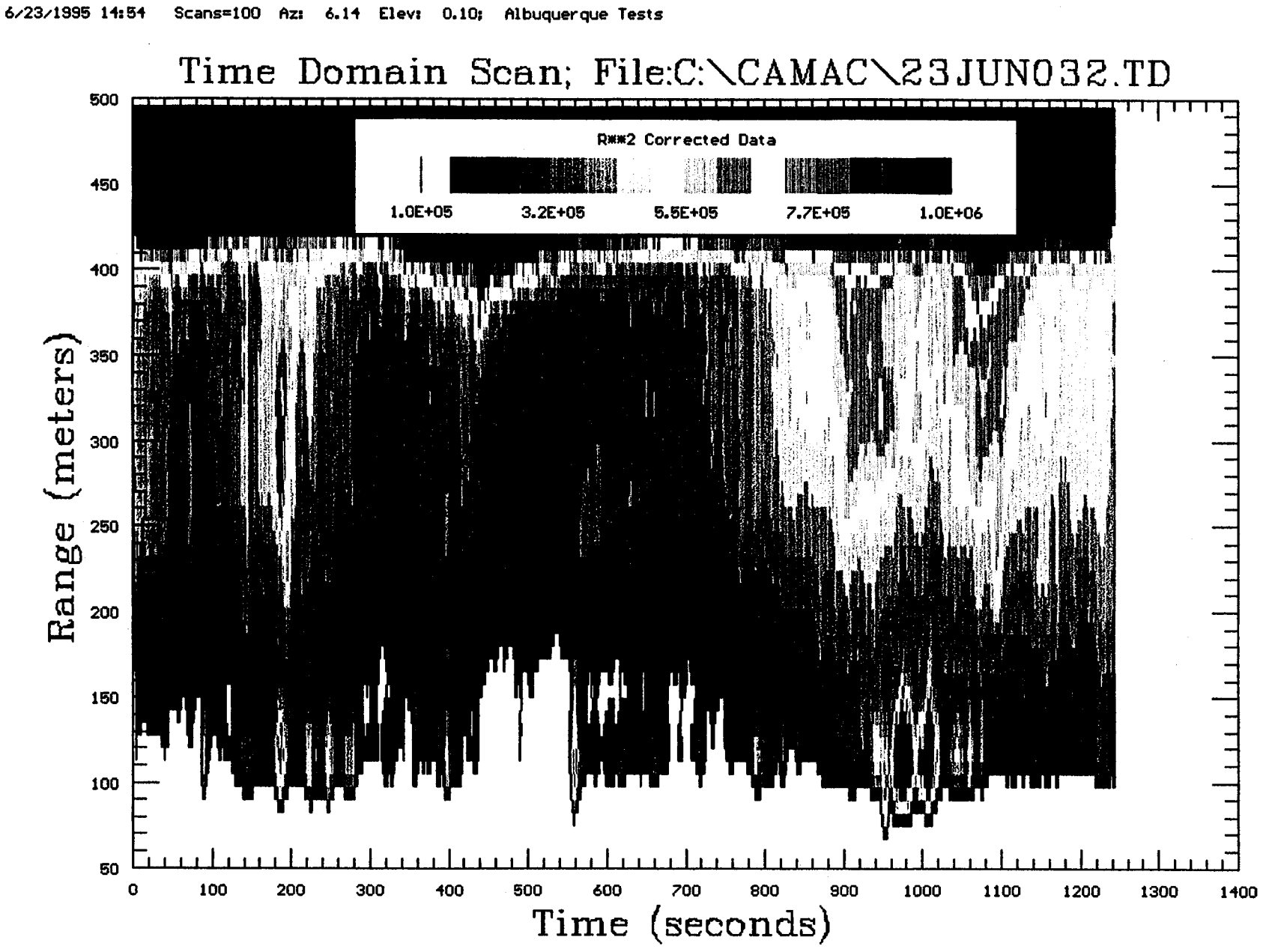
6/23/1995 14:54 Scans=100 Az: 6.14 Elev: 0.10; Albuquerque Tests
Time Domain Scan; File:C:\CAMAC\23JUN032.TD
R**2 Corrected Data
1.0E+05
3.2E+05
5.5E+05
7.7E+05
1.0E+06
Range (meters)
500
450
400
350
300
250
200
150
100
50
0
100
200
300
400
500
600
700
800
900
1000
1100
1200
1300
1400
Time (seconds)

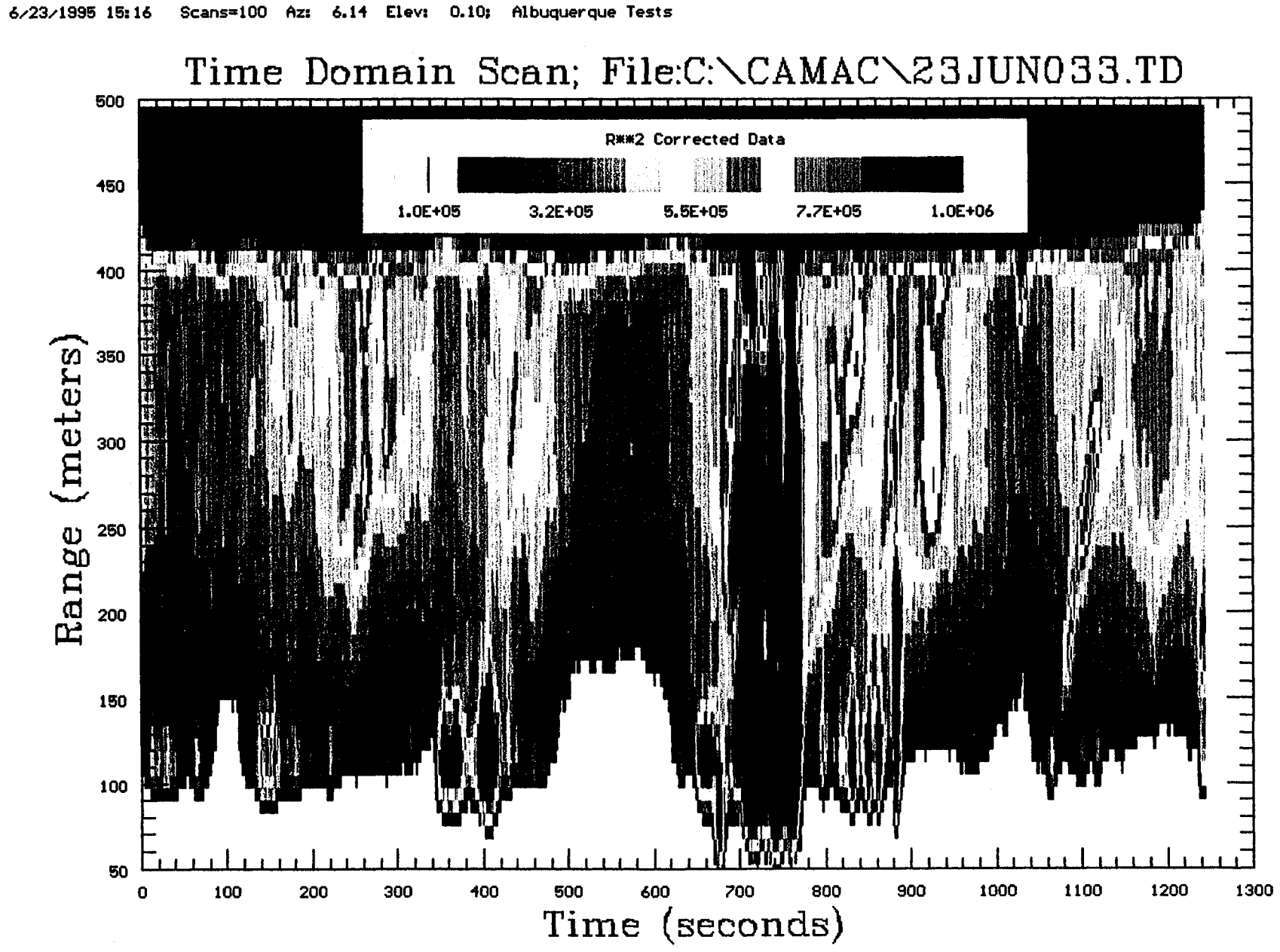
6/23/1995 15:16 Scans=100 Az: 6.14 Elev: 0.10; Albuquerque Tests
Time Domain Scan; File:C:\CAMAC\23JUN033.TD
R**2 Corrected Data
1.0E+05
3.2E+05
5.5E+05
7.7E+05
1.0E+06
Range (meters)
500
450
400
350
300
250
200
150
100
50
0
100
200
300
400
500
600
700
800
900
1000
1100
1200
1300
Time (seconds)

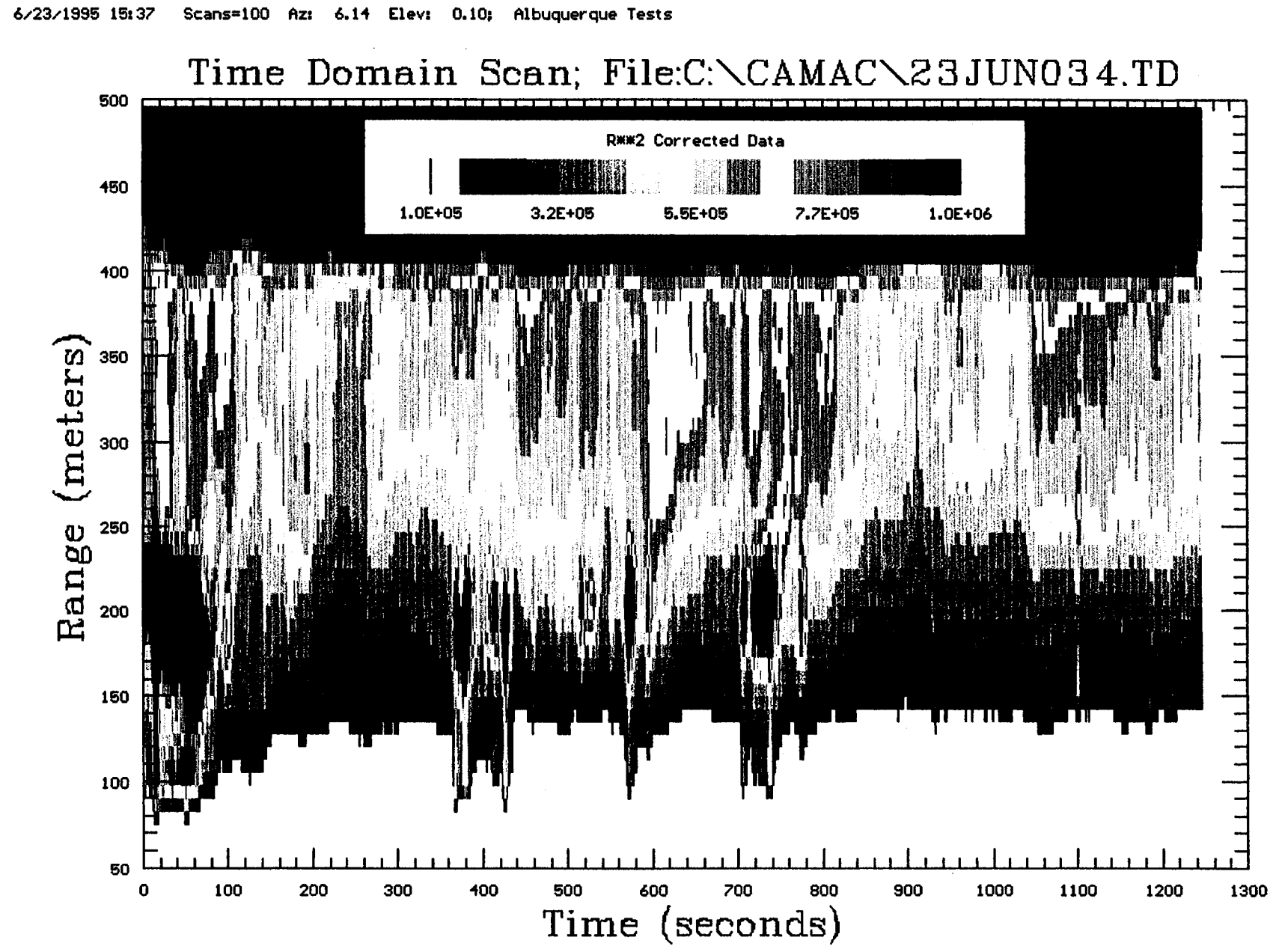
6/23/1995 15:37 Scans=100 Az: 6.14 Elev: 0.10; Albuquerque Tests
Time Domain Scan; File:C:\CAMAC\23JUN034.TD
R**2 Corrected Data
1.0E+05
3.2E+05
5.5E+05
7.7E+05
1.0E+06
Range (meters)
500
450
400
350
300
250
200
150
100
50
0
100
200
300
400
500
600
700
800
900
1000
1100
1200
1300
Time (seconds)

6/23/1995 15:58 Scans=100 Az: 6.14 Elev: 0.10; Albuquerque Tests

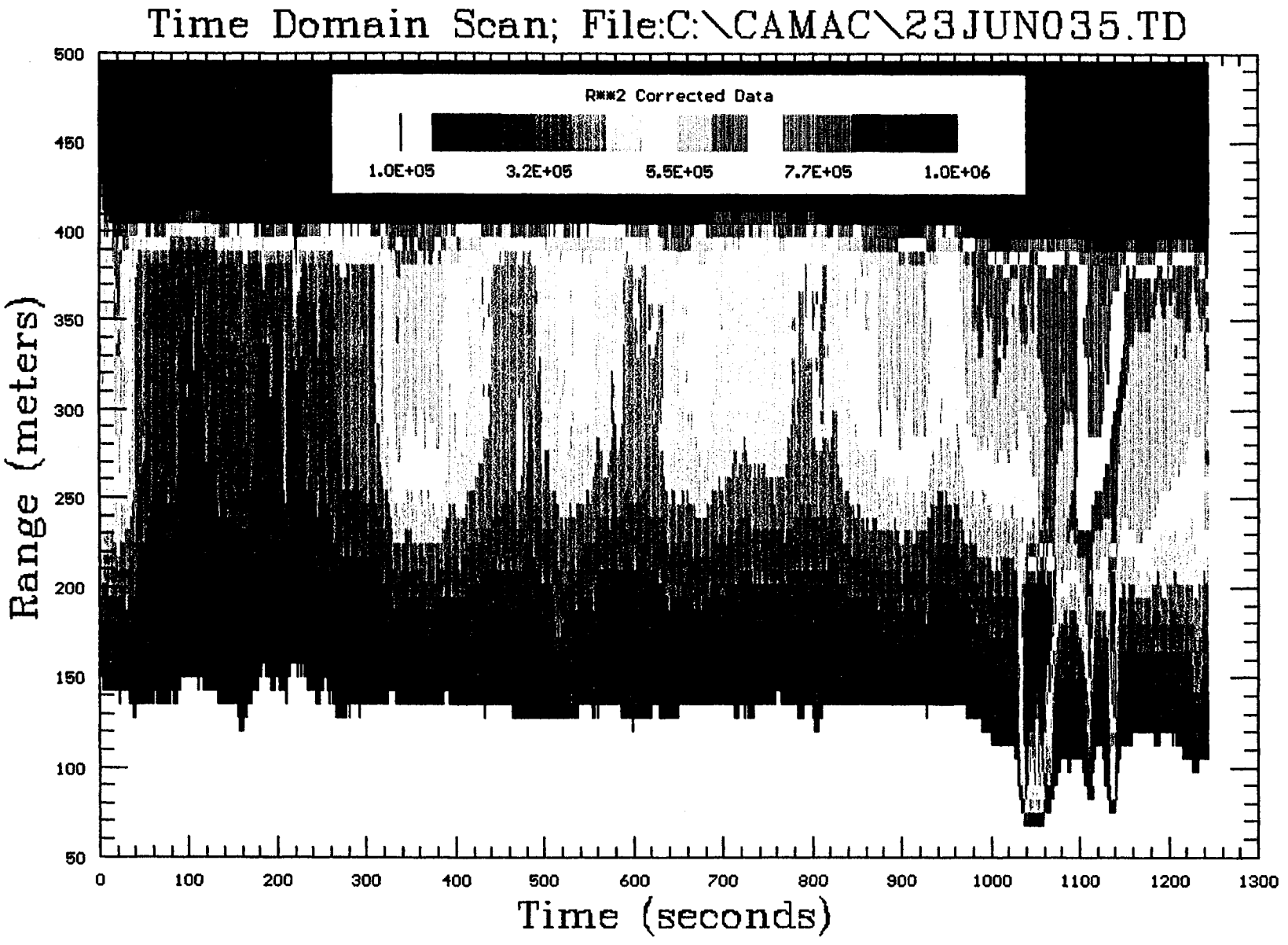

6/23/1995 16:19 Scans=100 Az: 6.14 Elev: 0.10; Albuquerque Tests

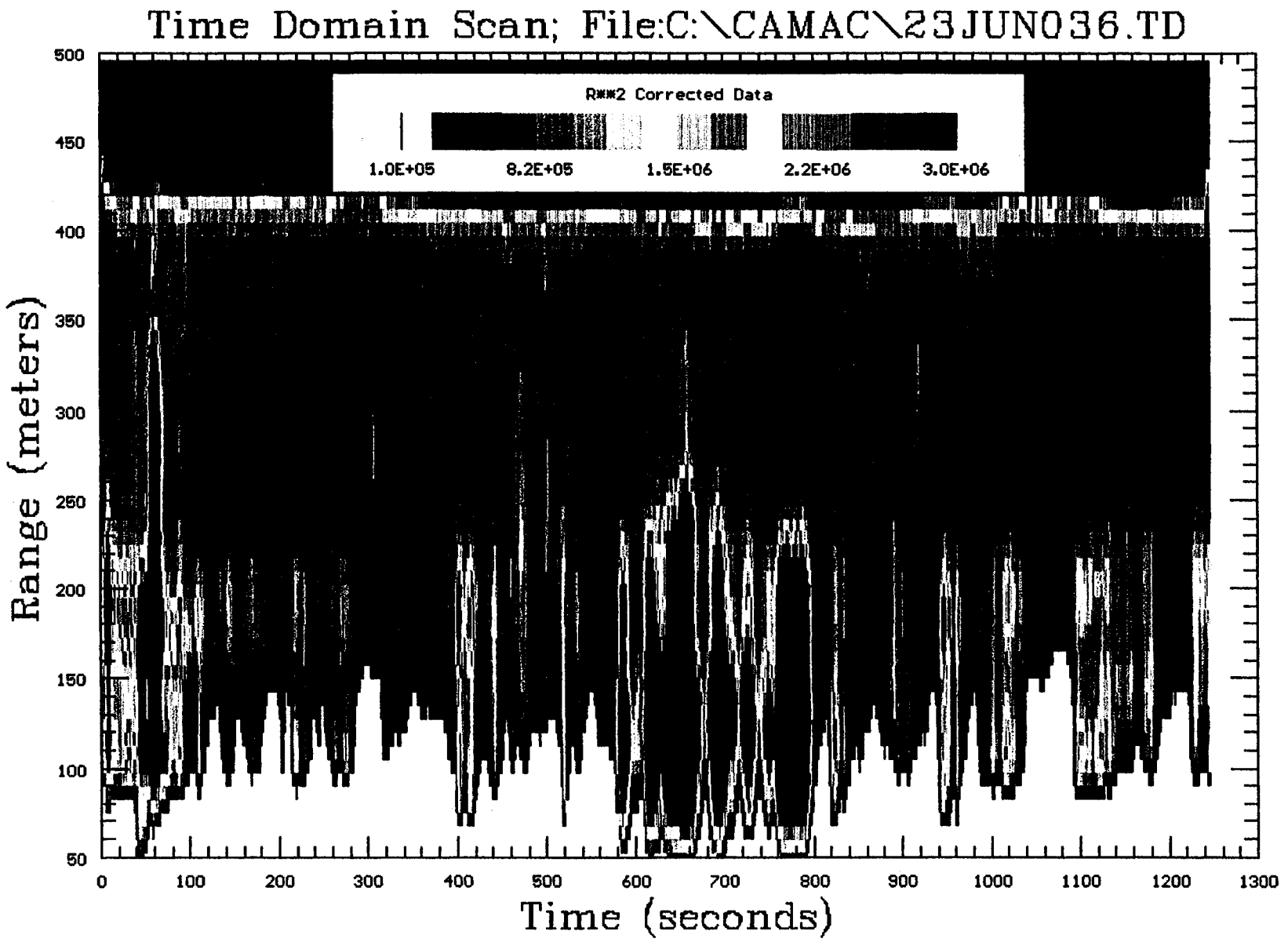

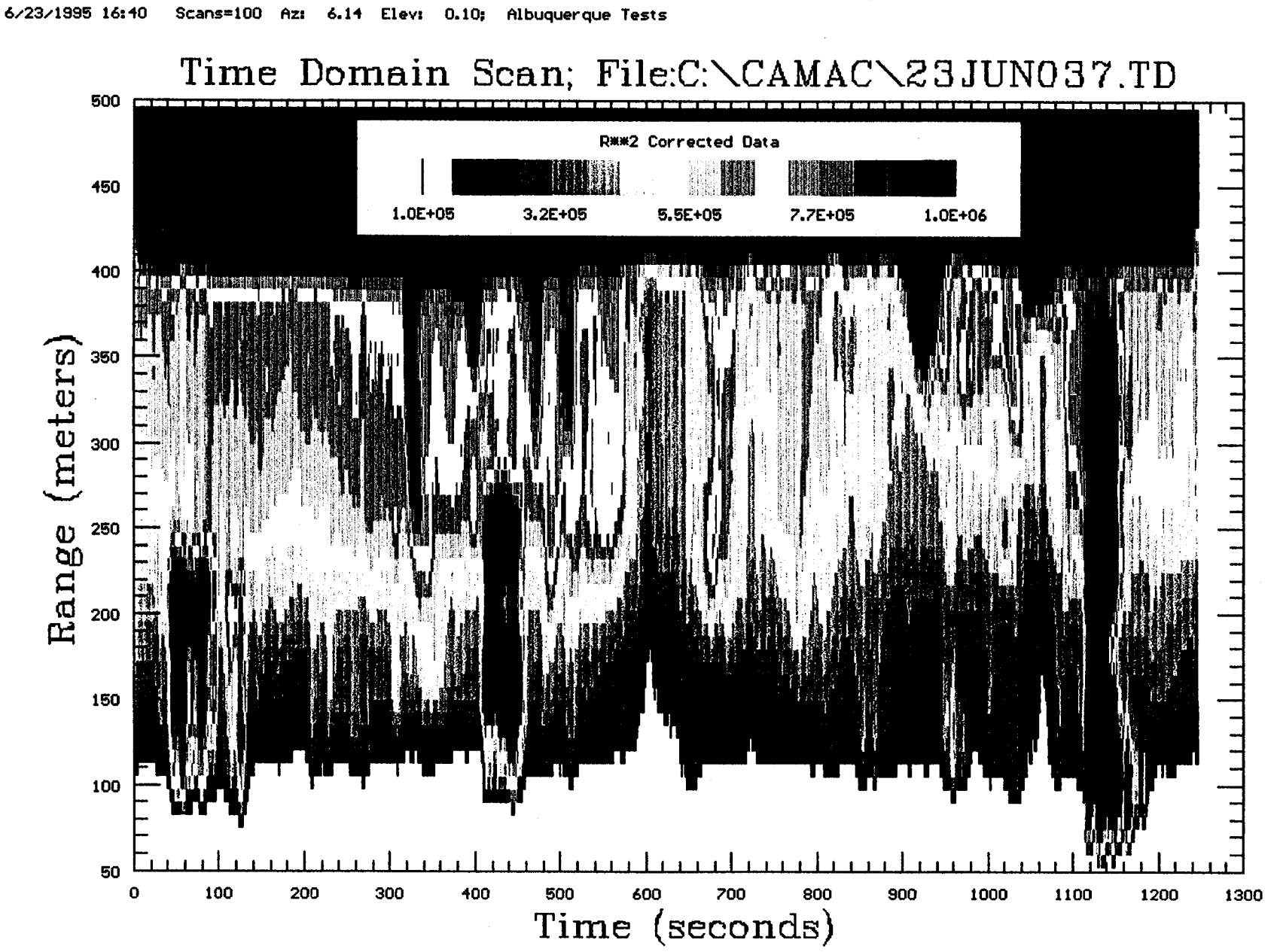
6/23/1995 16:40 Scans=100 Az: 6.14 Elev: 0.10; Albuquerque Tests
Time Domain Scan; File:C:\CAMAC\23JUN037.TD
R**2 Corrected Data
1.0E+05
3.2E+05
5.5E+05
7.7E+05
1.0E+06
Range (meters)
Time (seconds)
500
450
400
350
300
250
200
150
100
50
0
100
200
300
400
500
600
700
800
900
1000
1100
1200
1300

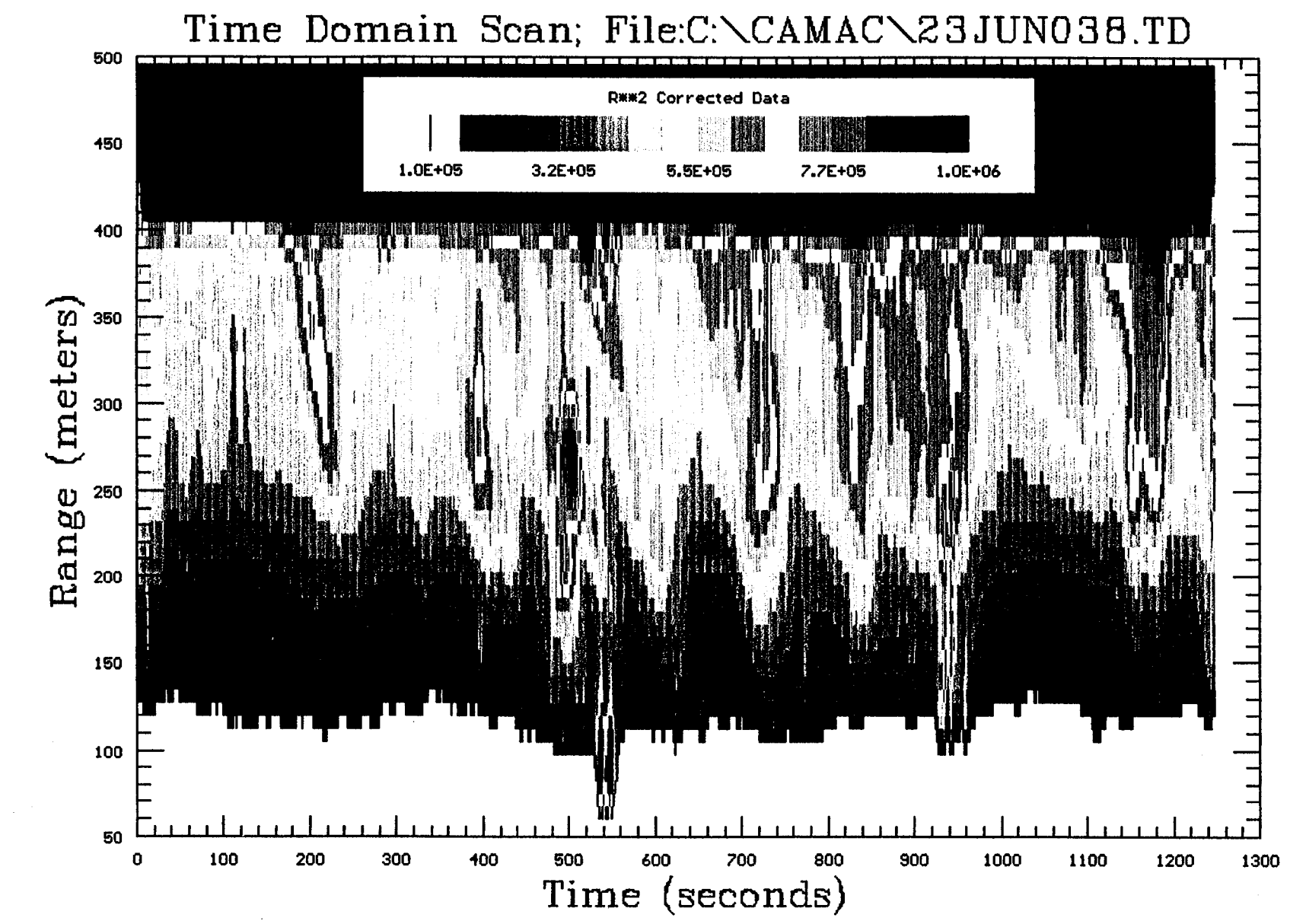
6/23/1995 17:01 Scans=100 Az: 6.14 Elev: 0.10; Albuquerque Tests
Time Domain Scan; File:C:\CAMAC\23JUN038.TD
R**2 Corrected Data
1.0E+05
3.2E+05
5.5E+05
7.7E+05
1.0E+06
Range (meters)
500
450
400
350
300
250
200
150
100
50
0
100
200
300
400
500
600
700
800
900
1000
1100
1200
1300
Time (seconds)

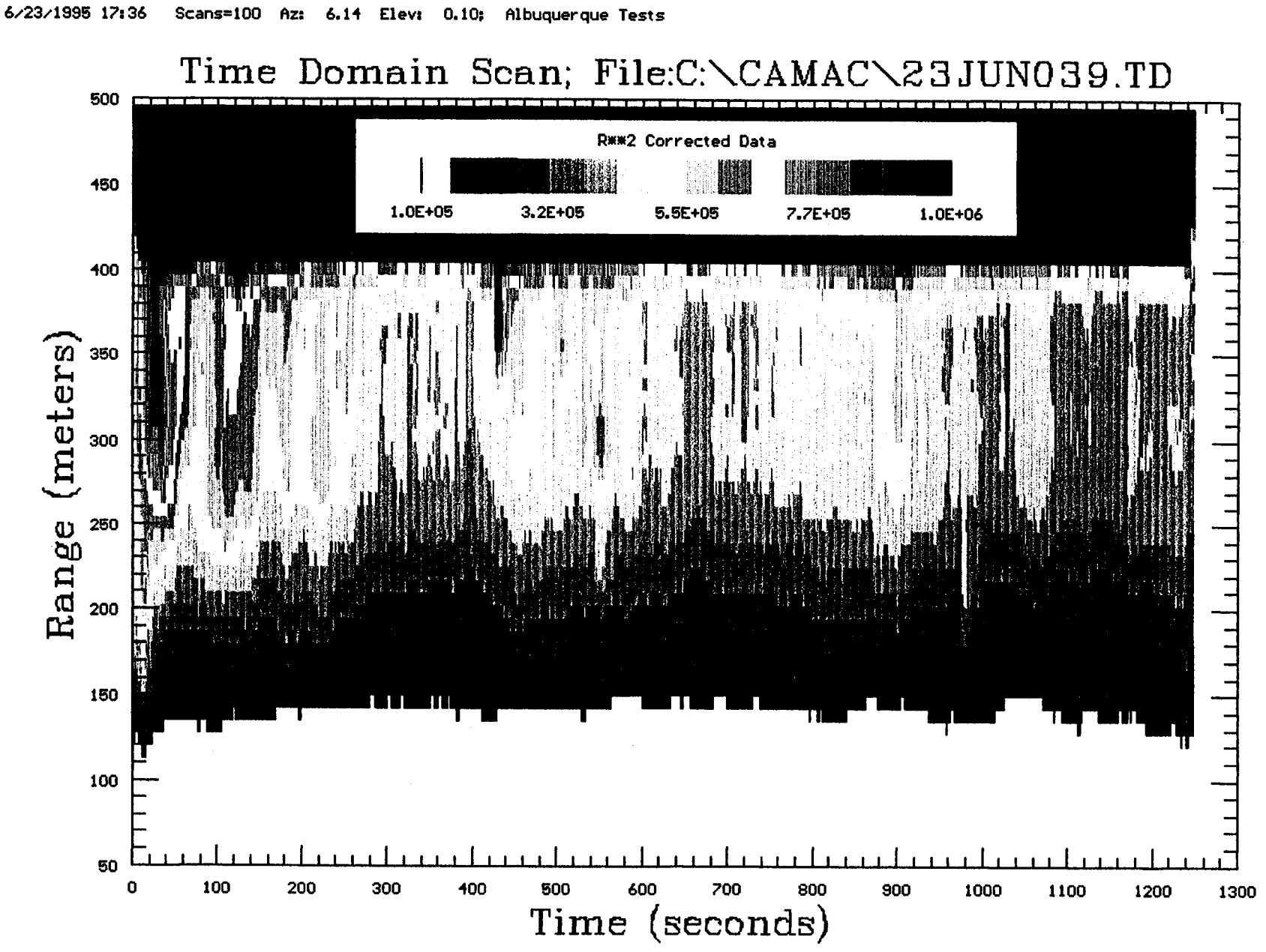
6/23/1995 17:36 Scans=100 Az: 6.14 Elev: 0.10; Albuquerque Tests
Time Domain Scan; File:C:\CAMAC\23JUN039.TD
R**2 Corrected Data
1.0E+05
3.2E+05
5.5E+05
7.7E+05
1.0E+06
Range (meters)
500
450
400
350
300
250
200
150
100
50
0
100
200
300
400
500
600
700
800
900
1000
1100
1200
1300
Time (seconds)

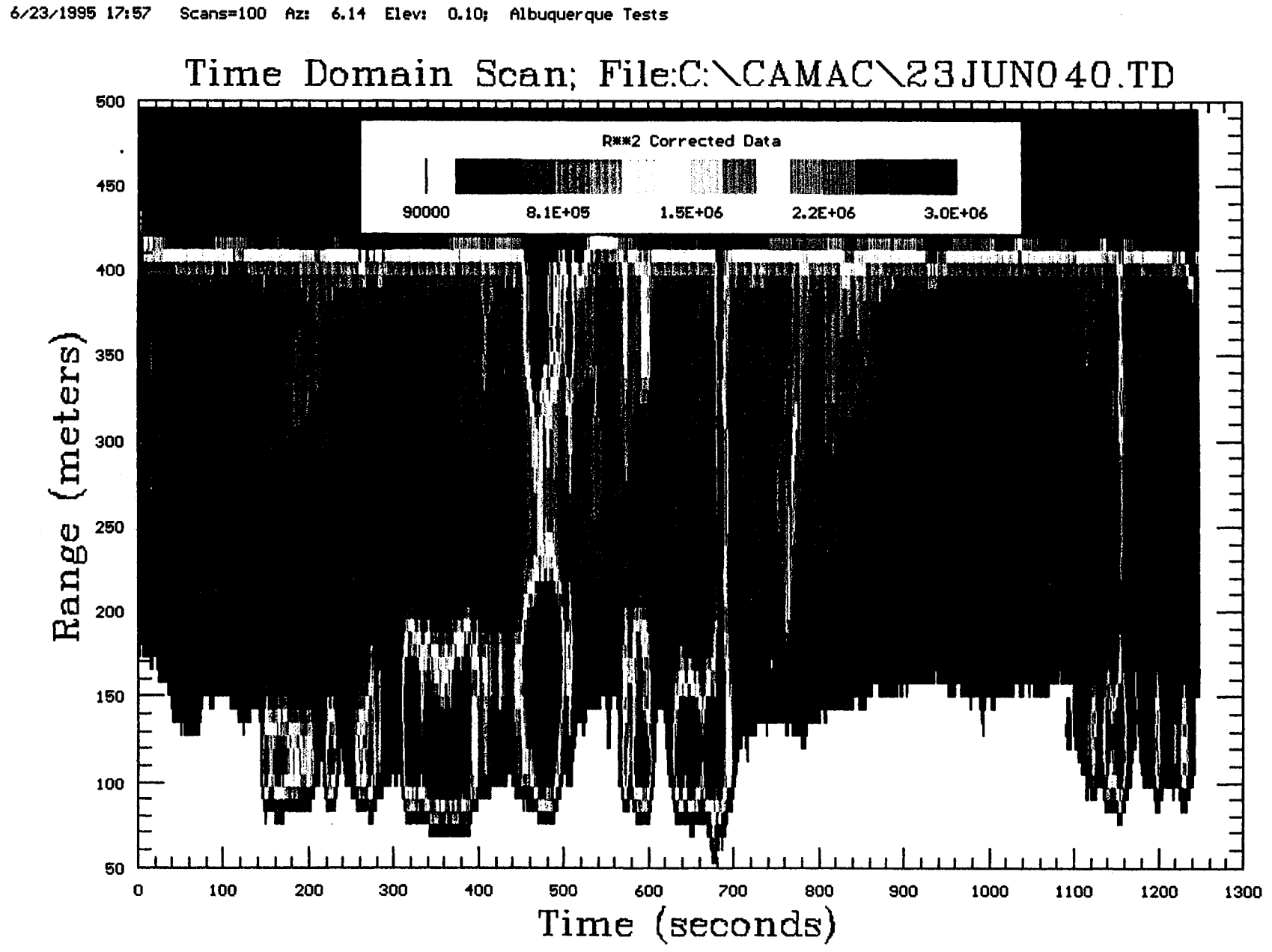
6/23/1995 17:57 Scans=100 Az: 6.14 Elev: 0.10; Albuquerque Tests
Time Domain Scan; File:C:\CAMAC\23JUN040.TD
R**2 Corrected Data
90000
8.1E+05
1.5E+06
2.2E+06
3.0E+06
Range (meters)
500
450
400
350
300
250
200
150
100
50
0
100
200
300
400
500
600
700
800
900
1000
1100
1200
1300
Time (seconds)